ISSN: 2354-5917

PROCEEDINGS
of

INTERNATIONAL SEMINAR ON CHEMICAL ENGINEERING

IN CONJUNCTION WITH

SEMINAR TEKNIK KIMIA SOEHADI REKSOWARDOJO (STKSR) 2017

Clean-Sustainable Process and Product Technology

2-3rd October 2017
East Hall and West Hall
Institut Teknologi Bandung

Organized by:

Sponsored by:

PT PETROKIMIA GRESIK

Supported by:

PROCEEDING

International Seminar on Chemical Engineering in conjunction with Seminar Teknik Kimia Soehadi Reksowardojo (STKSR) 2017

"Clean-Sustainable Process and Product Technology"

ISSN: 2354-5917

2nd-3rd October 2017
West and East Hall
Institut Teknologi Bandung
Jl. Ganesha 10 Bandung INDONESIA

Organized by

Department of Chemical Engineering
Faculty of Industrial Technology
Institut Teknologi Bandung

INTERNATIONAL SCIENTIFIC COMMITTEE

Prof. Johan Sanders. Wageningen University, the Netherlands
Prof. Ir. Dwiwahju Sasongko, M.Sc., Ph.D
Prof. Dr. Eng. I Made Joni, M.Sc
Assoc. Prof. Dr. M. Akbar Rhamdani, Ph.D
Assoc. Prof. Dr. Oki Muraza

STEERING COMMITTEE

Prof. Dr. Herri Susanto. Institut Teknologi Bandung
Prof. Dr. Subagjo Institut Teknologi Bandung
Prof. Dr. Ir. Mubiar Purwasasmita Institut Teknologi Bandung
Prof. Tjandra Setiadi, Ph.D. Insitut Teknologi Bandung
Prof. Dr. Yazid Bindar. Institut Teknologi Bandung
Prof. Johnner Sitompul, Ph.D. Insitut Teknologi Bandung
Prof. I. G. Wenten, Ph.D Insitut Teknologi Bandung
Assoc. Prof. Tatang Hernas Soerawidjaja. Institut Teknologi Bandung

ORGANIZING COMMITTEE

Chairman: Hary Devianto, Ph.D.

Dr. Pramujo Widiatmoko
Ardiyan Harimawan, Ph.D.
M.T.A.P. Kresnowati, Ph.D.
Dr. Antonius Indarto
Dianika Lestari, Ph.D.
Dr. Jenny Rizkiana
Dr. Vita Wonoputri
Dr. Dian Shofinita
Meiti Pratiwi, M.T.
Dr. Anggit R.

Agnes Veronica Victoria
Devina Regina
Catharine Bella
Agatha Victoria
Vania Elita Krisnandika
Nicholas George Stanley
The Arif Setio Nugroho
Catherine Melinda
Bonar Mangara Trijaya Manurung
Ghiffary Azka Nur Aulia
Judistira
Faisal Anggi Rangkuti
James Wijaya
Vincentius Ferry
Budi Prakarsa
Yeremia William Susanto
Kreszen Livianus Gatalie

ISSN: 2354-5917

MESSAGE

Welcome to all honorable keynote speakers, presenters, and participants in the International Seminar on Chemical Engineering in conjunction with Seminar Teknik Kimia - Soehadi Reksowardojo (STKSR) 2017. This annual seminar has been an event of research dissemination and knowledge sharing for chemical engineering community in Indonesian, as well as neighboring countries.

Chemical engineering concern to produce, transform, transport, and properly use of chemical, material, and energy. This field of engineering is therefore closely related to industry development in a country. Process design and analysis of technology, chemical reaction engineering, and safety analysis are the main object of chemical engineering. Chemical engineering has also significant role to fulfill one of millennium development goals, i.e. to ensure environmental sustainability. With limit on resources and increasing environment effect due to industries, we need to move toward a clean-sustainable processing technology.

We encourage youth and motivated professional to develop and share their innovation in the clean-sustainable product and process technology through this seminar. Hopefully, the seminar will bring a productive and fruitful discussion. Lastly, we greatly thanks all sponsors and contributors to support this seminar.

Prof.Dr.Ir. Kadarsah Suryadi, DEA.

Rector of Institut Teknologi Bandung (ITB)

ISSN: 2354-5917

MESSAGE

Dear Colleagues,

On behalf of the Organizing Committee of the International Seminar on Chemical Engineering, I am gladly welcome you all to Institut Teknologi Bandung, Bandung, Indonesia. This year, the Seminar which is held in conjunction with Seminar Teknik Kimia - Soehadi Reksowardojo (STKSR) 2017 raises the topic of 'Clean-sustainable Process and Product Technology'. Through this topic, we are promoting an awarness on global warming issues and sustainable production.

Those topics will be addressed in several categories, i.e. bionergy, chemurgy, alternative energy, fossil energy and mineral processing, process technology, and advance science in plenary lectures and parallel sessions. Here, we encourage young and inspiring keynote speakers to share their energy and experiencies. In end of seminar, we invite speakers in a workshop session who will share their industrial/field experiences.

We have prepared social (get-together) event, so that delegates may meet and communicate one another. Finally, the committee gratefully addressed all sponsors and ChemEng-ITB Alumni for funding and supports. We also thank all International/Technical Committee members, all the plenary and invited speakers and all oral/poster presenters for their kind efforts and contributions in making this conference a success.

Thank you

Hary Devianto, Ph.D.

Chairman of STKSR 2017

ISSN: 2354-5917

ACKNOWLEDGEMENT

The completion of this undertaking could not have been possible without the participation and assistance of so many people whose names may not all be enumerated. The contributions are sincerely appreciated and gratefully acknowledged. However, we would like to express our especially deep appreciation and gratitude to the following.

1. Institut Teknologi Bandung, Faculty of Industrial Technology, Department of Chemical Engineering.
2. Lembaga Penelitian dan Pengabdian kepada Masyarakat Institut Teknologi Bandung (LPPM ITB)
3. PT. Petrokimia Gresik
4. Medco Foundation
5. Ir. Rauf Purnama, IPU
6. Biomass Gasification Research Group Department of Chemical Engineering Institut Teknologi Bandung

for their support toward STKSR 2017. We sincerely hope that our good cooperation can extend to other opportunities in the future.

ISSN: 2354-5917

PT PETROKIMIA GRESIK

TABLE OF CONTENT

ISSN: 2354-5917

POSTER PRESENTATION SESSION

ISSN: 2354-5917

GENERAL PROGRAM STKSR 2017

1ST OF OCTOBER 2017: GET TOGETHER

VENUE: GALERI TK ITB

TIME	PROGRAM
14.00-14.30	Open Gate and Registration
14.30-14.45	Opening
14.45-14.50	Welcoming Speech by Chairman of STKSR 2017: Dr. Hary Devianto
14.50-15.50	Brief Introduction of Keynote Speakers
15.50-16.50	Free Session for All Participants
16.50-17.00	Closing

Every participant is welcome to attend the Get Together event.

2ND OF OCTOBER 2017: GALA DINNER

VENUE: ITB EAST HALL

Time	Program
18.30-19.00	Open Gate and Registration
19.00-19.15	Opening
19.15-19.20	Welcoming Speech
19.20-20.30	Dinner and performance
20.30-20.40	Short sharing session
20.40-21.00	Closing

ISSN: 2354-5917

2nd OF OCTOBER 2017: PLENARY AND PARALLEL SESSIONS

VENUE: ITB WEST HALL AND EAST HALL

TIME	PROGRAM			
	WEST HALL	EAST HALL		
	R01	R02	R03	R04
07.30-08.00	Open Gate and Registration			
08.00-08.10	Safety Induction and Program Report			
	-Safety Induction			
	-Program Report			
08.10-08.25	Welcoming Speech by Head of Faculty of Industrial Technology Faculty-ITB			
08.25-08.35	Opening of STKSR 2017 by Chairman of STKSR 2017: Dr. Hary Devianto			
	PLENARY SESSION 1			
08.35-09.00	Keynote 1:			
	Assoc. Prof. Dr. M. Akbar Rhamdani, Ph.D			
09.00-09.25	Keynote 2:			
	Assoc. Prof. Dr. Oki Muraza			
09.25-09.50	Keynote 3:			
	Prof. Dr. Eng. I Made Joni, M.Sc			
09.50-10.15	Discussion			
10.15-10.45	**COFFEE BREAK**			
	PLENARY SESSION 2			
10.45-11.10	Keynote 4:			
	Prof. Dwiwahju Sasongko M.Sc., Ph.D			
11.10-11.35	Keynote 5:			
	Prof. Dr. J.P.M. (Johan) Sanders			
11.35-12.00	Discussion			
12.00-12.20	**Flash Poster Presentation**			
12.20-13.30	**LUNCH BREAK (EAST HALL)**			
PARALLEL SESSION				
13.30-13.45	CE01	BE01	PT01	FEMP 01
13.45-14.00	CE02	BE02	PT02	FEMP 02
14.00-14.15	CE03	BE03	PT03	FEMP 03
14.15-14.30	CE04	BE04	PT04	FEMP 04
14.30-15.00	**COFFEE BREAK (EAST HALL & WEST HALL)**			

ISSN: 2354-5917

15.00-15.15	CE05	BE05	PT05	FEMP 05
15.15-15.30	CE06	BE06	PT 06	PS01
15.30-15.45	CE07	BE07	PT07	PS02
15.45-16.00	CE10	AE01	AE05	PS03
19.00-21.00		**GALA DINNER (EAST HALL)**		

R01: WEST HALL
R02-03-04: EAST HALL

For Parallel Session, the allocated time is 10 minutes for presentation and 5 minutes for discussion

ISSN: 2354-5917

3rd OF OCTOBER 2017: PARALLEL SESSION AND WORKSHOP SESSION

VENUE: ITB WEST HALL AND EAST HALL

TIME	PROGRAM			
	WEST HALL	EAST HALL		
	R01	R02	R03	R04
09.00-09.15	AS01	AE02	PT08	IA01
09.15-09.30	AS02	AE03	PT09	IA02
09.30-09.45	AS03	AE04	PT12	IA03
09.45-10.15	COFFEE BREAK (EAST HALL & WEST HALL)			
10.15-12.15	Poster Scoring Session	Workshop: Mr. Setyo Yanus Sasongko – PT. AIMTOP INDO Nuansa Kimia		Workshop: Mr. Antonius Dian Adhy Feryanto – CV Pavettia Kurnia Atsiri
12.15-13.15	LUNCH BREAK (EAST HALL)			
13.15-13.45	CLOSING AND AWARDING: -Closing by Chairman of STKSR 2017 Dr. Hary Devianto -Awarding: Best Paper, Best Presenter, Young Scientist Award, Best Poster			
13.45-14.15	COFFEE BREAK (WEST HALL)			

ISSN: 2354-5917


Medco
Foundation

KEYNOTE SESSION

Biobased Chemicals and Materials for Indonesia

Johan Sanders[a]*

[a]*Wageningen University and Research, Food and Biobased Research, Wageningen, the Netherlands.*

* *Corresponding Author's E-mail: Johan.sanders@wur.nl*

Abstract

The Paris CO2 reduction goals for 2050 give concrete challenges. Can we imagine how these can be obtained under economic conditions? How many new processes have to be designed and implemented? How much capital will be required?

High value products can only contribute with small overall CO2 reductions.
If on the bottom end of the ecopyramid biomass needs to compete with fossil resources just on its energy content the chances for biomass will be small, even more so when logistic properties are taken into account. Some waste streams will be available at limited volumes, but the waste streams often are heterogeneous in compositions and therefore set even more boundary conditions to their application. Since the availability of cheap waste is limited, the learning curves of these types of processes will only have limited application.

Biomass will have best economic chances when it is used because of its structural properties. These structures might be on molecular level and/ or on macroscopic level. Benefitting from its molecular structures, application of biomass in the chemical industry will need less heat exchanging process steps and therefore lead to lower capital requirements and therefore leaving more economic room for (the (biorefining and the production of) biomass. This leads to a significant increase in employment in the production of existing chemical building blocks without increase of the integral costprice. Anaerobic fermentation for the production of building blocks is one example of using the structure of biomass. The consequences on employment and the investment costs are compared of importing large amounts of lignocellulose for the supply of fermentation sugars is compared with the use of domestic sugar production.

Several examples will be given and also how they can be implemented under economic conditions.

ORAL PRESENTATION SESSION

Impact of Wastewatere Types and Electrolytes on Microbial Fuel Cell

Ardiyan Harimawan*, Brenda Kalista, Theresia Cecylia Ramli and Hary Devianto

Department of Chemical Engineering, Institut Teknologi Bandung, Bandung 40132 Indonesia

** Corresponding Author's E-mail:ardiyan@che.itb.ac.id*

Abstract
Microbial fuel cell is a cell that directly generates power using organic matter as fuel for exoelectrogenic microbes. The latter is different from the common fuel cell which uses hydrogen as its fuel. Until now, MFC has not been applied as a large scale power plant because it required high cost and power density produced is low. This research used bean curd wastewater and palm oil milling effluent (POME) and also carbon-based electrode to reduce cost. Furthermore, 10 g/L NaCl electrolyte was added to the feed as a trial variation. The results of this study indicate that MFC with POME wastewater as feed generate higher power compared to MFC with bean curd wastewater, due to higher nutrient content of POME. Biofilm formation is better in when 10 g/L NaCl was added to the feed, this caused the decrease of the MFC's charge transfer and ohmic resistance. However, in MFC with POME wastewater as feed, the addition of 10 g/L NaCl actually increased ohmic resistance due to the formation of $Ca(OH)_2$.

1. Introduction

The human population on earth is increasing every year. By 2050 human population is estimated to reach 9.4 billion (Lewis and Nocera, 2006). As the human population increases, the amount of energy demand also increases. Today, 85% of the world's energy needs are fulfilled with the burning of fossil fuels such as petroleum, natural gas, coal and others (Rackley, 2010). This conventional energy sources tend to be limited, so its price will increase every year. Another disadvantage of conventional energy sources is it produces very high carbon emissions and carbon emissions lead to global warming. In an effort to overcome this energy crisis, we need to look for alternative energy sources. One of the alternative energy sources that can be used is biomass. Generation of energy through biomass can be done using several methods, such as pyrolysis, fermentation, and microbial fuel cell (MFC). MFC, such as the fuel cell, require feed to generate energy. Wastewater can be used as MFC's feed because it contains biomass or organic materials that can be metabolized by microbes to generate electricity. Therefore, besides being able to generate energy, MFC can also be used as wastewater treatment technology. Currently, MFC cannot be applied on a large scale because the cost is high. The cause of the high cost required is the substrate used as MFC feed. Research conducted on MFC generally uses pure substrates such as acetic acid and glucose. The use of this pure substrate would be uneconomical when used on a large scale. Therefore, researchers starts to use industrial wastewater such as food, paper and beer industries as MFC feed. In Indonesia, palm oil milling effluent (POME) is abundant as a result of the large production of palm oil (indonesia-investments.com). In addition to POME, bean curd wastewater is also potentially used as MFC feed as it is easy to find and has not been studied enough. Thus, in this study, we used industrial bean curd wastewater manufactured in Bandung and POME as MFC feed. In addition to expensive fuel prices, MFC also cannot produce high power density. The cause is the high resistance in MFC due to the low concentration of compounds that can deliver electrons in the feed. This can be overcome by adding mediators such as pyocyanin, methylene blue, or salt such as NaCl (Logan, 2008). The addition of electrolytes such as NaCl is more desirable because it is cheaper and non-toxic to the environment. Based on the problems that have been described, this research has two

objectives, to determine the influence of the type of wastewater as feed on the performance of MFC and determine the effect of adding NaCl electrolyte on MFC performance.

2. Experimental

Figure 2.1 below shows a series of experiments conducted in determining the effect of wastewater type and electrolyte addition. We used double-chamber MFC, with the anode and cathode chamber capacity: 250 ml each. Figure 2.2 shows the MFC reactor used in this study.

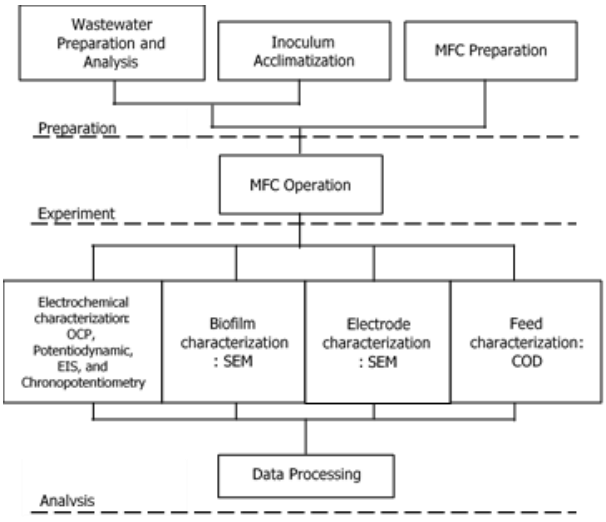

Figure 2.1 Experiment diagram

Figure 2.2 Double chamber MFC

The MFC used graphite sheet electrodes which had been activated using nitrate acid and sulfuric acid. Nafion 212 was chosen as the membrane to separate the anode and cathode chamber. The wastewater used are local bean curd wastewater and POME. The addition of NaCl with concentration 10 g/L in the feed was also tested. The inoculum used is derived from cow dung, it was first acclimatized in the YPG medium until the MLSS value reaches 1500-4000 mg/L. Before used, the wastewater pH was adjusted to 7 by using phosphate buffer. The anode chamber is filled with a wastewater and inoculum at a ratio of 1:1, whereas the cathode chamber is filled with 160ml $KMnO_4$ 0.02M and 40 ml of phosphate buffer solution. Potential is measured using multimetre until it reaches steady state, then electrochemical characterization is done by using potentiostat. Characterization of biofilm and electrode surface was done by SEM, while the COD removal efficiency of MFC was tested by COD test.

3. Results and Discussion

3.1. MFC COD removal efficiency

The wastewater used in this study was tested first at the Balai Laboratorium Kesehatan, the result is showed in Table 3.1 below. Table 3.2 shows the COD removal efficiency by various feed in MFC. MFCs with only wastewater as its feed (without the addition of inoculum) has the lowest COD removal efficiency, for the same type of wastewater. This indicates that microorganisms from cow manure are able to adapt and metabolize organic compounds contained in the bean curd wastewater and POME. On the other hand, the COD removal in bean curd wastewater is not as significant in POME. This is because the MFC with POME wastewater needs more time to reach steady state than MFC with bean curd wastewater. In MFC with bean wastewater, during the two-day interval, it is possible that microorganisms will metabolize the organic compound from its medium first, since MFC feed is a mixture of waste water with inoculum at a ratio of 1: 1.

Table 3.1 Wastewater characterization

No.	Parameter	Unit	Bean curd wastewater	POME
1.	Total N	mg/L	4,59	28,79
2.	COD	ppm O_2	4556	28282
3.	Phosphate	mg/L	3,78	15,58

Table 3.2 COD removal efficiency

Feed	Electrolyte	Inoculum added	COD removal	Time (Day)
Bean curd wastewater	-	1:1	13,9%	2
	NaCl 10 g/L	1:1	6,9%	2
	-	-	0,6%	2
POME	-	1:1	64,9%	11
	NaCl 10 g/L	1:1	46,4%	16
	-	-	20,0%	11

The addition of 10 g/L NaCl resulted in a lower COD removal than without the addition of electrolytes, either on MFC with bean curd wastewater or POME as its feed. This is because some types of microorganisms cannot survive, therefore organic compounds that can be metabolized by microbes are also reduced.

3.2. Open Circuit Potential (OCP)

MFCs with bean curd wastewater as its feeds either with or without the addition of 10 g/L NaCl reached its steady state within two days. On the other hand, MFC with POME reached its steady state in 11 days, whereas with the addition of NaCl, steady state was reached only after 16 days. The content of organic compounds as measured by the COD test, shows that the organic compound content in POME is more than five times that of bean curd wastewater. This means that there are more susbtrates that can be utilized by microorganisms, so electrons generated from the process of oxidation of organic compounds by microorganisms also increases. The operating time of MFC with the POME wastewater feed is much longer, therefore microbes have a longer time span to metabolize the substrate. The OCP value obtained does not come near to the maximum potential difference value, due to the presence of considerable internal resistance. Determination of resistance and effect of salt addition can be seen in sub-section of electrochemical characterization.

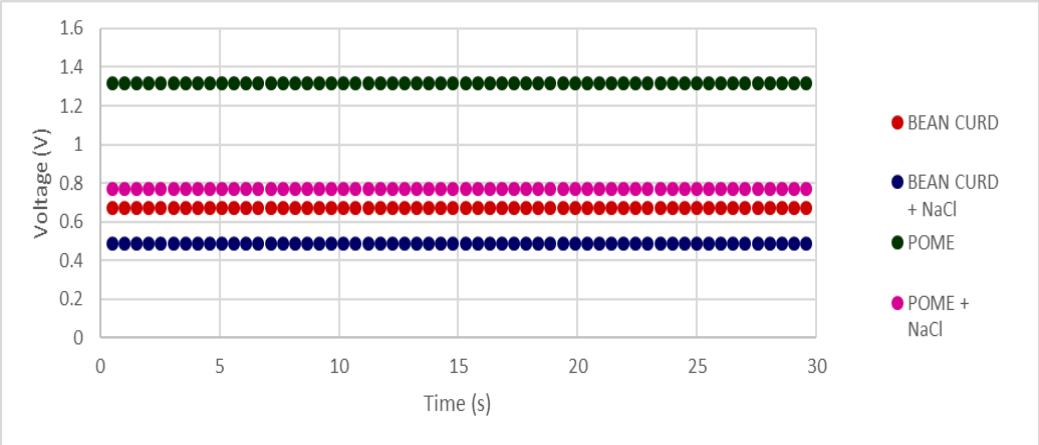

Figure 3.1 MFCs open circuit potential

3.3. Potentiodynamic

Figure 3.2 below shows I-V-P curve that was plotted from potentiodynamic measurement.

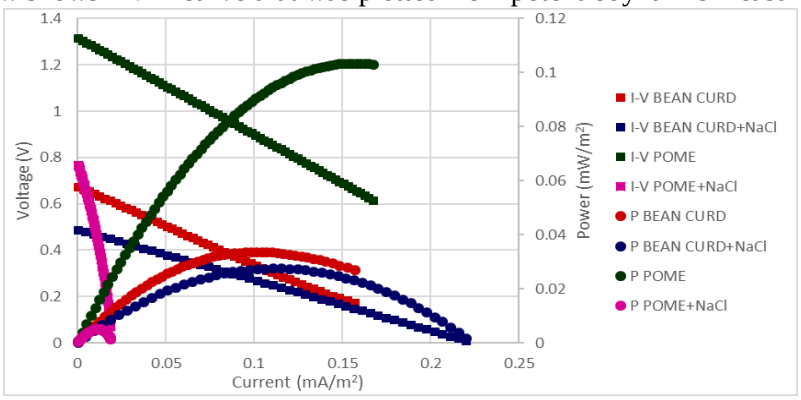

Figure 3.2 I-V-P curve based on different feed used in MFC

Based on the I-V-P curve, maximum power density obtained on the usage of POME without and with NaCl 10 g/L addition was 1.32 and 0.005 mW/m^2, meanwhile the usage of bean curd wastewater without and with NaCl addition was 0.034 and 0.027 mW/m^2. Salt addition will increase the ionic strength of the medium. The ionic strength of the medium will affect the conductivity of anolite solution and has been shown to affect power generation (Liu et al., 2005). On the other hand, higher ionic strength will inhibit microorganism, but a low ionic strength will limit power production (Logan, 2008). NaCl addition with 10 g/L concentration started to inhibit the growth of microorganism in anode chamber, but highest power density was obtained on 20 g/L NaCl concentration (Lefebvre et al., 2012). On this research, the addition of NaCl in 10 g/L concentration led to lower power density obtained, compared to the performance MFC without salt addition. There was a possibility in which microorganism on bean curd wastewater with NaCl addition can not survive in such high salinity solution. NaCl addition increased osmotic pressure, plasmolysed the cells in anode chamber. This decreased the organic matter that can be oxidized and the end led to lower number of electrons produced. The concentration of NaCl added to the medium was the same with literature (Lefebvre et al., 2012), but there were differences in medium and microorganism used in this research. The medium that was used on the literature was sodium acetate and the microorganism was obtained from domestic wastewater. On the other hand, in this research, bean curd wastewater and microorganism from calf faeces was used. Therefore, a further research is needed to determine a precise concentration for every wastewater types and inoculum sources, because a same salt concentration will deliver different result for different wastewater and inoculum. MFC system with POME with NaCl addition as anolyte, after the eighth day, became unstable and the potentiodynamic and electrochemical impedance spectrometry could not be measured any longer. If this result was compared with MFC performance with bean curd wastewater with NaCl addition as anolyte as previously described, it was clearly shown that MFC could attain a steady state system. POME contains more minerals than bean curd wastewater, so the addition of NaCl formed a more hypertonic solution, led to plasmolysis of the microorganism. This caused the MFC became unstable after the eighth day.

3.4. Electrochemical Impedance Spectrometry (EIS)

Characterization of MFC by EIS measurement was shown as Nyquist plot (Figure 3.3). MFC with POME with NaCl addition as anolyte cannot be characterized, as previously described. There are two types of resistance on MFC systems, ohmic resistance and charge transfer resistance. In order to know the value, a fitting towards Nyquist plot was done by equivalent circuit model (Figure 3.4). R_1, R_2 and C represented ohmic resistance, charge transfer resistance and double layer capacitance. Table 3.3 showed the fitting by equivalent circuit model result.

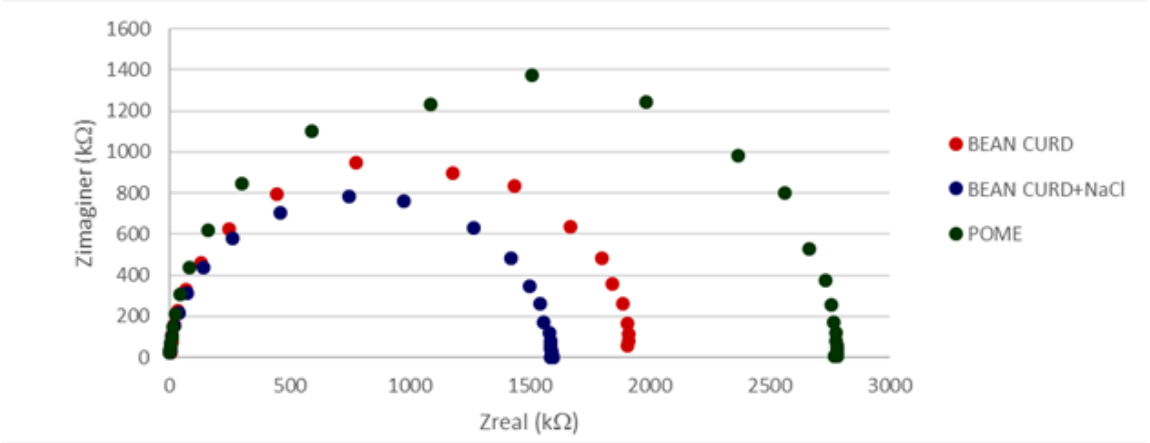

Figure 3.3 *Nyquist plot* for MFC with different anolyte

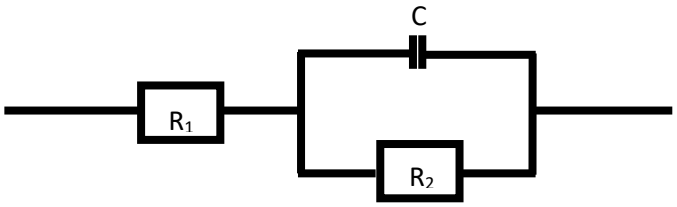

Figure 3.4 Equivalent circuit model

In bean curd wastewater with NaCl addition, it was shown that there was a decrease in both ohmic and charge transfer resistance. The decrease in ohmic resistance was caused by increasing ionic strength of the solution, so the proton was easier to move from anode to cathode chamber. Ionic strength of the solution was increasing because the addition of NaCl that acted as electrolytes in the medium. This fact was in tune with literature, that addition of electrolytes in MFC's medium will increase anolyte solution conductivity and power generation (Liu et al., 2005).

If internal resistance between bean curd wastewater and POME were compared, ohmic resistance in POME was lower. This was because the protein content in POME was higher than bean curd wastewater. Proteins content in POME is 12900 mg/L (Wu et al., 2007), while in bean curd wastewater is 226.06 to 434.78 mg/L (Ismail et al, 2014). Proteins roles as zwitter ion that aid electron delivery towards anode, hence decrease the ohmic resistance.

Table 3.3 Fitting by equivalent circuit model result

Symbol	**Bean curd**	**Bean curd + NaCl**	**Palm oil milling effluent**
R_1 (Ω)	1.86E+03	1.35E+03	1.22E+03
R_2 (Ω)	1.85E+06	1.59E+06	2.77E+06
C (F)	6.83E-10	7.15E-10	7.51E-10

Charge transfer resistance is closely related to biofilm formation on electrode surface. Biofilm formation is one of the microorganism stress response (Pan et al., 2010). The stress condition along MFC operation was caused by high salinity content, 10 g/L of NaCl. By saying so, salt addition in anolytes promoted microorganism to form biofilm, led to better electron transfer and lower the charge transfer resistance. In MFC with bean curd wastewater as anolyte, the addition of NaCl drove a thicker and equally formation of biofilm (Figure 3.5). This caused charge transfer resistance in MFC with

bean curd wastewater with NaCl addition was lower than MFC with only bean curd wastewater as anolyte.

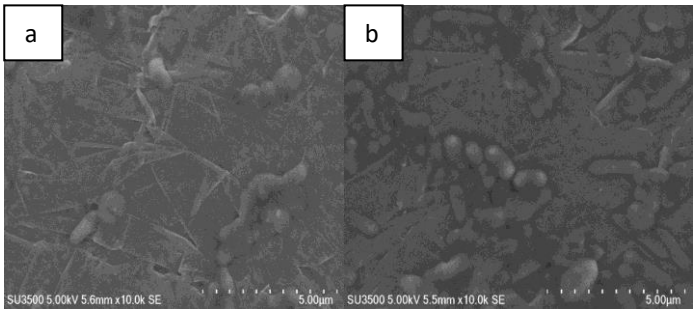

Figure 3.5 Biofilm on electrode on MFC with bean curd wastewater as medium (a) without and (b) with addition of NaCl 10 g/L

Charge transfer resistance in POME was higher than bean curd wastewater. This was because the biofilm formation on anode surface in POME is relatively higher than bean curd wastewater. Biofilm formed on anode in POME was less than bean curd wastewater, because nutrition content in POME is relatively higher. When microorganism is placed in rich medium, they tend to be in planktonic phase than sessile phase, where in sessile phase the biofilm formation is happened (Javaherdashti, 2008). Biofilm formation on anode surface in MFC with POME as medium was shown in Figure 3.6.

MFC with POME with NaCl addition could not be measured after the eighth day, meanwhile MFC with the same medium without any NaCl addition achieved a steady state system on the eleventh day. Therefore, to compare ohmic resistance between MFC system with and without NaCl addition, ohmic resistance value was measured by determining I-V curve's slope. Based on the slope, it was known that the ohmic resistance in MFC with palm oil milling wastewater as anolyte, without NaCl addition was 4189 Ohm and with NaCl addition was 37581 Ohm. Salt addition in anode chamber will decrease resistance in MFC, because of the increasing ionic strength (Liu et al., 2005). On the other hand, in this research, ohmic resistance was increasing as NaCl was added to the anode chamber. Based on SEM result on anode that was used in MFC with POME and NaCl as medium, it was shown that there was a lot of white sediment was formed on the anode surface (Figure 3.7).

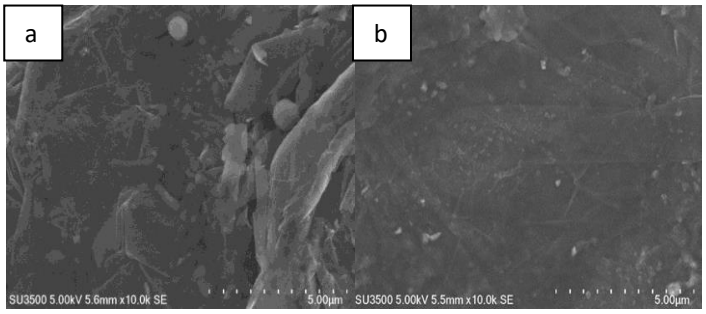

Figure 3.6 Biofilm on electrode on MFC with POME as medium (a) without and (b) with addition of NaCl 10 g/L

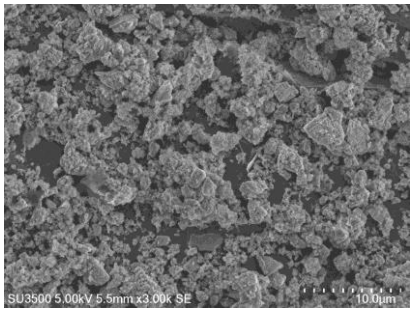

Figure 3.7 White sediment on anode surface

EDX test was done on the anode and it was indicated that the white sediment was calcium with proportion of 24,5% weight. There was a presumption that the white sediment on the anode was $Ca(OH)_2$. Calcium salt that easily precipitate was $Ca(OH)_2$ and $CaCO_3$. At the end of MFC operation, the final value of pH measured was 8.1, so the possibility of $Ca(OH)_2$ precipitation was higher. The base condition was caused by two possibilities. The first one was decomposition of organic matters that contain nitrogen to ammonium, because Total Nitrogen (TN) of POME based on Labkes test was 28.79 mg/L. Second, organic acids was carried away in the scum or foam, formed on the surface of anolyte. Scum was formed by saponification reaction between fatty acids and magnesium. Fatty acids sourced from the wastewater itself, cell fermentation and cell membrane. It should be noted that magnesium content in POME was also relatively high. Due to $Ca(OH)_2$ layer formation on anode surface, there was escalation on ohmic resistance value in MFC with POME with NaCl addition.

4. Conclusions

Based on this research, we can conclude that first, power density and COD reduction efficiency in MFC with POME was higher than MFC with bean curd wastewater. Second, there were two types of resistance on MFC used on this research, ohmic resistance and charge transfer resistance. Ohmic resistance in MFC using POME was lower than MFC using bean curd wastewater. Charge transfer resistance in MFC using POME was higher than MFC using bean curd wastewater. Third, NaCl addition in POME increased ohmic resistance due to $Ca(OH)_2$ precipitation on anode.

References

1. Eaktasang N, Kim D, et al. Enhancement of Electron Transfer by Electrochemical Treatment of Electrode in the Microbial Fuel Cell. International Conference on Chemical, Environmental Science and Engineering, (2012).
2. Ismail D, Rizkytata B T, et al. Industrial Tofu Wastewater as a Cultivation Medium of Microalgae Chlorella vulgaris. *Energy Procedia*; 47: 56-61(2015).
3. Javaherdashti, R. Microbiologically Influenced Corrosion. Springer, Manchester, (2008).
4. Lefebvre O, Tan Z, et al. Effect of increasing anodic NaCl concentration on microbial fuel cell performance. *Bioresource Technology*; 112: 336-340(2012).
5. Lewis N S, Nocera D G. Powering the planet: chemical challenges in solar energy utilization. PNAS 103; 43: 15729-15735(2006).
6. Little B J, Lee J S. Microbiologically Influenced Corrosion. John Wiley and Sons, New Jersey, (2007).
7. Liu H, Cheng S, Logan, B. Power Generation in Fed-Batch Microbial Fuel Cells as a Function of Ionic Strength, Temperature, and Reactor Configuration. *Environ. Sci. Technol.*; 39: 5488-5493(2005).
8. Logan, B E. Microbial Fuel Cells. John Wiley and Sons, New Jersey, (2008).

9. Pan Y, Breidt F, Gorski L. Syngergistic Effects of Sodium Chloride, Glucose, and Temperature on Biofilm Formation by Listeria monocytogenes Serotype 1/2a and 4b Strains. *Appl. Environ. Microbiol.*; 76: 1443(2010).
10. Rackley S A. Carbon capture and storage. Elsevier, Massachusettes, (2010).
11. Wu, T Y, Mohammad A W, et al. Palm oil mill effluent (POME) treatment and bioresources recovery using ultrafiltration membrane: Effect of pressure on membrane fouling. *Biochemical Engineering Journal*; 35: 309-317(2007).

Carbon Electrode Fabrication for *Dye-Sensitized Solar Cell*

Adriaan[1,*], Isdiriayani Nurdin[1], Pramujo Widiatmoko[1], Henry Natanail[1]

[1]*Department of Chemical Engineering, Institut Teknologi Bandung, Jalan Ganeca 10, 40135, Indonesia*

** Corresponding Author's E-mail:: widya.adriaan@gmail.com*

Abstract.
Solar cell is an environmental friendly technology used in many industries and household as an electricity source. The cell works by converting solar radiation directly to electric energy. The most common solar cell is silicon based solar cell. However, the fabrication of silicon-based solar cell is expensive. The main difference between DSSC and common solar cell is the use of dye to enhance cell's sensitivity. In DSSC, the counter electrode is made from platinum which is very expensive. To overcome the problem, carbon is being used to substitute platinum as counter electrode.
This research is focused on carbon electrode fabrication method and sources of carbon. The experimented-fabrication methods are metering rod, doctor blade and bubble deposition, while the source of carbon used are medicinal activated carbon and commercial activated carbon. DSSC performance are characterized using I-V curve and electrochemical impedance. Moreover, carbon electrode morphology are observed using Scanning Electron Microscopy (SEM) while carbon electrode surface area and porosity are observed using Brunauer-Emmett-Teller (BET).
Based on the research results, DSSC fabricated with bubble deposition method yield the highest efficiency. Meanwhile, medicinal activated carbon provides better efficiency than commercial activated carbon. The highest conversion efficiency of solar energy achieved is 3,763%.

1. Introduction

Solar energy is one of the renewable energy that has great potential in Indonesia. This is supported by the fact that solar energy in Indonesia reaches 4.8 kWh/m^2/day (Nurliyanti, 2012). Solar energy can be converted into electrical energy by solar cell. For that reason, solar cell is developed to become one of the alternative power generators.

Currently, the most common solar cell is silicon-based solar cell. The weakness of silicon-based solar cell is that it can only utilize high intensity light. Its efficiency will fall dramatically if used on low intensity light. To cope with this problem, solar cell is being developed into dye-sensitized solar cell (DSSC). DSSC can utilize diffuse light with higher efficiency than solar-based solar cell (Barber, 2011).

In Indonesia, solar energy radiation intensity is obtained relatively equal for each region because the location of Indonesia at the equator. Thus, solar energy has great potential to become renewable energy source for Indonesia. Utilization and development of DSSC can help indonesia to meet its targeted electrification ratio and solved the increasing energy demand in Indonesia.

One of the main component of DSSC is counter electrode. Counter electrode is where the electrolyte reduction reaction happened. Normally, DSSC utilize platinum metal as the material to make counter electrode, but platinum metal is expensive so that DSSC cannot be

sold comercially. Therefore, carbon is chosen to be the alternative material because it is cheaper.

2. Experimental

2.1. Main Equipments

In this research, doctor blade, bubble deposition, and metering rod are used to make carbon electrode.

1.1.1 Doctor blade

Carbon paste is applied on the conductive glass. The conductive glass area that wants to be coated is arranged with paper tape. Carbon film thickness can be adjusted by adjusting blade height. After the conductive glass are coated, the conductive glass are heated at 100^{o}C for 40 minute then cooled to room temperature.

1.1.2 Bubble deposition

Carbon solution is fed into bubble deposition. the conductive glass area that wants to be coated is arranged with paper tape. Air flowed through bubble deposition to form a bubble to coats the conductive glass surface. Then, the conductive glass are heated at 100^{o}C for 40 minute then cooled to room temperature.

1.1.3 Metering rod

Carbon paste is applied on the conductive glass. The conductive glass area that wants to be coated is arranged with paper tape. Carbon film thickness will be the same with the paper tape thickness. Then the conductive glass are heated at 100^{o}C for 40 minute then cooled to room temperature.

2.2. Dye preparation

In this research, the dye used was Eosin Y. the Eosin Y and acetone mixture were prepared by dissolving 0.0138 grams of Eosin Y into 20 mL acetone.

2.3. Working electrode preparation

TiO_2 paste is made by mixing 1 gram of TiO_2 powder with acetic acid solution. The acetic acid solution was prepared by mixing 3 mL glacial acetic acid with 12 mL of water. Then, 1 gram of TiO_2 powder is mixed with 30 drops of acetic acid solution in mortar and stirred until homogenous. The paste is applied into conductive glass surface. The conductive glass area that wants to be coated is arranged with paper tape. The coating are made using doctor blade methods. Then the conductive glass are heated at 500^{o}C and atmospheric pressure for 30 minute. Finally, the working electrode immersed into a dye solution for 24 hours in a sealed container

2.4. Electrolyte preparation

Electrolyte utilized in this experiment was iodine solution. The solution was made by mixing 0.496 g of potassium iodide with 0.076 g iodine inside 0.5 mL of water and 6 mL of asetonitril.

2.5. DSSC performance analysis

Short circuit current and open circuit voltage are measured by digital multimeters under irradiation of 100 W halogen lamp at a distance of 20 cm and perpendicular to DSSC. Resistor series can be used to assign loads to the DSSC to obtain variations in voltage and current data. In addition, impedance measurement were performed by electrochemical impedance spectroscopy (EIS) method using potentiostat tool. The EIS yields a nyquist curve which is the analyzed to obtain the desired resistance value. To minimize irradiation from the other sources, the DSSC is placed inside a box.

3. Results and Discussion

3.1 Titanium Dioxide Characteristic for Working Electrode

Titanium dioxide (TiO_2) act as electron acceptor. TiO_2 has three crystal structures. In this research, the desired crystal structure is anatase. According to Luttrell etc (2004), anatase crystals are more reactive than rutile crystals because they have a larger band gap than rutile crystals in the redox energy level diagram. Because of that, the oxidation capability is increasing and electron charge transfer is easier to perform. For that reason, XRD analysis is mandatory to determine the crystal structure of titanium dioxide used.

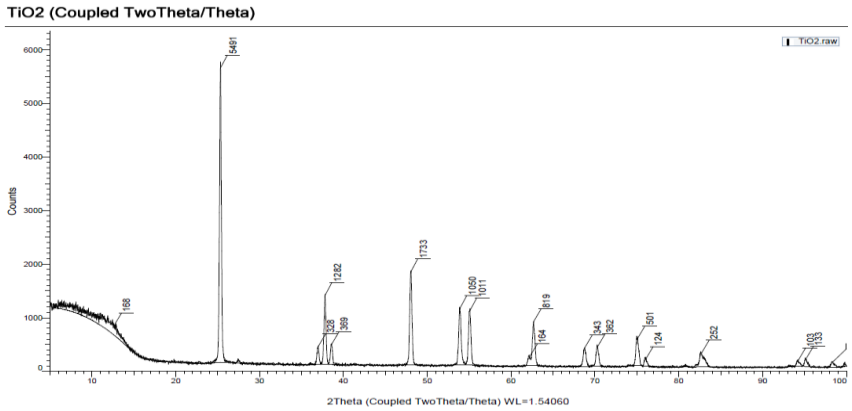

Figure 3.1 XRD test result

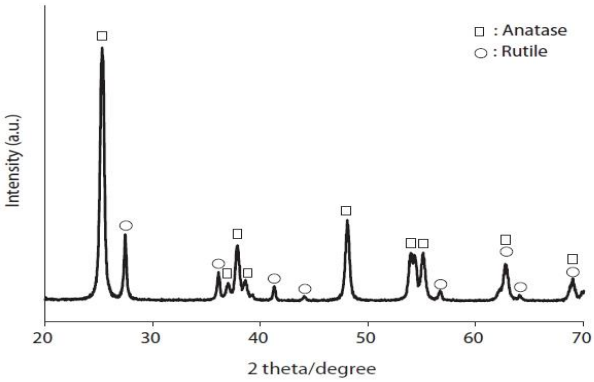

Figure 3.2 XRD reference for titanium dioxide (Cai, 2013)

Figure 3.1 is the XRD test result of titanium dioxide crystal structure, while 3.2 is the XRD reference result for Titanium dioxide crystal structure. According to the figure 3.2, the titanium dioxide used has anatase crystal structure.

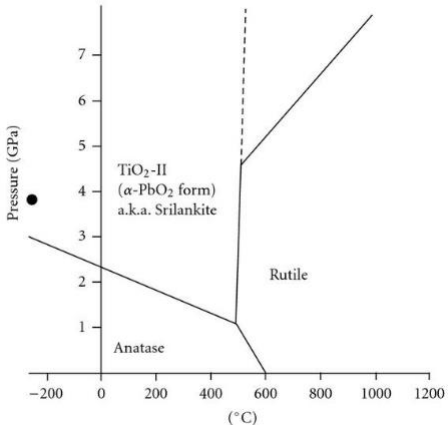

Figure 3.3 phase diagram for titanium dioxide (Nie, 2009)

Working electrode fabrication happen at 500°C and 0.1 GPa. According to figure 3.3, at 500°C and 0.1 GPa titanium dioxide is at anatase phase. This shows that the fabrication process doesn't change the titanium dioxide crystal structure.

3.2 Electrode Fabrication Methods Influence on Cell Performance's

In this research, the fabrication methods that will be discussed are metering rod, doctor blade, and bubble deposition. Other than that, activated carbon that are used as material are industrial-grade and medicinal-grade. The influence of variation on the fabrication method for both activated carbon are presented at figure 3.4 and table 3.1

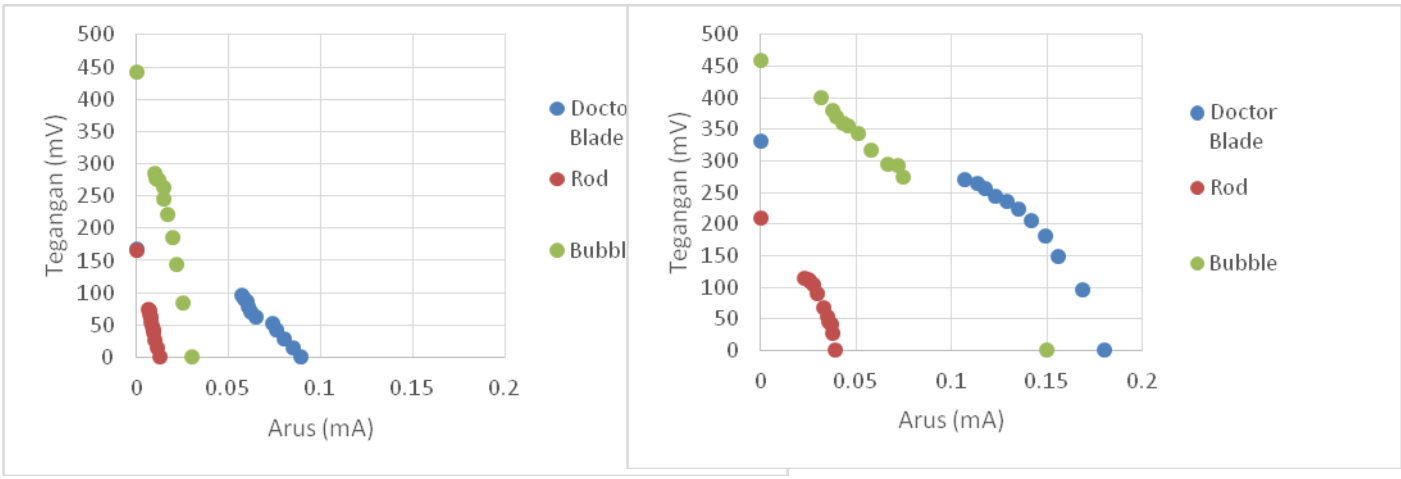

(a) (b)

Figure 3.4 Voltage to current graph for industrial-grade activated carbon (a) and medicine-grade activated carbon (b)

Table 3.1 The Calculation Results for Various Variations

Methods	**Activated Carbon**	**V_{OC} (mV)**	**I_{SC} (mA)**	**V_{max} (mV)**	**I_{max} (mA)**	**FF (%)**	**Efficiency (%)**
Doctor blade	Industrial-grade	168	0,089	97,2	0,059	38,35	0,82
Metering rod	Industrial-grade	210	0,0125	72,3	0,007	19,28	0,14
Bubble deposition	Industrial-grade	443	0,03	263	0,015	29,68	0,72
Doctor blade	Medicinal-grade	332	0,18	236	0,129	50,944	3,247
Metering rod	Medicinal-grade	165	0,039	105,2	0,028	45,775	0,350
Bubble deposition	Medicinal-grade	460	0,15	292	0,072	30,469	3,763

From table 3.1, Bubble deposition yields the highest voltage. This is because bubble deposition counter electrode film is the thinnest among the other methods. As the film of counter electrode getting thicker, the I_3^- concentration in counter electrode surface will be higher thus the potential energy at counter electrode will get closer to working electrode potential energy (Desilvestro,2013). The film thickness for each variations are analyzed with scanning electrode microscope (SEM) and presented at figure 3.5

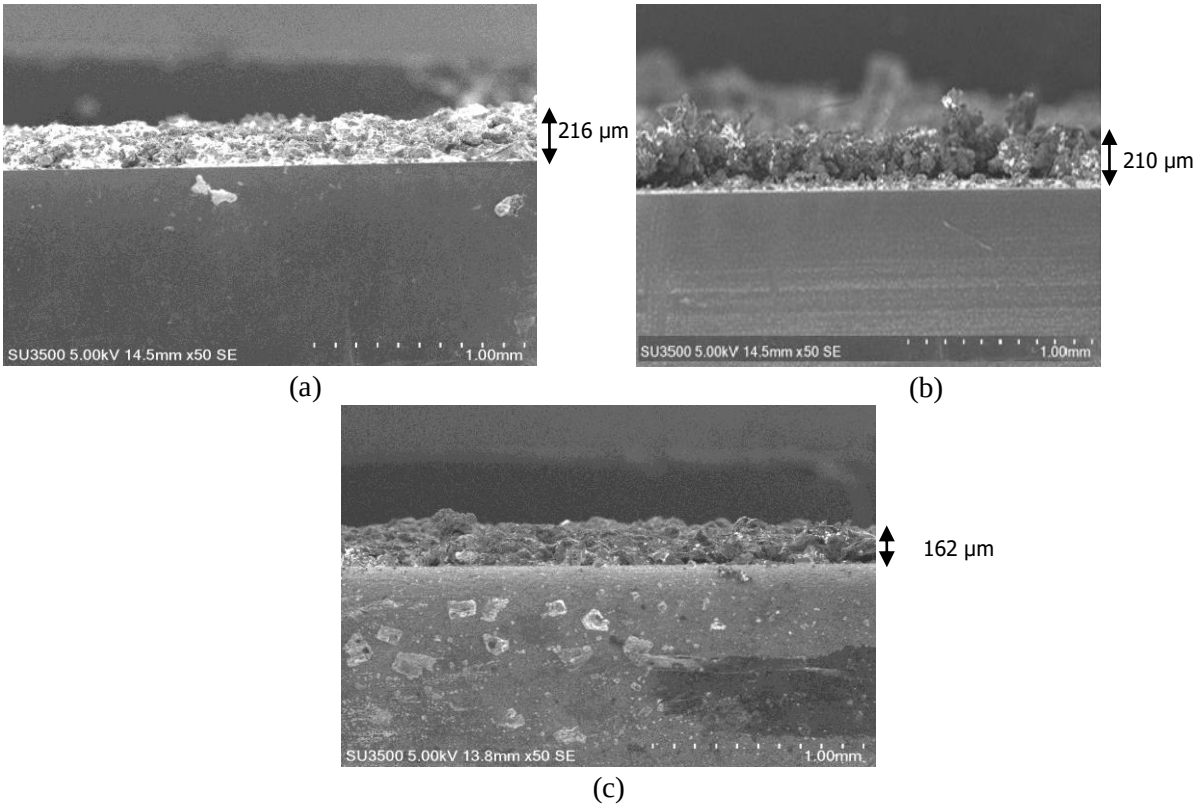

Figure 3.5 SEM result for *doctor blade* (a), *metering rod* (b), and *bubble deposition* (c)

From table 3.1 bubble deposition counter electrode yields less current than doctor blade counter electrode. This is due to excessive amount of electrolyte inside the electrode which result in flooding. Flooding will inhibit the reduction reaction inside the electrode (Desilvestro, 2013). Flooding happened because the amount of electrolyte used for each electrode is equal while the porosity for each electrode is different. The porosity and thickness value of doctor blade counter electrode are higher than bubble deposition so the doctor blade counter electrode can contain more electrolyte than bubble deposition. Bubble deposition counter electrode has 0.32 porosity while doctor blade has 0.71 porosity. The thickness for each counter electrode are presented at figure 3.5

3.3 Activated Carbon Influence on Cell Performance

In this research, the activated carbon used are industrial-grade activated carbon and medicinal-grade activated carbon. Table 3.2 presenting the characteristic for each carbon.

Table 3.2 activated carbon characteristic

Activated Carbon	***Average pore size* (nm)**	***Pore volume* (ml/g)**	***Surface area* m^2/g**
Industrial-grade	9,3	0,031	13,35
Medicinal-grade	13,5	0,018	5,32

Both activated carbons are obtained using a 100 mesh sieve. After that, the carbon are deposited on the conductive glass. Current and voltage are measured using variation of resistance, presented on the I-V curve. The performance for both carbon are shown in figure 3.6.

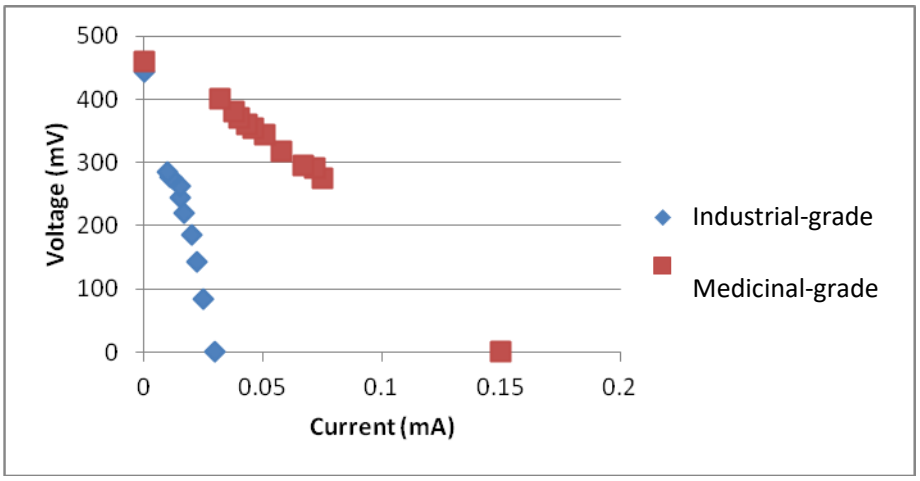

Figure 3.6 Cell performance for both carbon

From Table 3.2, industrial-grade activated carbon has wider surface area medicinal-grade activated carbon but from figure 3.6, medicinal-grade activated carbon has higher current and voltage than industrial grade activated carbon. According to Imoto (2002), reduction reactions happen inside counter electrode pore. Meanwhile, iodine ion has 3 angstrom (Å) and 6 angstrom (Å) diameter which is smaller than average pore diameter for both carbons. Because of that further analysis is required to determine each carbon composition.

Medicinal-grade activated carbon composition is activated carbon, gelatin, titanium dioxide, and iron oxide. According to literature, carbon electrical resistance is 60 x 10^{-5} ohm.m while iron oxide electrical resistance is 5 x 10^{-5} ohm.m (Heck, 1974). Because of that, medicinal-grade activated carbon are estimated to have better electrical conductivity property. Medicinal-grade activated carbons that are more conductive than industrial-grade activated carbon result in better performance as electrode material in DSSC.

3.4 The Influence of Counter Electrode Fabrication Methods on Cell Impedance

Charge transfer phenomenon inside DSSC can be illustrated using EIS analysis. EIS analysis result for each fabrication method are shown in figure 3.7.

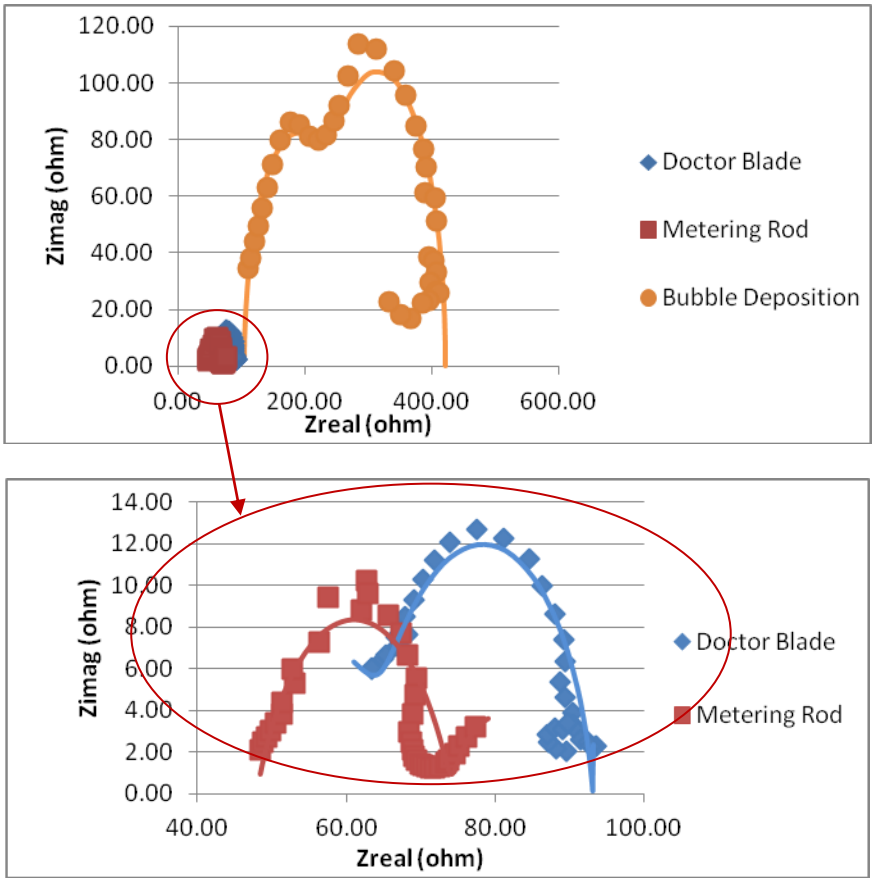

Figure 3. 7 DSSC Nyquist Graph

The DSSC nyquist graphs have 3 domes which represent the phenomena occurring inside the DSSC. The first dome describes the charge transfer that occurs between the counter electrode and the electrolyte. The second dome describes the isotherm diffusion and the reaction between the metal oxide and electrolyte that occurs inside TiO_2. While the third dome shows the diffusion if I_3^- in the electrolyte solution. From figure 3.7, it can be seen that bubble deposition method has greater resistance than doctor blade and metering rod methods. In addition to that, bubble deposition has 3 domes that are relatively large so further analysis is required to describe specifically the influence of counter electrode in DSSC performance.

Further analysis is done by making a symmetrical cell which consist of 2 counter electrode cell. The EIS test results are shown in table 3.3.

Table 3.3 resistance value for each *counter electrode*

Parameter	Resistance (ohm)		
	metering rod	*doctor blade*	*bubble deposition*
R_{CE}	6,709	30,37	130,8
R_{Sheet}	26,74	37,79	24,62

Bubble deposition methods give the highest resistance while metering rod give the lowest resistance. R_{CE} value represents the resistance values that happen between counter electrode surface and electrolyte. Bubble deposition R_{CE} value that is high are supporting the flooding phenomena claim that has been discussed earlier.

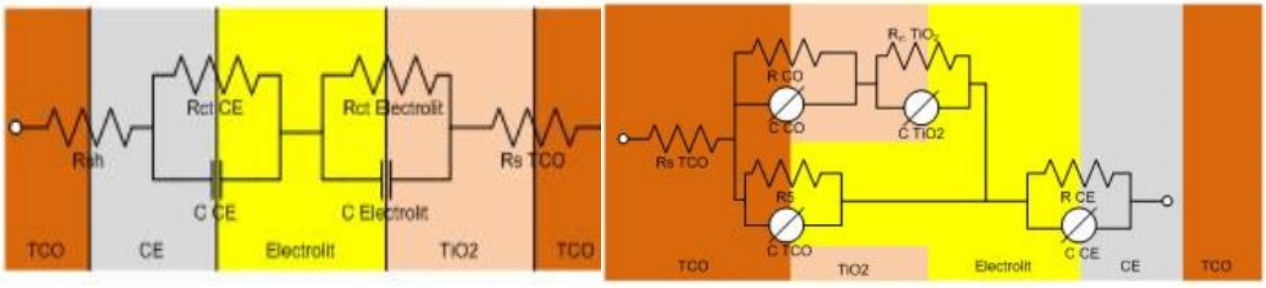

(a) (b)

Figure 3.8 Equivalent Circuit for bubble deposition method (a) (Lee, 2011) and Equivalent circuit for doctor blade and metering rod methods(b) (Sarker, 2014)

3.5 Cell Stability Analysis

DSSC uses liquid electrolyte so that DSSC tend to be more unstable compared to silicon-based solar cells. Therefore, cell stability test are necessary to determine the feasibility of DSSC.

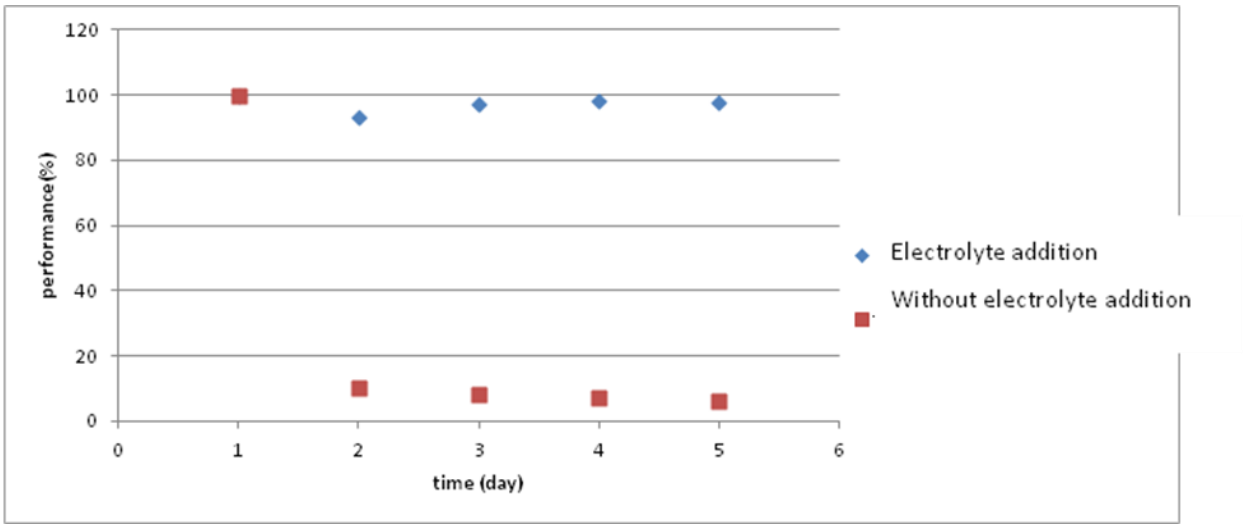

Figure 3. 9 DSSC Stability Graph

From figure 3.9, cell performance can be maintained at its peak with electrolyte addition every day. Meanwhile, Cell performance will drop significantly without electrolyte addition. This happened because the electrolyte is volatile and can be evaporated easily in room temperature. After 5 days, no structural damage was found in DSSC cells. This shows that the cell performance is only influenced by the amount of electrolytes contained in the DSSC cells. According to Lee (2008), DSSC performance can be kept optimum for 60 days without electrolyte addition by using seal made from polymer. The polymer seal will prevent the electrolyte from evaporating so that the cell performance can be maintained at optimum condition.

4. Conclusion

Carbon electrodes that are fabricated using bubble deposition methods has the highest efficiency but also has the highest impedance. Meanwhile, medicinal-grade activated carbon has higher efficiency because medicinal-grade activated carbon contain iron oxide that can improve carbon conductivity. From the cell stability analysis, DSSC stability depend on electrolyte inside the cell.

Acknowledgements

References

1. Barber, Greg. “Utilization of Direct and Diffuse Sunlight in a Dye-Sensitized Solar Cell – Silicon Photovoltaic Hybrid Concentrator System”. Journal of Physical Chemistry Letters. (2011): 581-585.
2. Cai, Y; Stromme, M; Welch, K. “Photocatalytic Antibacterial Effects are Maintained on Resin-based TiO2 Nanocomposites After Cessation of UV Irradiation”. PLOS ONE 8(10). (2013).
3. Desilvestro, Hans. “What Physical Factors Affect Current-Voltage Charateristics of Dye Solar Cells”. Dyesol, 2008.
4. Heck, Carl. “Magnetic Material and their Application”. Butterworths, 1974.
5. Imoto, Kiyoaki; Takahashi, Kohshin; Yamaguchi, Takahiro; Komura, Teruhisa; Nakamura, Junichi; Murata, Kazuhiko. “High Performance Carbon Counter Electrode for Dye-Sensitized Solar Cells”. Solar Energy Materials & Solar Cells. (2003):459-469.
6. Lee, Won Jae; Ramasamy, Easwaramoorthi; Lee, Dong Yoon; Song, Jae Sung. “Performance variation of carbon counter electrode based dye-sensitized solar cell”. Solar Energy Materials & solar Cells 92. (2008): 814-818.

7. Lee, Kyoung-Jun; Kim, Jeong-Hoon; Kim, Ho-Sung; Shin, Dongsul; Yoo, Dong-Wook; Kim, Hee-Je."A study on a solar simulator for dye sensitized solar cells". International journal of Photoenergy Volume 2012 (2012) 11 pages.
8. Nurliyanti, Vetri; Pandin, Marlina; Pranoto, Bono. Pembuatan Peta Potensi Energi Surya. Pusat Penelitian dan Pengembangan Teknologi Ketenagalistrikan, Energi Baru, Terbarukan, dan Konservasi Energi. (2012).
9. Luttrell, Tim; Halpegamage, Sandamali; Tao, Junguang; Kramer, Alan; Sutter, Eli; Batzill, Matthias. "Why is Anatase a Better Photocatalyst than Rutile?- Model Studies on Epitaxial TiO_2 Films". Scientific Reports. (2014).4:4043.
10. Sarker, Subrata; Ahammad, A. J. Saleh; Seo, Hyun Woo; Kim, Dong Min. "Electrochemical Impedance Spectra of Dye-Sensitized Solar Cells: Fundamental and Spreadsheet Calculation". International Journal of Phoyoenergy. (2014): 17 pages

Characterization of Poly-Acrylamide Based Nanopolymer for Water Shut-off In Enhanced Oil Recovery

Stevanus Alvin[1], Ricardo Nainggolan[1], Michael D. M. Sitompul[2], Dendy Adityawarman[1], Taufan Marhaendrajana[2], Johnner P. Sitompul[1]

[1]*Department of Chemical Engineering, Faculty of Industrial Technology*
[2]*Department of Petroleum Engineering, Faculty of Mining and Petroleum Engineering*
Institute of Technology Bandung, Jl. Ganesha 10, Bandung, 40132, Indonesia

[*] *Corresponding Author's E-mail:sitompul@che.itb.ac.id*

Abstract
The objective of the paper is to develop formulation of nano-polymer for EOR application especially for water shut off. The synthesis of nano-polymer was conducted in two stages, production of nano-emulsion and followed by phase polymerization in producing nano-polymer. The nano-emulsion was formulated by varying hydrophilic lipophilic balance (HLB) of oils at optimum temperature. The phase polymerization were conducted by varying composition of acrylamide as a main ingredient and addition of initiator and crosslinking into the nano-emulsion in order to produce nano-polymer in the respective mixture. The physical properties of nano-polymer are analyzed by measuring absorbance level and oil recovery was conducted in sandstone core using heavy oil. Further, permeability was determined by using an empirical equation correlating permeability with porosity and water saturation. Experimental results showed that molecular weight of nano-polymer was 1.05 x 10^6 g/mol, water absorbance level of nano-polymer mixture reached 121.98 times initial weight and salt absorbance level of the mixture reached 69.99 times initial weight. The two parameters showed high capability of nano-polymer for water shut off during EOR. The oil recovery test has resulted 20.53% original oil in place (OOIP) with nano-polymer concentration 1.0%, lower compared with that of APS flooding, around 23.53%. Moreoever, permeability reduction using nano-polymer reached 99.85% of initial permeability.

Keywords: acrylamide, EOR, nanopolymer, absorbance, water shut off, permeability

1. Introduction

Excessive water production is a common problem in reservoir as result of a long period during waterflooding in secondary recovery of oil. It often becomes environmental problem such as pipe corrosion that will cause reservoir closure. To prevent excessive water production, polymer such as PAM utilized as blocking agent to block high permeability area or thief zone. Thief zone shutdown will direct water injection from waterflooding to flow through lower permeability that still contains significant hydrocarbons. Generally, the PAM used as blocking agent is hydrophile polymer with three dimension structure, thus polymer is not water-soluble but swelling and outgrowing the polymer size. The PAM supposed to have high absorbency, in order to shut down entire the thief zone. The type of polymer used to block the high permeability area is so called water shut-off polymer. The polymer for water shut-off can be synthesized in-situ and preformed. In situ type polymer, such as nanoemulsion and crosslinker will be then injected into the reservoir and the initial solution has not formed a

gel yet. Nanoemulsion was initially introduced by Hour and Schulman in 1943 and may defined as a system consisting of oil, water, and amphiphile which is a single optically isotropic and and thermodynamically stable (Danielsson and Lindman, 1981). The stability causes constant droplet size in a continuous phase at all time. Furthermore, nanoemulsion droplet is stable due to strong brown movement related to micro-size particle (McClements dan Rao, 2011). In general, the parameter in determining nanoemulsion zone consists of oil composition, water, and surfactant and can be grouped as α and γ denoting respectively oil mass divided by oil total mass and water and surfactant mass divided by surfactant total mass, water, and oil.

Polymerization experienced after formation of nanoemulsion with addition of initiator and will form nanopolymer. Polymerization method in this research is inverse-nanoemulsion polymerization (IMP). Initiator added in nanoemulsion is water-soluble and thermal-activated. Initiator solubility within the oil is not significant and could be negligible. When initiator added in nanoemulsion and heated, initiator will form radical. Then, the free radical cause the monomer is active and chain the extension that forms oligomers. Then, termination phase occur and forms nanopolymer within the droplets. There are two IMP stages in PAM synthesis, determining nanoemulsion zone and polymerization phase. Firstly, determining nanoemulsion zone intends to determine the condition and optimum composition to obtain nanoemulsion. Temperature, HLB, and oil type may influence nanoemulsion zone, thus these variables are various in this research. Then, crosslinker number, initiator, and composition of acrylamide solution may influence nanopolymer absorbence in polymerization phase. In general, the purpose of this research is to develop formulation of nano-polymer for EOR application especially for water shut off, by measuring the permeability. The nano-polymer will then be applied in core flooding test for OOIP.

2. Experimental

2.1.Nanoemulsion Production

Nanoemulsion was synthesized by formulating certain amount of oil, surfactant and acrylamide solution and the emulsion properties were characterized both qualitatively and quantitatively. Oil that used are xylene and kerosene. The surfactant, were *polyethylene glycol sorbitan trioleate* (Tween 85) and sorbitan monooleate (Span 80), supplied by chemical company. Acryalmide solution was prepared by mixing acrylamide (>99%) with a weight of 50% in the mixture with aqua dm and crosslinker N.N'methylenebisacrylamide (MBA).

2.2.Polymerization

Polymerization was carried out after producing nanoemulsion in order to produce nanopolymer. Before polymerization, nanoemulsion will be purged using Nitrogen gas for about 30 minutes. Ammonium persulfate as an initiator was added to the nanoemulsion to start up the polymerization. The polymerization was carried out for 150 minutes. Polymerization step will be stopped by adding excess acetone fluid. The mixture was then filtered to obtain a solid and then dried in the oven for 24 hours at 600^0C. A number of physical properties of nanemulsion were then measured nanoemulsion particle diameter, nanopolymer molecular weight, and absorbance rate.

2.3.Core Flooding Test

Nanopolymer will be mixed with formation water and injected to the core which contain heavy oil. This core flooding test is conducted to measure OOPI. The schematic diagram and procedure for measuring OOIP can be found elsewhere (Sitompul *et al.* 2017).

3 Results and Discussion

3.1 Determinination of nanoemulsion zone

3.1.1 Influence of oil type towards nanoemulsion zone

Nanoemulsion may be observed qualitatively with visualization of phase behaviour forming one phase and transparent. According to transparent/clear nanoemulsion characteristic, nanoemulsion zone was determined by the mixture of kerosene/xylene oil, acrylamide solution, and surfactant. Nanoemulsion zone was determined qualitatively by connecting experimental data from *alfa* (α) = 0.65, 0.75, 0.85, and 0.95. Initially, the influence of oil type could be identified from ternary plot or diagram below. Result from determining nanoemulsion zone by xylene and kerosene oil is presented in Figure 1 to Figure 5 for temperatures of 25^{o}C, 50^{o}C, 75^{o}C and constant HLB

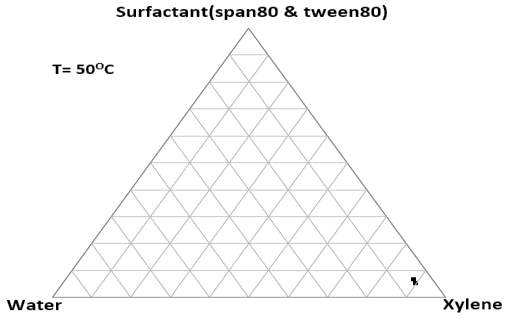

Figure 10 Ternary diagram using xylene at temperature 50^{o}C

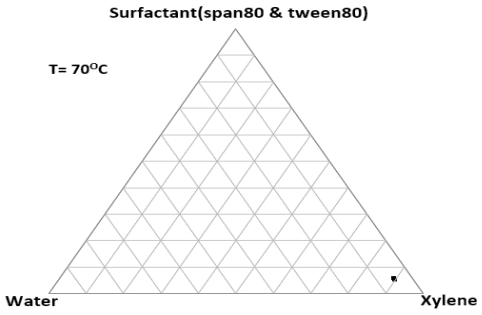

Figure 2 Ternary diagram using xylene at temperature 75^{o}C

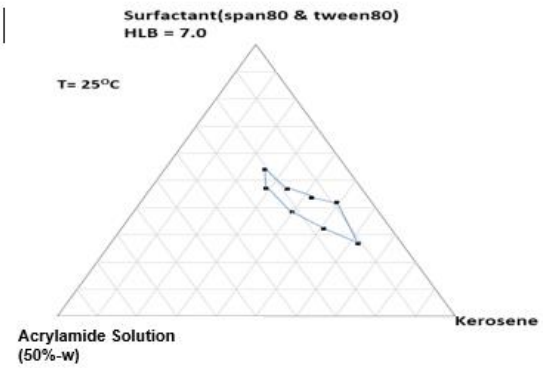

Figure 3 Ternary diagram using kerosene at temperature 25^{o}C

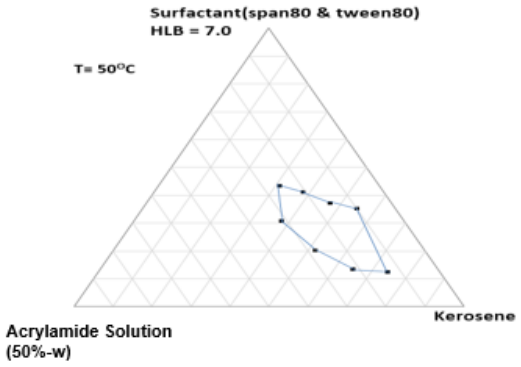

Figure 4 Ternary diagram using kerosene at temperature 50^{o}C

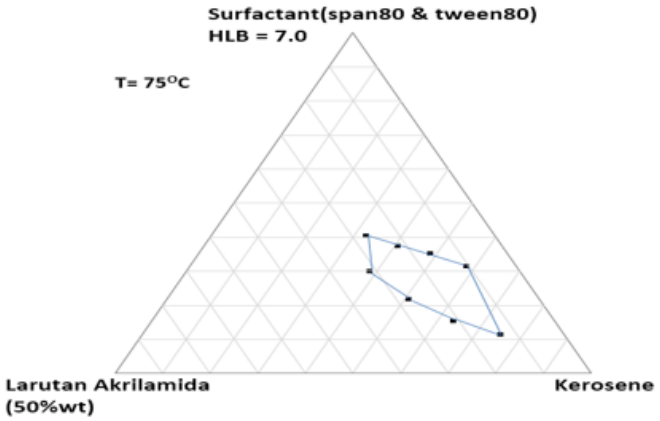

Figure 5 Ternary diagram using xylene at temperature 75°C

The images above described that the kerosene has wider nanoemulsion zone rather than xylene. The result showed that kerosene has advanced characteristic than xylene if applied Tween 80 and Span 80 as surfactant, respectively. Kerosene emulsion is more stable than xylene emulsion, because the presence of Ostwald ripening effect due to low oil phase viscosity (Flanagan & Singh, 2006). Note that Xylene viscosity is 0.812 cP, lower than that of kerosene, 1.640 cP at 20°C. Based on viscosity data, the experimental results supported data from literature that kerosene has enhanced characteristic than xylene to use as oil phase in the process of nanoemulsion production.

3.1.2 Influence of temperature to nanoemulsion zone

Range of temperatures studied in this research was 25°C to 75°C. Experimental results are presented in ternary diagram on Figure 3 to Figure 5. Ternary diagram showed that 50°C temperature on nanoemulsion formation has the widest area, with optimum temperature for nanoemulsion zone at 50°C. The graphic also explained that more surfactant addition could decrease stabilization of nanoemulsion system.

3.1.3 Effect of HLB to nanoemulsion zone

Range of hydrophilic lipophilic balance (HLB) varies from 4.3 to 15 with similar temperature, 50°C, and oil type, kerosene. Experimental results are presented in Table 1.

Table 1 Nanoemulsion synthesis result with HLB variation

HLB = 4.3	HLB = 7.0	HLB = 9.0	HLB = 11.0	HLB = 13.0	HLB = 15.0
tidak	terbentuk	terbentuk	Terbentuk gel	Terbentuk gel	Terbentuk gel

Table 1 showed that nanoemulsion was only formed in HLB 7 and 9. Lower HLB would not form nanoemulsion because the HLB lipophilic type and cannot hold water capacity in water-oil mixture. In addition, for higher HLB, nanoemulsion was not formed in the mixture due to hydrophilic type for excessive HLB.

In order to produce gel structure, then only HLB 7 and 9 formed three-phase diagram, as shown in Figure 7 and Figure 8 for HLB 7 and 9, respectively.

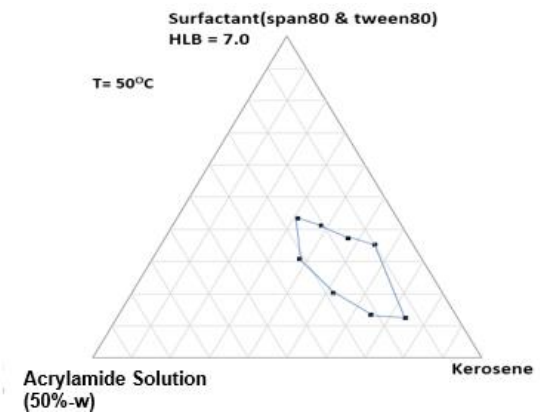

Figure 6 Terner diagram with HLB 7

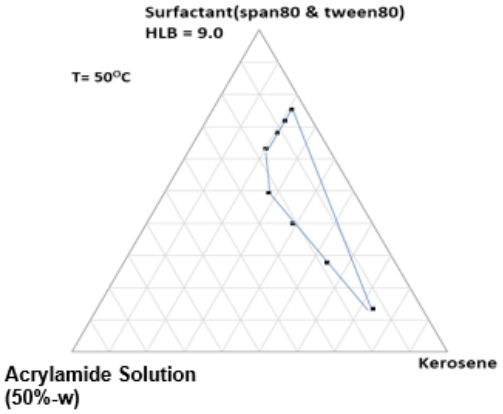

Figure 7 Terner diagram with HLB 9

Further, Figure 6 and Figure 7 show that nanoemulsion with HLB 9 has wider area than that of HLB 7. However, HLB 9 required much surfactant that HLB 7 considering economical cost for operation although the recycle method might be applied.

Table 2 Nanoemulsion composition at HLB 7 and 9

HLB	T(^{O}C)	Acrylamide Solution (%)	Kerosene(%)	Surfactant(%)
7.0	25	23.81	29.10	47.09
7.0	50	31.17	38.09	30.74
7.0	75	31.02	37.92	31.06
9.0	50	22.78	27.84	49.39

Table 2 shows that HLB 7 with the temperature the formation of 50^{0}C is the optimum operating condition to produce nanoemulsion with regards to highest acrylamide composition and low surfactant composition. Hence, HLB 7 and temperature formation of 50^{0}C with a composition which stated in table 2 were then applied to synthesize nanopolymer during polymerization stage.

3.2 Polymerization Stage for Synthesis of Nanopolymer

3.2.1 Influence of Acrylamide Solution Composition

Initial acrylamide monomer solution contained 50% by weight acrylamide. Further addition of acrylamide solution in a nanoemulsion system produced more nanopolymer. However, the excess of acrylamide in the solution could lead to the formation of solids during manufacture, so nanopolymer fail to be made. Based on the experimental results, it could form a solid phase polymerization for alpha (α) above 0.7 or equivalent to acrylamide solution composition above 28.02%.

With regards to nanopolymer formation using inverse-nanoemulsion polymerization method, the polymerization would be unstable and form flocculation or coagulation due to larger particle size (Wan, 2008). Larger particle sizes can occur because larger amount of acrylamide solution. Higher amount of acrylamide solution increases the amount of monomer, so many particles formed and even greater droplets and more solids formed. In this experiment, a solution of acrylamide varied below 28.02% in order to prevent the formation of solids during the polymerization and results is shown in Figure 8.

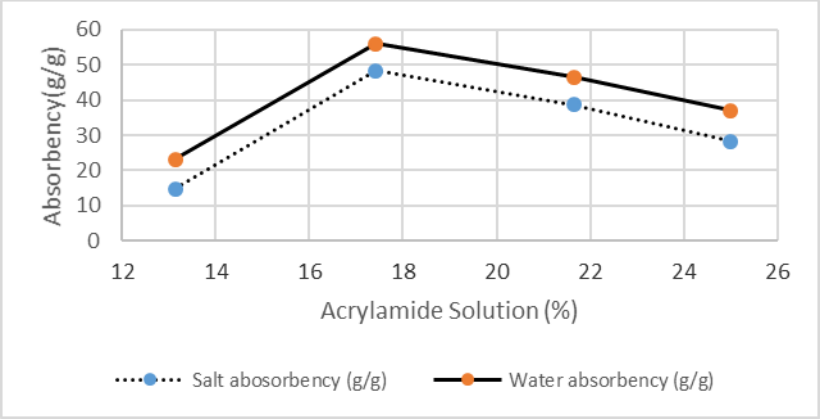

Figure 8 Influence of Acrylamide Solution Composition in nanoemulsion to Salt absorbance and water absorbance

Figure 8 shows increase of absorbance for acrylamide solution with acrylamide composition 13.14% to 17.42% in a nanoemulsion. Absorbance increases because higher composition of acrylamide solution would increase monomer so that the degree of polymerization increases. The higher degree of polymerization would then produce longer polymer chain with respect to polymer network and further more empty space in the nanoemulsion. The empty space was then used as a trap for molecules of water and hence much water absorbed. Thus, the highest absorbance was achieved when the composition of the solution of acrylamide in nanoemulsion 17.42% or alpha (α) 0.8.

3.2.2 Influence of Total Crosslinker

The amount of crosslinker can influence nanopolymer ability towards absorption. Crosslinker are useful to form the network on the polymer structure so that the hydrophilic polymer not too aqueous and higher strength of the polymer due to crosslinking. However, increasing crosslinker can also reduce the distance between the hydrogel bond.

Figure 9 shows the water absorbance and brine absorbance versus the amount of crosslinker. The addition of crosslinker more than 0.03% would lower water absorbance and brine absorbance of nanopolymer. While amount of crosslinker below 3%, the absorbance increase with additional amount of crosslinker. However, the addition of crosslinker more than 0.03%, cause too much crosslinker and hence nanopolymer produced higher density. Moreover, it could enhance the strength of the gel (fixed gel structure) and reducing the nanopolymer ability to expand to its maximum size.

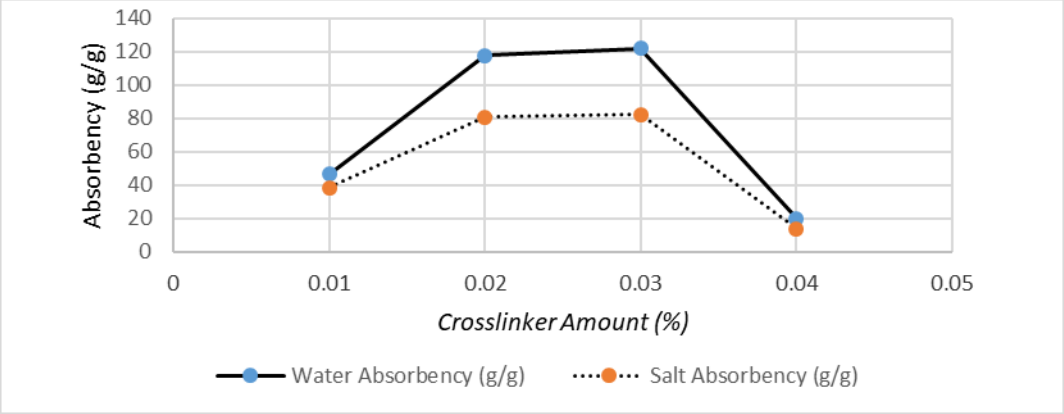

Figure 9 Relation number of crosslinker in nanoemulsion to salt absorbency and water absorbency

3.2.3 The Number of Initiator Influence

The effect of amount of initiator with regards to ability of nanopoyimer absorbance is shown in Figure 10. Figure 10 shows increase in absorbance from initiator concentration 0.05% to 0.1%. The addition of the initiator of more than 0.1 wt% decreases absorbance. If inisiator composition is lowered, then crosslinking reaction become slow and that affects polymer network result. Thus, water absorbance would be lowered too. The addition of the initiator more than 0.1 wt% may cause free radicals and occur more termination stage that produces short-chain polymers. Therefore, the addition of the initiator more than 0.1 wt% may lower the absorbance of the nanopolymer. Thus, the optimum initiator concentration is up to 0.01% wt.

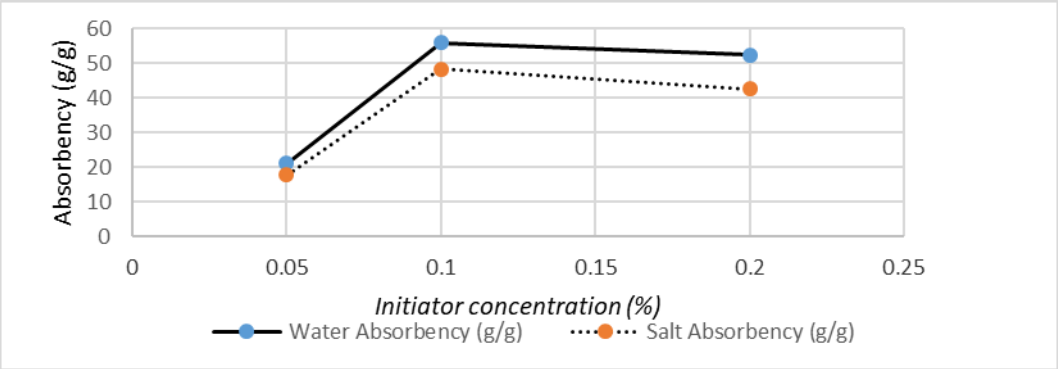

Figure 10 Relations initiator of concentration in nanoemulsion to salt absorbency and water absorbency

3.3 Nanoemulsion Particle Diameter Test

Nanoemulsion can be seen both qualitative (visual) and quantitative (using Particle Size Analyzer). Determination of the nanoemulsion area was done by visual (clear color showed formed nanoemulsion indicating nano-particle size). In order to prove that the clear mixture is a nanoemulsion, then the mixture particle diameter was tested by using Particle Size Analyzer. Results of quantitative analysis (using PSA) of bimodal distribution of particle size in the nanoemulsion are shown in Table 3.

Table 3 Particle diameter distribution

Distribution Result		
Peak	Diameter (nm)	Std. Dev
1	22.1	4.2
2	373.6	104.6
Average	51.9	102.7

Table 3 above shows that the peaks of particle diameter of the mixture is 22.1 and 373.6 nm, respectively, with an average particle diameter of 51.9 nm approving nanoemulsion mixture.

3.4 The Application of Nanopolymer for Water Shut-off in EOR

Nanopolymer samples with highest absorbance were tested in the core flooding test in order to see the performance. The core was made of sand stone with a length of 3.88 cm and a diameter of 2:55 cm. The core has permeability range between 70-110 mD. The results of permeability as well as the oil recovery gained both at the time of injection of formation prior to water injection and after injection nanopolymer presented in Table 4.

Table 4 Nanopolymer injection testing results

Run	Polymer Concentration (%)	Permeability before polymer injection (mD)	Permeability after polymer injection (mD)	Oil Recovery by Water flooding (%)	Incremental Oil Recovery (%)
1	1.0	71.32	0.1034	23.09	20.53
2	1.5	100.96	0.0014	29.01	26.37
3	2.0	86.88	0.0006	29.84	27.12

Table 4 showed that permeability of cores could be reduced to 99.85% after using HPAM. Hence, the polymer can almost close the permeable region as a whole as complete impermeability area (100%) of polymer injection for water shut-off required for application. The permeability reduction is quite high, but the oil recovery obtained was still lower, 20.53 % for 1% nanopolymer, than the literatures shown in the Table. Oil recovery using microgel nanospheres reached OOIP 24.27% (Wang, 2012). This might be due to too low fraction of core with lower permeability after nanopolymer blocking of higher permeability of the core. Reduced permeability by higher polymer concentrations (1.5 wt% and 2 wt%) can reduce permeability up to 99.99%. However, these higher polymer concentrations were not checked further because polymer concentrations of 1.5 wt% and 2 wt% may damage the reservoirs in their actual applications. Compared with the literature data as shown in Table 4, the permeability reduction obtained is greater than 99%. This indicates that permeability reduction meets the criteria, but need to be further developed to achieve actual permeability in the field.

Table 4 also indicates that the higher concentration of polymer, the higher oil recovery obtained. The highest oil recovery 27.12% using the polymer concentration 2.0%. However, upon application, the maximum concentration of the polymer to be injected lower than 1% wt because higher concentration may damage the reservoir. Accordingly, Table 5 shows compilation of permeability data and core condition for water shut-off application in literature. It can be concluded that 1% nanopolymer of this work can achieve 99.85% permeability reduction which is very good result compared with other literature results.

Table 5 Permeability data and core condition for *water shut-off* application from literature

No.	Researchers	Temperature core (°C)	Initial permeability (mD)	Final permeability (mD)	Permeability reduction (%)
1	Prada *et al.* (2000)	60 - 121	1145	10	99,12
2	Wang *et al.* (2010)	55	-	-	-
3	Mack *et al.* (1994)	45	20 – 1000	-	-
4	Shafian *et al.* (2010)	80 - 120	30,5	0,11	99,6
5	Vasquez *et al.* (2005)	135-170	-	-	97
6	Al-Muntasheri *et al.*(2006)	90	47	0	100
7	This research	70	71.32	1.077	99.85%

4. Conclusion

Experimental results showed that molecular weight of nano-polymer was 1.05 x 10^6 g/mol, compared with literature around 1.0 x 10^6 g/mol for water shut off application. Furthermore, water absorbance level of nano-polymer mixture reached 121.98 times initial weight while salt absorbance level of the mixture reached 69.99 times of initial weight. The two parameters showed high capability of nano-polymer for water shut off application during EOR. The oil recovery test has resulted OOIP 20.53% with nano-polymer concentration 1.0%, slightly lower compared with results of APS flooding, around 23.53%. Then, permeability reduction using nano-polymer reached 99.85%. Hence, the experimental data showed that nano-polymer has great potential to improve enhanced oil technology especially for water shut-off application.

Acknowledgement

The author would like to thank Mr Sumantri and Mr. Taufik from PT ZEKINDO, Cikarang, Indonesia, for supplying chemicals for this research. We are grateful for the financial support from Institute of Technology Bandung through Research Group funding.

Symbol

α: the fraction of oil in the oil-solvent mixture of acrylamide [-]
γ: the fraction of the surfactant in the nanoemulsion [-]

References

1. Alias, N.; Jaafar,M.R.; Bakar, W.; Ghazali, N.; Mohd, T. ; Taib, N.; Ramlee, N.; Ismail, S.,” Nanoemulsion Applications in Enhanced Oil Recovery and Wellbore Cleaning: An Overview, Dept. of Oil and Gas Engineering , Faculty of Chemical Engineering, Universiti Teknologi Mara 2012
2. Bai, B.; Zhou, J.; Yin, M., “A comprehensive review of polyacrylamide polymer gels for confomance control”, Petroleum Exploration and Development (2015), 42(4): 525-532.

3. Barari, M.; Abdollahi, M.; Hemmati, M., "Synthesis and characterization of high molecular weight polyacrylamide nanoparticles by inverse-emulsion polymerization", Iranian Polymer Journal 20 (1) (2011), 650-76.
4. Olajire, A.A., "Review of ASP EOR (alkaline surfactant polymer enchanced oil recovery) technology in the petroleum industry: Prospects and challenges", Energy 77 (2014), 963-982.
5. Ouyang, L.; Wang, L.; Schorck, F.J., "Synthesis and nucleation mechanism of inverse emulsion polymerization of acrylamide by RAFT polymerization: A comparative study", Polymer 52 (2011), 63-67.
6. Pei, H.; Zhang, G.; Ge, J.; Zhang, J.; Zhang, Q., "Investigation of synergy between nanoparticle and surfactant in stabilizing oil-in-water emulsions for improved heavy oil recovery", College of Petroleum Engineering, China University of Petroleum (2015)
7. Sarkar, Sume, "Evaluation of alkaline, surfactant, and polymer flooding for enhanced oil recovery in the norne e-segment based on applied resevoir simulation", Tesis Master, Norwegian University of Science and Technology, 2012.
8. Sitompul, J.P., Annisa N. Shabrina, A.N.; Ambardi, R., Sitompul, M.D.M, Siregar, H.S.; Lee, H.W., Experminetal Study of HPAM and Biodegradable Surfactant for ASP Flooding in Enhanced Oil Recovery, Proc. Int'l Conf. Chemical Engineering, Bandung, Indonesia, paper #, October 2017.
9. Timur, A. 1968. An Investigation of Permeability, Porosity and Residual Water Saturation Relationships for Sandstone Reservoirs. The Log Analyst 9(4).
10. Tobing, E.M.L., Peningkatan perolehan Reservoir Minyak dengan injeksi polimer skala laboratorium, Lembaran Publikasi Minyak dan Gas Bumi Vol. 46 No. 3, (2012), 95 – 106.
11. Wang, L.; Zhang, G.C.; Ge J.J.; Li G.H.; Zhang J.Q.; Ding B.D., "Preparation of microgel nanosphere and their application in EOR", SPE International 130357 (2010).
12. Wever, D.A.G ; Picchioni, F. ; Broekhuis A.A; "Polymers for enhanced oil recovery: A paradigm for structure–property relationship in aqueous solution", Progress in Polymer Science 36 (2011), 1558-1628
13. Yousefvand, H.; Jafari, A., "Enchanced oil recovery using polymer/nanosilica", Procedia Materials Science 11 (2015), 565-570.

SYNTHESIS AND CHARACTERIZATION OF ZINC PHOSPHATE MICROCRYSTALLINE

Alvika Meta Sari[1*], Tri Yuni Hendrawati[2], Erdawati[3]

[1,2]*Chemical Engineering Department, Engineeering Faculty, University of Muhammadiyah Jakarta, Jl.Cempaka Putih Tengah 27, Central Jakarta 10510, Indonesia*

[3]*Chemistry Department, State University of Jakarta, Jl. Pemuda 10, East Jakarta 13220, Indonesia*

[*]*Tel.:+62 21 4256023;*

** Corresponding Author's E-mail:alvika.metasari@ftumj.ac.id*

Abstract

This research was proposed to report the synthesis and characterization of nanosized zinc phosphate. Zinc Phosphate nanoparticles were synthesis from zinc acetate and ammonium hydroxide. The nanoparticles were produced in different condition of stirring time (60, 75 and 90 minutes). X-ray powder diffractometry (XRD) and particle size analyzer (PSA) was performed for microcrystalline characterization. The result showed that the zinc phosphate nanoparticles was confirmed as a nanoparticles of the XRD peaks and PSA. The crystalline size was analyzed from the XRD data which were verified by particle size analyzer. The XRD peaks revealed that average crystalline size of the synthesized zinc phosphate microcrystalline was of 250 nm. This was verified by particle size analyzer to be average 288.3 nm. The result of the XRD peaks confirmed the increase in the stirring time showed the decreased of microcrystalline size.

1. Introduction

Zinc phosphate is a non – toxic material widely used in coating for anti-corrosion material due to its low solubility in water / biological environment[1,2]. It used can be applied as paint pigment in numerous binders, which found the widest application among the phosphates. Zinc phosphate can be produced from zinc oxide and phosphoric acid or zinc salt and phosphates[3]. The nanocystallize zinc phosphate also can be obtained using nano zink oxide particles[4]. It`s anti-corrosion properties due to the un-smoothness of the surface of metal basement[5] and depend on the distribution of the particle size[3]. Hence, it is aimed to obtain the appropriate size. The nanoparticles would be the most advantageous size for the best characterization its application. The single particle of nanoparticles does not exceed 100 nm.

Although the common technology of zinc phosphate production was hard to obtain nano scale, there are various techniques have been investigated for synthesis of zinc phosphate nanocrystals[5] such as hydrothermal method[6-8], sol-gel method[9], solid-state method[10] and the utilization of the inorganic compounds as the precursors[3]. However applying these method for synthesis the nanoparticle zinc phosphate was difficult due to the high cost and complicated technology[5].

In this paper, the microwave and ultrasonic were combined to produce the zinc phosphate nanoparticles. The using of microwave and ultrasonic in the synthesis process an decrease the particle diameter hence it did not modify the surface.

2. Experimental

2.1 Apparatus and reagent

All of the reagents zinc acetat, ammonium phosphate, ammonium solution were analytical grade and used as received without further purification.

2.2 Synthesis of zinc phosphate

37.5 mL of zinc acetate 0,1 M aqueous solution was put into a conical flask, and 25 mL of diammonium phosphate 0,1 M solution was added dropwise with a dropping funnel with continuous stirring. The nanoparticles were produced in different condition of stirring time (30, 45, 60, 75 and 90 minutes). Then 4 mol L^{-1} of ammonia solution was used to adjust the pH of the mixed solution (pH=8), and then a certain amount of deionized water was added to the mixed solution to a total volume of 80 mL. After stopping stirring, the conical flask with the mixed solution was put into a conventional microwave oven (Panasonic with the output power of 800W) for microwave radiation for 2 min, and then it was cooled down. Then the conical flask was placed in the ultrasonic (ultrasonic frequency 20 kHz) for ultrasonic vibration for 20 min. Then, the flask was put into a water bath with constant preset temperature to age for 2 h. The white products were collected by centrifugation, washed with deionized water and ethanol twice, respectively, and dried at 70 ℃.

2.3 Characterization

The structure of the obtained nanoparticle zinc phosphate were characterized with X-ray powder diffraction (XRD) in BATAN, and Fourier transform infrared spectroscopy (FTIR). The microstructures and morphologies. The size distribution of zinc phosphate were characterized with Particle Size Analyzer (PSA).

3. Results and Discussions

3.1. Structure of zinc phosphate

Fig. 1 shows the high-resolution SEM images of three-dimensional flower-like zinc phosphate prepared after water bath reaction at 90 ℃ for 2 h with microwave-assisted sonochemical method. As shown in the figure, each petal is multi-layered sheet structure composed by two-dimensional nanosheets, and numer-ous layered structures form the three-dimensional flower-like zinc phosphate by self-assembly.

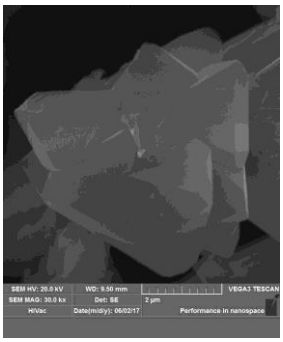

Fig.1. SEM images of zinc phosphat microcrystalline

Fig. 2(a) shows that, the diffraction peaks with 2θ values at 9.85°, 17.58°, 18.48°, 19.60°, 20.25°, 25.86°, 26.47°, 31.50° were from the (020), (210), (011), (040), (111), (240), (221) and (241) planes of orthorhombic zinc phosphate tetrahydrate (JCPDF 33- 1474), indicating that the prepared samples are composed of single component $Zn_3(PO4)_2$.$4H_2O$. It can be considered that the as-obtained samples have a good crystallinity and no other impurities were observed in the products. The peaks of sample

obtained at 90 °C are obviously more sharp than those of the other three patterns, because the crystallinity of the sample is much better with the reaction temperature increasing.

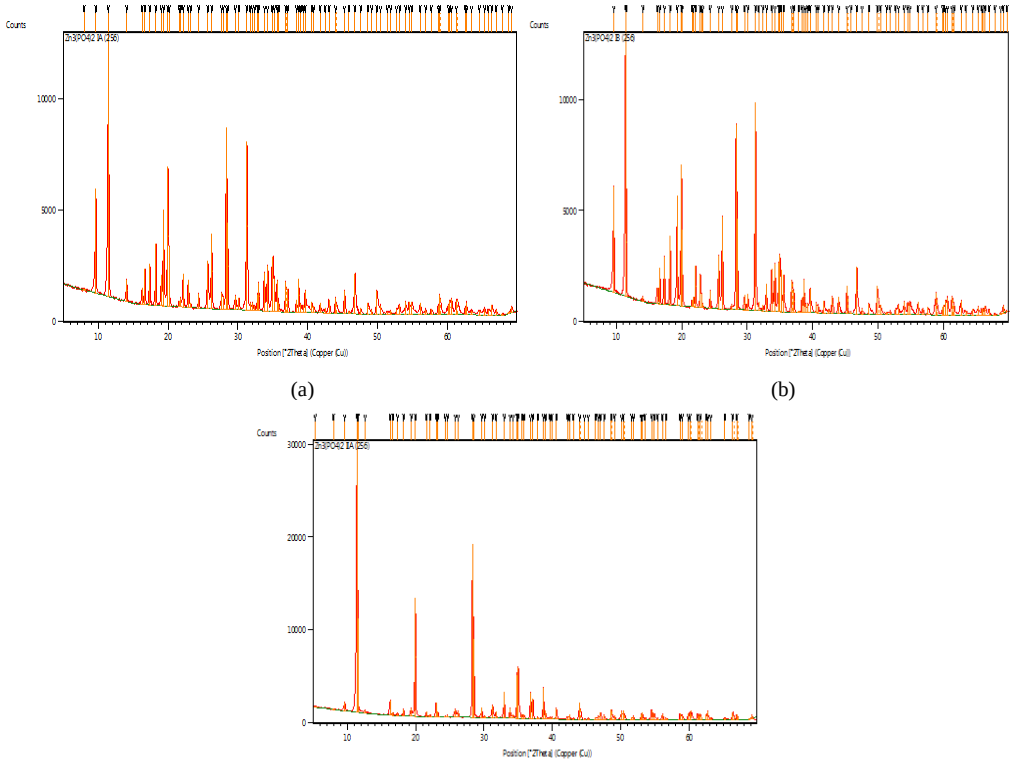

(a) (b)

(c)

Fig.2. XRD analysis of zinc phosphate microcrystalline of stirring time variable (a) 60 minutes, (b) 75 minutes, (c) 90 minutes

3.2. 3.3. The effect of stirring time on the Particle Size Distribution of zinc phosphate microcrystalline

The effect of stirring time on the Particle Size Distribution of zinc phosphate microcrystalline can be seen on Fig 3.

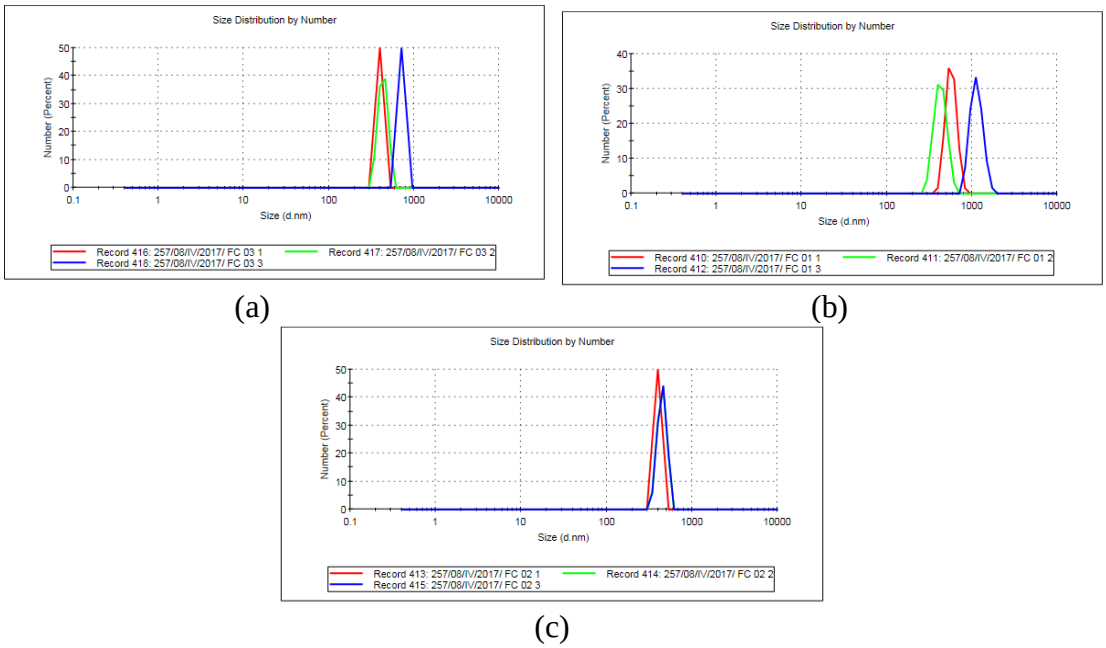

Fig. 3. The Particle Size Analyzer of zinc phosphate microcrystalline variable stirring time (a) 60 minutes, (b) 75 minutes, (c) 90 minutes

3.3. The effect of stirring time on the Rendement of zinc phosphate microcrystalline

The effect of stirring time on the Rendement of zinc phosphate microcrystalline was shown on table 1 below.

No	Stirring time (minutes)	Rendement (%)
1	60	1.18
2	75	1.16
3	90	1.24

4. Conclusions

The result showed that the zinc phosphate nanoparticles was confirmed as a nanoparticles of the XRD peaks and PSA. The crystalline size was analyzed from the XRD data which were verified by particle size analyzer. The XRD peaks revealed that average crystalline size of the synthesized zinc phosphate microcrystalline was of 250 nm. This was verified by particle size analyzer to be average 288.3 nm. The result of the XRD peaks confirmed the increase in the stirring time showed the decreased of microcrystalline size.

Acknowledgments

Thanks to University of Muhammadiyah Jakarta and Communnity Service, Directorate General for Research and Development, Ministry of Research and Technology Higher Education in accordance with the Letter of Agreement for the Implementation of Research Grant No.0404/K3/KM/2017, 24 May 2017 for the research funding.

References

1. B. D. A. R. Romagnoli, V. F. Vetere and L. S. Hernandez. Study of the Anticorrosive Properties of Zinc Phosphate in Vinyl Paints. *Progress in Organic Coatings,* Vol. 33, No. 1, 1998, pp. 28-35. doi:10.1016/S0300-9440(97)00124-0

2. B. Czarnecka and J. W. Nicholson. Ion release, Dissolution and Buffering by Zinc Phosphate Dental Coments, *Journal of Materials Science: Materials in Medicine,* Vol. 14, No. 7, 2003, pp. 601-604. doi:10.1023/A:1024018923186

3.Grzmil.B. Kic.B and Lubkowski.K.,Studies on Obtaining of Zinc Phosphate Nanomaterials. *Rev.Adv.Mater.Sci*.;14:46 - 48 (2007).

4. Wang.J.D. Li.D. Liu.J.K. Yang.X.H. He.J.L. and Lu.Y.One-Step Preparation and Characterization of Zinc Phosphate Nanocrystals with Modified Surface. *Soft Nanoscience Letters*;1:81-85(2011)

5. Tamilselvi.M. Kamaraj.P. Arthanareeswari.M. and Devikala.S. Nano zinc phosphate coating for enhanced corrosion resistance of mild steel. *Applied Surface Science*; 327: 218 - 225(February 2015).

6. B. Yan and X. Z. Xiao, "Hydrothermal Synthesis, Controlled Microstructure, and Photoluminescence of hydrated Zn3 (PO4)2: Eu3+ Nanorods and Nanoparticles," Journal of Nanoparticle Research, Vol. 11, No. 8, 2009, pp. 2125-2135. doi:10.1007/s11051-008-9578-6.

7. B. Boonchom, R. Baitahe, S. Kongtaweelert and N. Vittayakorn, "Kinetics and Thermodynamics of Zinc Phosphate Hydrate Synthesized by a Simple Route in Aqueous and Acetone Media," Industrial & Engineering Chemistry Research, Vol. 49, No. 8, 2010, pp. 3571-3576. doi:10.1021/ie901626z.

8. O. Pawlig and R. Trettin, "Synthesis and Characterization of -hopeite Zn3(PO4)2·4H2O," Materials Research Bulletin, Vol. 34, No. 12, 1999, pp. 1959-1966. doi:10.1016/S0025-5408(99)00206-8.

9. B. I. Lee, W. D. Samuels, L. Q. Wang and G. J. Exarhos, "Sol-gel Synthesis of Phosphate Ceramic Composites," Journal of Materials Research, Vol. 13, No. 6, 1996, pp. 134-143. doi:10.1016/S0025-5408(99)00206-8.

10. Q. A. Yuan, S. Liao, Z. F. Tong, J. Wu and Z. Y. Huang, "Synthesis of Nanoparticle Zinc Phosphate Dihydrate by Solid State Reaction at Room Temperature and Its Thermochemical Study," Materials Letters, Vol. 60, No. 17- 18, 2006, pp. 2110-2114..

Biohydrogen and Biomethane Production from Palm Oil Mill Effluent

Rien Rakhmana[1,*], Tjandra Setiadi[2]

[1]*Department of Bioprocess Engineering, Institut Teknologi Del, Laguboti, 22381, Indonesia*
[b]*Department of Chemical Engineering, Institut Teknologi Bandung, Bandung, 40132, Indonesia*

[*] *Corresponding Author's E-mail:rienrakhmana@gmail.com*

Abstract

The treatment of wastewater by the dark fermentation (DF) and anaerobic digestion is the promising approach to treat wastewater as well as produce bioenergy. Both of methods produce biohydrogen and biomethane. This research was held to study the parameters affected fermentation processes in such a way that the bioenergy can be achieved at the maximum yield. The DF was done with various conditions of temperature (34, 55 and 76°C), pH (5; 5.5; and 6) and substrate concentration (10-50 g/L). In DF, sample was treated in the anaerobic digestion to study the potential of biomethane production. Before the DF, sample was heated at 100°C for 45 minutes. This step was proven inhibit the activities of methanogenic bacteria. The highest yield of biohydrogen was achieved at thermophilic fermentation (55°C), pH 5.0 and substrate concentration 10 g/L with the yield of 0.128 mol/g COD. The DF process does not only produce biohydrogen, but also volatile fatty acids (VFAs) as the by-product. The VFAs composition is dominated by acetic acid (79%), then butyric acid (6-10%), and the trace of propionic acid. This VFAs potentially becomes precursor for bioplastic production. The remaining organic residues can be converted to biomethane for reducing COD's value. In this research, the method used was the Biochemical Methane Potential (BMP). The BMP process was conducted with incubation of remaining residues 35°C for 30 days. The highest efficiency of COD removal was achieved at 34°C (54.50%), followed by 55°C (48.79%) and 76°C (21.06%).

1. Introduction

At present, the main objective of wastewater treatment has shifted from the reduction of the COD (Chemical Oxygen Demand) value of wastewater to profitable energy production for agro industry[1]. During this time, energy demand is still dominated by fossil energy sources whose reserves are decreasing[2], while energy demand continues to increase along with growth of development. One of the alternative energy sources studied is biohydrogen. Biohydrogen is an environmentally friendly energy source because it is predicted to produce no waste at all. Its combustion products are water vapor and energy[3].

Agro-industrial wastewater is one of the proper substrates for the fermentation process for biohydrogen-producing bacteria[4]. This wastewater contains organic compounds which can be broken down by anaerobic bacteria to produce hydrogen and volatile fatty acids (VFAs). Palm oil mill effluent (POME) is one of the substrate that has great potential for anaerobic biohydrogen production.

However, from various studies that have been done, there are still constraints on the final product of the fermentation process. The obtained fermentation product is usually a hydrogen, alcohol, and VFAs which are organic pollutants. So far, research on the production of biohydrogen that has been done shows that the content of COD from the DF of wastewater is still high. Therefore, it is proposed of integration[5] techniques of DF and anaerobic degradation in the wastewater treatment process.

With anaerobic degradation techniques, VFA compounds that are products of the DF are converted to biomethane. The advantages of integration of DF and anaerobic degradation techniques are produce more bioenergy (biohydrogen and biomethane) and the COD level of the degradation effluent has been reduced so that the pollution load will decrease when it is discharged into free waters.

Therefore, the purpose of this research is to produce bioenergy (biohydrogen and biomethane) from POME. Bioenergy production is carried out by studying the operating conditions during the fermentation process in order to obtain maximum bioenergy and the remaining wastewater that can discharged into the waters.

2. Experimental

Broadly speaking, there are three stages of this research. The first stage is the initial analysis of wastewater conditions to study. The second is the development stage of inoculum. And the last stage is the production stage of biohydrogen and biomethane from POME. In the initial analysis phase, characterized of POME such as COD, TKN (Total of Kjeldahl Nitrogen), TSS (Total of Suspended Solid), and pH of wastewater used. At the acclimatization stage, it uses cow dung as a source of bacteria. The last stage is the production of biohydrogen and biomethane. At the DF stage is performed in batch with volume 100 mL. By a ratio of 1:9 between the inoculum and the substrate of POME. Prior to the fermentation process, the inoculum was preheated at a temperature of 100°C for 45 minutes. The DF process is done by varying the temperature, pH and substrate concentration.

After the DF, the residue is further processed using anaerobic digestion. The anaerobic digestion used is the BMP (Biochemical Methane Potential) test to see the potential for biomethane production. The test was performed using 40 mL of sample (residue of DF), 30 mL of medium solution, and 30 mL inoculum in the dark colored glass bottle. The test is done by inserting the sample bottle into an incubator at temperature 35°C for 30 days. The resulting gas is measured every 5 days using a syringe method.

2.1 Equipment and Materials

Equipment used is for analysis COD, TKN, TSS, and pH meter. In process of bioenergy production, it uses dark colored glass bottles. Operating conditions are set by pH setting using pH meter and waterbath. The product of DF and anaerobic digestion was measured using GC (Shimadzu GC-8A) with TCD detector and Porapak Q column. While the resulting VFA content was measured using HPLC (Waters 2695) with refractive detector (Waters 2414) column HPX-87H.

The material used is cow dung as a source of bacteria, the substrate used is POME from PT. Mutiara Agam (West Sumatera), and reagents necessary for characterization of POME.

2.2 Experiments Variations

Experimental variations in the DF process comprises fermentation temperatures (34, 55, and 76°C), pH (5; 5.5; and 6) and the substrate concentrations (10,30 and 50 g/L).

3. Results and discussion

3.1 The charateristics of POME

In Table 1, the characteristics of wastewater (POME) to be processed as follows:

Table 1 Characteristics of POME

Parameter	Unit (mg/L, except for pH and color)
COD	47,600-49,000
TSS	5,200
TKN	4,937
pH	5.2 – 5.4
Color	Brown

3.2 The production of biohydrogen by dark fermentation

3.2.1 The effects of early inoculum treatment on biohydrogen production

Inoculum preliminary treatment aims to inhibit the performance of hydrogen-feeding methanogenic bacteria. In Figure 1, it appears that fermentation operation at 34°C resulted in a larger biohydrogen in the inoculum which is not preliminary treated (2.8%) compared to the inoculum given the initial treatment (1.5%). The least of these biohydrogen yield is thought to be due to the presence of hydrogen produced during fermentation utilized by hydrogen-consuming bacteria to form methane. It shows from the presence of detected methane (3%). However, this phenomenon corresponds to the initial assumption, that is, if there is acitivity of bacteria consuming hydrogen, and then the yield of biohidrogen will decrease.

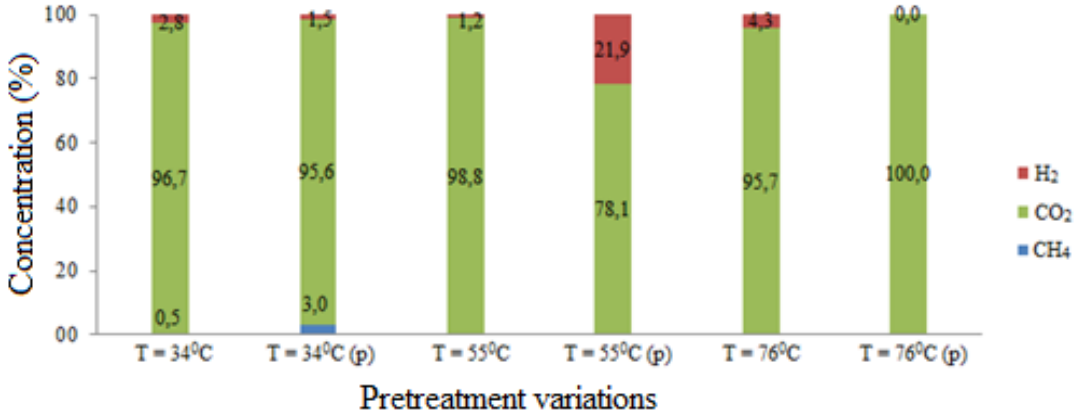

Figure 1 Inoculum initial treatment effect on dark fermentation process

This assumption is supported also from the yield of biohydrogen at 55 and 76°C temperature fermentation. In both conditions, biomethane is not formed. In the 55°C temperature fermentation, it appears that the inoculum given the initial treatment yielded a larger biohydrogen (21.9%) than the unflavored sample (1.2%). In accordance with that, it is proposed by Andreas[6] that the initial treatment on the inoculum makes the yield of biohydrogen becomes larger.

3.2.2 The influence of temperature and pH inoculum on the production of biohydrogen

Figure 2 shows that the temperature and pH of fermentation influence the yield of biohydrogen.

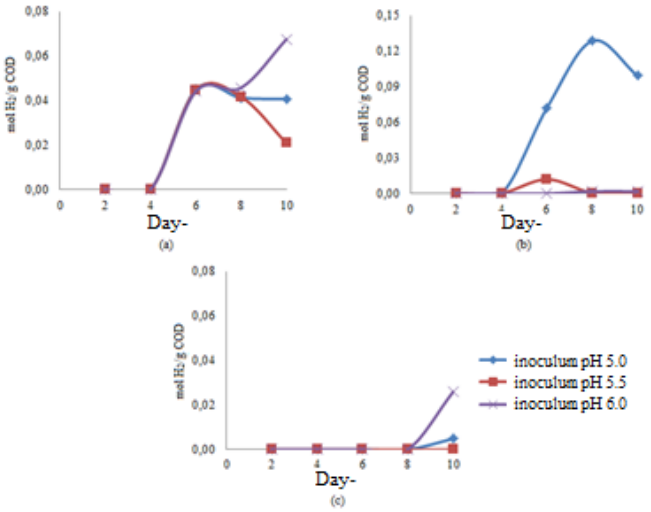

Figure 2 Production of biohydrogen at (a) 34°C, (b) 55°C, and (c) 76°C fermentation temperatures in pH range 5-6

Maximum biohydrogen is gained at 55°C fermentation temperature, which is 0.128 mol/g COD followed by fermentation temperature 34°C with hydrogen gain 0.068 mol/g COD. The lowest yield at a fermentation temperature of 76°C with a biohydrogen gain of 0.026 g/mol COD. The effects of temperature can be explained thermodynamically in terms of Gibss energy and reaction enthalpy[7]. The equation of the biohydrogen production reaction as follow:

$$C_6H_{12}O_6 + 2H_2O \rightarrow 2\ CH_3COOH + 4H_2 + 2CO_2$$
$$\Delta G = 176.1\ kJ/mol$$
$$\Delta H = +\ 90.69\ kJ/mol$$

When viewed from the above reaction equation, the reaction is endothermic. From the van't Hoff equation, if the temperature is raised with a fixed substrate concentration, then the equilibrium will shift toward the product. Therefore, increasing the fermentation temperature will produce more hydrogen. The yield of biohydrogen under thermophilic conditions (55°C) is greater than mesophilic (34°C)[8]. In line with the research conducted, the maximum biohydrogen production is obtained under thermophilic operating conditions.

In hyper-thermophilic fermentation conditions (76°C), it is gained the smallest biohydrogen. This is suspected because the high operating temperatures can cause the occurrence of higher protein denaturation that affect the performance of bacteria. Therefroe, Lee et al.[9] suggested that high temperatures potentially inhibit cell growth due to denaturation of enzymes needed in bacterial metabolism.

In addition to temperature, it also studied the effect of fermentation pH on the production of biohydrogen. One of the goals of pH regulations is to ensure the absence of active methanogenic bacteria. Setiadi[10] revealed that methanogenic bacteria work actively in the pH range from 6.5 to 7.7. However, if the pH of fermentation is too low then the production if biohydrogen will also decrease. The low pH of fermentation occurs because during the fermentation will from VFAs. This low pH condition can inhibit the bacteria producing bacteria producing hydrogen, so bacteria cannot work maximally. Vijayaraghavan[11] stated that in the variation of fermentation with pH 4, 5, 6 and 7, the largest COD removal gained in fermentation with pH 5, followed by pH 6, 7 and 4. Andreas[12] also stated that the largest biohydrogen recovery in fermentation with pH 5. In this research, fermentation is done by batch. The weakness of this technique is the absence of pH control during fermentation. Rasdi et al.[13] said that the fermentation process performed by controlling the pH is able to produce biohydrogen 2 times more and the production rate is 2 times greater than the fermentation that is not done pH control.

3.2.3 The Effects of substrate concentration on biohydrogen production

In figure 3, it is obtain the production of biohydrogen with substrate variations of 10, 30 and 50 g/L.

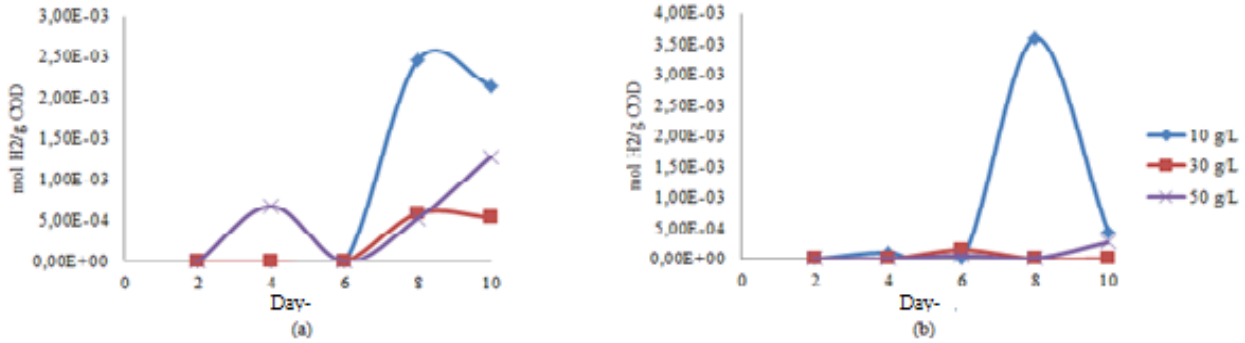

Figure 3 The production of biohydrogen at concentration variations at the fermentation temperature of (a) 34°C and (b) 55°C

From Figure 3, it can be seen that the highest production of biohydrogen is at substrate concentration of 10 g/L whether going for operating temperatures of 34 or 55°C with consecutive biohydrogen recovery of 3.6 mmol/g COD and 2.5 mmol/g COD. From the Figure 3, it appears that too high substrate concentration has the potential to decrease the production of biohydrogen gas. Substrate concentrations are too high to cause the organic load to be consumed by hydrogen producers is too high and exceed the ability of the bacteria. In addition to the overly high organic load, the performance of the producing bacteria is also affected by the amount of VFAs contained in the medium solution during the fermentation process. The yield of VFA during the fermentation process with substrate concentration variations as follows:

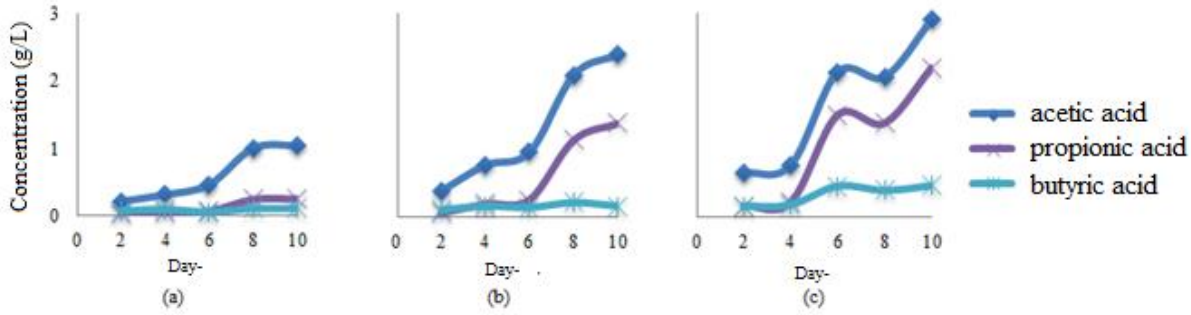

Figure 4 The production of VFA at a temperature of 34°C with the substrate concentration variation of (a) 10 g/L, 30 g/L, and (c) 50 g/L

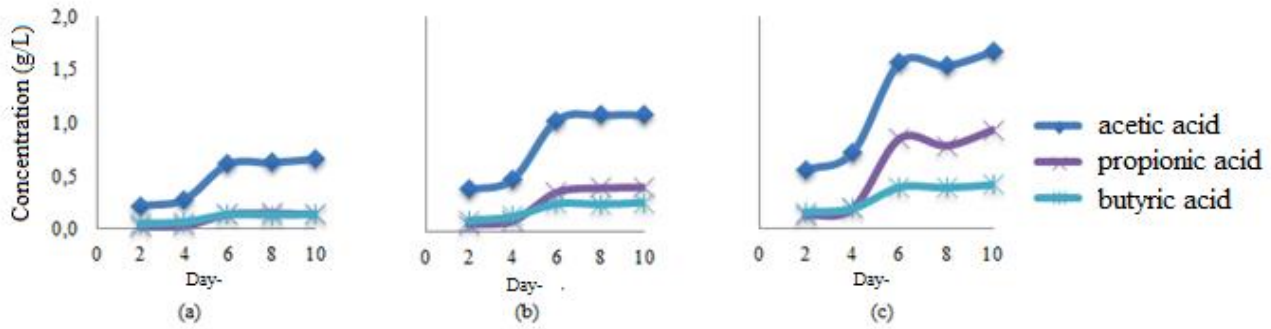

Figure 5 The production of VFA at a temperature of 55°C with the substrate concentration variation of (a) 10 g/L, 30 g/L, and (c) 50 g/L

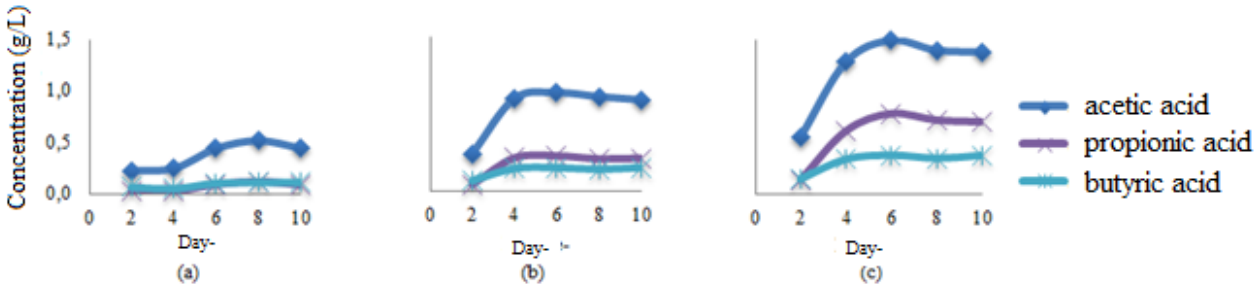

Figure 6 The production of VFA at a temperature of 76°C with the substrate concentration variation of (a) 10 g/L, 30 g/L, and (c) 50 g/L

Figure 4, 5 and 6 show that there is an increase in the production rate of VFAs as the substrate concentration used. The highest VFA production was obtained at a substrate concentration of 50 g/L with a fermentation temperature of 34°C. Oh et al.[14] and Wang et al.[15] stated that there was a relationship between the production of biohydrogen and the concentration of VFA in the medium solution. The increase in concentration of acetic and butyric acid are in line with the production of biohydrogen. However, the concentration of acetic acid and butyric acid are too high to be an inhibitor for the bacteria producing biohydrogen. In contrast to acetic acid and butyric acid, the high content of propionic acid signifies that the resulting biohydrogen content is reduced. This is because bacteria producing propionic acid can inhibit the performance of biohydrogen producing bacteria. Therefore, if in a solution containing high propionic acid, the biohydrogen recovery will decrease.

3.2.3 The potential of biomethane formation (BMP)

In this study, residues resulting from the DF were further treated in anaerobic degradation. Anaerobic degradation techniques performed using Owen et al.[16]. In anaerobic degradation, the VFAs of the DF process will be converted to biomethane and also studied the effectiveness of reduced effluent COD. Figure 7 shows the amount of COD samples decomposed during the anaerobic degradation process.

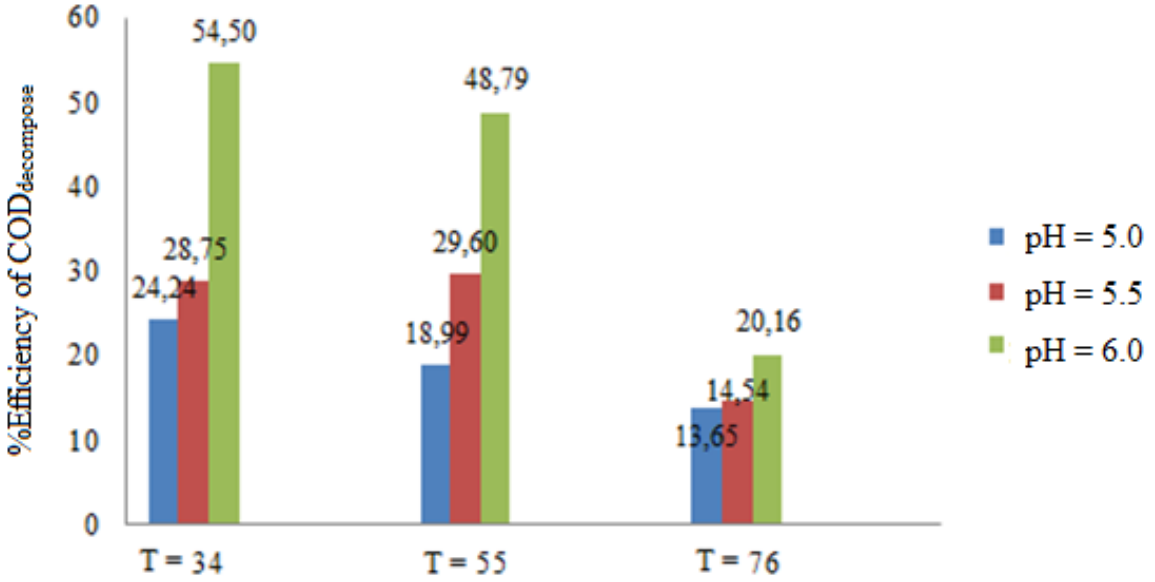

Figure 7 Efficiency of COD decomposes

In the figure above, it appears that the greatest COD degradation in the sample comes from the fermentation process at the temperature of 34°C, and then followed by a sample derived from DF at a temperature of 55°C and last at 76°C. In the BMP test, a sample derived from DF at temperature 34°C giving the greatest COD degradation. This is assumed because at the time of BMP test, sample degradation is done in incubator with temperature 35°C. The difference in the magnitude of this degradation is due to the absence of spikes or changes in temperature drastically.

4. Conclusions

The conclusions can be drawn from the results of research are:

1. Initial treatment of the inoculum with heated at a temperature of 100°C for 45 minutes gives a higher biohydrogen recovery than inoculum which is not given pretreatment.
2. Thermophilic fermentation conditions provide the highest biohydrogen with biohydrogen produced in thermophilic, mesophilic and hyper-thermophilic fermentation processes respectively of 0.128 mol/g COD, 0.068 g/mol COD and 0.026 g/mol COD.
3. The effect of pH during the fermentation process is in the range 5-6. Under thermophilic conditions, the maximum biohydrogen gained is achieved at pH 5.
4. Too high substrate concentrations interfere the performance of hydrogen-producing bacteria. The optimum substrate concentration for the production of biohydrogen is at 10 g/L.
5. The higher substrate concentration, the more increase production of propionic acid. The high proportion of propionic acid has the potential to be an inhibitor for hydrogen-producing bacteria, resulting in decreased biohydrogen production.
6. In the BMP test, the organic compound residue of the dark fermentation process is converted to biomethane and carbon dioxide.
7. In the BMP test, the samples derived from DF process with temperature 34°C make up the most biomethane, seen from COD value decomposed by 54.50%, then followed by sample temperature 55°C (COD decomposed by 48.79%) and last sample temperature 76°C (20.16%).

References

1. Premier. G.C., Kim, J.R., et al. Integration of Biohydrogen, Biomethane and Bioelectrochemical Systems, *Renewable energy*, 49: 188-192 (2013).
2. Show, K.Y., Lee, D.J., Tay, J.H., Lin, C.Y., dan Chang, J.S. (2012) : Biohydrogen Production: Current Persperctives and The Way Forward, *International Journal of Hydrogen Energy*, 37, 15616-15631 (2012).
3. Kapdan, I.K. dan Kargi, F. (2006) : Bio-hydrogen Production From Waste Materials, *Enzyme and Microbial Technology*, 38, 569–582.
4. Ntaikou, I., Antonopoulou, G. dan Lyberatos, G. (2010) : Biohydrogen Production From Biomass and Wastes via Dark Fermentation: A Review, *Waste & Biomass Valorization*, 1, 21-39.
5. Premier. G.C., Kim, J.R., Massanet-Nicolau, Kyazze, G., Esteves, S.R.R., Penumasha, B.K.V., Rodriguez, J., Maddy, J., Dinsdale, R.M., dan Guwy, A.J. (2013) : Integration of Biohydrogen, Biomethane and Bioelectrochemical Systems, *Renewable energy*, 49, 188-192.
6. Andreas, B. (2011) : Produksi biohidrogen dari air limbah *starch-rich* melalui fermentasi secara termofilik, Tesis, *Institut Teknologi Bandung*.
7. Vazquez, G.D., Arriaga, S., Mondragon, F.A., Rodriguez, A.d.L., Colunga, L.M.R., dan Flores, E. R. (2008) : Fermentative biohydrogen production : trends and perspectives, *Reviews in Environmental Science and Bio/Technology*, 7, 27-45.

8. Yossan, S., O-thong, S., dan Prasertsan, P. (2012) : Effect of initial pH, nutrients and temperature on hydrogen production from palm oil mill effluent using thermotolerant consortia and corresponding microbial communities, *International Journal of Hydrogen Energy*, 37, 13806-13814.
9. Lee, K.S., Lin, P.J., dan Chang, J.S. (2006) : Temperature effects on biohydrogen production from organic fraction of municipal solid waste, *International Journal of Hydrogen Energy*, 31, 465-472.
10. Setiadi, T. dan Dewi, R.G. (2003) : *Diktat Kuliah : Pengelolaan Limbah Industri*, Departemen Teknik Kimia ITB, Bandung.
11. Vijayaraghavan, K. dan Ahmad, D. (2006) : Biohydrogen generation from palm oil mill effluent using anaerobic contact filter, *International Journal of Hydrogen Energy*, 31, 1284-1291.
12. Andreas, B. (2011) : Produksi biohidrogen dari air limbah *starch-rich* melalui fermentasi secara termofilik, Tesis, *Institut Teknologi Bandung*.
13. Rasdi, Z., Mumtaz, T., Rahman, N.A. dan Hassan, M.A. (2012) : Kinetic Analysis of Biohydrogen Production from Anaerobically Treated POME in Bioreactor Under Optimized Condition, *International Journal of Hydrogen Energy*, 37, 17724-17730.
14. Oh, Y.K., Kim, S.H., Kim, M.S., dan Park, S. (2004) : Thermophilic biohydrogen production from glucose with trickling biofilter, *Biotechnology and Bioengineering*, 88, 690-698.
15. Wang, L., Zhou, Q., dan Li, F.T. (2006) : Avoiding propionic acid accumulation in the anaerobic process for biohydrogen production, *Biomass and Bioenergy*, 30, 177-182.
16. Owen, W. F., Stuckey, D. C., Healy, J. B., Young, L.Y., Jr., dan McCarty, P. L. (1979) : Bioassay for Monitoring Biochemical Methane Potential and Anaerobic Toxicity, *Journal of Water Resources*, 13, 485-492.

THE MAKING OF BIOETHANOL FROM DURIAN SEEDS THROUGH ENZYMATIC HYDROLYSIS AND FERMENTATION USING *Sacharomyces cerevisiae*

Fifi Rahmi Zulkifli, Elida Mardiah M.S, Marniati Salim M.S

Laboratory of Biotechnology, Department of Chemistry
Andalas University

The depletion of alternative fossil fuel and the significant increased of human population greatly affect the needs of energy for human life and economic and social activities. In the last five years, Indonesian national oil production has been decreased due to the reduction of oil reserves production in nature, whereas along with the increased of population number, the demand for transportation and industrial activities also rose. This results in an increased of the fuel consumption and demand.

One of the Vegetable based fuels is bioethanol. Bioethanol can be made from abundant biological resources that available in Indonesia. Bioethanol is made from sugary or starchy ingredients such as cassava, sugar cane, sapon, sorghum, sweet potatoes, and others. One of the countries that use bioethanol is Brazil. Bioethanol is a product that resulted from sugar fermentation process from carbohydrate sources (starch) with the help from *Sacharomyces serevisiae*. Bioethanol production from plants that containing starch or carbohydrates is done through conversion from carbohydrates into sugar (glucose) by several methods such as acid or enzyme hydrolysis. The enzymatic hydrolysis method is oftenly used because it is more environmentally friendly than the acid catalyst. The Glucose that obtained will be proccessed and fermented by adding yeast to obtain bioethanol as an energy source.

Durian plants (Durio zibethinus Murr) is one of the plantation crops that have long been known by the society. Durian seeds in durian fruit have not been fully utilized, whereas durian seeds have contents that can be utilized, such as starch 46% in a ripe durian seeds, protein, fat and others. Since durian seeds contain potential starch that can be processed into bioethanol by fermentation.

Before the fermentation process is done, hydrolysis process should be done first with the help of enzymes. The materials that containing starch can be hydrolyzed into simple sugars that is ready for fermentation. Hydrolysis by using α-amylase enzyme will break the polysaccharide bonds present in starch to be disaccharide and then proceed with hydrolysis using glucoamylase enzyme into monosaccharides (glucose). Research on Making Bioethanol from Durian Seed Through Enzymatic Hydrolysis and Fermentation Using Sacharomyces Cerevisiae has been done. This study aims to observe the effect of volume variation of enzyme α-amylase, glucoamylase and the variation of hydrolysis time and the effect of fermentation time on the produced ethanol concentration. 15 g durian seeds were washed first, cut into small pieces and dried under the sun, and grind the seeds until become powder by using a mill. Then the powder was dried again under the sun to avoid the growth of mushrooms in durian seed powder.

The dried durian seed powder was steved with 425μm. To obtain smaller and finer particles the powder durian seeds weighed 15 g each, Then put into a 250 mL erlenmeyer and added with 100 mL distilled water. Next, into each erlenmeyer, α-amylase enzyme was added with variation of volume starting from 4; 5; 6; 7; and 8 mL, then stirred using a shaker for 2 hours at 55^{o}C and pH 5. The temperature setting here was done because the α-amylase enzyme works optimally at 80 ° C. The hydrolyzed sample is then centrifuged to obtain the filtrate. The obtained filtrate was measured of its

absorbance by a spectrophotometer. The highest absorban value was continued for hydrolysis process by using glucoamylase enzyme. The same thing was done for variations in the addition of glucoamylase enzyme and the variation of hydrolysis time which was then continued in the fermentation process. From the hydrolysis process that has been done using α-amylase enzyme and glucoamylase with volume variation of 4, 5, 6, 7, and 8 mL and variation of hydrolysis time of 1, 2, 3, 4, 5 hours. The glucose produced was analyzed by using the Somogy-Nelson method. Hydrolysis with 6 mL addition of α-amylase enzyme and 7 mL glucoamylase for 3 hours gave optimum glucose concentration of 58.51 g / L.

The hydrolyzate produced from the hydrolysis process was continued in the fermentation process using Saccharomyces cerevisiae isolated from fermipan. The ethanol content of the fermentation product was analyzed by GC with operational conditions: Helium carrier gas, pressure 52.3 kPa, Rtx5MS column used with 30 m in column length and 0.25 μm inner diameter, 60^0C oven temperature, injection temperature 150 ° C, injection volume 0.5 μL, 0.94 mL / min total flow and FID detector. The maximum ethanol production was achieved after 4 days of fermentation with ethanol concentration obtained at 3.54%.

Keywords: bioethanol, durian seeds, hydrolysis, fermentation, gas chromatography

Intrinsic factors affecting co-gasification performance of low rank coal and biomass

Jenny Rizkiana[a*], Ryzka Pranata[a], Hasna Nisrina[a], Dwiwahju Sasongko[a], and Guoqing Guan[b]

[a] *Department of Chemical Engineering*
Institut Teknologi Bandung, Bandung 40132 Indonesia
[b]*North Japan Reasearch Institute for Sustainable Energy*
Hirosaki University, Japan

[*] *Corresponding Author's E-mail:jr@che.itb.ac.id*

Abstract
Co-gasification of coal and biomass is an alternative way to produce hydrogen. Co-gasification can be considered as clean coal technology as it utilizes coal with a lower carbon footprint due to the existence of biomass. Besides, mixing coal and biomass may increase the hydrogen production because of the presence of synergistic effect. Several factors may affect the performance of co-gasification process and the present study focused on the effect of intrinsic factor of the feedstocks. Based on the study, it is found that as intrinsic factors such as ash content and porosity significantly affect the co-gasification performance. Mineral contents in the biomass ash provide catalytic effect since some minerals such as alkali and alkaline earth metal (AAEM) is known to have a good catalytic effect towards carbon decomposition. Furthermore, more porous feedstock allows the gasifying agent i.e. steam to further penetrate the feedstock as such more carbon can contact and thus gasification rate increase.

Keywords: biomass, catalyst, co-gasification, deashing, low rank coal

1. Introduction

Hydrogen is one of the most used material in chemical industry, such as in the ammonia synthesis, fertilizer production, nickel and iron production, and many other processes [1]. Hydrogen is also used to produce electricity through fuel cell and gas turbine system. Hydrogen can be produced from water electrolysis, steam reforming of natural gas or petroleum, and gasification of biomass or coal. Water electrolysis could produce hydrogen rapidly and simply, but it needs a lot of electricity. Currently, the applied and commercial processes of hydrogen production are using steam reforming of natural gas or petroleum and gasification process. These processes have been implemented in Indonesia. Indonesia has potency to develop these processes due to abundant fossil energy resources. The amount of fossil energy sources reserves is shown in **Table 1** as follows.

Table 1. Fossil energy resources [2]

Fossil energy sources	Unit	Resources	Reserves	
Petroleum	Billion barrels		Proven	3.6
			+Potential	7.4
Natural gas	TSCF		Proven	100.3
			+Potential	149.3
Coal	Billion tons	124.8	32.27	

Assuming no new reserves are found, based on the reserve/production ratio calculation, the petroleum will be run out within 12 years, natural gas in 37 years, and coal in 70 years [2]. From these data, coal is potentially used as a raw material to produce hydrogen through gasification process.

2. Gasification

Gasification is defined as thermal conversion of carbonaceous materials into synthesis gas in limited air condition with gasifying agent. Synthesis gas that produced includes hydrogen, carbon monoxide, carbon dioxide, and methane [3]. As shown in **Fig.** 1, the steps of gasification process including drying, pyrolysis, combustion, and gasification reactions [4]. Generally, gasification involves the reaction of carbon by oxygen, air, steam, carbon dioxide, or mixture or such gases at temperature of 700°C or more to produce electricity and heat or feedstock for the chemical industry, liquid fuel, or gas fuel such as hydrogen [5].

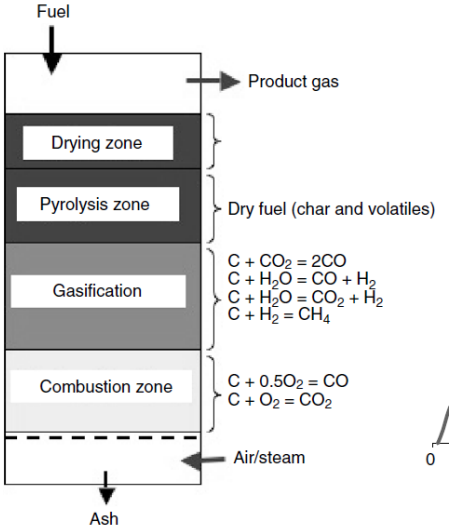

Fig. 1. Stages of gasification in an updraft gasifier [6]

The reactions that occur in the gasification process are as follows [6]:

$$C + CO_2 \leftrightarrow 2CO \quad (1)$$

$$C + H_2O \leftrightarrow CO + H_2 \quad (2)$$

$$CO + H_2O \rightarrow CO_2 + H_2 \quad (3)$$

One of the differences between gasification process and other thermal conversion is the presence of gasifying agent. These gasifying agents react with carbon and heavy hydrocarbon to produce light gases such as carbon monoxide and hydrogen [6]. As shown in **Fig. 2**, the composition of gas product depends on the gasifying agent. Gasifying agent that can be used in gasification process are as follows

- Oxygen
  According to [6], oxygen is popular gasifying agent, though it is primarily used for the combustion step. As shown in **Fig. 2**, using oxygen as gasifying agent could increase carbon-based compound in gas product such as CO and CO_2.
- Air
  Gasifying agent in form air has disadvantage by reducing the heating value of gas product in the gasification process. As shown in **Table 2**, using air as gasifying agent

could reduce the heating value of gas product due to the high amount of nitrogen (heating value of nitrogen = 0) [7].

- Steam
  If steam is used as gasifying agent, the product gas will produce gas product with higher H/C ratio than other gasifying agents as shown in **Fig. 2**. The addition of steam rate could increase the hydrogen as the final product, increase the conversion of solid carbon into gas molecules, and reduce the tar forming from gasification products [7].
- Carbon dioxide
  The use of carbon dioxide as gasifying agent could increase the reduction reaction between CO_2 and solid carbon [8]. The reduction reaction produces CO as following reaction.

$$C + CO_2 \rightarrow 2CO \quad (4)$$

Table 2. Heating value of gas product based on the gasifying agent

Gasifying agent	Heating value (MJ/Nm^3)
Air	4-7
Steam	10-18
Oxygen	12-28

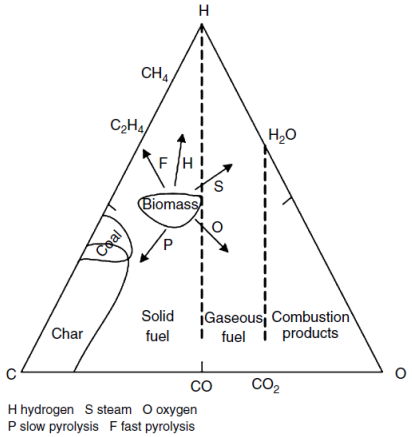

Fig. 2. Diagram of C-H-O of the gasification process [6]

There are 3 types of product that produced from gasification process, i.e. gas, solid, and liquid in form of tar. The gas products consist of hydrogen, carbon monoxide, carbon dioxide, and methane. The product gas yield became the main focus in this paper. However, the solid products, i.e. char can also be used as supercapacitor materials. Char – which mainly consist of carbons – from low rank coal gasification has porous structures thus it is favourable as electrode materials in capacitor. Through carbonization at certain temperature, coals become porous chars [9]. Meanwhile, carbon materials which have large surface area (about 1 to 2 thousand(s) m^2 g^{-1}) and well distributed pores are suited for the supercapacitor fabrication material [10].

Reactors that commonly used for gasification process (gasifier) are as follows.

- **Fluidized Bed Gasifier**
  In fluidized bed type gasifier, the fuel is entered from the side or top of gasifier as shown in **Fig. 3**. Generally, fuel particles undergo drying and pyrolysis rapidly to

produce gas and char. Fluidized bed gasifier operates in low temperature so prone to cause agglomeration. Agglomeration in fluidized type gasifier could be prevented by set temperature of gasifier at 800-1000^{o}C [4].

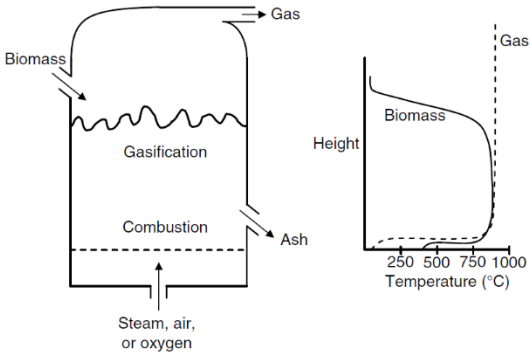

Fig. 3. Shematic of fluidized bed gasifier [11]

- **Fixed-bed Reacto**r

There are two common types of fixed-bed reactor, i.e. updraft gasifier and downdraft gasifier. Both types of reactors are described as follows.

Updraft Gasifier

In updraft gasifier, fuel is injected from the upper part of gasifier, while the gasifying agent is injected from the bottom and travel upward, thus the gas and solids are in counter-current mode [6]. The produced gas leaves from the top as shown in **Fig. 4.** This type of reactor is suitable for high-ash (up to 25%), high moisture (up to 60%) biomass. The tar produced from gasification with this type of reactor is very high, which makes it unsuitable for high-volatility fuels. Meanwhile, as a counter-current unit, an updraft gasifier utilizes combustion heat very effectively [6].

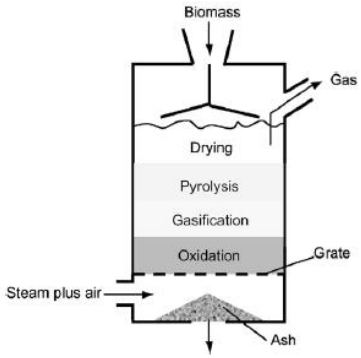

Fig. 4. Shematic of updraft gasifier [6]

Downdraft Gasifier

In downdraft gasifier, the gasifying agent enters the gasifier at a certain height below the top, while fuel (biomass or coal) enters from the top via hopper or distributor. The product gas flows downward and leaves through a bed of hot ash, as shown in **Fig. 5.** Since it passes through the high-temperature zone of hot ash, the tar in the produced gas finds favourable conditions for cracking. Thus, a downdraft gasifier has a lowest tar production rate.[6]

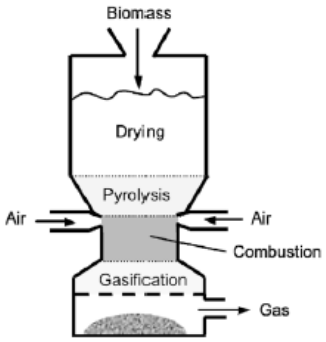

Fig. 5. Shematic of downdraft gasifier [6]

3. Co-gasification of coal with biomass

Co-gasification is defined as gasification of a mixture of waste/biomass and coal which offers several opportunities, especially to utility companies and customers, to protect the environment by reducing GHG emissions from existing process equipment [4]. Co-gasification could increase the product gas yield, especially hydrogen [12]. Several compounds in biomass ash could be catalyst to gasification process, i.e. alkali and alkaline earth metal (AAEM) in the form of carbonate. Alkali and alkaline earth compounds are highly volatile. In pyrolysis step, alkali and alkaline earth compounds leave from biomass then attach the coal surfaces to produce catalytic effect. Potassium carbonate has most significant effect in the gasification process with steam as the gasifying agent [13]. The existence of potassium makes the rate of WGSR (water gas shift reaction) increases to produce potassium salt [14]. The increase of reaction rate will increase the product gas yield.

The mechanism of catalyst addition in gasification process is as follows [15].

$$M_2CO_3 + 2C \rightarrow 2M + 3CO \quad (5)$$

$$2M + 2H_2O \rightarrow 2MOH + H_2 \quad (6)$$

$$2MOH + CO \rightarrow M_2CO_3 + H_2 \quad (7)$$

with M = alkali and alkaline earth.

Meanwhile, there is one coal ash content that should be avoided from co-gasification, i.e. silica in form of SiO_2. It causes deactivation of alkali and alkaline earth compounds as co-gasification catalysts by reduce their volatilities. If coal ash content is high, the co-gasification efficiency decreases and inhibits carbon conversion [16]. Coal ashes have higher silica content and lower alkali and alkaline earth metals content than biomass.

4. Effect of ash to the cogasification performance

Rizkiana et.al. [17] has conducted an experiment of addition of biomass ash in coal gasification. The results show that the biomass ash could increase the product gas yield in certain compositions and conditions. The most common elements of biomass ash are Cl, S, K, Na, and Sr. In addition, there are elements with relatively few compositions, i.e. Ni, Mn, Cd, Cr, Zn, Co, Si, Mo, Li, Mg, Pb, Ca, Cu, Ba, P, Se, Al, Sb and Fe [18]. All the biomass ash shows the catalytic activity in coal gasification process. This activity is due to the alkali and alkaline earth metal content which is still contained in biomass ash.

In contrast to biomass ash, coal with high ash content decreases the efficiency of gasification processes by inhibiting carbon conversion [16]. Coal ash has a higher silica content and lower alkali metal content when compared to high quality biomass for gasification. It has been mentioned that silica can be an inhibitor by decreasing the catalytic activity of AAEM. Meanwhile, low alkali metal content in coal also cannot raise carbon conversion in gasification.

Coal ash content, which is mostly silica, can be removed by a technique called deashing. In general, coal is mixed with HF or HCl solution. The mixture is inserted into a stirrer-equipped glass beaker. The solids are separated by a Buchner funnel or PP, dried in the oven to remove water content in the solid [19].

5. Conclusions and Future Outlook

From time to time, oil and gas production in Indonesia is decreasing. To meet the energy needs, the government's policy made Indonesia as one of fuel oil and LPG importer. In addition, the utilization of new and renewable energy has not been efficient yet. It is the price that cannot be compared to fossil energy. The new and renewable energy price is not competitive, and the energy subsidies are not on target [20].

As one of the primary energy, the use of coal is planned to be increased until 2050. From [20], coal utilization in 2050 is planned at 256 MTOE, or three times higher than this year. As the increase of coal needs, coal export should be stopped in 2046. By that time, the technologies to utilize coal must have been advance and sustainable. This makes the development of coal processing technologies is important.

To produce energy, coal is processed mostly via thermal conversion. However, it causes several environmental problems. The clean coal technology is the answer, due to its abundant reserves of low rank coals such as brown coal, lignite and subbituminous in Indonesia. It is important to utilize the low rank coals effectively and in an environmentally friendly way, such as co-gasification. The pre-treatment of this low rank coal also an important job to do co-gasification more efficiently. Thus, co-gasification of deashed low rank coal with biomass could decrease environmental problems and also meet the needs of hydrogen.

Acknowledments

This Research is supported by ITB through P3MI research scheme.

References

[1] A. Midilli, M. Ay, I. Dincer, and M. A. Rosen, "On hydrogen and hydrogen energy strategies I : current status and needs," vol. 9, pp. 255–271, 2005.
[2] BPPT, *Indonesia Energy Outlook 2016*. Pusat Teknologi Sumber Daya Energi dan Industri Kimia (PTSEIK), 2016.
[3] U. Arena, "Process and technological aspects of municipal solid waste gasification. A review," *Waste Manag.*, vol. 32, no. 4, pp. 625–639, 2012.
[4] S. Farzad, M. A. Mandegari, and J. F. Görgens, "A critical review on biomass gasification, co-gasification, and their environmental assessments," *Biofuel Res. J.*, vol. 3, no. 4, pp. 483–495, 2016.
[5] A. H. Demirbas and I. Demirbas, "Importance of rural bioenergy for developing countries," *Energy Convers. Manag.*, vol. 48, no. 8, pp. 2386–2398, 2007.
[6] P. Basu, *Biomass Gasification and Pyrolysis: Practical Design and Theory*, vol. 53, no. 9. 2013.
[7] F. Pinto *et al.*, "Effect of experimental conditions on co-gasification of coal, biomass and plastics wastes with air/steam mixtures in a fluidized bed system," *Fuel*, vol. 82, no. 15–17, pp. 1967–1976, 2003.
[8] T. H. Duan, C. P. Lu, S. Xiong, Z. Bin Fu, and Y. Z. Chen, "Pyrolysis and gasification modelling of underground coal gasification and the optimisation of CO2 as a gasification agent," *Fuel*, vol. 183, pp. 557–567, 2016.
[9] F. L. Shea, "CARBON ELECTRODES FROM BITUMINOUS COAL," US Patent 2594226, 1952.
[10] A. G. Pandolfo and A. F. Hollenkamp, "Carbon properties and their role in

supercapacitors &," vol. 157, no. 1, pp. 11–27, 2006.
[11] C. Higman and M. van der Burgt, *Gasification*, 2nd ed. Elsevier, 2008.
[12] J. Rizkiana *et al.*, "Effect of biomass type on the performance of cogasification of low rank coal with biomass at relatively low temperatures," *Fuel*, vol. 134, pp. 414–419, 2014.
[13] M. Shahbaz and D. O. Patrick, "The influence of catalysts in biomass steam gasification and catalytic potential of coal bottom ash in biomass steam gasification : A review," *Renew. Sustain. Energy Rev.*, vol. 73, no. October, pp. 468–476, 2017.
[14] M. Kajita, T. Kimura, K. Norinaga, C. Z. Li, and J. I. Hayashi, "Catalytic and noncatalytic mechanisms in steam gasification of char from the pyrolysis of biomass," *Energy and Fuels*, vol. 24, no. 1, pp. 108–116, 2010.
[15] H. Iwaki, S. Ye, H. Katagiri, and K. Kitagawa, "Wastepaper gasification with CO 2 or steam using catalysts of molten carbonates," vol. 270, pp. 237–243, 2004.
[16] K. V. Kumar, M. Bharath, V. Raghavan, B. V. S. S. S. Prasad, S. R. Chakravarthy, and T. Sundararajan, "Gasification of high-ash Indian coal in bubbling fluidized bed using air and steam – An experimental study," *Appl. Therm. Eng.*, vol. 116, pp. 372–381, 2017.
[17] J. Rizkiana *et al.*, "Promoting effect of various biomass ashes on the steam gasification of," *Appl. Energy*, vol. 133, pp. 282–288, 2014.
[18] S. V Vassilev, D. Baxter, L. K. Andersen, and C. G. Vassileva, "An overview of the composition and application of biomass ash . Part 1 . Phase – mineral and chemical composition and classification," *Fuel*, vol. 105, pp. 40–76, 2013.
[19] K. M. Steel, J. Besida, T. A. O. Donnell, and D. G. Wood, "Production of Ultra Clean Coal Part I — Dissolution behaviour of mineral matter in black coal toward hydrochloric and hydrofluoric acids," pp. 171–192, 2001.
[20] P. of the R. of Indonesia, *Peraturan Presiden Republik Indonesia Nomor 22 Tahun 2017 Tentang Rencana Umum Energi Nasional*. 2017, p. 6.

Thermodynamic simulation of two-stage gasification and combustion of very wet biomass including solid municipal waste

Muflih Arisa Adnan[1] and Herri Susanto[2*]

[1]*Department of Chemical Engineering, Islamic University of Indonesia, Yogyakarta 55584, Indonesia*
[2]*Department of Chemical Engineering, Bandung Institute of Technology, Bandung 40132, Indonesia*

** Corresponding Author's E-mail: herri@che.itb.ac.id*

Abstract

Oil palm empty fruit bunches (EFB) are generated in large amount together with the production of palm oil. While municipal solid wastes (MSWs) are always generated in line with the human being activities and often gives serious disposal problems. These two types of biomasses have a large potential as renewable energy sources despite of their large moisture contents of up to 70%. Two stage processes consisting of drying and pyrolysis as the first, and char combustion or gasification as the second ones have been proposed in many literatures. Successful demonstration plants of two stage incineration of MSW have been reported in China, and a demonstration unit is going to be installed in Jakarta soon. In order to get an initial overview on the capability of this process, several configurations of this two stage process are being studied using the thermodynamic, and mass and energy balance. This two stage process is simulated to evaluate the possibility of the implementation of the incineration of MSW and in the gasification of EFB. These the thermal conversions of biomass might be used to produce electricity.

1. Introduction

The increase of the human population and the economic development cause the significant increase of both the energy consumption and the waste production including the municipal solid waste (MSW). Recently, the energy demand is mainly supplied from the fossil fuel which release a massive amount of CO_2-emission[11]. The improper treatment of MSW also can causes the environmental problem such as the green house effect due to the formation of CH_4 formation during landfilling and toxic gases after inceneration[21]. It is worth noting that the MSW usually present in various types of materials with high moisture content (up to 70%)[24].

The attention to the gasification for MSW management is increaseing due to its ability to convert the MSW into the usable energy with minumum negative impact[8]. In addition, a considerable volume of research reported that the gasification shows high performance in term of overall efficiency[8, 26], cold gas efficiency[9] and high H_2 production[10, 19]. Indeed, the composition of the syngas varies with the variation of the properties of the MSW and the gasification technique [14].

A considerable number of litrature has focused on the development of the gasifier to optimize its performance. To cite a few, a moving bed gasifier with internal recycle system has been designed by Susanto and Beenackers[20], reporting the producer gas with a minimum tar concentration. The effect of steam injection to the counter-current reduction zone has been investigated by Adnan et al.[2], showing higher H_2 productions at higher steam to carbon ratio. The two-stage gasifier with the capacity of 100 kW has been developed by Brandt et. al.[6]. A negligible amount (15 mg/Nm^3) of tar in the producer gas was observed on their experiment. The two types of two-stage gasifier for gasification of wet biomass have been developed by Beňo et. al.[25]. The difference of the gasifier types lays on the drying and pyrolysis process which defined as the AS concept and the TARPO concept, as depicted in Fig. 1 and Fig. 2, respectively.

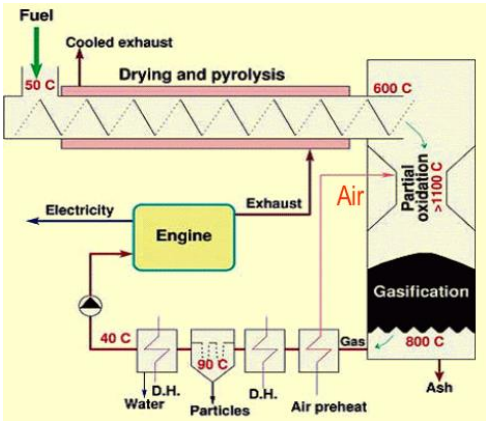

Fig. 1. The two-stage gasifier with AS concept (adapted from Beňo et. al.[25]).

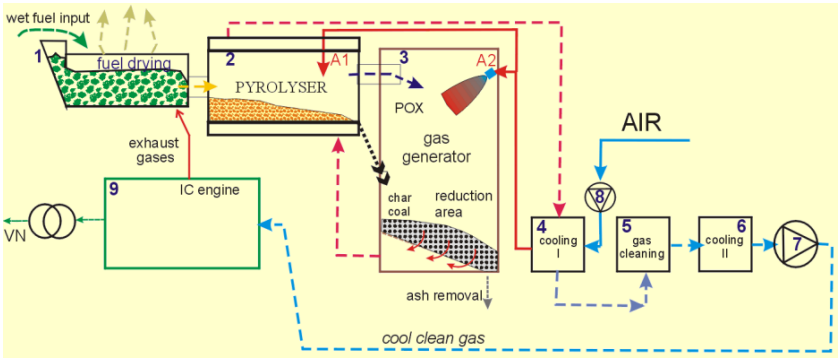

Fig. 2. The two-stage gasifier with TARPO concept (adapted from Beňo et. al.[25]).

Many studies have investigated the biomass gasification using thermodynamic analysis. The minimization of Gibbs free energy, a non-stoichiometric equilibrium approach, has been widely used for thermodynamic study on the gasification with a good agreement with the experimental results[17]. For instance, the gasification performance of various biomasses including microalgae using a thermodynamic analysis has been investigated by Adnan et al.[3]. The operation of CO_2-gasification of the biomass has been studied using a thermodynamic analysis by Chaiwatanodom et. al.[7] in order to find the optimum condition of the process. A modified moving bed downdraft gasifier has been simulated by Adnan et. al.[2] using a thermodynamic method with considering the tar formation to enhance the H_2 production of the gasifier.

In the present study, we investigate the performance of the two-stage gasifier for gasification of high water content MSW to obtain the preliminary estimation for the application of gasification of wet biomass. The gasifier consists of two-stage processes: (1) drying and pyrolysis to convert wet MSW into char by releasing the moisture and the volatile matter from the feedstock, and (2) combustion or gasification to convert char into the gaseous products and char. Two configurations of the two-stage gasifier are investigated using various type of biomass such as food waste, paper waste, empty fruit bunch (EFB), sewage sludge and palm kernel shell (PKS). For gasification of wastes, the performance of the gasifier for gasification of the mixture of food waste and paper waste is investigated as well.

2. Process Description

In the study herein, two configurations (i.e., configuration-1 and configuration-2) of the two-stage gasifier are investigated. In the configuration-1, the high moisture content feedstock at atmospheric presure and 30°C are sent to the drying and pyrolysis zone. In the drying and pyrolysis stage, the moisture content is completely vaporized and the feedstock is decomposed into volatile matter and char due to the high temperature (400°C). It is worth noting that the heat in the drying and pyrolysis stage is supplied by the exhaust gas (F_{eg}) using indirect contact. The properties of the fedstocks and the char are summarized in Table , while the block diagram of the process is depicted in Fig. 3. The products of the drying and pyrolysis stage (F_{vm}) is directed to the gasification stage. In the gasification

stage, the F_{vm} stream is converted into producer gas (mainly consists of H_2, CO, CH_4 and H_2O) using the heated air (F_{ha}) with the equivalence ratio (ER) of 0.3. The ER is the ratio of actual air to biomass weight ratio per stoichiometric air to biomass weight ratio for complete oxidation.

Table 1. The properties of the biomass, MSW and char.

	Food waste[24]	Paper waste[24]	EFB [4]	Sewage sludge [23]	PKS [18]	Wood char[a)13]
Proximate (wt%)						
Moisture	70	10.2	60.0	84.1	13.1	0.0
Volatile matters	21.4	75.9	34.8	7.4	66.8	31.0
Fixed carbon	3.6	8.5	3.7	0.2	11.0	69.0
Ash	5	5.4	1.5	8.3	9.2	0.8
Ultimate (wt%)						
C	73	43.3	44.9	20.6	35.61	78.9
H	11.5	5.8	6.2	3.11	5.49	4.3
O	14.8	44.4	44.0	21	35.22	16.7
N	0.4	0.3	1.2	1.63	0.9	0
S	0.1	0.2	0.0	1.23	0.35	0.06
Ash	0.2	6	1.5	8.3	0.16	0
Heating value (MJ/kg)	4.6	16.7	n.r. [b)]	7.67	14.3	33.1

[a)]after pyrolysis at 400°C
[b)]n.r. : not reported

The producer gas (F_{pg}) goes to the air preheater to transfer the heat from the producer gas to the air. The producer gas (F_{pg}) flows to the gas treatment in order to remove the solid fraction (i.e., ash and unconverted char) from the gaseous products and to reduce the temperature up to 40 °C. The condensed water in the producer gas (F_{fp}) is drained in the flash tank. The producer gas (F_{fg}) is directed to the gas engine for power generation. The power generation consists of the gas turbine driver and electric generator. The air with the excess air of 100% is injected to the gas turbine generator as the oxidation agent. The exhaust of the producer gas goes to the drying and pyrolysis stage as the heat source, and flows to the atmosphere.

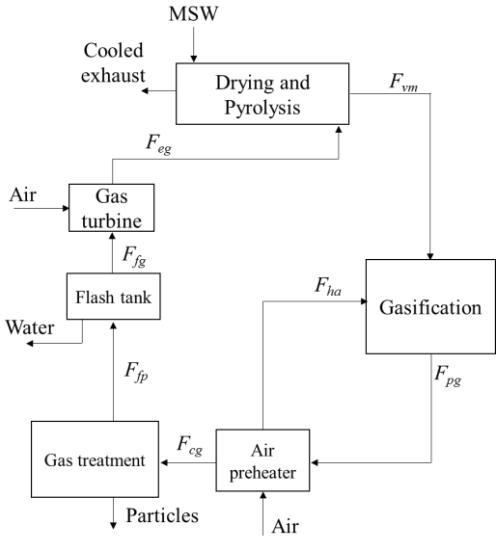

Fig. 3. The block diagram of the configuration-1.

The gasification process of the configuration-2 is similar to the gasification process of the configuration-1 with the modification on the treatment of the feedstock. In the configuration-2, the moisture content of the feedstock is removed separately from the pyrolysis process using direct contact with the exhaust gas, producing dried biomass (F_{db}). Prior entering the dryer, the high tempearture

exhaust gas (F_{eg}) is utilized as the heat supply in the pyrolyser with indirect contact. The high temperature producer gas (F_{pg}) from the gasifier is used as the heating medium for the air preheater to increase the inlet temperature of the air in the gasifier. The block diagram of the configuration-2 is depicted in Fig. 4.

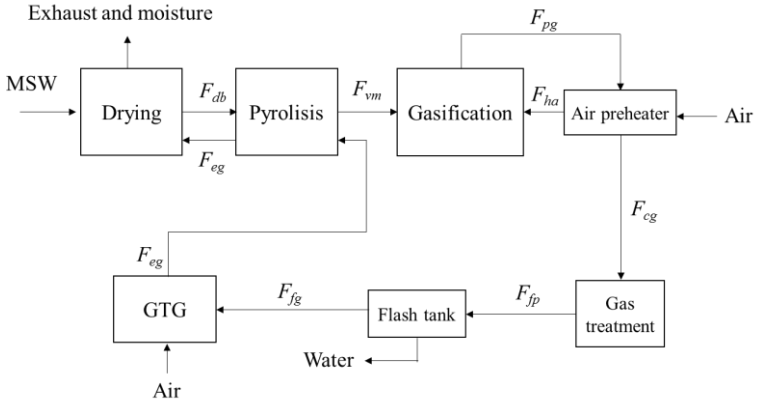

Fig. 4. The block diagram of the configuration-2.

3. Model development

The Gibbs minimization method (Peng-Robinson) is used for all calculations. It is worth noting that (1) ash and N_2 are considered as the inert material and (2) pressure drop and mass transfer limitation are considered to have a minor effect on the process. In addition, an adiabatic condition is assumed in the simulation except for the drying and pyrolysis stages.

A 100 kg/h of the MSW is fed to the drying and pyrolysis stage. In this stage, the moisture content in the MSW is assumed to be completely vaporized due to the high temperature (400^{o}C). In addition, the pyrolysis process takes place in this stage, converting the MSW into the volatile matter and char. The composition and the temperature of the input and output of this stage calculated based on the elemental balance and the heat balance, respectively.

For the elemental balance, the amount of char is predicted using the following equation[15]:

$$Y_C = 0.106 + 2.43 \times \exp(-0.66 \times 10^{-2} \times T) \quad (8)$$

where Y_c and T are char mass yield in kg ash-free char/kg daf biomass, and pyrolysis temperature in ^{o}C, respectively.

The products of the drying and pyrolysis stage is gasified in the gasification stage using the air as the gasifying agent. The composition and the temperature of the producer gas is calculate using the Gibbs free energy minimization method. Given the expected operating temperature is possible to facilitate the reactions reach the equilibrium[1].

Prior to the power generation, the producer gas is sent to the air preheater, cyclone and gas cooler for heat recovery and cleaning purposes. The dried and cooled producer gas is directed to the power generation which consists of compressors (i.e., compressor of the producer gas and combustion iar), a combustor and a gas turbine. The compressors work at the compression ratio of 10. The isentropic efficiency of the compressors and gas turbine is set to be the same at 90%, while the mechanical efficiency of the GTG is 90%.

4. Results and discussion

The properties of the feedstock has a significant influence on the gasification performance, particularly the moisture content[12, 23]. In the study herein we investigate the effect of the moisture content on the gasificaton performance. The temperature of the dring and pyrolysis stage of the configuration-1 is constant at 400^{o}C for all simulation, while in the configuration-2, the temperature of drying and pyrolysis are constant at 100^{o}C and 400^{o}C, respectively. The feasibility of the process is represented by the net energy in the drying and pyrolysis. The positive net energy means the gasification produces an excess energy while the negative net energy represents the amount of the required external energy supply in order to run the process.

The performance of the gasification using two-stage gasifier with various types of biomass is

presented in

Table 2. It can be clearly seen in Table 2 that the gasification temperature of the configuration-1 is lower than that of the configuration-2. The reason for this lays on the fact that the gasification temperature of configuration-2 is higher than its counterpart of configuration-1. This is because the moisture content of the feedstock entering the gasification process in the configuration-1 is higher than its counterpart of the configuration-2. Indeed, higher moisture contents cause lower gasification temperatures due to higher energy for water vaporization. The similar pattern was reported experimentally by Xu et. al[23], which was reflected on the organic material residue (OMR). In their study, higher amount of OMR was observed on the gasification of the sewage sludge at higher moisture content.

It is clearly shown in

Table 2 that the configuration-2 delivers higher concentration of CO, and lower concentration of H_2 when compared to the configuration-1. The similar trend is observed for PKS and sewage sludge. This is the results from the endothermicity of the Bouduard reaction which favors higher temperature due to the exothermic hydrogen oxidation reaction. This is confirmed by the decrease of the CO_2 concentration and H_2 concentration as show in

Table 2. This is also confirmed experimentally by Turn et al.[22] .They found that the CO concentration increased from 18.6% to 19.3% and the H_2 concentration decreased from 38.8% to 38.3% as the gasification temperature was increased from 850 to 900 ºC.

It is clearly shown in

Table 2 that the configuration-1 produces higher amount of producer gas when compared to its counterpart of configuration-2. The flowrate of the producer gas from the gasification of EFB and sewage sludge decrease in a similar fashion as well. This is attributed to the higher char conversion via steam reforming reaction as the consequence of higher water content in the gasification stage of the configuration-1. This is also confirmed by the lower gasification temperature due to the endothermicity of the steam reforming reaction. A similar pattern was reported experimentally by Billaud et al.[5] showed the presence of steam reduce the amount of soot. This was also confirmed experimentally by Niu et al.[16].

Table 2 shows that the negative net energy is observed on the gasification of EFB, PKS and sewage sludge using configuration-1. This indicates that operation of the gasification of EFB, PKS and sewage sludge require 267.71 MJ/h, 41.69 MJ/h and 187.92 MJ/h of external energy supplies, respectively. The lower external energy requirement is found on the configuration-2. The reason of this lays on the fact that the heat duty of the pyrolysis process of the configuration-1 is higher than that of the configuration-2. Indeed, the moisture content of the feedstock in the configuration-1 is higher than its counterpart in the configuration-2.

In this study the gasification of the MSW is run in the configuration-1 gasifier. The variation of moisture content is conducted by the variation of the mixture of food waste and paper waste (the analysis is summarized in Table), while keeping the mass flowrate of the biomass constant at 100 kg/h. It can be clearly seen in Fig. 5 that the net energy and the power output increase as the moisture content of the feedstock decreases. For instance, when the biomass with the moisture content of 70% is fed to the gasifier, the negative net energy (-91 MJ/h) is observed. However, the positive net energy (16 MJ/h) is observed when the biomass with the moisture content of 46% is fed to the gasifier. It is worth noting that when the moisture content of biomass is higher than 52%, the negative sign of the net energy is observed. This indicates that the additional energy supply is required for the gasfication of the biomass with the moisture content of higher than 52%. In addition, higher moisture content in the biomass require higher amount of the external energy supply. The similar result is also reported by Adnan et al.[3], indicating the gasification of rice husk (9.5wt% moisture) requires higher amount of exernal energy supply as compared to the gasification of palm frond (5.3wt% moisture), which reflecs on the lower gasification system efficiency.

Table 2. The composition, the flow rate and temperature of producer gas.

	Configuration-1 (stream F_{pg} in Figure 3)			Configuration-2 (stream F_{pg} in Figure 4)		
Biomass	EFB	PKS	Sewage Sludge	EFB	PKS	Sewage Sludge
Composition (%wt db)						
CO	0.11	0.25	0.01	0.25	0.27	0.28
CO_2	0.16	0.06	0.25	0.06	0.05	0.04
CH_4	Trace	Trace	Trace	Trace	Trace	Trace
H_2	0.29	0.23	0.39	0.20	0.22	0.22
N_2	0.44	0.47	0.36	0.50	0.47	0.46
Mole flow, kmol/h	3.51	8.98	1.05	3.12	8.87	0.83
T gasifier	1436	2010	867	2219	2114	1925

Table 3. The composition, the flow rate and temperature of producer gas.

	Configuration-1			Configuration-2		
Biomass	EFB	PKS	Sewage Sludge	EFB	PKS	Sewage Sludge
Power output, kW	27.03	85.87	6.70	21.14	65.78	6.46
Net energy, MJ/h	-267.71	-41.69	-187.92	-199.39	457.12	-115.60

It can be clearly seen in Fig. 5 that the power output of the gasification process increases when the moisture content of the biomass decreases. For example, the gasification produces electricity with the capacity of 52 kW as the biomass with the moisture content of 70% enters the gasifier. The capacity of power generation increase up to 81 kW when moisture content of the biomass is decreased to 46%. The reason of this finding lays in the fact that higher moisture content consume larger amount of energy for water vaporization. This is in line with the previous study by Adnan et. al. [3], reporting that higher moisture content has an adverse effect on the gasification performance in term of cold gas efficiency. In addition, Xu et al. [23] also reported that lower yield of combustible gas was observed at higher moisture content.

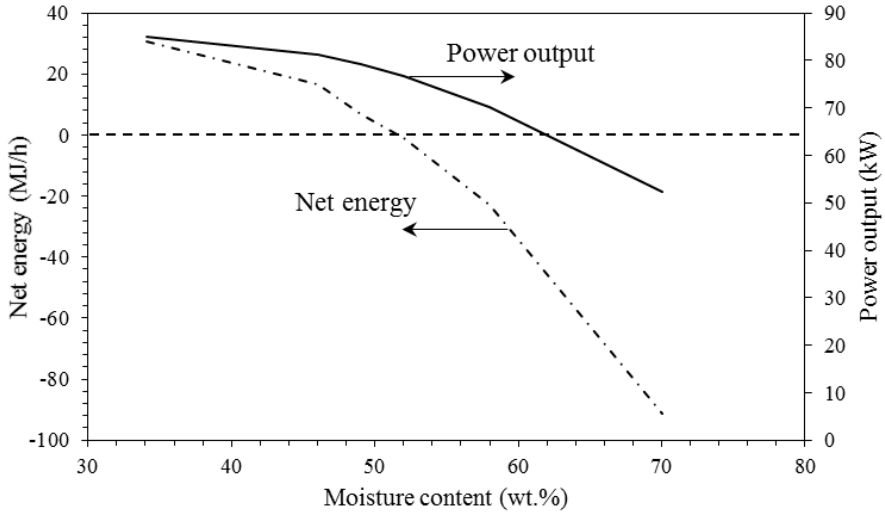

Fig. 5. The net energy and the power output of the gasification process.

The performance of the two stage combustion for incineration is presented in Table 4. During incineration, the air with ER of 1.2 is injected to the process. The configuration-2 shows a better performance in term of the energy production as compared to the configuration-1. This is attributed to lower moisture content of the biomass entering the combustion stage. The energy production can be

potentially used for steam generation. It can be clearly shown in Table 4 that the incineration of EFB required an external energy supply. This is because the heating value of the EFB is countered by the high moisture content of the EFB.

Table 4. The performance of the incinerator.

Biomass	Configuration-1, MJ/h	Configuration-2, MJ/h
Food waste	325.84	348.17
EFB	-29.66	-3.29

5. Conclusions

The two-stage gasifier has been investigated using the thermodynamic, and mass and energy balance methods. The gasification of various biomass using two-stage gasifiers (i.e., configuration-1 and configuration-2) showed the significant influce of moisture content in the biomass on the gasification performance. The configuration-1 showed a fair performance for gasification of wet biomass. A good performance was observed on the gasification of the wet biomass using configuration-2. Higher content of moisture in the biomass has an adverse effect on the gasification using configuration-1 and configuration-2. The highest power output exhibited on the gasification of PKS in the configuration-1 and configuration-2 with the power output of 85.87 kW (requires 187.92 MJ/h of external energy supply) and 65.78 kW (produces 457.12 MJ/h of heat energy), respectively. These results indicate that the two-stage gasification process can potentially be a promising technology for gasification of wet biomass with further optimization.

Acknowledgement

The authors acknowledge the financial support provided by Kemenristekdikti to this research under project no PN-7-17-2017 for "Integrated hydrothermal treatment for empty fruit bunch conversion to solid fuel and feedstock of potasium fertilizer".

References

1 Adnan M A, Muraza O, et al., Iron Oxide over Silica-Doped Alumina Catalyst for Catalytic Steam Reforming of Toluene as a Surrogate Tar Biomass Species. *Energy & Fuels*2017).
2 Adnan M A, Susanto H, et al., Enhancement of Hydrogen Production in a Modified Moving Bed Downdraft Gasifier – a thermodynamic Study by Including Tar. *International Journal of Hydrogen Energy;* 42: 10971-85 (2017).
3 Adnan M A, Susanto H, et al., Feed Compositions and Gasification Potential Of several Biomasses Including a Microalgae: A thermodynamic Modeling Approach. *International Journal of Hydrogen Energy;* 42: 17009-19 (2017).
4 Aziz M, Kurniawan T, et al., Advanced Power Generation Using Biomass Wastes from Palm Oil Mills. *Applied Thermal Engineering;* 114: 1378-86 (2017).
5 Billaud J, Valin S, et al., Influence of H2o, Co2 and O2 Addition on Biomass Gasification in Entrained Flow Reactor Conditions: Experiments and Modelling. *Fuel;* 166: 166-78 (2016).
6 Brandt P, Larsen E, et al., High Tar Reduction in a Two-Stage Gasifier. *Energy & Fuels;* 14: 816-19 (2000).
7 Chaiwatanodom P, Vivanpatarakij S, et al., Thermodynamic Analysis of Biomass Gasification with Co2 Recycle for Synthesis Gas Production. *Applied Energy;* 114: 10-17 (2014).
8 Couto N, Monteiro E, et al., Hydrogen-Rich Gas from Gasification of Portuguese Municipal Solid Wastes. *International Journal of Hydrogen Energy;* 41: 10619-30 (2016).

9 Couto N D, Silva V B, et al., Assessment of Municipal Solid Wastes Gasification in a Semi-Industrial Gasifier Using Syngas Quality Indices. *Energy;* 93, Part 1: 864-73 (2015).
10 Guan Y, Luo S, et al., Steam Catalytic Gasification of Municipal Solid Waste for Producing Tar-Free Fuel Gas. *International Journal of Hydrogen Energy;* 34: 9341-46 (2009).
11 Hossain M M, and de Lasa H I, Chemical-Looping Combustion (Clc) for Inherent Co2 Separations—a Review. *Chemical Engineering Science;* 63: 4433-51 (2008).
12 Korus A, and Szlęk A, The Effect of Biomass Moisture Content on the Igcc Efficiency. *Biomass and Bioenergy;* 80: 222-28 (2015).
13 Mafu L D, Neomagus H W J P, et al., Chemical and Structural Characterization of Char Development During Lignocellulosic Biomass Pyrolysis. *Bioresource Technology*2017).
14 Monteiro E, Sotton J, et al., Experimental Study of Syngas Combustion at Engine-Like Conditions in a Rapid Compression Machine. *Experimental Thermal and Fluid Science;* 35: 1473-79 (2011).
15 Neves D, Thunman H, et al., Characterization and Prediction of Biomass Pyrolysis Products. *Progress in Energy and Combustion Science;* 37: 611-30 (2011).
16 Niu Y, Han F, et al., Experimental Study on Steam Gasification of Pine Particles for Hydrogen-Rich Gas. *Journal of the Energy Institute;* 90: 715-24 (2017).
17 Renganathan T, Yadav M V, et al., Co2 Utilization for Gasification of Carbonaceous Feedstocks: A Thermodynamic Analysis. *Chemical Engineering Science;* 83: 159-70 (2012).
18 Samiran N A, Jaafar M N M, et al., Progress in Biomass Gasification Technique - with Focus on Malaysian Palm Biomass for Syngas Production. *Renewable and Sustainable Energy Reviews;* 62: 1047-62 (2016).
19 Shehzad A, Bashir M J K, et al., System Analysis for Synthesis Gas (Syngas) Production in Pakistan from Municipal Solid Waste Gasification Using a Circulating Fluidized Bed Gasifier. *Renewable and Sustainable Energy Reviews;* 60: 1302-11 (2016).
20 Susanto H, and Beenackers A A C M, A Moving-Bed Gasifier with Internal Recycle of Pyrolysis Gas. *Fuel;* 75: 1339-47 (1996).
21 Teixeira S, Monteiro E, et al., Prospective Application of Municipal Solid Wastes for Energy Production in Portugal. *Energy Policy;* 71: 159-68 (2014).
22 Turn S, Kinoshita C, et al., An Experimental Investigation of Hydrogen Production from Biomass Gasification. *International Journal of Hydrogen Energy;* 23: 641-48 (1998).
23 Xu Z R, Zhu W, et al., Influence of Moisture Content on the Direct Gasification of Dewatered Sludge Via Supercritical Water. *International Journal of Hydrogen Energy;* 37: 6527-35 (2012).
24 Young G C, 'Municipal Solid Waste and Properties', in *Municipal Solid Waste to Energy Conversion Processes* (John Wiley & Sons, Inc., 2010), pp. 135-54.
25 Zdeněk Beňo J B, Jaroslav Moško and Michael Pohořely, 'Experience with Operation of Multi-Stage (Two-Stage) Fixed-Bed Gasifiers in the Czech and Slovak Republic', in *The 8th International Freiberg Conference on IGCC & XtL* (Cologne, Germany: 2016).
26 Zhang Q, Dor L, et al., Gasification of Municipal Solid Waste in the Plasma Gasification Melting Process. *Applied Energy;* 90: 106-12 (2012).

Steam Gasification of Char from Pyrolysis of Palm Kernel Shell – Effect of Gasification Temperature on Hydrogen Production Rate

Joko Waluyo[a], Jie Lin[b], Mi Yan[b], and Herri Susanto[a*]

[a]*Department of Chemical Engineering, Institut Teknologi Bandung, Bandung 40132, Indonesia*
[b]*Institute of Energy and Power Engineering, Zhejiang University of Technology, Hangzhou-310014, China*

** Corresponding Author's E-mail:herri@che.itb.ac.id*

Abstract
Experimental study on the production of hydrogen from palm kernel shell (PKS) was conducted in a tubular reactor with a diameter of about 25 mm. The particle diameter of PKS was about -2.8/+1.5 mm, and its bulk density was about 1 mg/mL. About 2 – 6 gram oven dried PKS was firstly pyrolyzed up to 500°C, under the flowing of N_2 at a constant flow rate 200 mL/min (1 bar and 30°C). After keeping at 500°C for about 10 minutes, the reactor temperature was then increased to desired gasification temperature of 700, 800, or 900°C. When this reaction temperature was reached, steam at 110°C was injected into the N_2 flow, with the steam rate of about 0.12 g/min (1 bar and 30°C). The composition of gaseous product from gasification was measured every 10 minutes using a gas chromatography. After normalization to exclude N_2, the composition of gaseous product from gasification at 700°C were: 72.0% H_2, 11.4% CO, 15.8% CO_2, and 0.8% CH_4. The carbon conversion was about 92% at 900°C. The hydrogen production rates at the gasification temperature of 700, 800 and 900°C were about 52, 71, and 93 H_2 mol/kg of Char respectively.

Keyword: pyrolysis, steam gasification, synthesis gas

1. Introduction

Gasification is the process of thermal conversion into synthesis gas which can be utilized for power generation as well as for chemical synthesis. The gasifying medium affects the resulting gas composition and the heating value of syngas. To obtain syngas with higher hydrogen production rate as well as higher H_2/CO molar ratio also lower tar content by using steam gasification of char is the best choice [1]. Steam as a gasifying medium can produce syngas with a heating value of about 10-18 MJ/Nm^3 [2].

In order to produce clean synthesis gas from tar, the palm kernel shell was done pretreatment through pyrolysis. With pyrolysis, the volatile matter content and moisture content of biomass will decrease, resulting in char having properties or lower volatile matter content, higher fixed carbon, higher carbon element and lower oxygen [3]. Char also contains some minerals such as sodium, potassium, calcium, silicon, and magnesium, whose presence can give catalyst effects on gasification reactions [4]. Otherwise minerals at high temperatures, they produce solid materials that deposit on the char pore, so char reactivity will decrease [5]. To optimize the mineral content of char pyrolysis results, biomass can be pretreatment by a hydrothermal process to decrease mineral content especially sodium and potassium.

Char gasification with steam as a gasifying medium will produce syngas suitable for

utilization applications to synthesize chemical compounds such as ammonia, methanol, DME and Fischer tropsch.

In steam gasification, operating parameters that affect the yield of hydrogen are char characteristics, gasification temperature, and steam/carbon ratio. In this study, the palm kernel shell was obtained from Lampung-Indonesia which had undergone a hydrothermal pretreatment to reduce the mineral content and volatile matter. After hydrothermal treatment continued PKS pyrolysis treatment to produce char. Char from PKS then conducted steam gasification on temperature variation to determine the effect of temperature on the composition of syngas and hydrogen production rate/ yield of hydrogen.

2. Material and Methods

2.1 Biomass preparation

The PKS was obtained from local oil palm factory on Lampung – Indonesia. Samples PKS were crushed into specific particle size between 1.5 – 2.8 mm. The proximate and ultimate analysis of PKS as shown in Table 1.

Table 1 Proximate and ultimate analysis of Palm Kernel Shell

No	Characteristic	Value
1	Proximate analysis	
	Moisture	8.19%
	Volatile matter	70.45%
	Fixed Carbon	18.89%
	Ash	2.47%
2	Ultimate Analysis	
	Carbon	48.25%
	Hydrogen	6.41%
	Oxygen	42.69%
	Nitrogen	0.15%
	Sulfur	0.03%
3	Heating value (kJ/kg)	19820

Pretreatment of PKS conducted on hydrothermal processes, 10 gram biomass were fed into the autoclave and then added 50 gram of water. The autoclave was heated to 180℃ and held for 60 minutes. After finished, biomass was separated from the liquid and dried into the oven.

2.2 Experimental procedure

About 2 – 6 gram oven dried PKS was firstly pyrolyzed up to 500°C, under the flowing of N_2 at a constant flow rate 200 mL/min (1 bar and 30°C). After keeping at 500°C for about 10 minutes, the reactor temperature was then increased to desired gasification temperature of 700, 800, or 900°C. When this reaction temperature was reached, steam at 110°C was injected into the N_2 flow, with the steam rate of about 0.12 gram/min (1 bar and 30°C).

2.3 Sampling and analysis

The composition of gaseous product H_2, CO, CO_2, and CH_4 from gasification was measured every 10 minutes using a gas chromatography GC 2014A Shimadzu (MS5A and Porapak-Q column). The sample was analyzed in thermal conductivity detector (TCD) at 150°C.

2.4 Data Analysis

The hydrogen production rate or yield of Hydrogen was defined as:

$$Y_{H2} = \frac{n_{H2}}{Char\_weight} \quad (1)$$

The yield potential of Hydrogen can be developed in the presence of CO. This is because the water gas shift reaction from CO is an exothermic reaction and easily carried out.

$$Y_{H2+CO} = \frac{n_{(H2+CO)}}{Char\_weight} \quad (2)$$

For carbon conversion of Char, could be determined as

$$X_C = \frac{n_{(CO+CO2+CH4)}}{n_{Carbon\_in\_Char}} x100\% \quad (3)$$

Yield of by-product (CO, CO_2 and CH_4) was calculated as

$$Y_{Ci} = \frac{n_{(Ci)}}{n_{Carbon\_in\_Char}} x100\% \quad (4)$$

3. Result and Discussion

3.1 Biomass pretreatment

PKS was conducted pretreatment hydrothermal before being pyrolyzed. Hydrothermal is done to adjust the composition of the mineral, which affects the reactivity of the char when undergoing the steam gasification process. The minerals are mainly K, Si, P and Fe. The ratio of these minerals will affect the order of reaction and the rate of reaction of steam gasification. The mineral composition of fresh biomass and after hydrothermal is presented in Table 2.

Table 2 Mineral composition of Fresh PKS and after pretreatment hydrothermal

No	Mineral	Fresh PKS	After HT 180°C, 60 min
1	K	2.42	1.79
2	Si	26.47	28.31
3	P	0.55	0.00
4	Fe	0.83	0.89
	Ratio K/(Si+P)	0.09	0.06

After pretreatment with hydrothermal, it showed that potassium and phosphorous minerals decreased and the ratio of K/Si+P was also below 1, indicating gasification reaction is still relatively slow. However, Fe content in char can increase the yield of hydrogen as a gasification catalyst[6]. By decreasing some minerals, it can increase the pores of the char that have an impact on increasing the effectiveness of the char reactions to the steam.

3.2 Pyrolysis

Char production from Palm kernel shell conducted on intermediate pyrolysis with a heating rate 50°C/minute at temperature 500°C and 700°C. The product yield from the pyrolysis (Table 3), there was no significant changes with increasing pyrolysis temperature from 500 to 700°C. The char yield decreased about 1% as the final pyrolysis temperature was raised from 500 to 700°C.

Table 3 Yield of pyrolysis product at a heating rate 50°C/min and particle size of 1.5–2.8 mm

No	Pyrolysis product	Temperature	
		500°C	700°C
1	Char	26.10%	25.37%
2	Oil	50.35%	49.97%
3	Gas	15.36%	16.44%

Experiment for intermediate pyrolysis usually generates a char of 25% [7]. From the experimental results at the temperature 500°C and 700°C obtained char with a higher value than fixed carbon in fresh PKS, because char is not fully fixed carbon. From some experiments show that char has fixed carbon of about 75-90% depending on temperature pyrolysis [8, 9].

3.3 Effect of Temperature on Steam Gasification of Char

Char from pyrolysis of PKS were conducted on steam gasification at a different temperature. The effect of reaction temperature varying from 700°C to 900°C and Steam to Carbon ratio about 2. The syngas composition and the ratio of H_2/CO are influenced by the temperature of the gasification reaction (Table 4).

Table 4 Effect temperature on gas composition at S/C=2

No	Temperature	700°C	800°C	900°C
1	Gas Composition (%mol)			
	H_2	71.98%	63.91%	65.07%
	CO	11.38%	14.72%	17.20%
	CH_4	0.81%	1.08%	0.49%
	CO_2	15.83%	20.29%	17.24%
2	Heating value (MJ/NM^3)	10.93	10.43	10.65
3	H_2/CO ratio (mol/mol)	6.33	4.34	3.78
4	H_2/CO_2 ratio (mol/mol)	4.55	3.15	3.77

The gasification steam reaction can be represented by reactions (1) - (3).

$$C + H_2O \leftrightarrow CO + H_2 \qquad \Delta H_{298K} = +131 \text{ kJ/mol} \qquad (1)$$

$$C + 2H_2O \leftrightarrow CO_2 + 2H_2 \qquad \Delta H_{298K} = +109.8 \text{ kJ/mol} \qquad (2)$$

$$C + CO_2 \leftrightarrow 2CO \qquad \Delta H_{298K} = +172 \text{ kJ/mol} \qquad (3)$$

Gasification results showed that with increasing temperature makes the concentration of CO continues to rise while the H_2 concentration is relatively constant. The concentration of CO_2 and CH_4 increased first then decrease when temperature change from 700°C to 900°C. This corresponds to the thermodynamic equilibrium that, after a temperature 850°C the equilibrium constant of reaction (K) for CO_2 formation (reaction 2) is lower than that of the equilibrium constant for CO formation (reaction 1) as shown in Fig. 1.

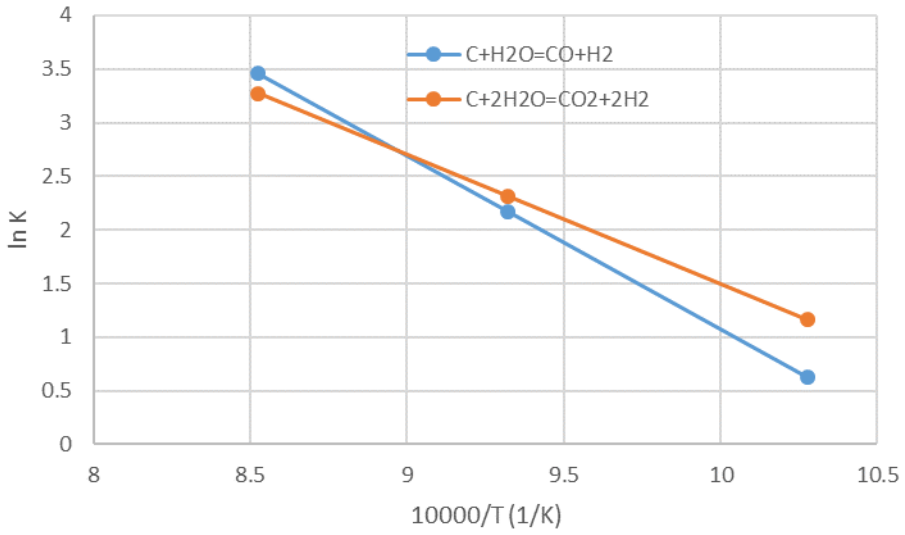

Fig. 1 Equilibrium constant as a function of temperature

In steam gasification of char with rising temperatures will result in higher H_2 yield and potential H_2 yield (Fig. 2). This is because the main gasification reactions such as Water gas, Boudouard and steam reforming are endothermic reactions, so it would be favorable if operating at high temperature. Increasing temperature from 700°C to 900°C, obtained hydrogen production rate increase from 52 mol/kg char to 93 mol/kg char. The H_2 yield potential is 118 mol/kg char at 900°C.

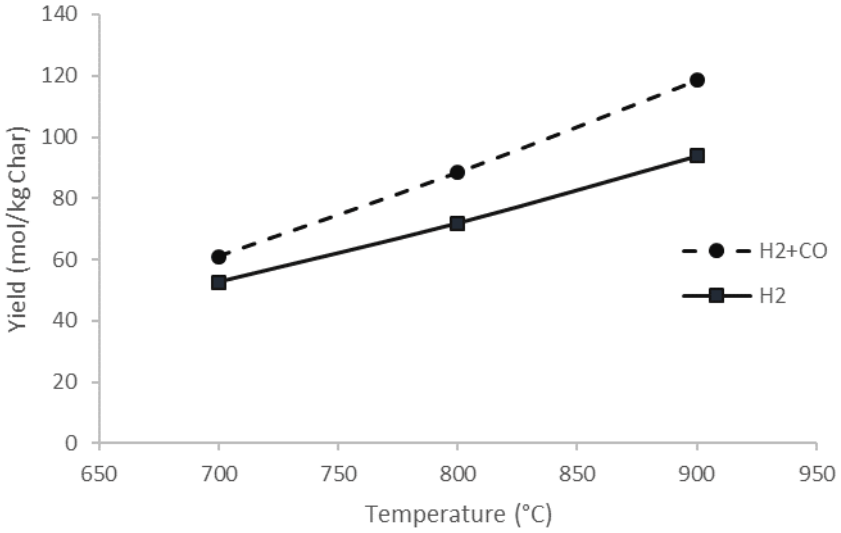

Fig. 2 Effect of temperature on H_2 yield

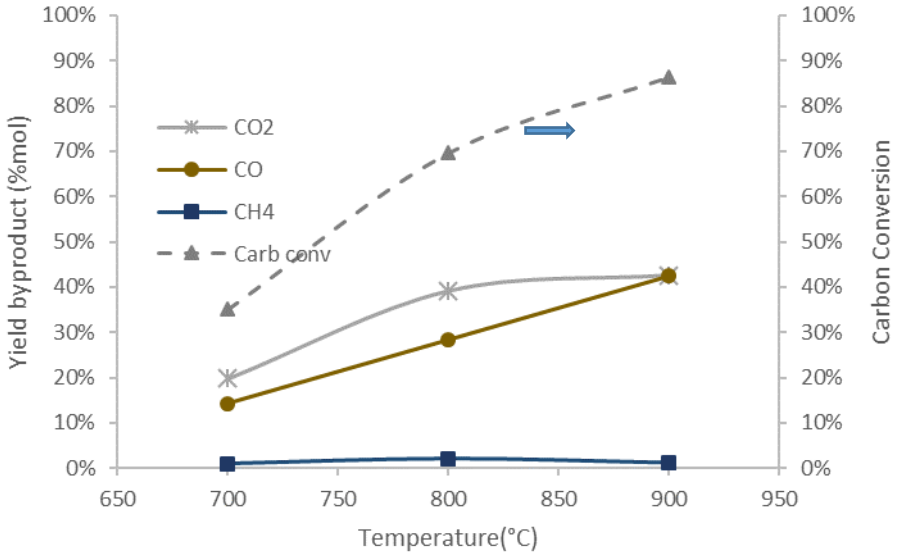

Fig. 3 Effect of temperature on by-product yield and carbon conversion

In PKS steam gasification, at high temperature indicate that char is highly reactive. Increasing the temperature from 700°C to 900°C, obtained carbon conversion increase from 35% to 86% (Fig. 3). As shown in Figure 3, yields of CO_2 and CH_4 decreased during the reaction when temperatures were raised more than 800°C. This is due to the reaction of water gas shift (reaction 1) and boudouard reaction (reaction 3) which is an endothermic reaction, more dominant at high temperature. The synthesis gas having higher H_2/CO ratio is desired for convert syngas to ammonia synthesis as well as hydrogen utilization for a fuel cell.

4. Conclusions

Hydrothermal treatment can reduce mineral (ash) content. The result of pyrolysis palm kernel shell has a char yield about 25%. In the steam gasification of char with Steam/carbon ratio 2, resulting in a H_2/CO ratio 3 – 6 depending on the operating temperature. Water gas reaction more dominant than water gas shift reaction at temperature reaction more than 850°C. Increasing the temperature of the gasification could increase by 86% carbon conversion and hydrogen production rate of 93 mol/kg char at a temperature 900°C.

Acknowledgments

The author would like to acknowledge the financial support from *Hibah Pasca Sarjana Dikti 2017*, *Hibah MP3I ITB 2017* and *Program Penelitian Luar Negeri ITB 2017*.

Reference

1. Sattar, A., et al., Steam gasification of rapeseed, wood, sewage sludge and miscanthus biochars for the production of a hydrogen-rich syngas. *Biomass and Bioenergy*. **69**: p. 276-286.(2014)

2. Basu, P., *Chapter 7 - Gasification Theory*, in *Biomass Gasification, Pyrolysis and Torrefaction (Second Edition)*. 2013, Academic Press: Boston. p. 199-248.
3. Beis, S.H., Ö. Onay, and Ö.M. Koçkar, Fixed-bed pyrolysis of safflower seed: influence of pyrolysis parameters on product yields and compositions. *Renewable Energy*. **26**(1): p. 21-32.(2002)
4. Dupont, C., et al., How inorganic elements of biomass influence char steam gasification kinetics. *Energy*. **109**: p. 430-435.(2016)
5. Zolin, A., et al., The Influence of Inorganic Materials on the Thermal Deactivation of Fuel Chars. *Energy & Fuels*. **15**(5): p. 1110-1122.(2001)
6. Saw, W., et al., Production of hydrogen-rich syngas from steam gasification of blend of biosolids and wood using a dual fluidised bed gasifier. *Fuel*. **93**(Supplement C): p. 473-478.(2012)
7. Bridgwater, A.V., Review of fast pyrolysis of biomass and product upgrading. *Biomass and Bioenergy*. **38**: p. 68-94.(2012)
8. Mafu, L.D., et al., Chemical and structural characterization of char development during lignocellulosic biomass pyrolysis. *Bioresource Technology*. **243**(Supplement C): p. 941-948.(2017)
9. Ma, Z., et al., Hydrogen Production from Bio-Char via Steam Gasification in a Fluidized-Bed Reactor. *Chemical Engineering & Technology*. **36**(9): p. 1599-1602.(2013)

Hydrothermal Treatment of Palm Kernel Shell for Recovery of Potassium

Yusuf Ahda[a] , Aisyah Ardi[a], and Herri Susanto[a*]

[a] *Department of Chemical Engineering*
Institut Teknologi Bandung, Bandung 40132, Indonesia

** Corresponding Author's E-mail:herri@che.itb.ac.id*

Abstract
In line with a large production of palm oil, palm biomass are potential for renewable energy and chemicals resources. Experimental study on the hydrothermal treatment (HT) of oil palm kernel shell (PKS) has been conducted to get a refined solid fuel for gasification process and also to recover potassium originated in the ash. Experiments on HT were carried out in a digester of 500 mL, and the liquid to water ratio of 5 mL/g. Temperature were varied in the range of 150 to 220^{0}C, holding time of 30 - 120 min, and particle sizes of PKS of 0.2-5 mm. Temperature of hydrothermal treatment gave a more significant effect compared to that of holding time on the dissolution of potassium from PKS. Potassium content in the liquid product of HT as high as 187 mg/L was obtained from the HT ata temperature of 200^{0}C and a holding time of 30 min.

Keywords: hydrothermal treatment, energy from biomass, biochar, potassium

1. Introduction
The result of increasing population and economic growth from a nation, always followed by higher energy demand. During this economic growth, energy supplies always depending from fossil fuel. The consumption of fossil fuels such as oil, coal and natural gas has increased rapidly. Indonesia goverment develops a long-term development planning targets to suport economic growth. Indonesia goverment plan to reduce the fossil fuel dependence and start to using renewable energy. In 2025, Indonesia plans to 25% energy demand supplied from renewable energy [1]. Palm Oil is one of the most popular comodity in global market. Indonesia is one of the largest Palm Oil producers in the world. Palm Oil waste recognize as a biomass. Oil Palm Kernel Shell (PKS).

PKS is one of waste from Crude Palm Oil production. Every 1 ton fresh palm fruit contain 5-6% PKS. PKS contain more high bulk density, high calorific value so its very potential as a solid fuel. In current condition in palm industry, PKS often used as a fuel for boiler. Direct combustion still be the most using methods to utilize PKS. Alkali content in PKS could caused slagging, fouling and scaling on the furnace in boiler. To minimize the fouling effect, biomass pretreatment and choose the thermochemical conversion technology process are very important to obtain better properties of PKS for solid fuel.

Thermochemical conversion process is based on the thermal breakdown biomass which contain hemicelulose, celullose, and lignin into fuel and some valuable product. Moisture content of biomass could be the one important factor for deciding the suitable process to use. High moisture content will reduce the combustion temperature. Hydrothermal Treatment is one of pre-treatment introduced by Shell Oil Company in 1980s. In this method, the thermal degradation of biomass take place in water and affect the physicochemical of water [2]. Organic compound are insoluble in water in normal condition, water can be a good solvent for non-polar subtances under supercritical condition. In Hydrothermal, higher moisture content of raw material are suitable for raw material for hydrotermal. In other thermochemical

process, raw material must dried first. This require additional cost if it applied in industrial application [4]. Moreover HT may used to remove some volatile matter, it can reduce tar formation if it applied in gasification. Beside remove some volatile matter, HT able to reduce some alkali content in biomass like Na, Ca, K, Mg, K, Fe, and Mn [8-9].

The objective of this research is improving the solid fuel-like properties of PKS by HT. HT products expexted to be gasification feedstock. This research focused the effect of temperature, holding time and size particle of PKS in HT based on potassium removal.

2. Methode

2.1. Materials

The biomass feedstock used for this experiment is palm oil shell (PKS) collected from Palm Oil Mill Industry in Lampung, Sumatera, Indonesia. The biomass was cutting and screened in several diameter particle size : particle A (>5mm) and B (0.2-3mm). The feedstock wrapped in sealed plastic bag and kept at the room temperature. The feedstock biomass was first analyzed before the experiment. Ultimate and proximate analysis of palm oil shell feedstock shown in Table 1.

2.2. Experiments

Experiments were performed on a batch reactor. This isolated reactor equipped by electric heater and also provide with thermocontrol to maintain the operating temperature (Fig 1). A 100 grams of palm kernel shell (PKS) sample and 500 mL water was loaded into the reactor and the electric heater heated at desired operating temperature (120, 150, 180, and 200^{0}C), The holding time at each set temperature are (30, 60, 90, and 120 minutes). After the hydrothermal completed, the product was discharged from the reactor. The solid product (biochar) was separated from the liquid by using the fitration, then oven dried for 24 hr, and wrapped in a sealed bag for analysis. The liquid product filled in the sterilized bottle and kept in a refrigerator.

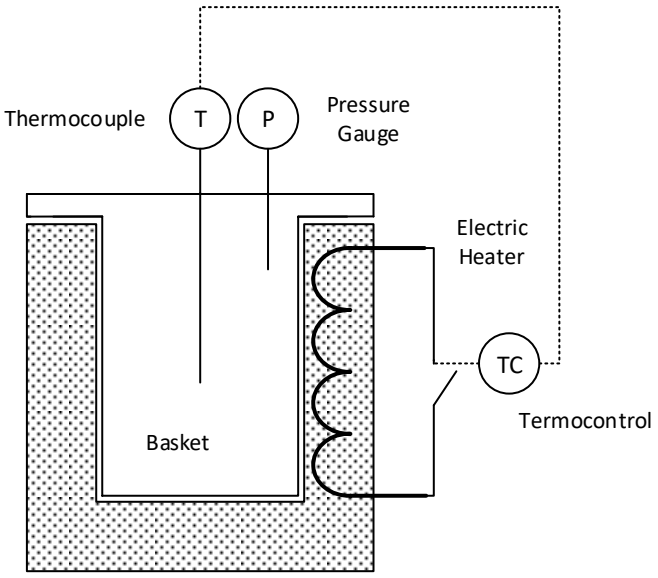

Figure 1. Hydrothermal Treatment Reactor

2.3. Analyze

Raw PKS was analyzed with ultimate and proximate analysis performed based on ASTM D 3172. PKS also analyzed the ash compostion for the baseline. The HT product solid and liquid separated. The liquid analyzed the potassium content in liquid analyze with Standart Methods for Examination of Water and Wastewater 22nd Edition 2012. Using APHA-3500-K-B methods to trace amounts of potassium can be determined in either a direct-reading or

internal-standard type of flame photometer.

3. Result and Discussion

3.1. Proximate and Ultimate Analysis of PKS

PKS characteristic include chemical and physical properties is needed to determined the baseline before the HT process started. PKS for this research contain about 18.89% wt. The volatile matter in PKS is the biggest part baout 70-75%. High volatile matter could affect tar formation if it used to be a gasification feedstock. PKS Ash content based on proximate analysis about 2.47% which is dominated by Si, Ca and K. Si formed in SiO_2 and Ca formed in CaO. The focus of this research is potassium removal. Potassium content in raw PKS is the third biggest ash content. Potassium content in PKS formed in K_2O is about 5.84%. The elemental ash composition shown in Table 2. The percentage gained from spectroscopy analysis in oxide form.

Table 1. Proximate and Ultimate Analysis

Parameters	PKS Riau 1 [11]	PKS Riau 2 [11]	Present Work
Proximate (mass fraction adb)			
MC	9,76%	8,44%	8,19%
Ash	2,87%	1,74%	2,47%
VM	75,70%	76,99%	70,45%
FC	21,43%	21,28%	18,89%
Ultimate			
C	47,87%	48,96%	48,25%
H	6,15%	6,15%	6,41%
O	42,92%	42,87%	42,69%
N	0,33%	0,32%	0,15%
S	0,14%	0,12%	0,03%

Table 2. Ash Content of PKS and HT Product

No	Parameters Temperature Holding Time	Feedstock *	HT Present Work **			
			120^0C (60)	150^0C (60)	180^0C (60)	200^0C (60)
1	SiO_2	56,73%	60,26%	60,46%	60,67%	61,12%
2	Al_2O_3	1,99%	2,11%	2,12%	2,13%	2,14%
3	Fe_2O_3	2,37%	2,52%	2,53%	2,53%	2,55%
4	K_2O	5,84%	4,97%	4,66%	4,33%	3,61%
5	Na_2O	0,60%	0%	0%	0%	0%
6	CaO	23,46%	24,92%	25,00%	25,09%	25,28%
7	MgO	2,77%	2,94%	2,95%	2,96%	2,98%
8	TiO_2	0,20%	0,21%	0,21%	0,21%	0,22%
9	MnO	0,13%	0,14%	0,14%	0,14%	0,14%
10	P_2O_5	2,57%	0%	0%	0%	0%
11	LOI	1,81%	1,92%	1,93%	1,94%	1,95%
12	H_2O	0,13%	0%	0%	0%	0%
13	SO_3	1,23%	0%	0%	0%	0%

*measured

** calculated from potassium mass balance

3.2. Effect of HT on Potassium Recovery

The HT could decrease the ash content of PKS as shown in several table. The effect of temperature on potasium removal shown at Figure 2. In this picture shown that temperature is the most influential variables in HT process. It related by termal degradation of biomass component range temperature. At higher temperature HT, PKS becomes more porous. Porous form structure could absorb some inorganics compound, which explain the increase potasssium content in liquid at increased temperature. Additionally, increasing temperature could increase the solubility some inorganics compound. Most of biomass content such as cellulose and lignin are insoluble in ambient water but are soluble in high temperature or supercritical water [4]. From Figure 2. HT process At 200^0C, potassium content in liquid 187 gr/mL.

The effect of holding time of HT result shown in Figure 3. Increasing holding time did not show significant result. Although increasing holding time from 30–120 minutes. HT process at 180^0C, potassium content in liquid at 30 minutes only reach 79,2 gr/mL and at 120 minutes at the same temperature reach 87,8 gr/mL. It can explain that temperature most influence parameter in HT process.

The effect of holding time of HT result shown in Figure 3. Increasing holding time did not show significant result. Although increasing holding time from 30–120 minutes. HT process at 180^0C, potassium content in liquid at 30 minutes only reach 79,2 gr/mL and at 120 minutes at the same temperature reach 87,8 gr/mL. It can explain that holding time only give little effect in potassium removal HT.

The effect of size particle of HT result displayed in Figure 4. The experiment compared two size particle (particle A and particle B). The different size particle gives different result. At the same operating condition, Particle B (0.2-3mm) gives better result than particle A (>5mm). Particle B with small size particle have bigger surface area. Wider surface area lead the contact area between biomassa (PKS) and solvent (water). Wider surface area also could increase the potassium removal efficiency. From Figure 3, average potassium content in liquid product, particle B (91 gr/mL) gives much higher result compared than particle A (74 gr/mL).

The biomass PKS contain sillicon and potassium as their principal ash forming compounds. Utilize HT on PKS can reduced potassium which formed in K_2O, the HT could recovery the potassium average 30% from raw PKS based on operational temperature, size partcle and holding time as shown as Figure 5. Decreasing the potassium content expected to minimize the potency of ash agglomeration during gasification or combustion. The losses of potassium and some alkali and soluble compound effect the SiO_2 and CaO content increasing respectively shown as Table 2. SiO_2 content in HT given from calculation potassium mass balance from PKS and potassium content in liquid. The calculation of Table 2 assume that Na_2O, P_2O_5, SO_3 compund in solid removed completetely during HT. Si, Al, Fe, K, Ca content in solid from raw PKS and after HT displayed in Figure 6. Si, Al, Fe, and Ca increased along with a potassium decrease. Si, Al, Fe, and Ca assumed a unsoluble in water so there is only potassium, Na, P, and S dissolved in water shown in Table 2.

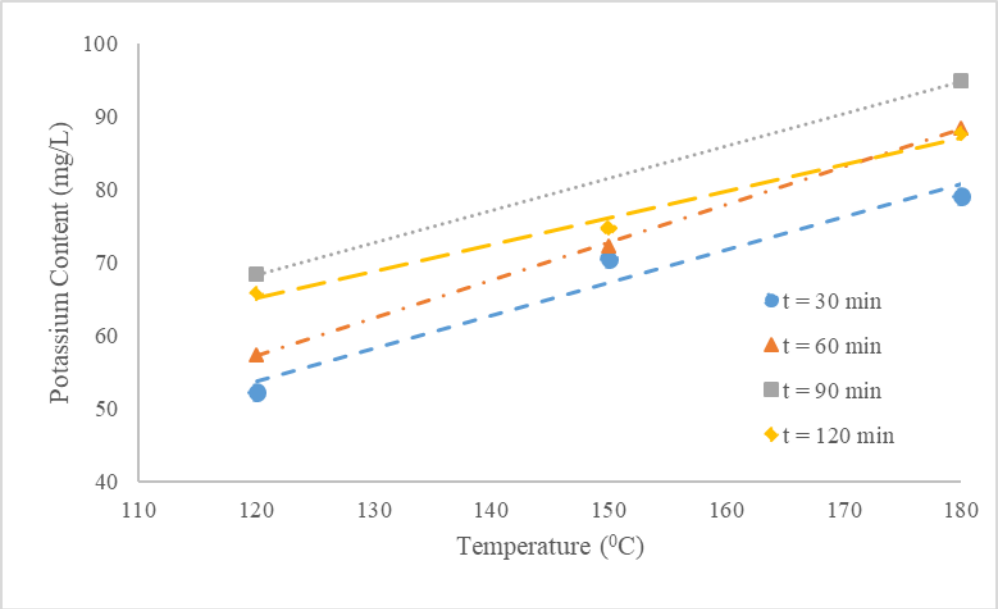

Figure 2. Effect of Temperature on Potassium Content Size A (>5mm)

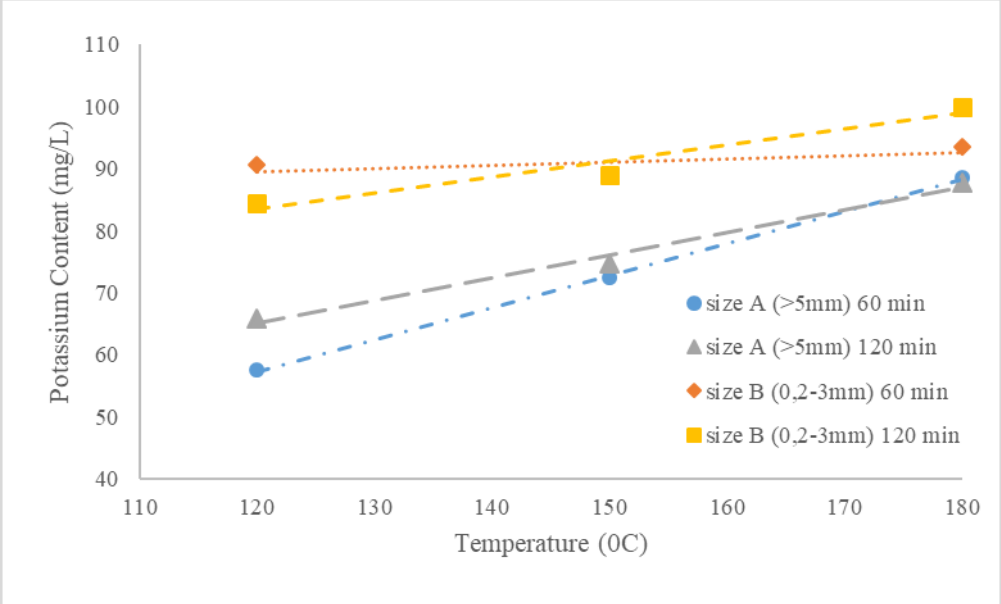

Figure 3. Temperature Effect on Potassium Content size A (>5mm) & Size B (0.2-3mm)

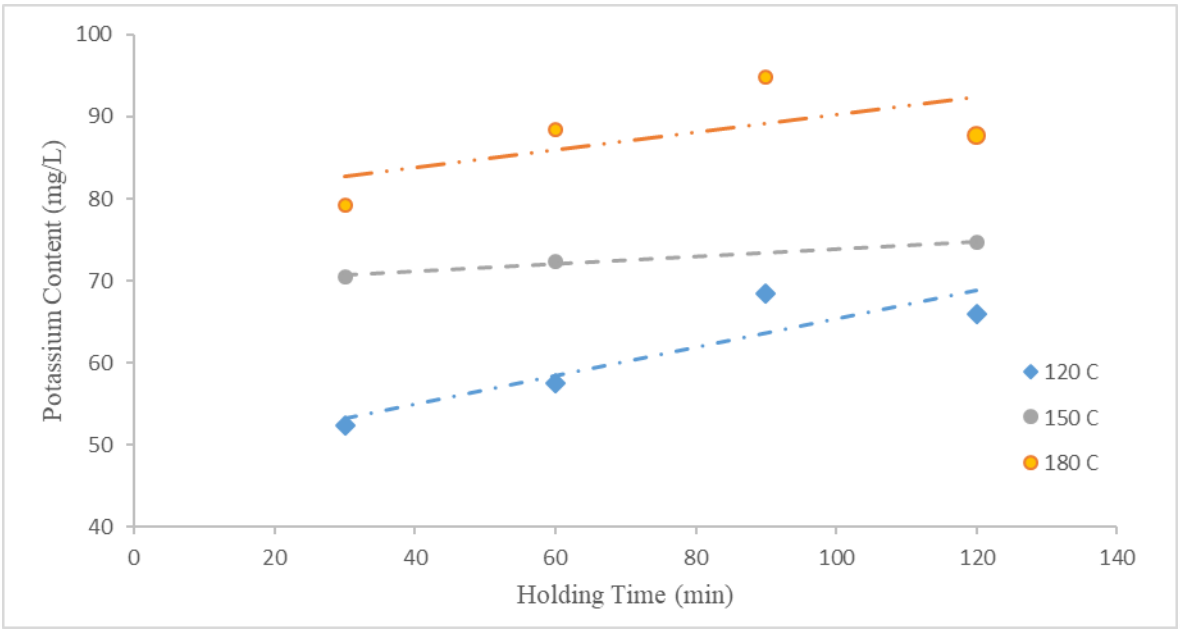

S

Figure 4. Effect of Holding Time on Potassium Content (size A)

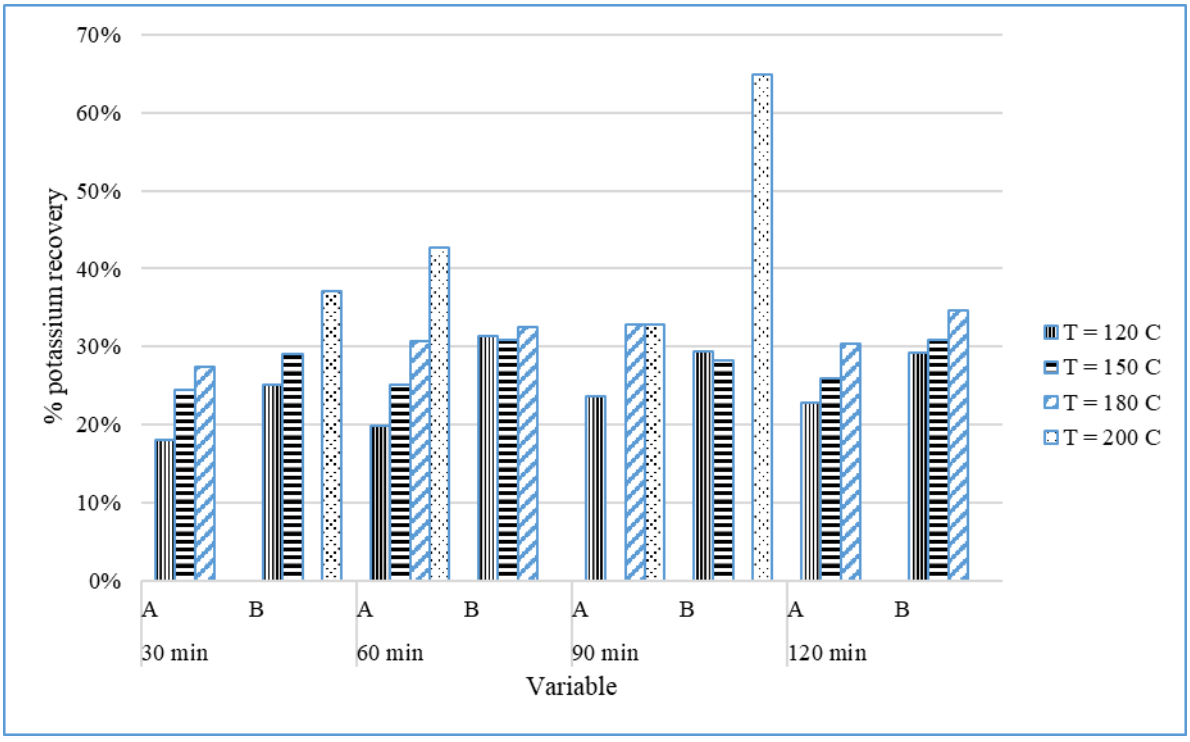

* Size A (>5mm), ** Size B = (0,2-3mm)

Figure 5. Effect of Parameter Operation in Potassium % Recovery

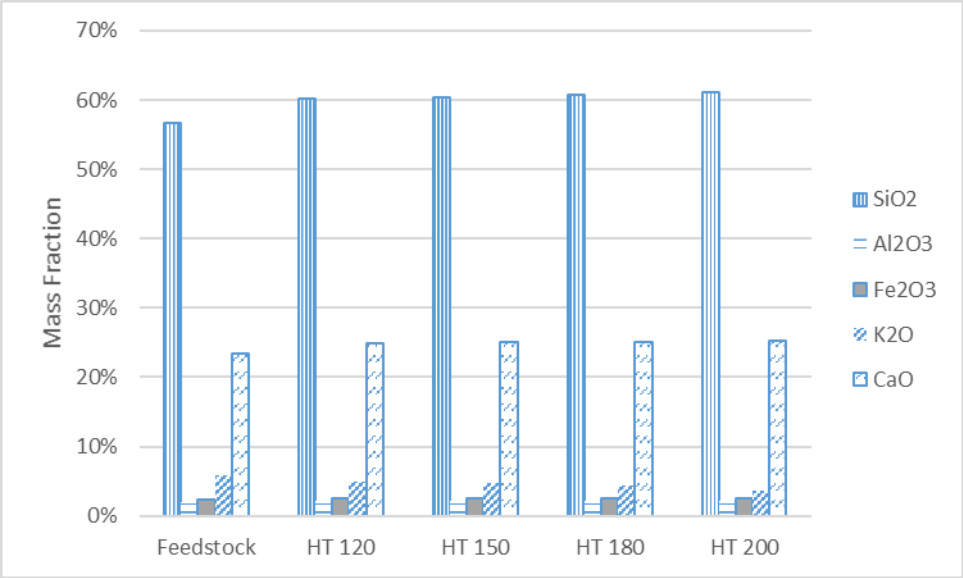

Figure 6. Effect of HT in Ash Composition

4. Conclusions

This present work is focusing on PKS utilization with Hydrothermal Treatment (HT). The improvement shown that HT could decrease the potassium content of PKS. The potassium removal efficiency show improvement based on graph shown that Temperature HT is the most influential parameter. At 200^0C, potassium content in the liquid product of HT as high as 187 mg/L. It was obtained from the HT at temperature of 200^0C and a holding time of 30 min. Other parameter like holding time and size particle are slightly affected the potassium removal process. The increase of potassium content during longer holding time and smaller size particle. Particle B (0,2-3 mm) which have smaller size than size A (>5mm) shown better performance. As expected that HT process could reduce potassium in PKS. Decreasing potassium content in could minimize ash agglomeration tendency during gasification.

Acknowledgement

The authors acknowledge the financial support from Kemenristekdikti under *Hibah Pascasarjana* for the research project entitled *Hydrothermal Treatment of Palm Kernel Shell for Production of Solid Fuel and Recovery of Potassium*. The authors like thanks to Institut Teknologi Bandung for the financial support under *World Class University Program 2017*.

References

[1] Pusdatin ESDM. Handbook of Energy & Economic Statistic of Indonesia 2014. Center of Data and Information (Pusdatin), Ministry of Energy and Mineral Resources Indonesia; 2014

[2] Elliot, DC. (2011) : Hydrothermal Processing, Thermochemical Processing of Biomass : Conversion into Fuels. In Brown RC, editor . Chemical and Power. Chicester, UK : John Wiley & Sons Ltd, p 200-31

[3] Hrncic, M.H. (2016) : Hydrothermal Treatment of Biomass for Energy and Chemical. *Energy 1-11*.
[4] Kubilay, T. A. (2014) : Review of Hydrothernal Biomass Processing. *A Renewable and Sustainable Energy Review*, **40,** 673-687.
[5] Liu Z. (2013) : Production of solid biochar fuel from waste biomass by hydrothermal carbonization. *Fuel*, **103,** 943–949.
[6] Libra, J.A, dkk. (2011) : Hydrothermal carbonization of biomass residuals: a comparative review of the chemistry, processes and applications of wet and dry pyrolysis. *Biofuels* **2(1)**, 89–124.
[7] Ninduangdee, P. (2015) : Thermogravimetric Studies of Oil Palm Empty Fruit Bunch and Palm Kernel Shell: TG/DTG Analysis and Modeling. *Energy Procedia*, **79**, 453-458.
[8] Novianti, S. (2014) : Upgrading of Palm Oil Empty Fruit Bunch Employing Hydrothermal Treatment in Lab-Scale and Pilot Scale. *Procedia Environmental Science***, 20,** 46-54
[9] Novianti, S. (2015) : Low Potassium Fuel Production from Empty Fruit Bunch by Hidrotermal Treatment Processing and Water Leaching. *Energy Procedia* **75**, 584-589.
[10] Nurdiawati, A. (2016): Production of Low-Potassium Solid Fuel from EFB by Employing Hydrothermal Treatment and Water Washing Process. *Journal of the Japan Institute of Energy*, **94**, 775-780.
[11] Susanto, H. (2017) *Hydrothermal Treatment of Oil Palm Empty Fruit Bunch for a Feedstock of Gasification Process*. Submitted to Bioenergy and Bioenergy.

Comparison of Double Decomposition and Direct Method to Produce Basic Metallic Soaps and Their Decarboxylation into Liquid Biohydrocarbon

Meiti Pratiwi*, Godlief F. Neonufa, Lidya Elizabeth, Astri Nur Istyami, Ronny Purwadi, Tirto Prakoso, and Tatang H. Soerawidjaja

Department of Chemical Engineering, Institut Teknologi Bandung, Bandung 40132 Indonesia

Basic metallic soap is one of the main feedstocks to produce liquid biohydrocarbon via decarboxylation process. In general, metal soaps were carried out with double decomposition method. It was proven could resulted liquid biohydrocarbon as renewable fuels (e.g. green diesel, jet bio fuel, and bio-gasoline) by pyrolysis and decarboxylation. However, the double decomposition method has two drawbacks; first, it was processed by two steps reaction, saponification vegetable oil or triglycerides with sodium hydroxide and followed by Na ion exchange with 2 or more valence metals ion to produce basic soaps; second, it could result a lot of salt waste as side product.

The manufacture of basic soap via direct reaction of triglycerides with metal hydroxides has been reported by Blachford (1982). This method conducted only by one step reaction and didn't result salt waste. The properties of basic soap from direct method as feed to produce liquid biohydrocarbon, especially renewable fuels would be investigated.

The decarboxylation products characteristics determined by the metal soap characteristics. Therefore, the objective of this research is to investigate the properties of basic magnesium soaps from palm stearine and their decarboxylation liquid products carried out from direct reaction and double decomposition method.

Palm stearine was used in this experiment consisted of 0.6%-mol lauric acid, 1.2%-mol myristic acid, 62.8%-mol palmitic acid, 5.7%-mol stearic acid, and 23.1%-mol oleic acid. Basic magnesium soaps were carried out with double decomposition and direct reaction palm stearine with magnesium hydroxide at 185°C for 3 hr.

The double decomposition process started by mixing oils and hot ethanol. Then, stirred the mixture with an aqueous solution of sodium hydroxide at 20% (w/w) until it has reached a firm consistency. While continually stirring, to this mixture is then added slowly a solution of $Mg(OOC_2H_5)_2.4H_2O$ in distilled water. The resulting basic soaps were filtered, washed and dried. Double decomposition process was performed in a glass batch reactor.

The direct reaction was carried out at 185 °C for 3 hours by reacting palm stearine, magnesium hydroxide, and water. The magnesium soaps were washed with distilled water and methanol, filtered, and dried at 60 °C. The dried soaps was grounded into magnesium basic soaps powder. The direct reaction was carried out in 100 ml SS mini-autoclave.

The decarboxylation process was performed in a 100 ml glass batch reactor at atmospheric pressure with water-cooled condenser. Decarboxylation proceeded at temperatures up to 370°C for 5 hours. The liquid products were collected in a beaker. These products were analyzed by gas chromatograph (Shimadzu 2010) equipped with a capillary column (RTX-1) and flame ionization detector.

The magnesium soaps were tested with a Scanning Electron Microscope (SEM) (Hitachi SEM SU3500). The SEM pictures showed that the basic magnesium stearine produced from

double decomposition and direct method have amorphous morphology. From infra-red analysis showed both saponification method have similar wavelength characteristics. The basic magnesium soaps from direct method is comparable with the double decomposition basic soaps.

The primary liquid hydrocarbon product decarboxylation of basic magnesium soaps is alkane. Decarboxylation of basic magnesium soaps via direct reaction yield greater alkene and i-alkane than double decomposition method. The main decarboxylation product is hydrocarbon C15, diesel range hydrocarbon.

This research is funded by Grand Riset Sawit (GRS K-16) Programme from BPDPKS – Indonesian Ministry of Finance 2016

References

[1] S. B. Elliott, The Alkaline-Earth and Heavy-Metal Soaps, 1946.

[2] Q. Dou, and K. M. Ng, Powder Technology, 2016, 301, 949-958.

[3] M. Gönen, et al., Ind. Eng. Chem. Res., 2005, 44, 1627-1633.

[4] T. O. Egbuchunam, et al., Polymer Degradation and Stabillity, 2007, 92, 107-116.

[5] C. C. Chang, S. W. Wan, Ind. Eng. Chem, 1947, 39, 1543-1548.

[6] H. Lappi and R. Alen, Journal of Analytical and Applied Pyrolysis, 2011, 91, 154-158.

[9] J. Fu, The Journal of Chem Sus Chem, 2011, 4, 481-486.

[10] A. Demirbas, et al., Energy Sources, 2006, 28, 619-626.

[11] K. S. Markley, Fatty Acids Their Chemistry, Properties, Production, and Uses, 1961.

[12] J. Fu, The Journal of Energy and Env. Sci., 2010, 3, 311-317.

[13] G. F. Neonufa, M. Pratiwi, A. N. Istyami, L. Elizabeth, S. S. Dewi, R. Purwadi, Proceeding of IJCAET 2016, 2016.

[14] J. Blachford, US Patent No 4,316,852, 1982.

[15] M. Pratiwi, et al., Proceeding of SOMCHE 2016, 2016.

[16] E. Santilan-Jimenes, M. Crocker, J Chem Technol Biotechnol, 2012, 87, 1041-1050.

---

*mei@che.itb.ac.id

Improvement of Process Control Course at Chemical Engineering Department UGM through the Use of MATLAB/SIMULINK

Muhammad Mufti Azis* and Sarto

Chemical Engineering Department, Faculty of Engineering, Universitas Gadjah Mada
Jl Grafika No. 2, Kampus UGM, Sleman, D.I. Yogyakarta 55281 Indonesia

** Corresponding Author's E-mail muhammad.azis@ugm.ac.id*

Abstract
Since 2014, undergraduate program of Chem. Eng. UGM is internationally accredited by IChemE. The department aims to improve a number of courses to obtain M-level accreditation in the near future by introducing a number of advanced material in undergraduate program. Process control course in semester VI embeds advanced material under the 2016 curriculum by increasing the portion of computer simulation. Here, we demonstrated the introduction of water heater simulation with MATLAB/SIMULINK to improve student's understanding on: open and closed loop simulations with SIMULINK. Although it appears as a simple problem at first, many students found that the water heater problem is very attractive as it offers flexibility which allows them to work from a simple SISO problem to a more complex MIMO problem. The use of SIMULINK helps students to visualize the simulation as well as to understand the stability of a system. The course evaluation showed that many students were very satisfied with the delivery of the water heater project as it may improve their skills on computer programming and help them to understand better the process control course.

Keywords: Process control course; computer simulation; MATLAB; SIMULINK

1. Introduction

Chemical Engineering Department UGM has updated the undergraduate curriculum in 2016. The spirit of Outcome Based Education (OBE) has been renewed in 2016 curriculum. The latest IChemE accreditation which took place in November 2016 has inspired Chem. Eng UGM to increase the B level to the M level of IChemE accreditation. This is going to be achieved through the introduction of advanced material (breadth, depth, practice and design) in undergraduate education[1]. The undergraduate program is accredited by IChemE since 2014. The latest evaluation was conducted in 2016 and currently Chem. Eng. UGM still holds the B level IChemE accreditation to 2022.

Process control course (TKK 3262) is one of the course that has been modified in 2016 Curriculum[2]. The credit has been increased from 2 to 3 SKS under 2016 Curriculum to increase the portion of computer simulation. In addition, an advanced course namely Process Modeling and System Dynamics (2 SKS) is also offered as an elective course for advanced course in Process Computation elective track[2].

Table 1. The learning outcome of Process Control (TKK 3262)[2]

1.	To explain types and working principles of measurement systems, controllers, control valves, and process control.
2.	To develop mathematical and transfer function models for dynamic processes.
3	To predict process stability and dynamic responses, and to design feedback control system.
4	To explain the advantages and disadvantages of some process control strategies.
5	To synthesize control system for certain equipment

Process Control course is offered in Semester VI with the prerequisite of Applied Chemical Engineering Mathematics and completion of Computation Lab work. In the course, the students learn the concept and principles of simple process control. The course subject covers modeling dynamic behavior of processes, control strategies, analysis and design of feedback control system, and principles of some common control structures in chemical industries. The learning outcomes of Process Control course are presented in Table 1.

Computer simulation is believed as an effective tool to improve student understanding to the process control mechanism. A number of recent textbooks have used MATLAB/SIMULINK package to illustrate the process control in chemical engineering processes, for instance in [3,4] and [5].

The aim of this article was to present the introduction of continuous water heater problem as a part of Process Control module which implement the utilization of MATLAB/SIMULINK. SIMULINK is a part of MATLAB that can be used to simulate dynamic systems. To facilitate model definition, SIMULINK adds a new class of windows called *block diagram* windows.

2. Modul description

2.1 Problem statement

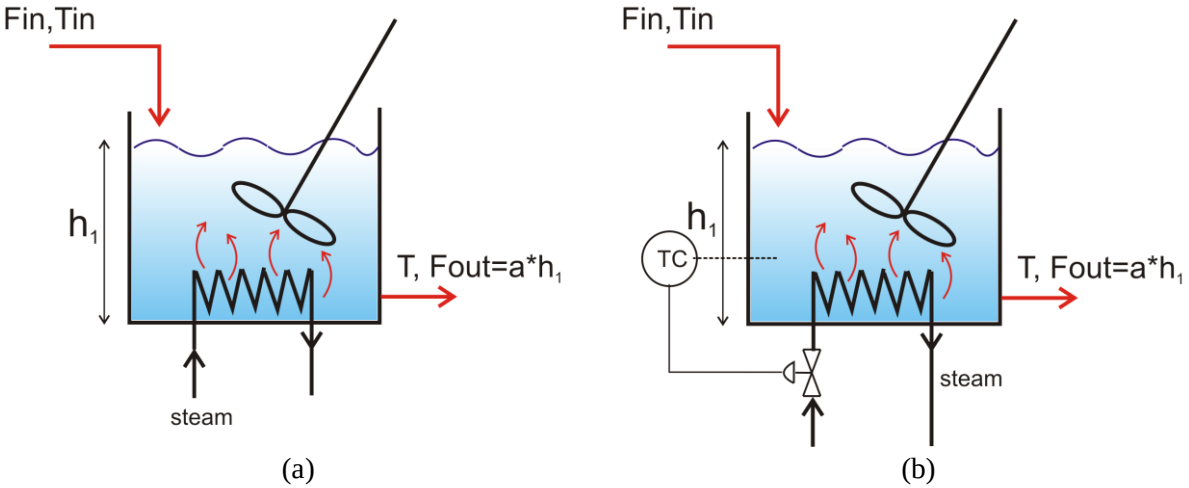

Fig. 1. Problem statement of a continuous water heater for (a) open loop and (b) closed loop system.

A continuous water heater is used to increase the water temperature from Tin to T with the aid of a coil steam heater. The coil whose steam temperature of Tst has been installed in the heater. The schematic diagram of the problem is described in Fig. 1. In this case, we would like to investigate the dynamic of

tank level as well as water temperature in the tank. For this purpose, we would like to simulate the system both in open loop and closed loop simulation. For open loop (Fig. 1a), the water heater operates without any controller. In contrary, the closed loop system (Fig. 1b) used feedback control mechanism to control the temperature by manipulating the flow of steam in the coil. The relationship between the steam flow and heat transfer coefficient UA is generally available as shown in [4]. Hence, temperature control is basically performed by manipulating the value of UA. Here, both *disturbance rejection* and *set point tracking* simulations have been conducted with P,PI and PID controller scheme. A number of assumptions were taken for the simulation:

a. The water density as well as heat capacity are constant despite of temperature change. The temperature fluctuation is expected to be relatively low in the present case.

b. The tank is perfectly mixed which cause the temperatures at all points inside the tank are the same.

c. The volumetric flow of Fout is assumed to have a linear relationship with the liquid level.

d. Transport delay is assumed to be negligible in the present case. It means that the response is immediate between the input and output of the system.

2.2 Problem formulation: mass and energy balances

Initially, one may assume that the system is in steady-state condition. The mass balance of the system with constant density can be written as:

$$A\frac{\partial h}{\partial t} = Fin - Fout$$

$$A\frac{\partial h}{\partial t} = Fin - a \cdot h \qquad (1)$$

Conversion to Laplace transform in *deviation variables* terms gave:

$$h'(s) = \frac{Fin'(s)}{A \cdot s + a} \qquad (2)$$

The deviation variable is defined as:

$$Y' = Y - Y_{steady\ state} \qquad (3)$$

In order to simulate the dynamic of temperature, one may set up the energy balance. The energy balance of the system can be written as:

$$\rho \cdot Fin \cdot Cp \cdot (Tin - Tref) - \rho \cdot Fout \cdot Cp \cdot (T - Tref) + UA \cdot (Tst - T) = \rho \cdot Cp \cdot A\frac{\partial}{\partial t}(T \cdot h) \qquad (4)$$

By assuming *Tref* = 0, we may obtain:

$$Fin \cdot Tin - a \cdot h \cdot T + \frac{UA}{\rho \cdot Cp} \cdot Tst - \frac{UA \cdot T}{\rho \cdot Cp} = A\frac{\partial T}{\partial t} + A\frac{\partial h}{\partial t} \qquad (5)$$

With the aid of linearization method, we yield:

$$Fin \cdot Tin - a \cdot h_{ss} \cdot (T - T_{ss}) - a \cdot T_{ss} \cdot (h - h_{ss}) + \frac{UA}{\rho \cdot Cp} \cdot Tst - \frac{UA_{ss}}{\rho \cdot Cp} \cdot (T - T_{ss}) \quad (6)$$

$$-\frac{T_{ss}}{\rho \cdot Cp} \cdot (UA - UA_{ss}) = A\frac{\partial T}{\partial t} + A\frac{\partial h}{\partial t}$$

Here, we set that Fin, UA, T and h may change with time. In contrary, parameters Tin, Tst, ρ and Cp were set to constant values. By using the Laplace transform and deviation variables, we may obtain the transfer functions. To simplify the derivation, let's denote that the left hand side on the equation (6) as LHS. Hence:

$$\left.\frac{\partial LHS}{\partial Fin}\right|_{ss} = Tin \qquad \left.\frac{\partial LHS}{\partial T}\right|_{ss} = -ah_{ss} - \frac{UA_{ss}}{\rho Cp}$$

$$\left.\frac{\partial LHS}{\partial UA}\right|_{ss} = \frac{Tst}{\rho Cp} - \frac{T_{ss}}{\rho Cp} \qquad \left.\frac{\partial LHS}{\partial h}\right|_{ss} = -aT_{ss}$$

Hence, the transfer function in Laplace domain and deviation variables is:

$$T'(s) = \frac{Tin}{(A \cdot s + C_2)} \cdot Fin'(s) + \frac{C_1}{(A \cdot s + C_2)} \cdot UA'(s) - \frac{(C_3 + A \cdot s)}{(A \cdot s + C_2)} \cdot h'(s) \quad (7)$$

Where:

$$C_1 = \frac{1}{\rho Cp}(Tst - T_{ss}) \qquad C_2 = a \cdot h_{ss} + \frac{UAss}{\rho Cp} \qquad C_3 = a \cdot Tss$$

3. Results and discussion

3.1 Block diagram of the system

From the formulation of the system (section 2.2), it is now possible to construct a block diagram which allows us to investigate simultaneous level and temperature dynamics by using SIMULINK. The simplified representation of the block diagram for open loop and closed loop simulations are shown in Fig. 2. As seen here, combination of equation (2) and (7) gave us the possibility to simulate the continuous water heater problem with level and temperature changes. It should be noted here that, arbitrary yet still reasonable numbers were used to define the transfer functions for the present case. Their definitions are:

$$G1 = \frac{Fin'(s)}{A \cdot s + a} = \frac{1}{2s + 1} \quad (8)$$

$$G2 = \frac{(C_3 + A \cdot s)}{(A \cdot s + C_2)} = \frac{2s + 30}{2s + 10} \quad (9)$$

$$G3 = \frac{Tin}{(A \cdot s + C_2)} = \frac{20}{2s + 10} \quad (10)$$

$$G4 = \frac{C_1}{(A \cdot s + C_2)} = \frac{0.1}{2s + 10} \quad (11)$$

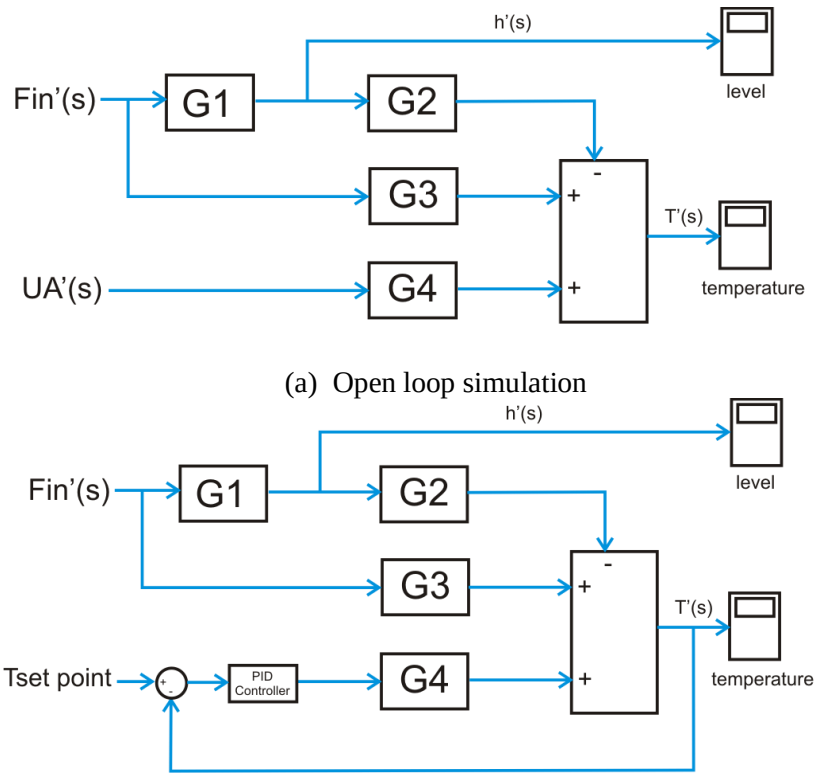

(a) Open loop simulation

(b) Closed loop simulation

Fig. 2. Block diagram of continuous water heater system for (a) open loop simulation and (b) closed loop simulation

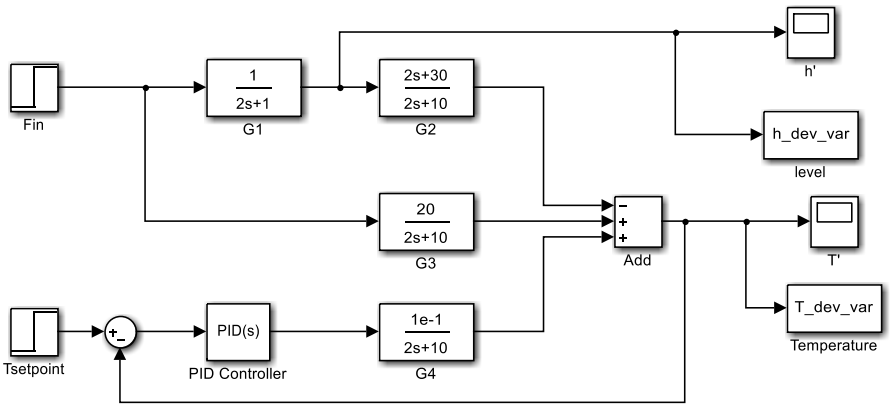

Fig. 3. SIMULINK block diagram for the simulation of a continuous water heater system. The system here can handle both the open loop and closed loop simulations. Open loop simulation can be conducted by deactivating the PID Controller block.

By setting up the transfer functions, it is now possible to set up the SIMULINK block diagram as presented in Fig. 3. The block diagram presented in Fig.3 was designed to simulate both the open loop and close loop simulation. The open loop simulation was performed by deactivating the PID controller. This is carried out by putting the value of P,I and D parameters to zero.

As seen in Fig 3, although it appears that the water heater case is a simple problem, it ,however, offers flexibility to students to investigate SISO and simple MIMO problems. Thus, the use of SIMULINK

has been able to help students to visualize the simulation as well as to understand the stability of a system.

3.2 Open-loop simulation

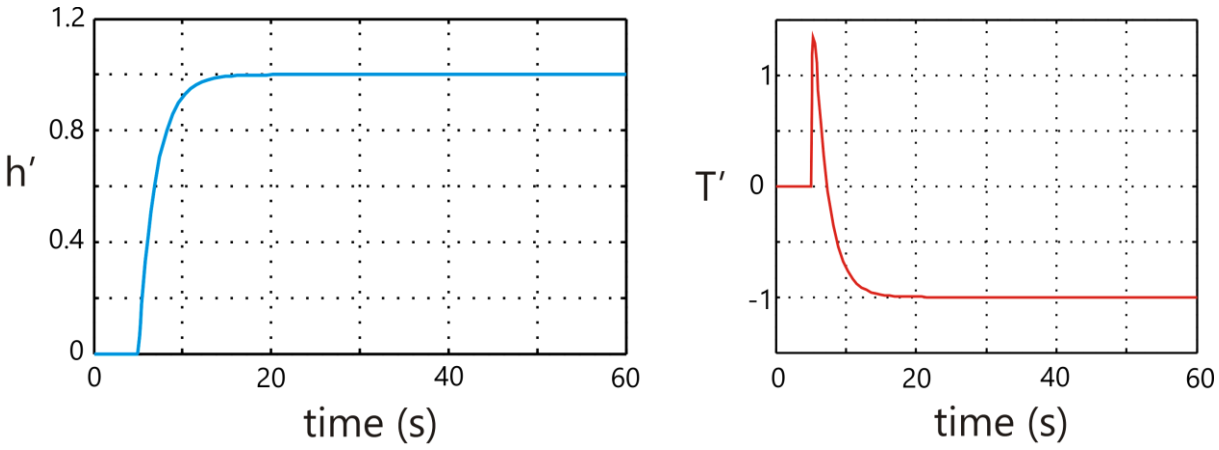

Fig. 4. The dynamic of tank level (left panel) and temperature (right panel) as a result of step increase of Fin 1 unit at t=5 s.

For the open loop simulation, a step increase of 1 unit in Fin was introduced at t=5 s. The response of the level and temperature is depicted in Fig. 4. As expected, the level increased immediately. As a result, the increase of liquid volume is accompanied by the decrease of temperature. The response is generally immediate at ca.15s to reach new steady state points. It is also important to note that there was an initial spike of temperature increase at t=5s upon the increase of Fin. This is not clearly understood and might be due to numerical issue in the simulation.

3.2 Closed loop simulation

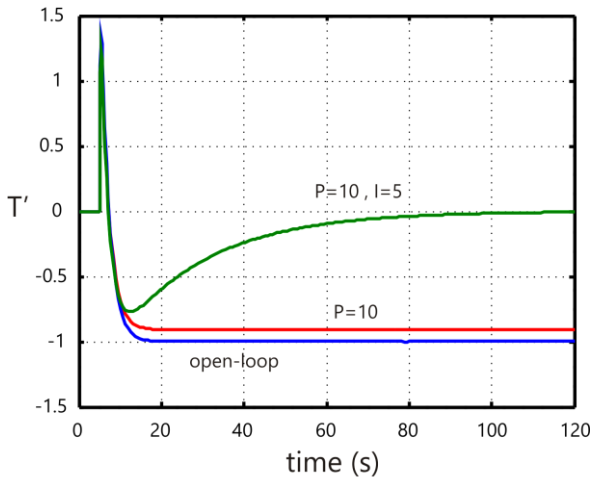

Fig. 5. The closed loop simulation result for disturbance rejection. The Fin had a step increase of 1 unit at t=5 s. The temperature response for P and PI controllers are shown. PID controller gave the same result as the PI controller and thus not shown.

The result of closed loop simulation can generally be divided as *disturbance rejection* case (Fig. 5) and *set point tracking* (Fig. 6). For disturbance rejection case (Fig. 5), an increase of Fin as much as 1 unit occurred at t=5s. The simulation results from the use of P and PI controllers were presented. As seen here, P only controller is unable to recover the temperature to the steady state value (0) with permanent

offset. Introduction of PI controller improve the performance of the system. The response is rather sluggish which took nearly 100 s to recover the temperature to steady state point. This is indeed can be improved by using different setting of P and I parameters. The result of PID controller is not shown as it typically gave the same response as the PI controller.

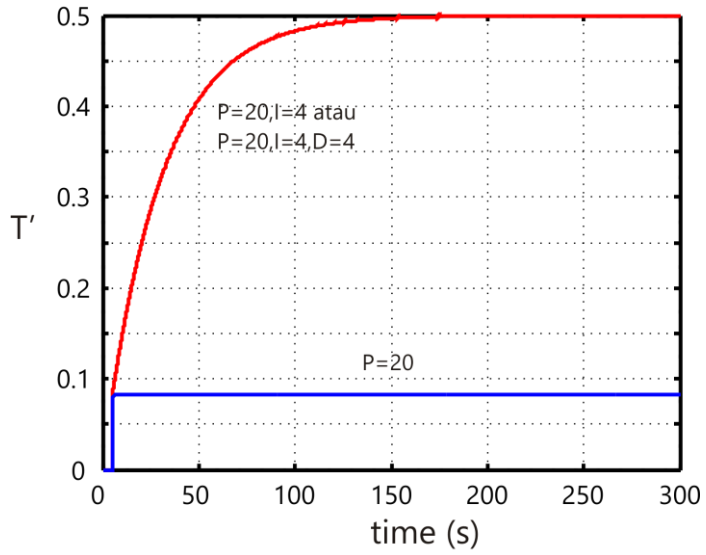

Fig. 6. The closed loop simulation result for set point tracking. The T set point had a step increase of 1 unit at t=5 s. The temperature response for P and PI controllers are shown. Similar to Fig. 5, the PID controller gave the same result as the PI controller.

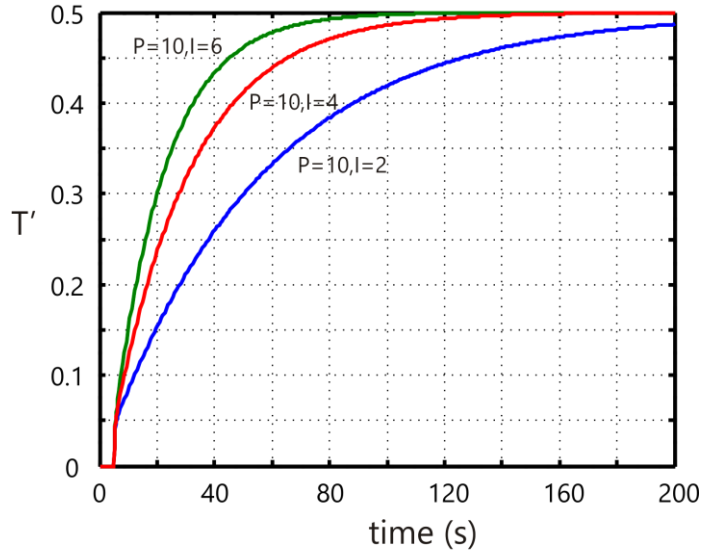

Fig. 7. The influence of Integral parameter in a set point tracking case. The T set point had a step increase of 0.5 unit at t=5 s.

The result from set point tracking case is presented in Fig. 6. Here, the T set point was increased 0.5 unit at t=5 s. Similar to the Fig 5, P only controller is unable to reach the new set point and exhibits permanent offset. However, PI controller as well as PID controller improved the performance and able to reach the new set point. The time to reach the target is ca. 150 s which is more than 2 minutes. It is also worth noting that the response of PI and PID are nearly identical which indicates that the D parameter plays a minor role in PID controller for the present case.

Fig. 7 shows the sensitivity analysis of temperature response by varying the integral parameter I for set point tracking case. As expected, the increase of I clearly increased the pace of temperature response.

3.3 Student evaluation

The student evaluation was conducted in the last week of the semester and the result is presented in Fig. 8. Here, we have 22 respondents which answers 4 evaluation criteria which is relevant for this study. The scoring is between 1 (poor) to 5 (excellent). Within that range, the average score for the evaluation criteria is between 3 to 3.7. As a result, it can be concluded that the level of student satisfaction as well as acceptance rate are relatively high.

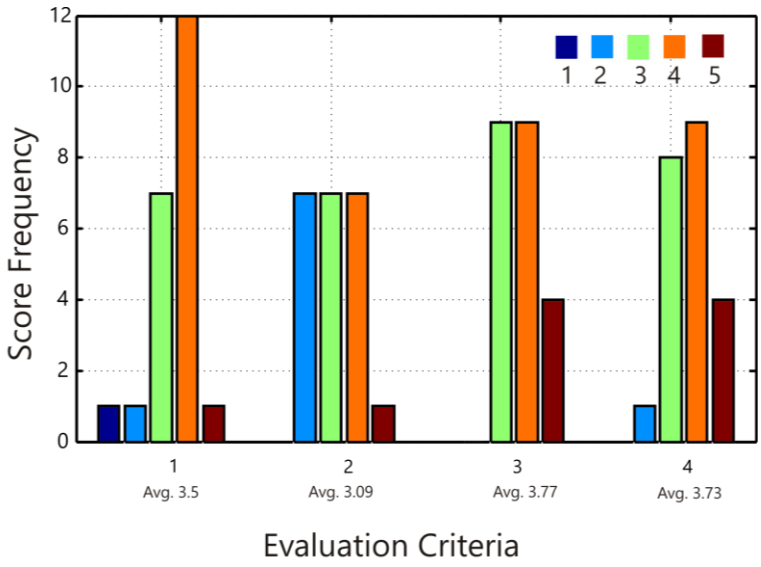

Fig. 8. The result of student evaluation form for 4 evaluation criteria: (1) The ability of teacher to explain the course material (2) How the course stimulates the student to learn (3) How the material relates with the learning outcomes (LO) of course (4) The benefit of the course for students. The sample population is 22 students.

It should be noted that utilization of SIMULINK was a new thing for the students under the 2016 curriculum. There was a learning curve for many of them and the course emphasized the ability of students to construct a block diagram from scratch. During the course, combination of MATLAB and SIMULINK approaches were employed which tested their skills in dynamic programming as well. In addition, the project that was delivered to student was actually larger. It had 3 modules to simulate water heater, isothermal CSTR and non-adiabatic and non-isothermal CSTR. Students worked in a group of 3 students. Project presentation as well as peer scoring sheet have been applied to the overall scoring. At the end of the course, each group shows their reflection on the course especially for the improvement of the course in the upcoming years.

4. Conclusions

There has been renewed interest to improve the implementation of outcome based education (OBE) at Chemical Engineering Department UGM. Process control course has been modified under the 2016 undergraduate curriculum to increase from 2 to 3 SKS. This modification was made to facilitate larger portion of computer simulation in the course. Here, we have introduced utilization of MATLAB/SIMULINK to simulate the dynamic process of water heater system. Understanding of the basic principles from a simple dynamic model and convert it to block diagram in open and closed loop environment are essential to fulfil the learning outcome of the process control course. The use of

SIMULINK has been able to help students to visualize the system better. Eventually, student evaluation showed that many students were very satisfied with the delivery of the water heater project as it may improve their skills on computer programming and help them to understand better the process control course.

Acknowledgements

We would like to thank the students at Process Control Course 2017 for their input and suggestion to the course. Chemical Engineering Department UGM is greatly acknowledged for all the support to this study.

References

1. IChemE, Accreditation of chemical engineering programmes, IChemE, 2015.
2. Chem.Eng.Dept. UGM, Undergraduate Program Curriculum Chemical Engineering UGM, 2016
3. Seborg, D.E., Edgar, T.F, and Mellichamp, D.A., Process Dynamics and Control, John Wiley & Sons, New York, 1989.
4. Marlin,T.E., 2015,"Process Control: Designing Processes and Control Systems for Dynamic Performance" , available from http://www.pc-education.mcmaster.ca/, 2015.
5. Coughanowr, D.R. and LeBlanc, S.E., "Process System Analysis and Control", 3rd edition, McGraw-Hill's, New York, 2009

Catalytic Conversion of Glucose and Cellulose to Lactic Acid by Alkaline Catalyst

Apsari Puspita Aini, Carolus Borromeus Rasrendra*, Johnner P. Sitompul

Department of Chemical Engineering, Faculty of Industrial Technology, Institute of Technology Bandung, Jl. Ganesa 10, Bandung 40132, Indonesia

** Corresponding Author's E-mail: cbr@che.itb.ac.id*

Abstract

This research was conducted to determine the effect of the alkaline catalyst in hydrothermal conversion of glucose and cellulose to lactic acid. Calcium hydroxide and barium hydroxide were used as catalysts in this experiment. The results show that the yield of lactic acid from glucose was higher compared to cellulose as raw material, 32.08% C-mol, and 4.3% C-mol, respectively. It was caused by incomplete hydrolysis of cellulose to glucose. The high crystalinity of cellulose affects the catalyst access on cellulose chain. Another method for increasing the yield of lactic acid was by the addition of pressurized nitrogen and $NaHCO_3$ into the reactor during the reaction time.

Keywords : barium hydroxide, calcium hydroxide, glucose, cellulose, lactic acid

1. Introduction

Lactic acid is one of the platform chemicals that widely used for several applications in industry, such as food industry, pharmacy, textile, and as a feedstock to be converted into other chemicals, especially Poly Lactic Acid. Lactic acid is included in the top 30 platform chemicals with significant market growth potential in PLA and solvent industries. The growth rate in the industry segment is 19% per year. A market research and consulting company, Grand View Research, in 2014 reported that lactic acid global market is estimated to grow from 714.2 kilotons to 1960.1 kilotons[1]. Several methods can be carried out to produce lactic acid, such as fermentation route, chemical synthesis, and catalytic conversion[2–4]. Many researchers conducted the production of lactic acid with catalytic conversion due to some disadvantages possessed by other methods. Chemical synthesis must be depending on other chemicals as feedstock, i.e. lacto-nitrile, while fermentation route needs more intensive control during the reaction, such as pH, temperature, sterilization media, longer reaction time, etc.

Triose, hexose, cellulose or lignocellulosic biomass could be used as feedstock in the production of lactic acid[3,5–9]. The production of lactic acid with glucose and cellulose as raw materials in this study was the preliminary research before it will be applied to produce lactic acid from lignocellulosic biomass. Lewis acid catalyst is a highly selective catalyst in the production of lactic acid. However, the high level of toxicity, the finding for other alternative catalysts needs to be carried out[6,8,9]. In this study, i.e. $Ba(OH)_2$ and $Ca(OH)_2$ were used as catalyst. The selection of these catalysts was based on the research conducted by Esposito and Antoniette in 2013, and Li in 2014. Esposito and Antonietti (2013) conducted a research with glucose as a feedstock. The yield of lactic acid of 49%, 50%, and 53% were achieved at a temperature of 220°C using 0.05 M $Ca(OH)_2$, $Sr(OH)_2$, and $Ba(OH)_2$ with 12 h reaction time. Fewer by-product yield, such as formic acid (4.4-5.9%) and acetic acid (5-7.6%) showed that $Ca(OH)_2$, $Sr(OH)_2$, and $Ba(OH)_2$ were selective catalysts for production of lactic acid. In addition to achieving high yields, the alkaline catalyst is also safer for human or

environmental than other catalysts. The addition of pressurized nitrogen into the reactor during the reaction was intended to increase the yield of lactic acid, based on the previous research conducted by Wang in 2013 and Tang in 2014. The yield of lactic acid of 68% can be achieved with the addition of 20 bar N_2[8]. The objective of this research were to evaluate the effect of using alkaline catalysts $Ca(OH)_2$ and $Ba(OH)_2$ on the yield of lactic acid and other by-products, and to evaluate the methods for production of lactic acid from glucose and cellulose using catalytic conversion using a pressurized hydrothermal system (inert gas, at a pressure of 20-40 bar and temperature above 180°C).

2. Experimental

2.1 Materials

The raw materials in this experiment were glucose and cellulose microcrystalline. Glucose pro analysis was purchased from Merck, with purity of 99,9%. Microcrystalline cellulose was supplied from Kuraray Co., Ltd. Organic acids used in this experiment were purchased from Merck, i.e. lactic acid with purity of 90%, formic acid with purity of 98-100%, and acetic acid with purity of 100%. $Ba(OH)_2.8H_2O$ and $Ca(OH)_2$ from Merck were used as the alkaline catalyst in this experiment.

2.2 Conversion Glucose and Cellulose to Lactic Acid

This experiment was carried out in a high-pressure stainless steel autoclave reactor equipped with a stirrer to homogenize the raw materials and the catalyst. Raw materials were put into the reactor that contains 80 ml catalyst with concentration of 0.1 M. The solution was heated until it reached the desired temperature and was maintained at constant temperature for 4 h.

In order to increase the yield of lactic acid, pressurized N_2 and $NaHCO_3$ were also used in this experiment. The variation of pressurized nitrogen was 20-40 bar at 200°C. Before the reaction start, the reactor with raw material and catalyst was purged with N_2 to remove oxygen inside the reactor. Heating of the reactor was carried out until it reached the desired temperature. Then pressurized N_2 was inserted into the reactor. The variation of $NaHCO_3$ concentrations were 0.05 M and 0.31 M. The formation of CO_2 gas during the reaction using $NaHCO_3$ was expected to increase the yield of lactic acid.

2.3 Analytical Method

High Performance Liquid Chromatography (HPLC) was used for quantitative and qualitative analysis. Lactic acid and other organic acids as by-product were injected to HPLC. The HPLC was using Phenomenex Rezex ROA-Organic Acid H^+ column (300 x 7.8 mm) with an RI detector and 0.005 M H_2SO_4 as the mobile phase. It was operated at 60°C with flow rate 0.6 ml/min. Calibration of standard curve from several concentrations of D-Glucose, lactic acid, formic acid, and acetic acid were needed to determine the concentration of lactic acid from the conversion of glucose. All of the samples were eluted into column and the peak of organic acid was detected in certain retention time. Calibration curve for glucose and organic acid was made by plotting the concentration and the peak area of chromatography. The value of R square must be more than 98% to get high data accuracy.

3. Results and Discussion

3.1 Conversion glucose and microcrystalline cellulose to lactic acid

Conversion of glucose and cellulose to lactic acid was the preliminary experiment to choose the best alkaline catalyst, before converting lignocellulose biomass to lactic acid. It was also

examined to validate the experiments which have been done by previous several researchers[10,11]. This experiment was conducted in a stainless steel autoclave reactor at 200°C, with reaction volume of 80 ml, for 4 h reaction time. The concentration of glucose and microcrystalline cellulose were 0.025 M[10] and 5%w/v, respectively. The yield of lactic acid from glucose and microcrystalline cellulose showed in Table 1.

Table 1. The yield of lactic acid from glucose and cellulose

raw material	catalyst	Yield (% C-mol)			
		lactic acid	formic acid	acetic acid	levulinic acid
glucose	$Ca(OH)_2$	28,6	7	1,76	-
	$Ba(OH)_2$	32,08	3,6	3	-
a* glucose	PbO /γAl_2O_3	25.80	-	5.63	5.25
b* glucose	$PbCl_2$	17.38	-	2.13	24.67
microcrystalline cellulose	$Ca(OH)_2$	3,3	2,5	0,2	-
	$Ba(OH)_2$	4,3	1,1	0,3	-
c* Steam explosion EFB	$Ba(OH)_2$	21.57	7.16	14.7	6.6
d* Steam explosion EFB	$PbCl_2$	23.67	1.5	4.94	1.003

a* and b* Nabila and Nursyifa, (2015). Temperature 220°C. Glucose 13.8 mmol.
c* and d* were assumed as amorphous cellulose. Temperature 240°C. Biomass 5%w/v.

The yields of lactic acid were shown in Table 1. Lactic acid produced by using glucose as raw material have higher yield than those from microcrystalline cellulose. Glucose was the most constituent unit of carbohydrate so that it could be more easily converted into other compounds such as lactic acid. The reaction pathway of glucose conversion to lactic acid was shorter than those of microcrystalline cellulose. Microcrystalline cellulose needs hydrolysis process to form glucose before it converted to lactic acid. It was supported by the data shown in Table 1. The yield of amorphous cellulose (steam explosion EFB) higher than microcrystalline cellulose. It was in agreement with previous research conducted by Wang et. al (2013). Wang et al (2013) showed that the similar yield of lactic acid from ballmill cellulose (68% mol) and microcrystalline cellulose (62% mol) with crystallinity 85% were achieved in different reaction time. Ball mill cellulose needed shorter reaction time (4 h) than microcrystalline cellulose (15 h). It means that with high crystallinity, the catalyst was difficult to cleavage the cellulose chain into monosaccharide for afterward be converted to lactic acid[8].

The yield of lactic acid from glucose in this experiment (28.6% C-mol and 32.1% C-mol) was in agreement with previous research conducted by Esposito and Antonietti (2013) and Li (2014). The yield of lactic acid conducted in the experiment Esposito and Antonietti (2013) was 53%, 49%, and 40% using $Ba(OH)_2$, $Ca(OH)_2$, and $Sr(OH)_2$, respectively. Those yields of lactic acid were higher than those of our experiment. It was because the reaction time in their experiment was 12 h and the temperature was 220°C. In the experiment conducted by Li (2014), the yield of 56% C-mol lactic acid was achieved using 0.25 M $Ba(OH)_2$ as catalyst at 58°C. The higher the concentration of the catalyst used, the higher the yield of lactic acid can be achieved. Esposito and Antonitte showed that $Ba(OH)_2$ was the best alkaline catalyst compared with other catalysts. It was because the radius ionic of Ba^{2+} (0.136 nm) is larger than Ca^{2+}(0.1 nm). The larger the ionic radius, the better the catalytic effect occurs. It also occurs in the production of lactic acid from glycerin using $Mg(OH)_2$ and $Ca(OH)_2$ catalysts, where the yield of lactic acid obtained is 18.3% mol using $Ca(OH)_2$ and 15.7% mol using

$Mg(OH)_2$[12].Beside of producing lactic acid as a main product, the conversion of glucose and cellulose also produces other organic acids as by-products, such as formic acid, acetic acid, and levulinic acid. The conversion of lactic acid with glucose as a feedstock does not indicate the formation of levulinic acid. The chromatogram of glucose and cellulose conversion to lactic acid is shown in Figure 2. In chromatogram with glucose as a feedstock, there was no glucose peak (retention time ± 9.7 minutes). This shows that glucose was perfectly converted. In contrass, in chromatogram with cellulosic feedstock, there was still a peak of glucose but at very small concentration. The levulinic acid compound also neither appeared at the chromatogram (a) nor (b). In conversion of cellulose to lactic acid, an unidentified compound was detected at ± 11-12 minute retention time, which was predicted as an intermediate compound.

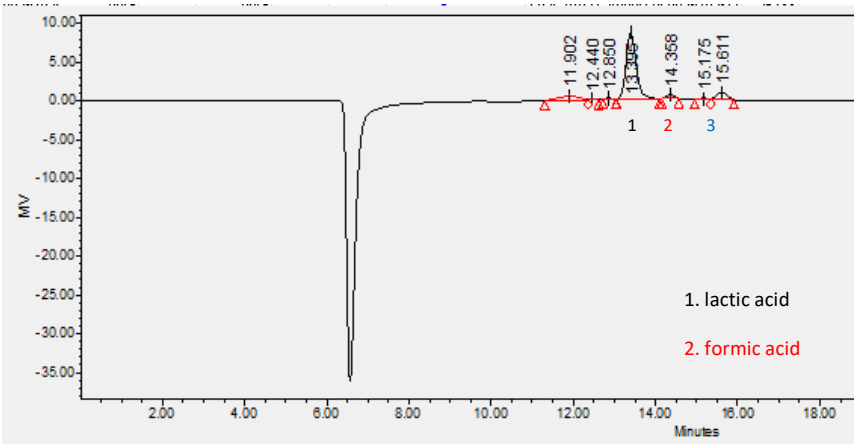

(a)

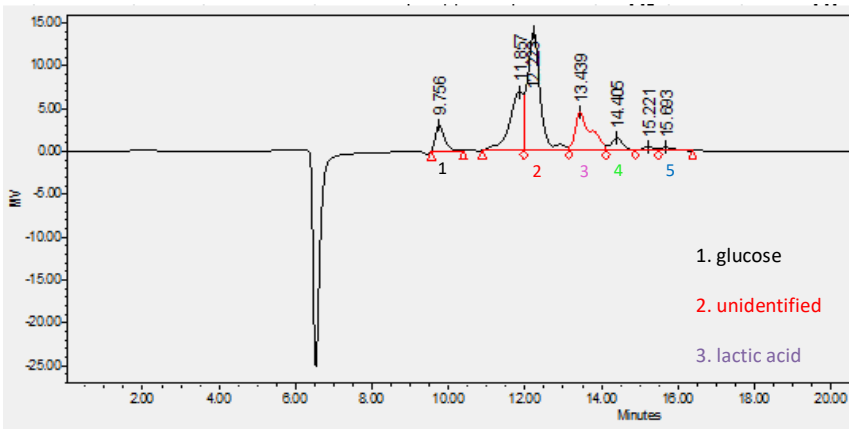

(b)

Figure 2. The HPLC Chromatograms of conversion glucose (a), and microcrystalline cellulose (b) to lactic acid at 200°C using 0.1 M $Ba(OH)_2$ during 4 h reaction time

Compared with alkaline catalyst, lewis acid catalyst (Pb) was more selective catalyst. It could be seen from the low yield of by-products obtained with glucose as a raw material. The highest yield of lactic acid (25.80% C-mol) was achieved using PbO/Al_2O_3 as heterogenous catalyst. However, due to of the high-level toxicity of Pb, the alkaline catalysts could be other alternative options.

3.2 The effect of pressurized nitrogen toward conversion of glucose to lactic acid

The addition pressurized N_2 was applied into an autoclave reactor that contains glucose as feedstock. The result of this experiment was showed in table 2. The temperature was conducted at 200°C with a glucose concentration of 0.025 M for 4 h reaction time.

Table 2. The yield of lactic acid from glucose with pressurized nitrogen

raw material	concentration	nitrogen (bar)	yield of lactic acid (%C-mol)
glucose	0.025M	-	32,08%
glucose	0.025M	20	32,12%
glucose	0.025M	30	29,33%
glucose	0.025M	40	29,67%

Table 2 showed that the addition of pressurized N_2 (0-40 bar) did not increase the yield of lactic acid. The results of this experiment were contradicted with the research done by Wang et al. 2013 on the conversion of cellulose to lactic acid with Pb^{2+}. The yield of lactic acid was 68 %-mol with operating conditions at 190°C and 20 bar N_2. Pressurized nitrogen and temperature of 200°C was used in the reactor to depolymerize cellulose to glucose, can cleavage C_6 into C_3, and converted it to lactic acid. At high temperatures the water ionization (kw) increases, causing weakening of the hydrogen bond and the increase in hydronium ions $(H_3O)^+$ which acts as catalyst for breaking the β-(1,4) glycosidic bonds at C_1 and C_4 atoms[13–15].

The effect of $NaHCO_3$ addition to increase the yield of lactic acid was also studied. $NaHCO_3$ was used as a substitute for CO_2 gas. When CO_2 gas dissolves into the water, HCO_3^- was formed, which contributes to the process of cleaving glucose chain to triose and afterward converted into lactic acid.

Table 3. The yield of lactic acid from glucose using $NaHCO_3$

raw material	concentration	$NaHCO_3$	Yield of lactic acid (% C-mol)
glucose	0.025M	-	32.08
glucose	0.025M	0.05357 M	24.51
glucose	0.025M	0.3125 M	11.38

Table 3 shows that the yield of lactic acid did not increase. Brown color appeared in product solution indicates that the addition of $NaHCO_3$ during reaction leads to the formation of byproducts such as HMF or furfural. However, due to the unavailability of standard solutions for both compounds, the product of the reaction could not be detected.

3. Conclusion

The highest lactic acid yield was achieved using $Ba(OH)_2$ as an alkaline catalyst. The yield of lactic acid with glucose as raw material (32.1% C-mol) was higher than others, followed by amorphous cellulose. It was due to the high crystallinity of cellulose which made the catalyst difficult to access the cellulose chain. The alkaline catalysts could be other alternative options compared with lewis acid catalyst due to high-level toxicity of Pb,

Acknowledgements

This research is funded by Indonesia Estate Crop Fund For Palm Oil through the Ministry of Finance and Research Incentive Program The National Innovation System through the Ministry of Research and Technology.

References

1. Research, G. V. Lactic Acid And Poly Lactic Acid (PLA) Market Analysis By Application (Packaging, Agriculture, Transport, Electronics, Textiles) And Segment Forecasts To 2020.(2014).
2. John, R. P., G.S., A., Nampoothiri, K. M. & Pandey, A. Direct lactic acid fermentation: Focus on simultaneous saccharification and lactic acid production. *Biotechnol. Adv.* 27: 145–152(2009).
3. Onda, A., Ochi, T., Kajiyoshi, K. & Yanagisawa, K. A new chemical process for catalytic conversion of d-glucose into lactic acid and gluconic acid. *Appl. Catal. A Gen.* 343**:** 49–54(2008).
4. Datta, R. & Henry, M. Review Lactic acid: recent advances in products, processes and technologies a review. *J. Chem. Technol. Biotechnol.* 82: 1119–1129(2006).
5. Bicker, M., Endres, S., Ott, L. & Vogel, H. Catalytical conversion of carbohydrates in subcritical water: A new chemical process for lactic acid production. *J. Mol. Catal. A Chem.* 239: 151–157(2005).
6. Rasrendra, C. B., Fachri, B. A., Makertihartha, I. G. B. N., Adisasmito, S. & Heeres, H. J. Catalytic conversion of dihydroxyacetone to lactic acid using metal salts in water. *ChemSusChem* 4: 768–777(2011).
7. Tang, Z. *et al.* Transformation of cellulose and its derived carbohydrates into formic and lactic acids catalyzed by vanadyl cations. *ChemSusChem* 7: 1557–1567(2014).
8. Wang, Y. *et al.* Chemical synthesis of lactic acid from cellulose catalysed by lead(II) ions in water. *Nat. Commun.* 4: 2141(2013).
9. Sitompul, J. P. *et al.* Catalytic Conversion of Empty Fruit Bunch of Palm Oil for Producing Lactic Acid. *Procedia Chem.* 9: 88–93(2014).
10. Esposito, D. & Antonietti, M. Chemical conversion of sugars to lactic acid by alkaline hydrothermal processes. *ChemSusChem* 6: 989–992(2013).
11. Li, M. Value-added Bioproducts Development from Lignocellulosic Biomass. (Auburn University, 2014).
12. Shen, Z. *et al.* Effect of Alkaline Catalysts on Hydrothermal Conversion of Glycerin into Lactic Acid. *Ind. Eng. Chem. Res* 2: 8920–8925(2009).
13. Chin, S. X., Tasirin, S. M., Chan, H. & Chia, H. Catalytic Conversion of Empty Fruit Bunch (EFB) Fibres into Lactic Acid by Lead (II) ions. 11: 2186–2201(2016).
14. Ruiz, H. A., Rodr??guez-Jasso, R. M., Fernandes, B. D., Vicente, A. A. & Teixeira, J. A. Hydrothermal processing, as an alternative for upgrading agriculture residues and marine biomass according to the biorefinery concept: A review. *Renew. Sustain. Energy Rev.* 21: 35–51(2013).
15. Chan, C. H., Chia, C. H., Zakaria, S., Sajab, M. S. & Chin, S. X. Cellulose nanofibrils: a rapid adsorbent for the removal of methylene blue. *RSC Adv.* 5: 18204–18212(2015).

The Effect of Propanoic Acid in Separation and Purification of Lauric Acid from Palm Kernel Oil

Ana Kemala Putri Jauhari[a], Ifan Murdiyadi[a], Johnner Sitompul[a,b*], and C. B. Rasrendra[a]

[a]*Department of Chemical Engineering*
[b]*Department of Food Engineering*
Faculty of Industrial Technology
Institute of Technology Bandung, Bandung 40132, Indonesia

[*] *Corresponding Author's E-mail sitompul@che.itb.ac.id*

Abstract

Lauric acid is one of the organic acids with a variety of applications in different industries. One of the widely available sources of lauric acid in Indonesia is Palm Kernel Oil (PKO). The amount of lauric acid in PKO is relatively high, typically 40-52%-wt. The objective of this research is to identify the effects of propanoic acid in the separation and purification of lauric acid from PKO. Furthermore, the key deliverables of this research is to determine optimum operating conditions at which lauric acid can be produced with the highest yield and purity. Both purification and separation methods for lauric acid are sequentially carried out through transesterification, vacuum distillation, and followed by hydrolysis. The transesterification was carried out using methanol and sulfuric acid as a catalyst, followed by distillation process at a vacuum pressure of 3.33 kPa. The hydrolysis was performed in the presence of sulfuric acid and propanoic acid as the catalysts. Moreover, propanoic acid was utilized as a catalyzing agent that navigated the hydrolysis reaction towards the formation of lauric acid. The purity of resulted lauric acid was then analyzed with a set of Gas Chromatography (GC) instruments. The experimental results showed that the highest yield of lauric acid 98.81%-wt with a purity level of 94.95%-wt. These results were obtained through hydrolysis process with a molar ratio of propanoic acid to methyl ester of 5, the ratio of mass of sulfuric acid to methyl ester 17.20%-wt, and an overall reaction time of 4 hours.

Keywords: Lauric acid; Hydrolysis; Yield; Purity; Propanoic acid

1. Introduction

Lauric acid is one of three saturated acids found in nature other than its two monologues, stearic acid and palmitic acid. Lauric acid has a broad range of applications in various industries, in food, chemical and pharmaceutical industries. It is widely used for the production of surfactants, transparent soap starting precursors, and drugs. In addition, pure lauric acid is required as a feedstock for the manufacture of Dodecanedioic Acid (DDDA). These compounds are being developed for the production of various polymeric materials. Its application is also extended to food industries where it is consumed as flavor enhancers, antimicrobial agents, and antifungal agents (Eavis et al., 1997; Rihakova et al., 2001; Sitompul et al., 2013; Walter et al., 2003).

As one of the largest palm oil producing countries in the world, Indonesia is a land abundant with palm oil and coconut oil resources which, in turn, render its derivatives, including and CNO and PKO, relatively easy to obtain. Currently, the demand for lauric acid is normally fulfilled from Coconut Natural Oil (CNO) and Palm Kernel Oil (PKO), due to its high lauric acid content of 44-52%-wt (Chempro Technovation Pvt, Ltd., 2015). Based on Cognis Oleochemicals (2015), a number of vegetable oils, likewise with CNO, have a high lauric acid content, one of which is Palm Kernel Oil

(PKO) with 40-52% of lauric acid as its content. This type of oil is classified as a vegetable oil produced from the palm oil industry. According to Basiron and Weng (2004), oil derived from palm fruits has advantages over other natural oils in the sense that they are more economically competitive and ready to use compared to all available vegetable oils. With its vast abundance, clipped with a high content of lauric acid, PKO can be considered as a potential raw material for producing lauric acid in a sizeable capacity.

With the broadly extensive applications of lauric acid in various industries, there is a growing request that the lauric acid output be boosted to meet the continuously increasing market demand. One of the methods to produce lauric acid is through transesterification reaction followed by hydrolysis. Previously, many researchers elsewhere have attempted to discover the optimum operating condition in transesterification process. On the other hand, there have not been many hydrolysis processes capable of producing lauric acid with high conversion and purity. Previously, Liu (2001) conducted an experiment of the hydrolysis reaction using propanoic acid and was able to produce lauric acid with a conversion of 90%-wt. This outcome was obtained under an operating temperature of 90^{o}C at atmospheric condition with a 2-hour reaction time. In industrial application, the lauric acid could be produced from high pressure hydrolysis of PKO, even though now the pressure has been significantly reduced by conducting methanolysis before carrying out hydrolysis (Cognis Oleochemicals, 2015).

Further research is needed to produce lauric acid with a higher conversion rate and relatively mild operation. Additionally, a certain level of purity standard is invariably applicable to lauric acid for industrial applications. Thus, it is necessary to investigate into the operating conditions that would lead to resulting in lauric acid with high purity. The objective of this research is to identify the effects of propanoic acid in separation and purification of lauric acid from RBDPKO. In addition, the key deliverables of this research include determining the optimum operating conditions at which the lauric acid can be produced with the highest yield and purity.

2. Experimental

2.1 Feedstock

The raw materials used are Refined, Bleached, and Deodorized Palm Kernel Oil (RBDPKO) obtained from local companies located in Sumatra Island. In the transesterification reaction, technical grade methanol is used as a reacting agent jointly coupled with pro analysis (p.a.) grade potassium hydroxide (KOH) as an alkaline catalyst. Both methanol and potassium hydroxide were supplied from local chemical company, Brataco. As for the hydrolysis stage, the reactants used are water and two compounds as the catalysts: sulfuric acid (98%-wt, p.a.) and propionic acid (p.a.). The latter two chemicals were supplied from Sigma Aldrich.

2.2 Transesterification

The transesterification reaction is carried out under conditions of room pressure (1 atm), temperature 65^{o}C, 350 rpm stirring rate, and reaction time 2 hours in a 3 liter reactor . KOH concentration is 1%-wt while the ratio of methanol to RBDPKO is 1: 3. The transesterification reaction is performed in a reactor equipped with a total reflux distillation column. In the transesterification, alcohol is generally in excess amounts to shift the reaction equilibrium toward product formation (Boz *et al*., 2015). Given the addition of excess alcohols, the concentration of diglyceride and monoglyceride products from transesterification results becomes insignificant as the reaction proceeds almost perfectly with triglycerides as a limiting reagent (Zheng *et al*., 2006).

First and foremost, KOH was dissolved in methanol. Furthermore the KOH-methanol mixture is divided into two parts by volume at a 70-over-30 ratio. Furthermore, the PKO was subjected to a temperature of 65°C. After reacting mixture attained such temperature, the 70 part of KOH-methanol

mixture was introduced into the RBDPKO. The duration of the reaction was timed from the second KOH-methanol mixture was fed into the reactor. The transesterification was carried out for an hour under a constant temperature at 65°C. Following this stage, the 30 part of KOH-methanol mixture was further fed and the reaction was allowed to take place under the same operating condition and for the same amount of time. To reduce the wasted heat, the transesterification reactor is coated with an insulator. The product of the transesterification reaction is an immiscible mixture of FAME and glycerol. A further separation process is physically performed based upon these two components' specific gravity. The FAME component moved upward as the top layer while the glycerol accumulated as the bottom layer. The FAME was then washed with demineralized water.

2.3 Vacuum Distillation

The formed FAME contains various methyl esters of varying chain length, with the main methyl ester content of which is methyl laurate. Therefore, it is necessary to do a gradual separation process to be able to isolate the methyl laurate with high purity. Because the boiling point of FAME is still high enough, the separation process is carried out by means of a vacuum distillation. A 2-liter vacuum distillation process was carried out at a pressure of 1-3 kPa. Measurement of methyl ester composition was conducted with a set of Gas Chromatography (GC) FID instruments.

2.4 Hydrolysis

The distillate with high methyl laurate purity (>98%) was then hydrolyzed to produce lauric acid. The hydrolysis reaction is carried out at an atmospheric pressure, temperature 90^{o}C, and 350 rpm stirring rate. The hydrolysis reaction is carried out in a reactor equipped with a distillation column. The distillation column is used to remove some of the products produced during the reaction. This is done in order to shift the equilibrium of the hydrolysis reaction toward the product formation. According to Earle (2004), the reaction equilibrium can be shifted toward the product formation by removing the product to the right of the reaction or adding the reactant to the left of the reaction.

The hydrolysis product is further crystallized to separate lauric acid from by-products and unreacted reactants. Crystallization is done to create the saturation condition of the solution. This condition can be achieved by decreasing the temperature of the solution on the saturated consti- tion or by increasing its concentration (Earle, 2004). In this study, the process of crystallization is conducted by direct crystallization method, by mixing the hot hydrolysis product with cold aqua dm directly. In the process of crystallization is the process of cooling lauric acid suddenly, due to heat transfer between lauric acid with aqua dm. Due to this sudden cooling, there is a crystallization process that can form lauric acid solids. The ratio of cold aqua dm volume used to hydrolysis product yield is 1:1.

The lauric acid solid was filtered using a Buchner vacuum and then dried for 7 days under room conditions (25°C, 1 atm) to remove the water content and propanoic acid remaining in the form of lauric acid solids. Analysis of the purity of lauric acid was carried out using High Performance Liquid Chromatography (HPLC) and Gas Chromatoraphy (GC) FID.

3. Results and discussion

3.1 Transesterification

In this study, the transesterification reaction followed by the washing and drying, can produce FAME with a yield of 95.65%-wt. According to Chandra and A'lim, (2015), the transesterification reaction carried out at a 65^{o}C in batch reactor using a homogeneous KOH catalyst can produce FAME with a yield of 91.7%-wt. Using the same operating conditions, another experiment can produce FAME with yield of 89.27%-wt. Compared to these two data, the yield of FAME obtained in this study is greater,

that is 95.66%-wt. Yield of FAME obtained in this study can be greater because the method of addition of KOH-methanol mixture is done gradually.

The acid number in the FAME was measured, about 0.21 mg KOH per gram FAM which is considerable small enough that it can be assumed that the transesterification reaction performed has been successful and no need for rinsing by using KOH. The methyl ester composition contained in FAME of transesterification results is presented in Table 1.

Table 1. Methyl ester composition in FAME from RBDPKO compared with literature (Chandra and A'lim, 2015)

Component	Experiment data (%-mole)	Literature data (%-mole)	Difference
Methyl caprylate (C8)	4.81	4.00	16.84%
Methyl kaprate (C10)	4.14	5.00	20.77%
Methyl laurate (C12)	53.55	51.00	4.76%
Methyl myristate (C14)	15.38	16.00	4.03%
Methyl palmitate (C16:0)	6.77	8.00	18.17%
Methyl stearate (C18:0)	1.47	2.00	36.05%
Methyl oleat (C18:1)	10.90	12.00	10.09%
Methyl linoleat (C18:2)	2.99	2.00	33.11%

According to Table 1, it can be seen that the methyl ester composition (FAME) has a composition comparable to that of composition from literature with variation of 4.03% to 36.05% for each fatty acid. The percentage difference of methyl laurate composition has a low value of 4.76%.

Overall, the transesterification process carried out under the vacuum operating conditions resulted in a high yield FAME of 95.65%-wt, low acid value of 0.21, and a methyl ester composition similar to that of literature data.

3.2 Vacuum Distillation

The profile of purity (percent mole) of methyl laurate and the yield of methyl laurate from FAME vacuum distillation to temperature is shown in Figure 1. At a vacuum pressure of 3.41 kPa, the highest methyl laurate composition was obtained when distillate removal was carried out at a temperature range of 150-155^{o}C with purity of 84.03%-wt. At that temperature, the yield of methyl laurate obtained also has the highest yield of 54.75%-wt. The yield obtained is quite good, because at that temperature, more than half of the methyl laurate can be isolated from other methyl esters. Thus, temperature of 150-155°C is the optimum condition to separate methyl laurate in FAME with considerable purity and yield.

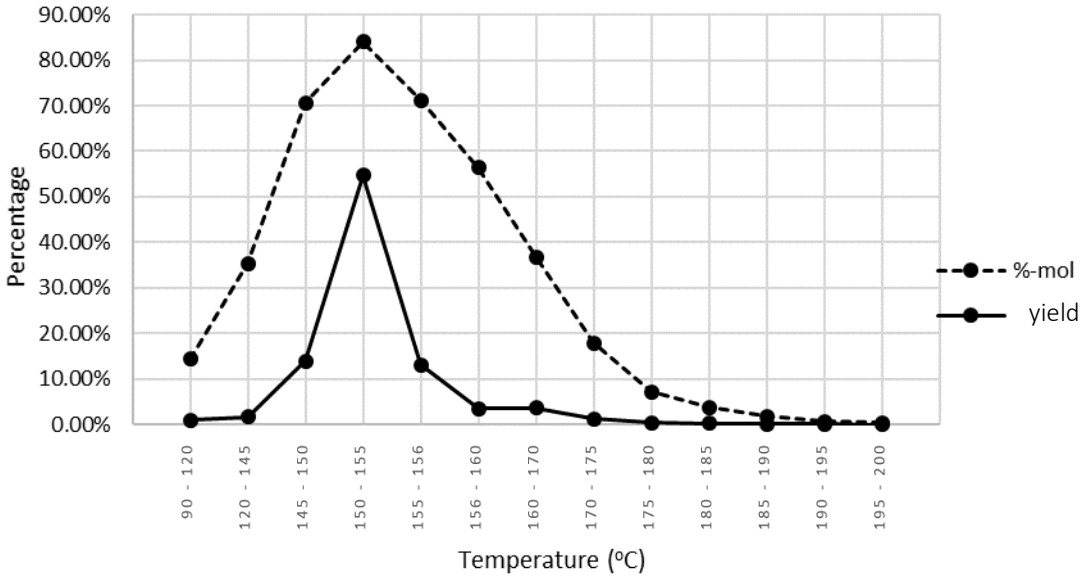

Figure 1. The purity profile (%-mole) and the yield of methyl laurate resulted from a FAME vacuum distillation to a temperature at a vacuum pressure of 3.33 kPa

3.3 Hydrolysis

The hydrolysis process is carried out by reacting methyl laurate with water and a catalyst mixture comprised of an organic weak acid (carboxylic acid) and a strong acid. The strong acid used is sulfuric acid while the carboxylic acid used is propanoic acid. The hydrolysis reaction occurring by using a mixture of these two catalysts comprises two stages of the reaction. The reaction stage occurred during the hydrolysis reaction using this catalyst mixture can be seen in Figure 2. The selection of the carboxylic acid catalyst is based on the boiling point of the methyl ester produced from the first-stage reaction compared with the methanol boiling point resulting from the second-stage reaction.

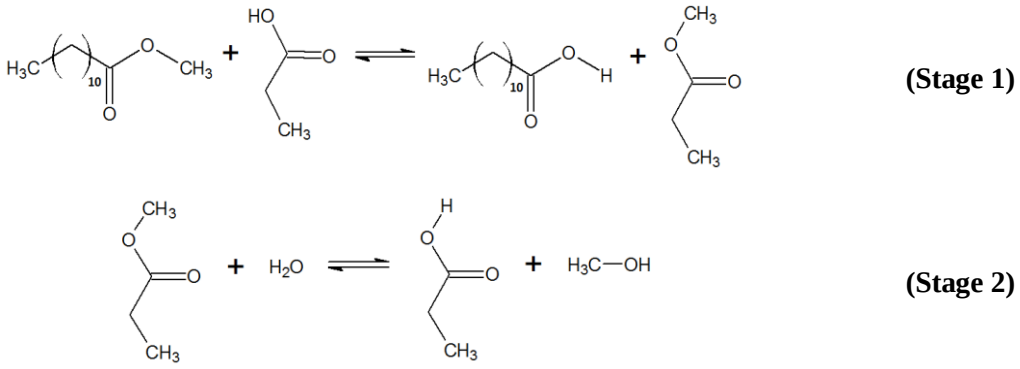

Figure 2. Stages of hydrolysis reaction of methyl laurate by using propanoic acid (Liu, 2001).

The hydrolysis reaction equilibrium can be shifted toward the formation of lauric acid by removing the methanol formed as the reaction product. Thus, in the system methanol must be the component with the lowest boiling point. The boiling point of the methyl ester produced from the first-stage reaction should be higher than that of methanol. This is done so that the component coming out of the system consists only of methanol which can shift the equilibrium reaction toward the formation of the product. At atmospheric pressure, methanol has a boiling point of 64.7°C, the methyl form has a boiling point of 31.8°C, methyl acetate having a boiling point of 57.1°C, and methyl propanoate

having a boiling point of 80°C. Thus, the carboxylic acid which may be used is a carboxylic acid with a carbon number greater than 2, for example propanoic acid (C3).

3.3.1 Results of Hydrolysis

The hydrolysis experiments were performed for producing higher purity of lauric acid by varying operating conditions such as molar ratio of propanoic acid to methyl laurate, ratio of mass of sulfuric acid to methyl laurate, and reaction time. The variables analyzed for each experiment were the purity of the obtained lauric acid and the conversion of the methyl laurate hydrolysis reaction. The experimental results of the hydrolysis reaction for each variation plot performed are presented in Table 2.

Table 2. Result of hydrolysis experiment

Run	*n* propanoic acid : *n* methyl laurate	*m* sulfuric acid : *m* methyl laurate	reaction time (h)	Conversion Rate (%-wt)
01	4	10%	3	90.98
02	5	10%	3	92.71
03	4	17.20%	3	93.76
04	5	17.20%	3	95.18
05	4	10%	4	95.80
06	5	10%	4	96.98
07	4	17.20%	4	97.71
08	5	17.20%	4	98.81
Average				**95.24**
09	**0**	**17.20%**	**4**	**0**

3.3.2 Effect of molar ratio of propanoic acid to methyl laurate

Table 2 showed that the effect of the molar ratio of propanoic acid to methyl laurate was observed by comparing the conversion obtained at the time of another variable value, those are the ratio of mass of sulfuric acid to methyl laurate used and the reaction time being carried out equally. Thus, the effect of these variables was done by comparing the results of the #1 run with that of the #2, #3 with #4, #5 with #6, and #7 with #8. The effect of the observed variables for the variation value of the mole ratio of propanoic acid to methyl ester of 4 and 5.

Based on the four comparisons that have been made, it is known that the molar ratio between propanoic acid to methyl laurate with value 5 resulted in higher lauric acid conversion when compared to other 4 values. This may be due to such higher amount of propanoic acid that the amount of methyl laurate which reacts with the propanoic acid may increase. Higher amount of methyl laurate which reacts produced higher conversion of hydrolysis because methyl laurate can react completely by acting as a limiting reagent on excess propanoic acid concentration. Thus, the conversion of lauric acid at the hydrolysis stage increases with increasing molar ratio between propanoic acid and methyl laurate used. In another comparison, the 9th run above was for hydrolysis reaction without the use of propanoic acid and that condition could not produce lauric acid at the end of the reaction. Based on the experimental data, the use of propanoic acid can direct the hydrolysis equilibrium reaction toward the production of lauric acid.

3.3.3 Effect of mass ratio of sulfuric acid to methyl laurate

Based on the experimental data presented in Table 2, the effect of the mass ratio of sulfuric acid to methyl laurate can be seen by comparing the conversion rate at the time of another variable condition, those are the molar ratio of propanoic acid to methyl laurate used and the reaction time being carried out equally. Thus, the effect of this variable could be identified by comparing the results of the #1 run with that of the #3, #2 with #4, #5 with #7, and #6 with #8. Thus, the observed variables for the value of variation in mass ratio of sulfuric acid to methyl laurate mass is between 10%-wt and 17.2%-wt.

Based on the four pairs of comparisons, the mass ratio of sulfuric acid to methyl laurate of 17.2%-wt could result in a higher lauric acid conversion rate compared to 10%-wt. The higher conversion rate would be achieved when higher amount of sulfuric acid involved during the reaction. This is definitely evident that higher amount of sulfuric acid would consequently lead to a faster reaction rate, allowing the reaction to come to its ultimate equilibria more quickly.

3.3.4 Effect of reaction time

Based on the experimental data shown in Table 2, the effect of reaction time could be observed through comparing varying conversion rate under different reaction time variants, 3 or 4 hours, when the remaining variables in those pairs of data were made the same. Therefore, the outcome could be identified by comparing the results of the #1 run with that of the #5, #2 with #6, #3 with #7, and #4 with #8.

From these comparisons, the inference would suggest that the 4-hour reactions compared with 3-hour produced higher conversion rate. As the reaction time elevates, more methyl laurate would be consumed which then eventually produced higher reaction yield. This further justified the thermodynamics perspective.

3.4 Significant variables affecting hydrolysis conversion

In order to identify the significant operating condition by each variable and their potential interaction in this research, a certain procedure of statistical analysis has completely been performed with a v17 Minitab software. Three varying attributes of the reaction were methodically examined: propanoic acid to methyl laurate molar ratio, sulfuric acid to methyl laurate mass ratio, and reaction time. The analysis was specified to focus on each of the variables implication towards the overall performance, as indicated by conversion rates, of the hydrolysis reaction in all experimental dataset.

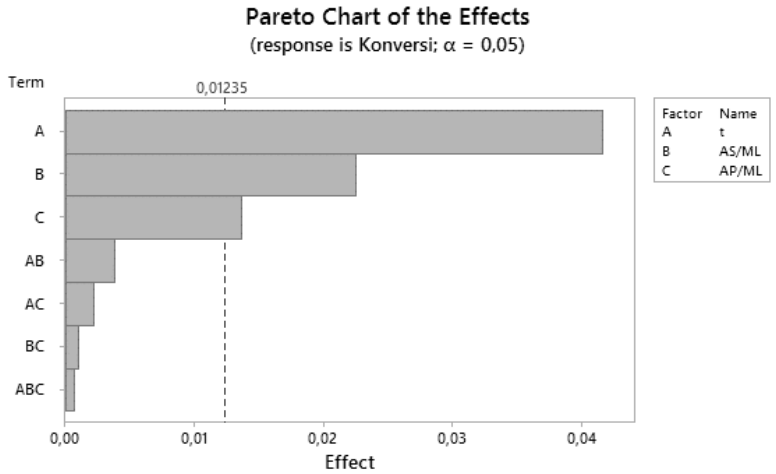

Figure 3. Pareto diagram of the effect of experimental variables on the conversion of methyl laurate at the hydrolysis stage

Based on Figure 3, the reaction time is the most significant value compared to the other two variables. Specifically, their influential level could be assessed based on the relative position of the individual Pareto bar chart to the baseline, illustrated as a dashed line in Figure 3. The overall effect brought about by the reaction time, propanoic acid to methyl laurate ratio, and sulfuric acid to methyl laurate ratio are quantified as response values of 0.04165, 0.02246, and 0.01365, respectively. Therefore, the conversion rate could be further effectively enhanced by carrying out the hydrolysis reaction for a longer duration compared with other two varying variables.

3.5 Physical and chemical properties of lauric acid

The quality of the lauric acid crystals was evaluated through some measurements of both physical and chemical properties. The products were characterized on their appearances, colors, and melting points, as well as purity and acid value. The average purity of lauric acid using all methods is shown in Table 3. Further, more details on the product melting point and acid value are presented in Table 4 below.

Table 3. The average purity of lauric acid from the three analytical methods

Method	Purity of C12 (%-wt)
HPLC	99.57
GC FID	94.95
Melting point	94.64

Table 4. Melting point and acid value of products and food grade standards

Run	Melting point (^oC)	Acid value
01	42 – 47	310.31
02	42 – 48	311.12
03	42 – 47	308.29
04	43 – 47.5	320.74
05	43 – 48	322.28
06	45 – 50	320.72
07	44 – 46	312.22
08	44 – 48	329.82
Average	**43.1 – 47.7**	**316.94**
Standard	**43 – 44**	**317.13**

From the HPLC measurements, the purity of lauric acid crystalline product was between 99.47-100%-wt or an average 99.57%-wt. In comparison, its overall purity as measured with the GC FID instrument and melting point apparatus stands at 94.95%-wt and 94.64%-wt, respectively. Based upon physical properties, lauric acid was produced as a solid, white-colored powder form at the room temperature and pressure. For the reference, the standardized grade lauric acid also exhibits similar appearances with the resulted products. The melting point of the lauric acid crystals was the range of 43.1-47.7^oC. This margin is not significantly different from the melting point reference of lauric acid which ranges between 43-44^oC. Furthermore, acid value of the product has been measured at 316.94, compared to that of standards at 317.13, with difference of approximately 0.06%.

4. Conclusions

The experimental data showed that the use of propanoic acid can direct the hydrolysis equilibrium reaction of FAME toward the production of lauric acid, producing better yield compared to only using sulphuric acid. The use of propanoic acid in hydrolysis reaction can direct the hydrolysis reaction towards the formation of lauric acid more effectively. The highest lauric acid conversion rate of 98.81%-wt and purity of 99.57%-wt could be achieved by performing hydrolysis reaction under the propanoic acid to methyl laurate ratio of 5, sulfuric acid to methyl laurate mass ratio at 17.2%-wt, and total reaction time of 4 hours.

Acknowledgement

We gratefully acknowledge the funding from the Government of Korea through Korea Research Institute of Bioscience and Biotechnology (KRIBB).

References

1. Basiron, Y., Weng, C.K., The oil palm and its sustainability. *Journal of Oil Palm Resource*; 16(1): 1–10 (2004).
2. Boz, N., Dogu, T., Murtezaoglu, K., Dogu, G., Effect of hydrogen ion-exchange capacity on activity of resin catalysts in *tert*-amyl-ethyl-ether synthesis. Applied Catalysis A: General; 268 (1–2): 175–182 (2004).
3. BPstats, Fatty acid composition of vegetable oils. *Cognis Oleochemicals*: Malaysia (2014).
4. BPstats, Fatty acid composition of some major oils. *Chempro Technovation Pvt, Ltd.*: India (2015).
5. Chandra C., A'lim, Z., Pemurnian asam laurat skala mini-pilot. *Skripsi Sarjana*: Institut Teknologi Bandung (2015).
6. Earle, R.L., Earle, M.D., Unit operations in food processing. *Web Edition, The New Zealand Institute of Food Science and Technology (Inc.)*, Palmerston North (2004).
7. Eavis, R.M., Booth E.J., Walker K.C., Taylor B.R., Wightman P.S., Agro-industrial crops for non-food uses. *SAC Crop Sci. Res. Rep*: 2–5 (1997).
8. Liu, W.T., Tan, C.S., Liquid-phase esterification of propionic acid with *n*-butanol. *Industrial and Engineering Chemistry Research*; 44: 3281–3286 (2001).
9. Sitompul, J.P., Rasrendra, C.B., Makertiharta, IGBN, Lee, H.W., Process development of chemical conversion of empty fruit bunch to platform chemical and its conversion to biodegradable plastics. Insinas Project Report, Minsitry of Research and Technology and Higher Education, 1-7 (2013).
10. Rihakova, Z., Plockova M., Filip V., Smidrkal J., Antifungal activity of lauric acid derivatives against Aspergillus niger. *Eur. Food Res. Tech.*; 213: 488–490 (2001).
11. Walters, D.R., Walker, R.L., Walker K.C., Lauric Acid Exhibits Antifungal Activity Against Plant Pathogenic Fungi. *Journal Phytopathology*; 151**:** 228-230 (2003).
12. Zheng, S., Kates, M., Dubé, M.A., Mclean, D.D., Acid-catalyzed production of biodiesel from waste frying oil. *Biomass and Bioenergy*; 30(3): 267–272 (2006).

CHARACTERISTIC STUDY OF BIOCOMPOSITE FILM POLY-LACTIC ACID (PLA) AND CELLULOSE FROM OIL PALM EMPTY FRUIT BUNCH (OPEFB)

Nina Juliana R. Turnip, Hyung Woo Lee, Johnner P. Sitompul, Tika Paramitha

Department of Chemical Engineering, Faculty of Industrial Technology
Institute of Technology Bandung, Jl. Ganesha 10, Bandung,40132,Indonesia

[*] *Corresponding Author's E-mail leehw@che.itb.ac.id; ninajr.turnip@gmail.com*

Abstract
PLA is known as synthetic polymer from renewable and environmentally friendly sources. However, PLA has weaknesses that are fragile and expensive. Therefore, PLA will be combined with other natural materials such as cellulose for producing bio-composite film through solvent casting method. Cellulose comes from oil palm waste such as empty fruit bunch of oil palm (OPEFB) containing high cellulose content that can be utilized as filler for producing film. The objective of this paper is to characterize and discuss biocomposite film of poly-lactic acid and cellulose through surface morphology. First, cellulose was isolated from OPEFB through a series of treatment processes so that the lignin was significantly reduced. Then the biocomposite film was then produced by the addition of OPEFB's cellulose till 30%-wt into PLA. The experimental results showed that characterization of biocomposite film in the form of mechanical properties such as elongation, biodegradation, and light resistance increasing through addition cellulose. Surface morphology also supports whole characterization results that showed spider-like web on spherical form.

Keywords: PLA, biocomposite film, cellulose from OPEFB, mechanical properties, biodegradability, morphology

1. Introduction

Poly-lactic acid (PLA) is an aliphatic polyester obtained from polymerization of L- and D-lactic acid, so called platform chemical. It is categorized as a promising polymer because it is made up of renewable resources. However, the PLA has a low percent elongation, around 2 to 10%, that limits of its use. The presence of polar ester groups affects the physico-chemical interactions between the polymer chains reducing the chances of shear chain during physical deformation[1]. In addition, PLA prices are quite expensive compared to synthetic polymers from petroleum derivatives. The approach to improving the utility of PLA is by producing new material that is biocomposite. Biocomposite is a blend of two or more polymeric materials based on natural materials to produce new materials at comparable or lower cost and have new properties. Cellulose is one of the options as a mixture of PLA. Cellulose used is sourced from oil palm plantation waste that is empty bunch of oil palm (OPEFB). OPEFB is a ligno-cellulosic waste that can be processed into various uses. First, ligno-cellulosic material is treated through a series of treatment processes to aim altering macroscopic and microscopic sizes, composition, and chemical structure. Challenge in producing biocomposite is in their interface properties. Different surface properties between PLA and cellulose will prevent the homogeneous dispersion. The approach to providing good adhesion is the use of coupling agents. The coupling agent increases cross-sectional level in the interface region and provides

suitable bonding results, as well as creates a high surface area for the interaction between cellulose and PLA.

Most of previous researches were conducted to synthesize bio-composite PLA blend from PLA with flax fibres. Oksman *et al.* reported the addition of triacetin (TAc) on PLA/flax composites gives an improvement in the elongation to break[2]. Furthermore, the stress and stiffness are decreased with the addition of high amounts of triacetin. Harmaen *et al.* stated that at 80% PLA and 20% OPEFB fiber increase tensile strength and Young's modulus with 5% triacetin[3]. The morphology of OPEFB fiber-reinforced PLA composites can be seen from the micrograph of Scanning Electron Microscopy (SEM). Generally, the indication of poor filler-matrix interaction is seen that many fiber pull out and the finding are in agreement with Rozman *et al.,* Oksman *et al.,* and Harmaen *et al.* Further, the insufficient adhesion between fiber and matrix is indicated by the cleanness of fiber surfaces. On the other hand, the good bonding indirectly implies that there is good adhesion. Hence, it is likely that the addition of triacetin in the matrix showed positive effect on the interface between OPEFB fiber and PLA.

This research is focused on the study of characteristics of PLA and cellulose biocomposite film. Cellulose was isolated from OPEFB through a series of treatment processes so that the lignin was significantly reduced. The agent coupling is then added to the biocomposite for improving the matrix. The effect of treatment on OPEFB and the addition of plasticizer on the mechanical properties, biodegradation, and light resistance will be further analyzed and discussed. Further, the interaction between filler-matrix is proven by the micrograph of Scanning Electron Microscopy (SEM).

2. Experimental

2.1 Materials

Poly-lactic acid (PLA), trade name PLA Ingeo 2003D, was supplied from Nature Work, USA. Oil palm empty fruit bunches (OPEFB) as cellulose source was supplied from PT Perkebunan Nusantara (PTPN) VII, Bogor, Indonesia. Triacetin (TAc) 99% as coupling agent was purchased from Sigma-Aldrich. Sodium hydroxide (NaOH), sulfuric acid (H_2SO_4), and chloroform ($CHCl_3$) were supplied from Merck, Inc. Sodium hypochlorite (NaClO) technical from PT. Brataco Chemica. Also, micro-crystalline cellulose was supplied from Kuraray Co., Ltd.

2.2 Isolation of cellulose from OPEFB

First, the OPEFB was milled and sieved on 30 mesh. 500 ml of NaOH 0.5 M was prepared and 50 g OPEFB was immersed for 2 hours, filtered, and placed in hydrothermal reactor. The principle of this reactor is steaming, so into the reactor is added 1 liter of water. The Reactor was closed tightly and heated. Water inside the reactor was boiled and and the water vapor produced to make the pressure rose. The pressure was maintained at 2 kg/cm^2 and the reaction time for about 30 minutes. After that, the OPEFB was treated, filtered, washed, and dried. The next step is to reduce the lignin content by bleaching method. At this stage, the OPEFB is treated in 5%-v agent bleaching with ratio the OPEFB/agent bleaching 1:50. After the series of treatment, OPEFB's cellulose was obtained, washed till neutral, and dried. It was analyzed before and after treatment with National Renewable Energy Laboratory (NREL) analytical procedures to confirm its chemical composition[4].

2.3 Preparation of PLLA/cellulose biocomposite Film

PLLA/cellulose bio-composite films were prepared by applying solution casting method. PLA and cellulose were prepared with total weight 3 gram and varied with weight ratio 90/10, 80/20, and 70/30. Then, PLA was dissolved in chloroform and agitated on stirring plate till

dissolved perfectly for 2 hours. Finally, cellulose was added into PLA solutions and mixed together and followed by adding 5% wt of triacetine. The mixture solution was agitated for 2 hours, casted onto a film applicator, evaporated in room temperature for 18 hours and also dried in vacuum oven for 6 hours to remove chloroform.

2.4 Characterization

The properties of film PLA/cellulose characterized using scanning electron microscopy (SEM), mechanical testing, film transparency, biodegradation, and gas permeability. All measurements are explained as follows : (1) scanning electron microscopy/SEM (Hitachi MC1000) was used to characterize the surface morphology, (2) tensile testing was carried out in accordance to ASTM D-882 (Tensile Properties of Thin Plastic Sheeting) using Universal Testing Machine (Lloyd Instrument, LRX Plus) with crosshead speed 12.5 mm/min, load rate 5 kN/min, (3) film transparency was measured by using Spectrotronic Unicam, Genesis 10 UV-Vis with wave length 600 nm. Specimen was measured 1×3 cm and placed inside the spectrophotometer cuvette, (4) biodegradation test performed at 37°C in shaking incubator. Beforehand, the sample was cut 2x1 cm then put into vial containing 5 ml of carbonate buffer (pH 8.5), 0.25 mg Proteinase K, and 1 mg sodium azide. Samples were taken periodically, washed, and dried[5] and (5) gas permeability was based on the ASTM Standard (1998).

3. Results and Discussion

3.1 Isolation of cellulose from OPEFB

According to result NREL's investigation, as shown in Table 1, methods of treatment was successful in reducing lignin and increasing cellulose content. Chemical treatment with sodium hydroxide as chemical agent has a function of destroying lignocelluloses media complex[6] while the hydrothermal treatment aims to maximizing physical changes material and minimizing hydrolysis of cellulose[7]. OPEFB have weight loss around 25-26% due to dissolved lignin during immersion and neutralization. Then, OPEFB's cellulose was sieved on 80 and 270 mesh sieve. The size of OPEFB's cellulose was tested using Beckman Coulter Particle Size Analyzer (PSA) instrument. The mean size of OPEFB's cellulose passing through 80 mesh is 7.6 μm. While the mean size of OPEFB's cellulose passing through 270 mesh is 2.3 μm.

Table 1. Chemical composition of OPEFB

Composition	Raw OPEFB (%-wt)	Treated OPEFB (%-wt)
Cellulose	38.3	71.6
Hemicellulose	14.3	6.9
Lignin	25.5	5.5
Other	21.9	16.0

3.2 Preparation of PLLA/cellulose biocomposite film

Biocomposite films were successfully produced with the addition of 30%-wt cellulose through a solvent casting method. Addition of more than 30%-wt cellulose causes film break when released from the applicator film (Fig. 1).

(a) (b) (c) (d) (e)

Fig.1. Biocomposite film with varying amount of cellulose (a) 0, (b) 10, (c) 20, (d) 30, and (e) 40%-wt

3.3 Characterization

3.3.1 Film transparency

Barrier from UV light for protecting the light-sensitive products during storage is sometimes required for certain products and this becomes an important character of film in its application as food packaging. A colorless film had high transparency because the light emitted by the instrument was not scattered by particles inside material. Neat PLA had a bad barrier in UV protection due to showed highest absorbance, the spectrum was visible at wavelength of 400 -700 nm[8]. Table 2 shows the effect of cellulose addition on biocomposite film transparency.

Table 2. Effect of cellulose addition on film transparency

Cellulose (%-wt)	Transparency (%)
0	85.0
10	17.3
20	12.7
30	6.1

The results presented in Table 2 show that the addition of cellulose resulted in a decrease in transparency. The white cellulose covered the clear PLA matrix body. Lower biocomposite's transparency made it more able to withstand the UV light. Previous researcher indicated that the cellulose is like a mirror that transmit and reflect UV light at the same time8.

3.3.2 Mechanical properties

The mechanical properties of neat PLA and biocomposites are summarized in Table 3 below.

Table 3. Mechanical results on film biocomposite with size variation of OPEFB's cellulose

Cellulose size (μm)	Cellulose (%-wt)	Tensile stress (MPa)	Elongation (%)
-	0	14,6	2,3
7,6	5	2,4	14,9
7,6	10	1,8	8,4
7,6	20	1,1	5,4
2,3	5	2,5	15,9
2,3	10	2,5	15,1
2,3	20	1,5	11,4

In general, neat PLA showed better tensile strength than PLA composites[3]. This research, neat PLA film has better tensile strength and lower elongation than these biocomposite films. In biocomposite film, cellulose could reinforce the matrix polymer by transferring the load to cellulose and distributed to matrix. Thus elongation was increased.

The size amount of cellulose affected on mechanical properties of biocomposite film. Smaller size of cellulose gave larger area of cellulose as filler in matrix, so that the load was transferred more uniformly to the matrix thus its mechanical properties were increased. In contrast, the high amount of cellulose reduced the mechanical properties of the biocomposite film because the matrix was not complete to wet out the fiber[3]. Furthermore, tensile strength was decreased due to fiber-fiber interaction and agglomeration of fiber in the matrix[9].

3.3.3 Biodegradation

The addition of cellulose improved the biodegradation properties of PLA. The natural and hydrophilic properties of cellulose could make it easy to decompose aerobically. According to Fig. 2, degradation rate of biocomposite film was increased with the addition of cellulose. The addition of 30%-wt cellulose and 5%-wt cellulose have lower degradation rate than the addition of 10%-wt cellulose and 20%-wt cellulose. If the addition of cellulose is low, it will form void in the matrix. While the addition of cellulose is high, the cellulose is not sufficiently wet by matrix so the cellulose is not completely dispersed.

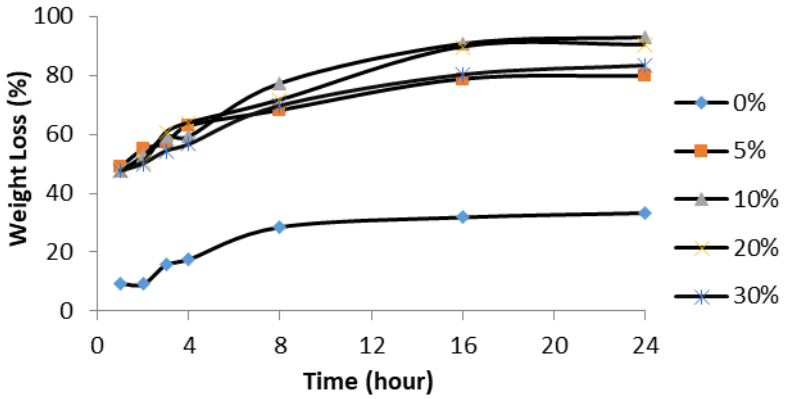

Fig.2. Biodegradation testing with variation amount of 7.6 μm cellulose in %-wt

3.3.4 Surface morphology

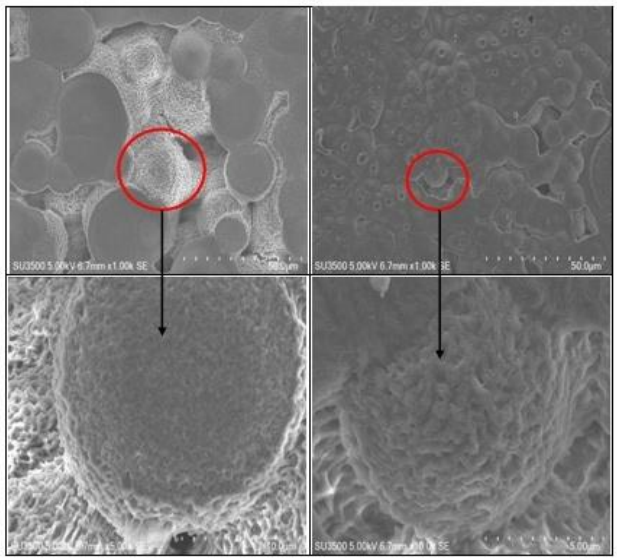

(a) (b)

Fig.3. SEM film biocomposite with size cellulose variation on 10%-wt of cellulose addition (a) 7.6 μm dan (b) 2,3 μm

The morphology of polymer network can be seen on the micrograph of Scanning Electron Microscopy in Fig.3. The polymer network was formed due to the addition of coupling agents that play a role as a bridge between PLA and cellulose to form a complex bond. From the morphological analysis, it could be described the mechanical properties of biocomposite film that the strength and elongation of the biocomposite is increased along with the smaller ball size. And the polymer fiber network covered on spherical cellulose particles caused that the gas permeation resistance was decreased and crystallinity of matrix was changed and then the biodegradation ability increased.

This morphology of biocomposite film produced without the addition of TAc as a coupling agent was analyzed. Fig.4 shows that cellulose was not form polymer network like in Fig.3 inside PLA matrix.

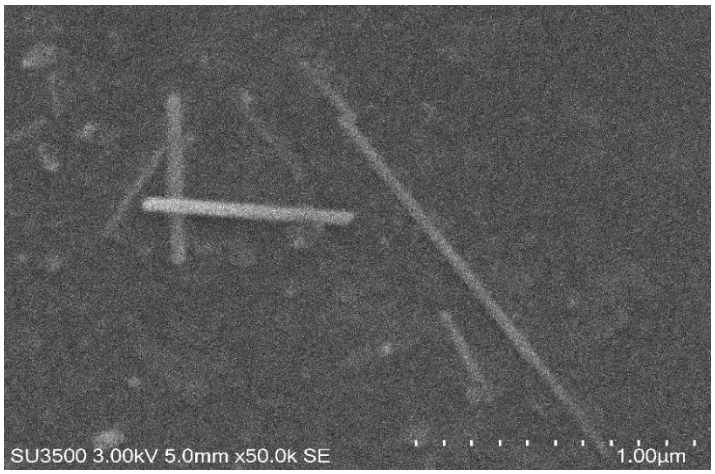

Fig.4. SEM biocomposite film 10%-wt of 7.6 μm cellulose without TAc addition

When the TAc was not added, the cellulose fibers were remained with stick type on the surface of biocomposite film, whereas, in the presence of Tac made the cellulose bind

together to form a spherical particles (Fig.3). Based on experiment, biocomposite film (10%-wt of 7.6 μm cellulose) without TAc yields a tensile stress of 12.3 MPa and elongation of 10.4%. The mechanical result showed that the elongation was increased without decreasing of tensile strength compare to biocomposite film with Tac (see Table 3).

4. Conclusion

The biocomposite film of poly-lactic acid and cellulose has been successfully produced. Cellulose was isolated from OPEFB through series of treatment could reduce lignin significantly and retain hemicellulose and cellulose components for biocomposite matrix. The addition of cellulose in biocomposite film affects transparency, biodegradation, and mechanical properties. The addition of 10%-wt of cellulose with 270 mesh showed a good result of biocomposite property. The use of TAc also plays a role in biocomposite film properties proved by morphology analysis. Furthermore, the experimental results showed that characterization of biocomposite film in the form of mechanical properties such as elongation, biodegradation, and light resistance increasing through addition of cellulose.

Acknowledgement

We are grateful for the financial support from *Grant Sawit* through BPDP Palm Oil, 2016 and *Riset Insentif Sistem Inovasi Nasional* (SINas) through the Ministry of Research and Technology and Higher Education, Indonesia, 2017. Dr. Hyung Woo Lee was supported by the National Research Foundation of Korea (NRF Korea) through the TPC program for this work.

References

1. Auras, Rafael, Loong-Tak Lim, Susan E.M., Hideto Tsuji. (2010): Poly(lactic acid) : Synthesis, Structures, Properties, Processing, and Application. Canada: *John Wiley and Sons, Inc.*
2. Oksman, K., Skrifvars, M., and Selin, J.F. (2003): Natural fibres as reinforcement in polylactic acid (PLA) composites. Composites Science and Technology , 63 : 1317–1324.
3. Harmaen, A.S., Khalina, A., Faizal, A.R., Jawaid, M. (2013): Effect of Triacetin on Tensile Properties of Oil Palm Empty Fruit Bunch Fiber-Reinforced Polylactic Acid Composites. Polymer-Plastics Technology and Engineering, 52 : 400–406.
4. Sluiter, A., et al. (2012): Determination of Structural Carbohydrates and Lignin in Biomass. *Technical Report of National Laboratory.* U.S: Departement of Energy.
5. Sitompul, Johnner, Insyani, R., et al. Polymer Properties and Biodegradable Performance of Blend Biodegradable Poli (L-Lactic Acid) (PLLA) Polymer. *Reactor*; 15 : 79-86 (2014).
6. Yuanisa, A., Ulum, K., and Wardani, A.K. Pretreatment Lignocellulose Oil Palm Stem As Initial Step Making the Second Generation Bioethanol: Reader Review. *Journal of Food and Agro-Industry;* 3: 1620-1626 (2015).
7. Aisyah, Siti, Uemura, Yoshimitsu, and Yusup, S. 'The Effect of Alkaline Addition in Hydrothermal Pretreatment of Empty Fruit Bunches on Enzymatic Hydrolysis Efficiencies." *Procedia Chemistry;* 9 : 151-157 (2014).
8. Yang, W., Fortunati, E., et al. Synergic effect of cellulose and lignin nanostructures in PLA based systems for food antibacterial packaging. *European Polymer Journal;* 79: 1-12 (2016).
9. Ibrahim, N.A., Wan Yunus, W.M.Z., Othman, M., Abdan, K. (2011): Effect of chemical surface treatment on the mechanical properties of reinforced plasticized poly(lactic acid) biodegradable composites. J. Reinf. Plast. Comp., 30, 381–388.

Granulation of NPK Fertilizers

I Dewa Gede Arsa Putrawan[1,*], Dendy Adityawarman[2],
Haris Askari[3], and Natal Bagus Jalu Buana[3]

[1]*Research Group on Chemical Product Design and Development,*
[2]*Research Group on Chemical Process Design and Development,*
[3]*Study Program of Chemical Engineering,*
Faculty of Industrial Technology, Institut Teknologi Bandung
Jalan Ganesha 10, Bandung 40132, Indonesia

* *Corresponding Author's E-mail: idewa@che.itb.ac.id*

Abstract
The purpose of this research is to study the physical granulation of mixed NPK fertilizers consisting of urea, diammonium phosphate, and potassium chloride. In addition, eggshell was used as filler. The granulation was carried out in a pan granulator with a pan diameter of 40 cm at a rotation speed of 35 rpm and an inclination angle of 45°. Aqueous molasses and water were used as binding liquid. The granulation variations included molasses concentration, location of liquid spray, and liquid-to-solid (LS) ratio. The granulation performance was evaluated by measuring the yield and compressive strength of onsize fraction (2-4 mm). Molasses concentration and LS ratio increased the onsize fraction. The optimum onsize fraction using hot water and 50%-molasses solution as binding liquid were 30% and 40%, respectively. Hot water resulted in higher compressive strength than 50%-molasses. Better granulation was found when the location of liquid sprayer was divided into two sections, on the bulk flows near scrapper and on the rolling regions of powder flow.

1. Introduction

NPK fertilizers are multinutrient fertilizers which contain all macronutrients needed by the plants, i.e., nitrogen (N), phosphor (P), and potash (K). Bulk production of NPK fertilizers are mainly in the granular form, with the advantage of having excellent storage, handling, and transport properties. Granular NPK fertilizers may be prepared by reactive granulation or physical granulation. In the former process, phosphoric acid is made to react with ammonia vapor to produce ammonium phosphate slurry. The slurry is then sprayed upon a tumbling bed of potassium chloride, recycled solid, filler and other solid materials to form NPK granules. In the later, mixed fertilizers are tumbled with the addition of binder. These two processes are sometimes called as slurry and solid routes, respectively[1].

Fillers are used to adjust the percentage of the nutrients to a desired ratio, prevent caking of the fertilizers, and increase the fertilizer weight[2]. Fillers dilute the concentration of fertilizer active ingredients, which can burn delicate roots and stems. Fillers contribute a significant portion in NPK formulation. NPK 20-10-10 granulated from urea, DAP (diammonium phosphate), and KCl, for example, contains 36% fillers by weight. Fillers are usually taken from inorganic minerals, such as zeolite, clay, dolomite, phosphate rock, and bentonite. These materials are not renewable and their reserves are, of course, limited. Alternatives for conventional filler materials are required.

In seeking alternatives for materials, attentions have to be paid on agricultural and livestock wastes. Eggshell can be considered as an alternative for NPK fillers. Fig. 6 shows the estimated volume of eggshell production which was estimated based on the world

production of eggs from FAO[3] and assuming that an average 11% weight of eggshell in egg[4]. As seen from the figure, the world production of eggshell reached 7 million tonnes per year.

Eggshell is a bio-ceramic composite material with an extracellularly assembled structure, whose function is to protect the contents of the egg and to ensure the calcium necessary for the formation of the chick's skeleton. Eggshells are comprised of a network of protein fibers, associated with crystals of calcium carbonate (96% of shell weight), magnesium carbonate (1%) and calcium phosphate (1%), and also of organic substances and water. Calcium carbonate ($CaCO_3$), the major constituent of the shell, is an amorphous crystal that occurs naturally in the form of calcite (hexagonal crystal)[5]. Although many works on NPK granulation have been published[6-10], intensive study on the granulation of NPK fertilizer with eggshell as filler is not available.

This research is aimed to study the physical granulation of NPK fertilizer with eggshells as fillers. In more specific, this research was proposed to study the particle size distribution and compressive strength of granules obtained from physical granulation of NPK fertilizers with eggshell as filler. Physical granulation was selected instead of reactive granulation as physical granulation requires lower capital cost and could be handled by home industries. Urea, DAP, and KCl were used as the nitrogen, phosphor, and potassium sources. Molasses and hot water were used as binder. At first, the flow behaviors of single materials during the granulation were observed. Secondly, the granulations of mixed fertilizer were studied by observing the particle size of the granulated products. The compressive strengths of onsize granules were then measured and compared to those of granules using bentonite, a representative of conventional fillers.

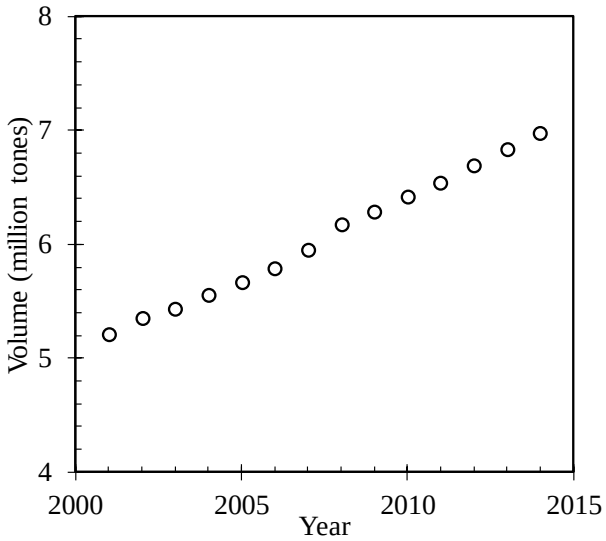

Fig. 6. World production of eggshell.

2. Experiments

2.1 Materials

Urea and KCl were purchased from market, having NPK analysis of 46-0-0 and 0-0-60, respectively. DAP having an analysis of 15-46-0 was kindly supplied by PT. Petrokimia Gresik. Eggshell was collected from a local cake shop. Molasses was kindly supplied by PT. Madukismo, Yogyakarta. All solid materials were milled until passing 100 mesh screen before granulated.

2.2. Equipment

Fig. 7 shows the schematic of the granulation apparatus used. The apparatus consists of an inclined pan equipped with a scrapper, supported on a frame which allows slope adjustment. The pan was rotated by a motor equipped with a speed reducer and an inverter. The pan was made from flexiglass, having a diameter of 40 cm and a rim height of 4 cm. The rotation speed and inclination angle were fixed at 35 rpm and 45°, respectively.

2.3. Procedure

The granulation was carried out in batch system. About 100 g grinded materials consisting of urea, DAP, KCl, and fillers were put into the pan and then rotated. After the mixtures were tumbled homogeneously, binder was sprayed onto the tumbling materials. The granulation was stopped after a determined time. The granules were then dried in oven at 70°C and then divided into three fractions, i.e., oversize (+5 mesh or ≥ 4 mm), onsize (+5 mesh/-10 mesh or between 2 to 4 mm), and undersize (-10 mesh or ≤ 2 mm).

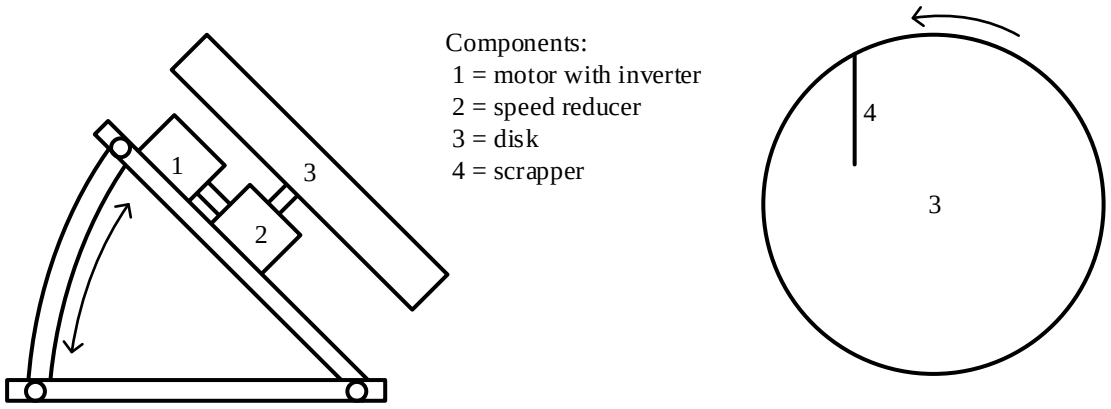

Fig. 7. Schematic of granulation apparatus.

3. Results

3.1 Flow pattern

Granulation in pan granulators are facilitated by tumbling process[11]. The homogeneity of the tumbling materials is very important when granulating solid mixtures. Studying the flow behavior of materials on a rotating pan can give description of the homogeneity of the materials when granulated. Fig. 8 presents the flow patterns arising on the pan granulator used of single materials as well as of mixed NPK and eggshell at 35 rpm. In general, flow patterns arising on a pan granulator include slipping, rolling, cascading, cataractering, and centrifuging[12]. Cascading and cataractering facilitate the consolidation of particles to collide eat other to enable growing. Rolling facilitates the colliding granules to form spherical shapes. Centrifuging is not expected because all materials are carried by centrifugal forces and adhere on the rim. Most materials used exhibited cascading, cataractering, and rolling. Eggshells which were used as fillers could be well tumbled and had almost similar pattern with bentonite. Urea, however, showed centrifuging pattern. It was caused by the low density of urea so that at the same rotation speed, urea is easily carried by centrifugal force. When eggshells were incorporated into NPK materials, consisting of urea, DAP, and KCl, the mixtures could be well tumbled. Good tumbling behavior is necessary for achieving homogeneous composition.

3.2 Effects of spray position

Spray position has important role on the extent of granulation as well as on the size distribution of granules. To study the effects of spray position, bentonite was granulated using molasses solution as binder for 5 minutes at molasses concentration of 30% and L/S ratio of 15%. There were four positions observed, i.e., at the top near the scrapper (T), at the bottom on the rolled material (B), at the middle between top and bottom (TB), and back and forth along the flowing particles between T and B (TB*). Fig. 9 shows the schematic of T, B, and TB position. The results were depicted in Fig. 10. It was found that spraying binder on the flowing material along the space from near scrapper to the rolling particles at the bottom gave the highest onsize yield (50% onsize). This spray method, however, requires that the sprayer is movable along the top and bottom.

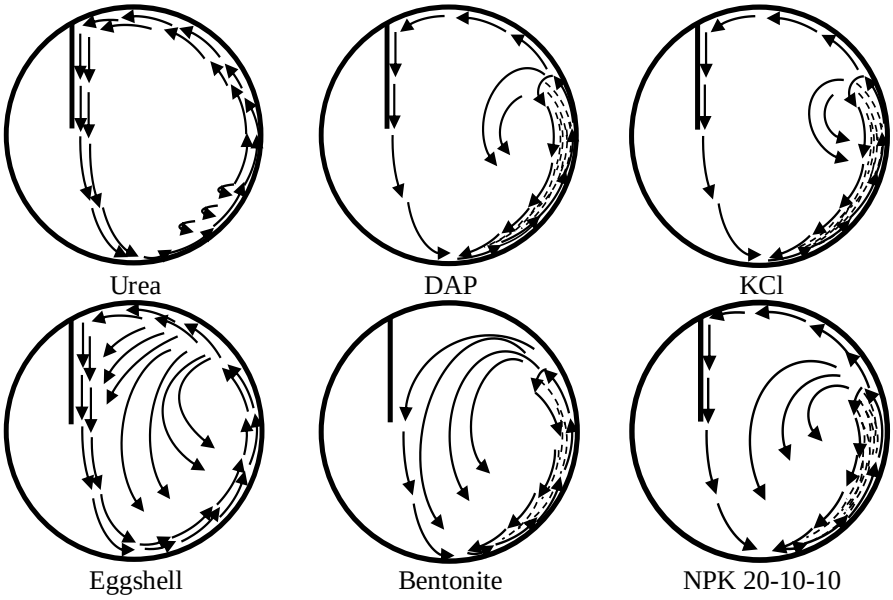

Fig. 8. Flow pattern of materials.

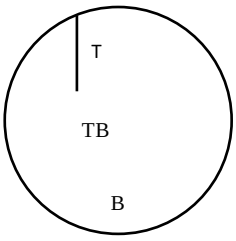

Fig. 9. Location of sprayer.

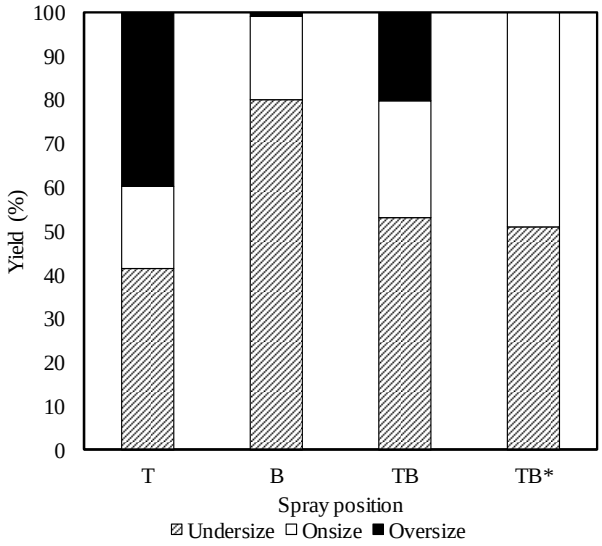

Fig. 10. Effect of sprayer position.

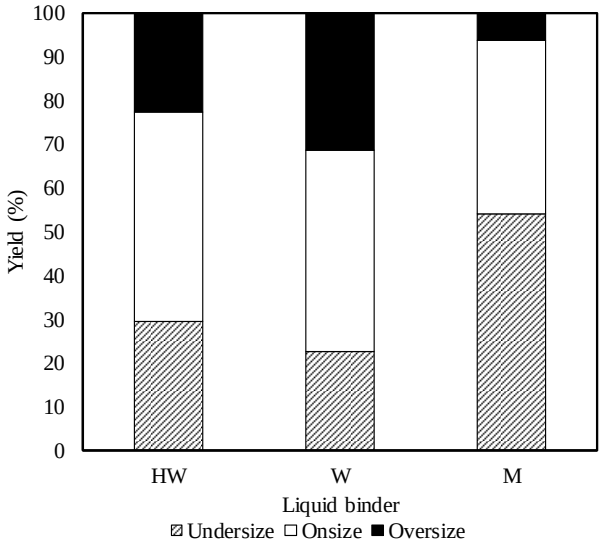

Fig. 11. Effect of binder.

3.3 Effects of binder

Three binding liquid solutions used in this research include molasses solution (M), cold water (W), and hot water (HW). The effects of liquid were studied by granulating bentonite-urea mixtures with 36% urea. This formula is corresponding to urea content of NPK 20-10-10 having high content of urea. The granulations were carried at L/S ratio of 20%. Molasses concentration used was 50%. The results are shown in Fig. 11. The order of binder in decreasing onsize yield are hot water, cold water, and molasses solution. Urea was known very soluble in water, 1079 g/L at 20°C[13]. Urea, therefore, functions not only as raw material but also as binder. The higher the temperature the higher the solubility and the faster the urea solubilizes. Molasses 50%, on the other hand, was very viscous that it is difficult to flow and to coat particles. In addition, for the same L/S ratio, it contained less water. Water without molasses, therefore, could granulate NPK particles containing urea. The role of urea as binder was convinced by granulating a bentonite-urea mixture containing 21% urea which is corresponding to NPK 15-15-15. It was found that to have the same extent of granulation to

that of NPK 20-10-10, an L/S ration of 35% was necessary. It means that lower urea content requires more liquid to achieve the same onsize yield.

3.4 Effect of L/S ratio

Effect of L/S ratio was studied by using NPK 20-10-10 and with eggshell as binder. The granulations were carried for 5 minutes using hot water as binder. The results are shown in Fig. 12. As comparison, Fig. 13 shows the results for the case bentonite as filler. Eggshell as binder gave approximately the same extent of granulation to that of bentonite. It could be understood as eggshell also chemically consists of mineral having density which is close to that of bentonite. Compared to bentonite-urea mixture, L/S ratio necessary for granulating NPK is lower than that for bentonite-urea mixture. It was caused by the existence of KCl which also contributed binding properties. The solubility of KCl used is 20 g/L at room temperature. The dissolved KCl played a role as binder, which also occurred for urea. More soluble material results in stronger coalescence bridges[14]. As can be seen also that L/S ratio higher than 5% decreased onsize fraction and increased oversize fraction. It means that the L/S interval in which the granulation operates well is narrow, i.e., 0 to 5%.

The sensitivity of NPK granulation to L/S ratio could also be seen from the flow pattern of NPK during the granulation. The flow patterns are shown in Fig. 9. The particles grew fast that in four minutes, fine powders vanished and the granules could not lifted or left rolled at the bottom.

3.5 Compressive strength

Fig. 15 shows the compressive strength of onsize NPK granules obtained using hot water and 50% molasses solution as binders. The strengths were determined from 20 granules. Molasses gave lower compressive strength than hot water. The very viscous solution when molasses used as binders made the binder difficult to penetrate into the particles. Hot water, on the other hand, solubilize urea and KCl and left stronger bridge after dried. In general, 7% L/S ratio gave the highest strength. However, the granules obtained did not satisfy the required strength of minimum 3 MPa.

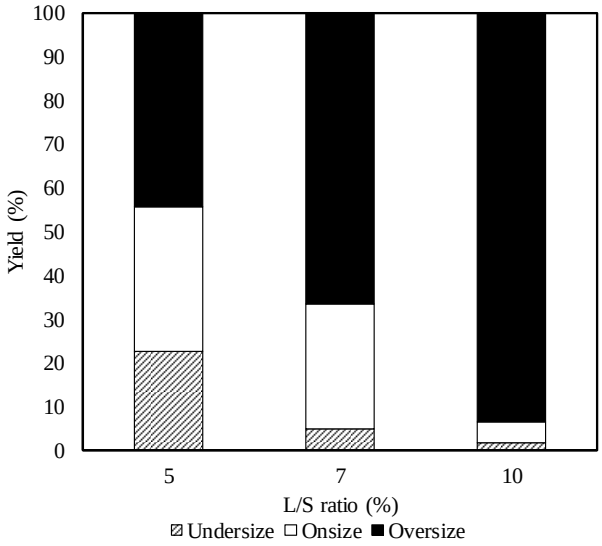

Fig. 12. Effect of L/S ratio on distribution size of NPK with eggshell as filler.

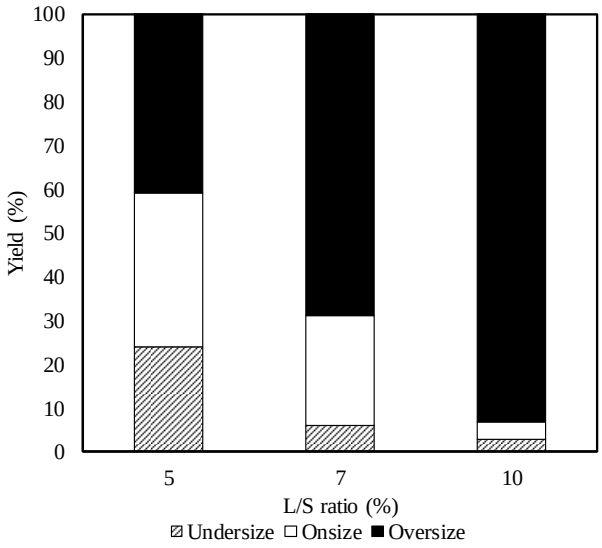

Fig. 13. Effect of L/S ratio on distribution size of NPK with bentonite as filler.

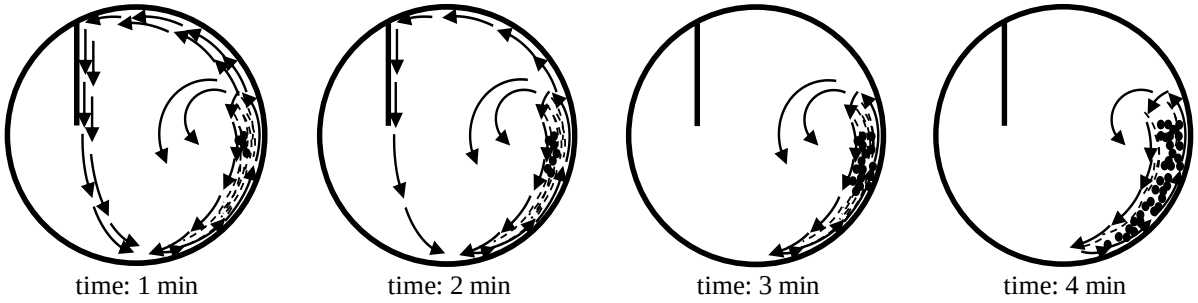

Fig. 14. Flow pattern during granulation of NPK.

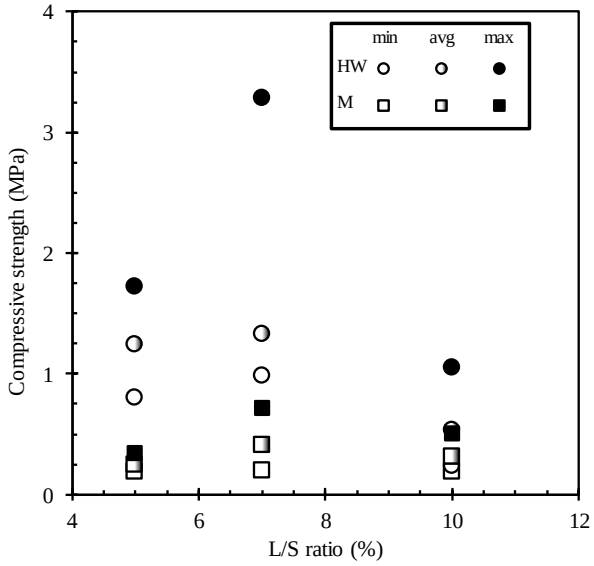

Fig. 15. Compressive strength of NPK granules.

4. Conclusions

NPK mixers consisting urea, DAP, and KCl have been granulated using a pan granulator and eggshell as filler. The granulation performance was evaluated by measuring the yield and compressive strength of onsize fraction (2-4 mm). The granulation using eggshell as filler had the same granulation extent to that using bentonite as filler. Hot water was found to be better binding liquid than cold water and molasses solution for facilitating the collisions of particles. Molasses concentration and L/S ratio increased the onsize fraction. The optimum onsize fraction using hot water and 50%-molasses solution as binding liquid were 30% and 40%, respectively. The yield of onsize fraction was significantly affected by liquid-to-solid ratio. Hot water resulted in higher compressive strength than 50%-molasses. Better granulation was found when the location of liquid sprayer was divided into two sections, on the bulk and on the rolling regions of powder.

Acknowledgements

We express our thanks to PT. Petrokimia Gresik for providing DAP and to PT. Madukismo for providing molasses. This research was supported by Institut Teknologi Bandung under the grant of P3MI 2017.

References

1. Hallsworth, J. A., Fortescue, W. F. Proceeding of Technical Meeting of IFA (1984).
2. Gowariker, V., Krishnamurthy, V. N., et al. The fertilizer encyclopedia. John Wiley, New Jersey (2009).
3. FAO. Livestock statistic report. http://faostat.fao.org (2017).
4. Zaheer, K. An Updated Review on Chicken Eggs: Production, Consumption, Management Aspects and Nutritional Benefits to Human Health. *Food and Nutrition Science*; **6**: 1208-1220 (2015).
5. Oliveira, D. A., Benelli, P., et al. A literature Review on Adding Value to Solid Residues: Egg Shells. *Journal of Cleaner Production*; **46**: 42-47 (2013).
6. Olive, B. M., Hardesty, J. O. Fertilizer Granulation, Effect of Particle Size of Potassium Chloride on Granulation of Mixed Fertilizer. *Agricultural and Food Chemistry*; **12**(6), 492-497 (1964).
7. Walker, G. M., Holland, C. R, et al. Drum granulation of NPK fertilizers. *Powder Technology*;107:282-288 (2000).
8. Walker, G. M., Holland, C. R., et al. Prediction of Fertilizer Granulation: Effect of Binder Viscosity on Random Coalescence Model. *Industrial and Engineering Chemistry Research*; **40**: 2128-2133 (2001).
9. Chudinova, O. A., Poilov, V. Z., et al. Physicochemical Foundations and Optical Parameters of the Granulation Process of NPK Fertilizers based on Ammonium Sulfate. *Russian Journal of Applied Chemistry*; **85**: 933-940 (2010).
10. Farahani, S. S., Rajabipour, A., et al. Energy Use and Economic Analysis of NPK-15:8:15 Fertilizer Granulation Process in Iran. *Journal of Saudi Society of Agricultural Sciences*; **16**:265-269 (2017).
11. Sherrington, P. J., Oliver, R. Granulation. Heyden&Son, London (1981).
12. Chadwick, P.C., Bridgwater, J., Solids Flow in Dish Granulators. *Chemical Engineering Science*; **52**: 2497-2509 (1997).
13. Green, D. W., Perry, R. H. Perry's Chemical Engineers' Handbook. McGraw-Hill, New York (2008).
14. A. A. Adetayo, J. D. Litster, M. Desai, The Effects of Process Parameters on Drum Granulation of Fertilizers with Broad Size Distributions. *Chemical Engineering Science*; 48: 395l-3961 (1993).

Synthesis of Methyl Tin Oxide as Raw Material for PVC Stabilizer

I Dewa Gede Arsa Putrawan [1,*], Denny [2], and Windy Wijaya[2]

[1]*Research Group on Chemical Product Design and Development*
[2]*Study Program of Chemical Engineering,*
Faculty of Industrial Technology
Institut Teknologi Bandung, Jln. Ganesha 10, Bandung 40132, Indonesia

** Corresponding Author's E-mail: idewa@che.itb.ac.id*

Abstract
This research is aimed to study the synthesis of methyl tin oxide as a raw material in producing thermal stabilizer for poly vinyl chloride from methyl tin chloride. Ammonium hydroxide and sodium hydroxide were used as bases. The synthesis was carried out in a semi batch stirred vessel. The experimental variables included base concentration (4~9 M), base flowrate (2~8 mL/min), and base excess (0%-20%). It was found that base flowrate did not influence the yield of methyl tin oxide. Stronger base resulted in lower yield of methyl tin oxide. The higher the base concentration, the larger the yield obtained. The optimum base excess was in the range of 5~10%. The tin content of methyl tin oxide obtained was in the range of 62% to 66%, a little bit lower than the maximum theoretical yield. The methyl tin oxide obtained was used to synthesize organotin thermal stabilizer. The thermal stabilizer has been tested using a two rolls mill and was found to be effective in stabilizing poly vinyl chloride.

1. Introduction

Poly vinyl chloride (PVC) is the third largest polymer in volume production in the world[1]. The annual production of PVC in Indonesia has reached 20,000 tons. PVC has wide applications and mixes well with additives due to the presence of polar chlorine groups. However, it can be thermally degraded due to autocatalytic dehydrochlorination reaction that start occurring at 70^{o}C. Thermal degradation of PVC is caused by the irregular structures in the form of allylic chloride[2]. It liberates hydrochloric acid so that the chlorines are detached from their bond and leave polyene structures (carbonyl group). This process destroys the backbone of PVC. Thermal degradation lowers the mechanical strength of PVC, PVC changes color when heated, from yellow, brown, and black. Thermal degradation of PVC needs to be prevented as most PVC processing involved heat.

PVC thermal degradation can be retarded by using thermal stabilizers. The thermal stabilizer works as a reactive nucleophile, reacts with the allylic chlorines and scavenge the liberated hydrochloric acid so that the propagation of dehydrochlorination reaction can be terminated[3]. There are various types of thermal stabilizers, such as lead, barium, zinc, and organotin[4]. Among all types of thermal stabilizers, organotin stabilizer is very potential to be developed in Indonesia. The main raw materials for organotin stabilizers are tin and fat. Both materials are abundant in Indonesia. Indonesia is the second largest tin producer in the world. According to the US Geological Survey, tin reserve in Indonesia reaches 60,000 tons/year. On the other hand, Indonesia as a tropical country is also rich in vegetable oils.

One of the synthesis routes of organotin stabilizers can be described in Fig. 16. The synthesis of organotin stabilizer involves two stages of reactions, namely (1) the synthesis of raw material, and (2) the synthesis of organotin stabilizer. The raw material in the form of methyl tin oxide (MTO) is synthesized from methyl tin chloride (MTC) and a base solution, while the other raw material in the form of mercapto ethyl ester of fatty acid (MEFA) is synthesized through a reaction between fatty acids and mercaptoethanol. At the second stage,

methyl tin oxide and MEFA are reacted to obtain organotin thermal stabilizer. Stage 1 and stage 2 might be carried in separate plants/places. This so called MTO route allows the production of organotin stabilizers without transporting MTC which is rather difficult as MTC is a toxic liquid at room condition.

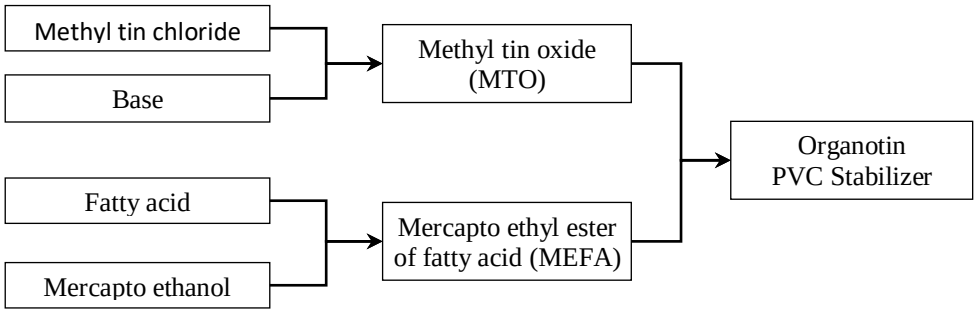

Fig. 16. The synthesis route of organotin PVC stabilizer.

There are two methods of synthesizing MTO. The first is by reacting tin powder and primary alcohols at temperatures of 200~400°C[5]. However, this method is considered to be unattractive because it involves high reaction temperatures and requires cooling at very low temperatures to obtain MTO[6]. The second is by hydrolysis in which n-alkyl tin halides are reacted with base solutions at 60~100°C. The yields of MTO via this reaction were found in the range of 97.9~98.9%[7]. The recommended concentrations of base were between 5% and 50%[8]. The reaction is also possible be carried at lower temperature.

Although the synthesis of organotin stabilizer from MTO and MEFA has been patented in 1968, however, there is no intensive study on this topic, especially on the more downstream, i.e., reacting the obtained MTO with MEFA to produce PVC stabilizer and testing the stability effectiveness. The production of organotin stabilizer via MTO is mostly kept as proprietary know-hows by the producers. It is the purposes of this research to synthesize organotin stabilizers using MTO and MEFA. In this paper, the works focus to the synthesis of MTO in which local MTC is used as a raw material. MTO was synthesized through hydrolysis, between base and MTC. The MTC used consisted of dimethyl tin dichloride and monomethyl tin trichloride. The reaction parameters studied are the types, concentration, flowrate, and excess of bases. Two bases were used, i.e., ammonium hydroxide and sodium hydroxide. The MEAL used was prepared from rice bran oil.

2. Experimental

MTC, a mixture of monomethyl tin trichloride and dimethyl tin dichloride containing 17.8%-w Cl, was kindly supplied by PT. Timah Industri. Aqueous solution of NH_4OH containing 25%-w NH_3 was purchased from a local supplier. NaOH with 99.99%-w purity was purchased from Merck. MEAL was obtained from the previous works[9,10,11]. The experimental set for preparing MTO is shown in Fig. 17. MTC of 200 g was first placed in the reactor. The base solution is then fed at a determined flowrate under stirring. The reaction temperature is maintained at 25~35°C by controlling the temperature of circulating water and feeding of base solution. The temperature controller stopped feeding base solution when the reaction temperature passes the maximum allowed temperature. The pH and temperature of the solution were recorded during the reaction. The reaction was stopped after all base was fed into the reactor. The solid phase was then separated using a separating funnel to obtain crude MTO. The crude MTO was then washed with water three times to obtain final products. Tin contents in products were measured using XRF.

The reaction was carried out at various base excess (0%, 5%, 10%, and 20%), base concentration (4.0, 6.6 M), and base flow rate (2, 4, 12 mL/min). Each run was performed twice. The experimental runs are presented in Table 1. As mentioned above, the used MTC consisted of monomethyl tin trichloride and dimethyl tin trichloride. The synthesis reactions can be written as follows:

$$2LOH_{(aq)} + (CH_3)_2SnCl_{2(aq)} \rightleftharpoons (CH_3)_2SnO_{(s)} + 2LCl_{(aq)} + H_2O_{(l)} \quad (1)$$

$$3LOH_{(aq)} + CH_3SnCl_{3(aq)} \rightleftharpoons CH_3SnOOH_{(s)} + 3LCl_{(aq)} + H_2O_{(l)} \quad (2)$$

The above reactions are very exothermic. This is the reason why the reaction temperature was controlled both using circulating water and by controlling the feeding rate of base.

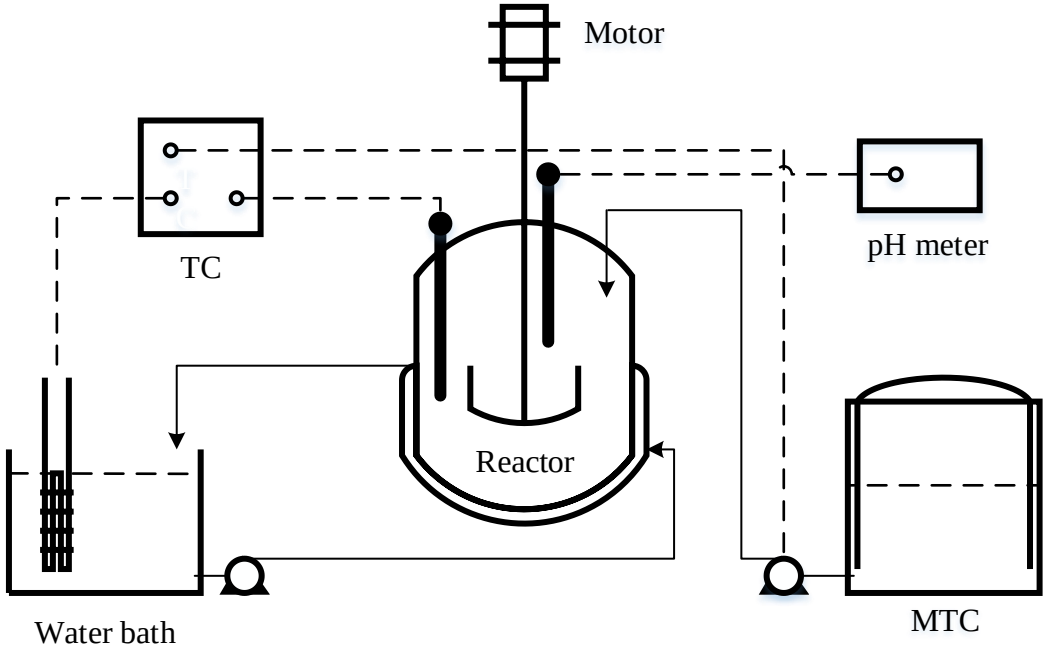

Fig. 17. Schematic of apparatus.

Table 1. Experimental runs.

Code	Base					Code	Description				
	Base	Molarity (M)	Flowrate (mL/min)	*Excess (%)*	Run		Base	Molarity (M)	Flowrate (mL/min)	*Excess (%)*	Run
SC1-1	NaOH	4.00	8.12	5	1	AF6-1	NH_4OH	8.79	12.19	5	1
SC1-2	NaOH	4.00	8.12	5	2	AF6-2	NH_4OH	8.79	12.19	5	2
SC2-1	NaOH	6.57	8.12	5	1	SE0-1	NaOH	6.57	8.12	0	1
SC2-2	NaOH	6.57	8.12	5	2	SE0-2	NaOH	6.57	8.12	0	2
SC3-1	NaOH	8.79	8.12	5	1	SE5-1	NaOH	6.57	8.12	5	1
SC3-2	NaOH	8.79	8.12	5	2	SE5-2	NaOH	6.57	8.12	5	2
AC1-1	NH_4OH	4.00	8.12	5	1	SE10-1	NaOH	6.57	8.12	10	1
AC1-2	NH_4OH	4.00	8.12	5	2	SE20-1	NaOH	6.57	8.12	20	1
AC2-1	NH_4OH	6.57	8.12	5	1	AE0-1	NH_4OH	8.79	8.12	0	1
AC2-2	NH_4OH	6.57	8.12	5	2	AE0-2	NH_4OH	8.79	8.12	0	2
AF1-1	NH_4OH	8.79	2.03	5	1	AE10-1	NH_4OH	8.79	8.12	10	1
AF1-2	NH_4OH	8.79	2.03	5	2	AE10-2	NH_4OH	8.79	8.12	10	2
AF2-1	NH_4OH	8.79	4.06	5	1	AE20-1	NH_4OH	8.79	8.12	20	1
AF2-2	NH_4OH	8.79	4.06	5	2	AE20-2	NH_4OH	8.79	8.12	20	2

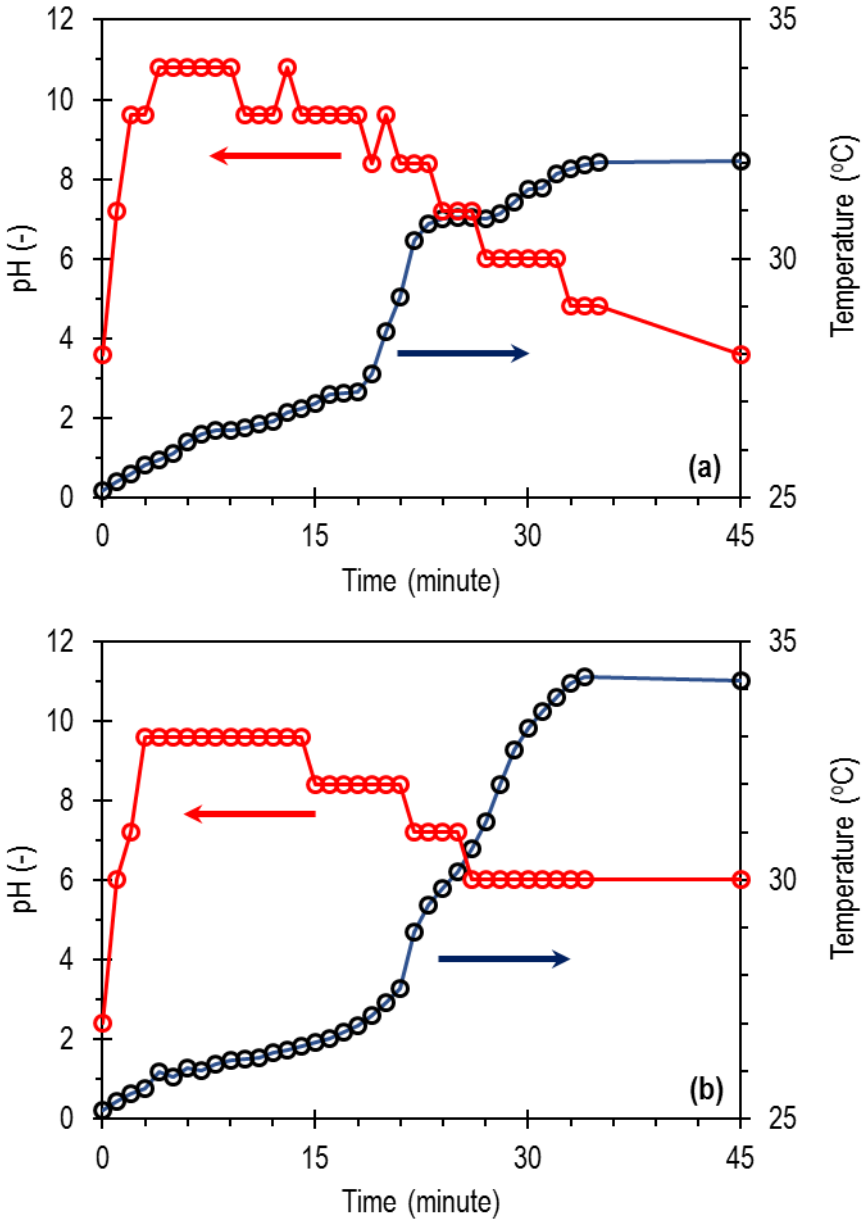

Fig. 18. Profiles of pH and temperature.

3. Results and Discussion

3.1. Profiles of pH and temperature

Fig. 18a and Fig. 18b show the pH and temperature profiles when ammonium hydroxide and sodium hydroxide were used as bases, respectively. The profiles were obtained at 4M base concentration and 5% base excess. The reaction temperature increased just after MTC was fed. It was due to the exothermic reaction occurred. After the reaction achieved a maximum point, the temperature decreased slowly as the liberated heat was absorbed by the solid phase and circulating water. When ammonium hydroxide was used, the reaction temperature could return to room temperature in 45 minutes. For sodium hydroxide, however, the temperature was still at 30°C in 45th minute. This indicate that, as sodium hydroxide is stronger that ammonium hydroxide, it gives higher reaction heat that the circulating water could not absorb the liberated heat as fast as in the case of ammonium hydroxide.

The pH of the reaction mixtures was increase continuously as the base solution was fed. The pH started at a low pH as MTC is acid. The addition of base solution neutralized part of

MTC so that pH was getting higher and higher. The equivalent points were clearly shown by the graphs. The final pH for sodium hydroxide was found to be higher than that for ammonium hydroxide. This occurred as sodium hydroxide is stronger than ammonium hydroxide.

3.2 Effect of base parameters on yield

The effects of base parameters on the yield of MTO are presented in Fig. 19a. Fig. 19a shows the effects of bases on yields both for ammonium hydroxide and sodium hydroxide. Lower yield was obtained for sodium hydroxide. This means that stronger base provides lower MTO yield. For the same excess, stronger base gave higher final pH. The higher the pH, the more soluble the MTO[11]. Higher solubility resulted in higher loss during washing and filtration. More MTO was carried away in the filtrate so that the yield decreased.

Fig. 19a also shows the effects of base concentrations on the obtained methyl tin oxide. Higher base concentrations result in greater yield. This is because the synthesis reaction of MTO is an equilibrium reaction. The addition of base concentration causes the system to shift toward MTO to minimize the impact of disturbance according to Le Chatelier principle.

Fig. 19b shows the effects of base flow rates on yield. The effect of base flow rate is observed by comparing runs AF1-1, AF1-2, AF2-1, AF2-2, AF6-1, and AF6-2. The data in Fig. 19b shows the effect of the base flow rate on the yield of methyl tin oxide product by 0-0.4%. The value of the change given is so small that the effect of the base flow rate on the yield of methyl tin oxide product can be neglected. This means that the reaction rate of methyl tin oxide formation is very fast due to a good agitation process.

The effects of base excess on yield is shown in Fig. 19c. The graphs show an optimum base excess both for ammonium hydroxide and sodium hydroxide. The best base excesses of 10% and 5% were found for ammonium hydroxide and sodium hydroxide, respectively. When base excess was increased at the lower region, the yield also increased. This happened as the increase in excess convinced the completion of reaction. However, when excessive base excesses were applied, the pH solution increased resulting in significant product losses due to solubility. These opposite effects resulted in an optimum base excess.

3.2 Tin Content

Fig. 20 shows the content of tin in product, at various base excess. The tin contents were in the range of 63-65 and 63-66 %-w for ammonium hydroxide and sodium hydroxide, respectively. The variations in tin contents were in the range of experimental errors. Thus, it could be said the tin contents were in an average value of 64%. The theoretical tin content, estimated from the stoichiometric reaction and chlorine content of MTC is 71%. From these values, the purity products obtained was around 90%. The tin contents were a little bit lower than the theoretical value. Analysis of metals in MTO of all experimental runs found that the tin contents were in the range of 98.9-99.5, as shown in Fig. 21. It means that there was no sodium or other metals left in the products. In other words, the excess sodium could be removed by washing. Thus, the fact that the tin contents were lower than the theoretical value should be caused by no metal containing side products. It is possible some products were hydrated which lowering the tin contents in the products. In contrast to yield, optimum base excesses of 10% and 5% were found for ammonium hydroxide and sodium hydroxide, respectively, for tin content. Thus, generally speaking, the optimum base excess was in the range of 5~10%.

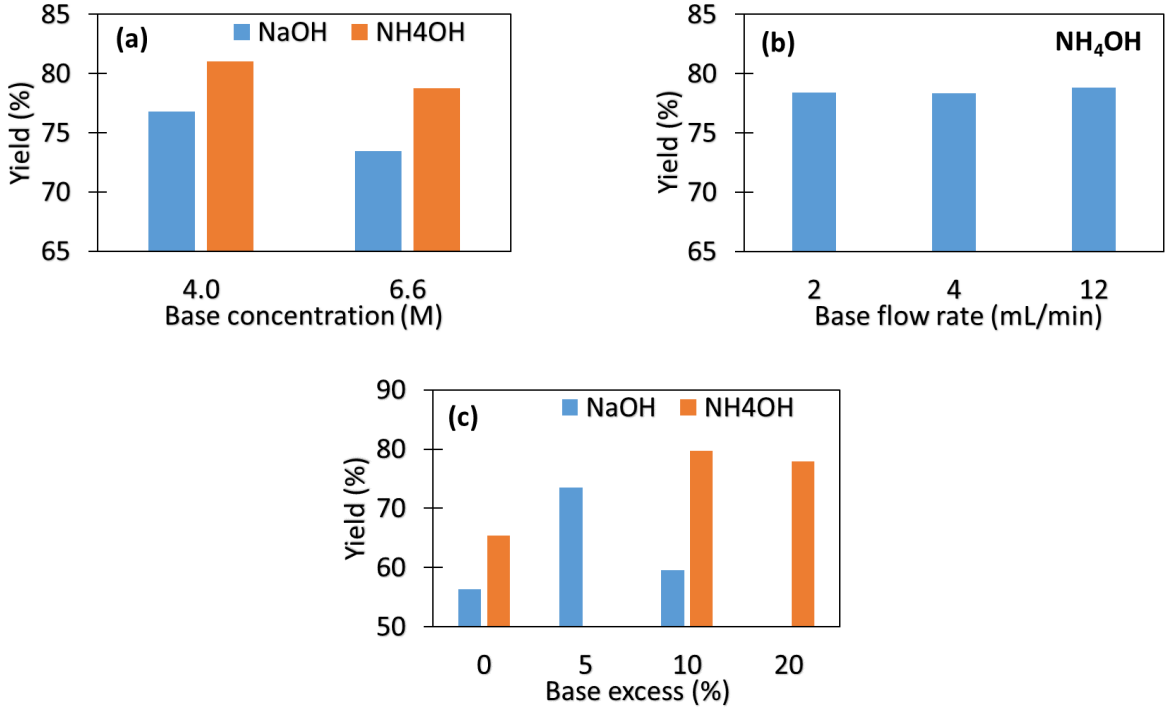

Fig. 19. Effects on yield of (a) base concentration, (b) base flow rate, and (c) base excess.

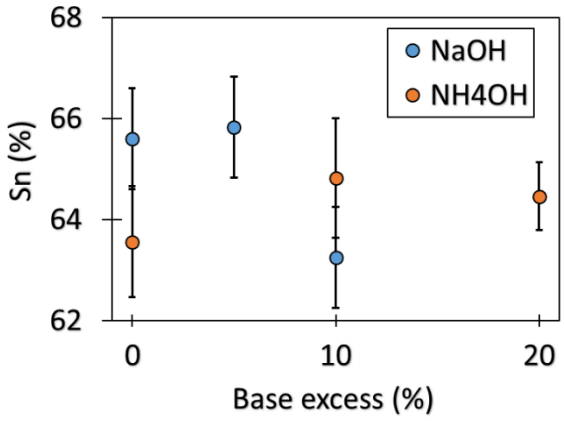

Fig. 20. Tin content of MTO, total base.

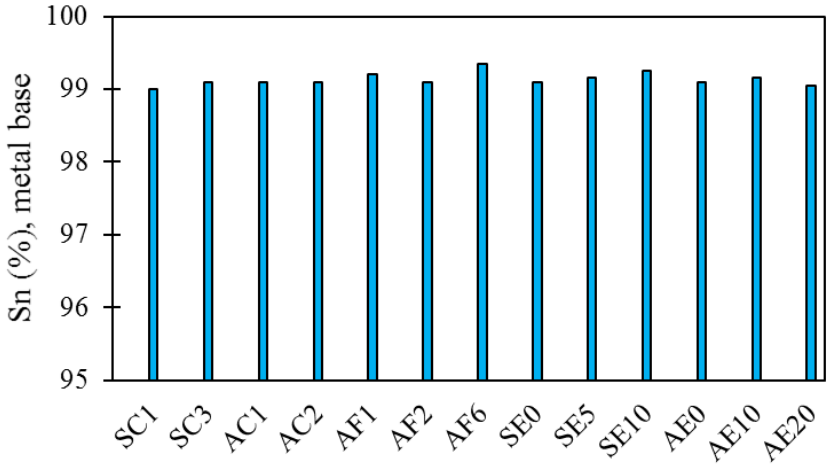

Fig. 21. Tin content of MTO (metal base).

3.3 Synthesis of stabilizer

The MTO produced was reacted with mercapto ethyl ester of rice bran fatty acid to synthesize organotin stabilizer. The reactions can be written as follows:

$(CH_3)_2SnO + 2\ RCOOCH_2CH_2SH \rightleftharpoons (CH_3)_2Sn(SCH_2CH_2OOR)_2 + H_2O$ (3)

$CH_3SnOOH + 3\ RCOOCH_2CH_2SH \rightleftharpoons (CH_3)_2Sn(SCH_2CH_2OOR)_2 + 2\ H_2O$ (4)

The reactions were carried at 80°C under rigorous stirring and vacuum. A clear oil phase was obtained in two hours of reaction. A formulation consisting of 1.5 phr the produced organotin stabilizer, 1.2 phr P-1141, 0.3 phr Loxiol G-78, 5 phr B-622, 1.5 phr PA-20, and 0.3 phr ACP 316-A was prepared. PVC resin having a k value of 57 was used. This formula is commonly applied in industry. The formulation was heated at 190°C in a two rolls mill. Samples were taken at every 5 minutes. The results are depicted in Fig. 22. Organotin stabilizer at 1.5 phr made in this research could stabilize PVC until 30 minutes. Practical extrusions require 15 minutes stability. The thermal stabilizer of this study, therefore, obeys the practical requirement. Observations during the synthesis of organotin stabilizer found that a very little solid left at the bottom of the flask. This confirms that the MTO obtained contained a small amount of impurity. Using pure MTO, no solid should be left at the end of reaction. The produced water, as a by product, evaporates due to vacuum. It is the additional advantage of using MTO route, that the synthesis of organotin stabilizer produced no waste.

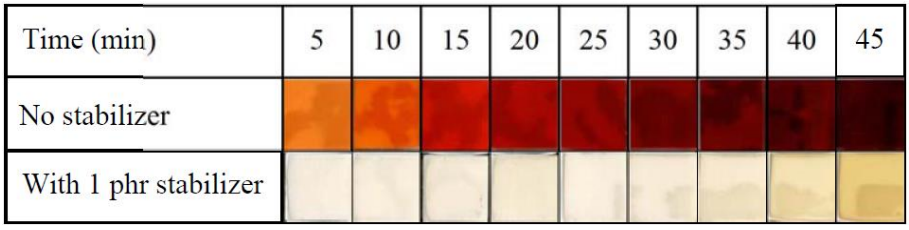

Fig. 22. Stability test.

4. Conclusions

Methyl tin oxides have been prepared from methyl tin chloride and base solution. It was found that base flow rate did not influence the yield of methyl tin oxide. Stronger base resulted in lower yield of methyl tin oxide. The higher the base concentration, the larger the yield obtained. The optimum base excess was in the range of 5~10%. The tin content of methyl tin oxide obtained was in the range of 62% to 66%, a little bit lower than the maximum theoretical yield. The methyl tin oxide obtained was used to synthesize organotin thermal stabilizer. The thermal stabilizer has been tested using a two rolls mill and was found to be effective in stabilizing poly vinyl chloride.

Acknowledgements

The authors wish to thank PT Timah Industri for providing methyl tin chloride. This research was supported by the Indonesian Estate Crop Fund for Palm Oil (BPDPKS) under GRS 2016.

References

1. Folarin O. M., Sadiku E. R. Thermal stabilizers for Poly (vinyl chloride): A review. *International Journal of The Physical Sciences*; 6: 4323-30 (2011).
2. Starnes, W.H. Structural Defects in Poly (vinyl chloride) and the Mechanism of Vinyl Chloride Polymerization: Comments on Recent Studies. *Procedia Chemistry*; 4: 1-10 (2012).
3. Steenwijk J., Es D.S., Haveren J., Geus J.W., Jenneskens L.W. The effect of (natural) polyols on the initial color of heavy metal- and zinc-free poly (vinyl chloride). *Polymer Degradation and Stability*; 91: 2233-40 (2006).
4. Murphy J. Additives for Plastics Handbook 2nd Ed. Elsevier Advanced Technology, 2001: United Kingdom.
5. Grossman. Synthesis of Organotin Oxide. *United States Patent Office*; 6,215,010 B1: 1-3 (2001).
6. Tang J. Y. Method of Preparing Oxidation Methyl Tin, *Google Patent*; CN101585852 B: 1-3 (2010).
7. Katsumura T., Kataoka H., Mizuno Y. Process for Preparing Dioctyltin Oxide. *United States Patent*; 3,390,159: 1-2 (1968).
8. Kiyama et al. Process for Fractional Production of Alkyl tin Oxide. *United States Patent*; 4,968,823: 1-12 (1990).
9. Putrawan, IDGA, Azharuddin, A., et al. Synthesis of Mercapto Ethyl Ester of Fatty Acid. 2nd International Conference on Biomass, Bogor (2017).
10. Wahyuni F., Hutami P. I. Synthesis of Mercapto Ethyl Oleate. Undergraduate Thesis, Institut Teknologi Bandung (2014).
11. Bestari D. K., Wicaksana C. A. Synthesis of Mercapto Ethyl Ester of Rice Bran Fatty Acids. Seminar on Chemical Engineering, University of Parahyangan, Bandung (2017).
12. Rochow E. G., Seyferth D. The Electrolytic Dissociation of Dimethyl tin Dichloride; 2877-78 (1953).

EXPERIMENTAL STUDY OF HPAM AND BIODEGRADABLE SURFACTANT FOR ASP FLOODING IN ENHANCED OIL RECOVERY

Johnner P. Sitompul[1,*], Annisa N. Shabrina[1], Rizky Ambardi[1], Michael D. M. Sitompul[2], Hasian P. Septoratno Siregar[2], and Hyung W. Lee[1]

[1]*Department of Chemical Engineering, Faculty of Industrial Technology*
[2]*Department of Petroleum Engineering, Faculty of Mining and Petroleum Engineering*
Institute of Technology Bandung, Jl. Ganesha 10, Bandung, 40132, Indonesia

[*] *Corresponding Author's E-mail: sitompul@che.itb.ac.id*

Abstract
The objective of this paper is to characterize and discuss partially hydrolyzed polyacrylamide (HPAM) and biodegradable surfactant formulated for alkaline-surfactant-polymer (ASP) flooding in enhanced oil recovery (EOR). HPAM was synthesized from acrylamide through aqueous solution polymerization and hydrolysis at the same time with potassium persulfate and sodium bisulfite. Surfactants used in this research were biodegradable , methyl ester sulfonate, formulated from the reaction of sulfuric acid and methyl ester, derived from the result of trans-esterification and fractionation of palm kernel oil. Alkaline used in this research was sodium carbonate while core flooding were performed with light oil and in sandstone cores. Phase behavior analysis and ASP flooding for EOR were applied and compared with SP flooding or polymer flooding, respectively. Experimental results showed that synthesized HPAM had high molecular weight of 27.7 x 10^6 g/mol. Phase behavior analysis showed maximum micro-emulsion formed at 0.5%-mass of surfactant. The addition of HPAM in injection fluid showed increasing viscosity in the solution while the addition of alkaline decreased the viscosity of the injection fluid. Core flooding analysis showed that ASP flooding has higher oil recovery compared to SP flooding or polymer flooding. The highest oil recovery from ASP flooding has resulted in 23.53% of original oil in place (OOIP).

Keywords: partially hydrolyzed polyacrylamide, biodegradable surfactant, phase behavior, ASP flooding, original oil in place, Enhanced Oil Recovery (EOR)

1. Introduction

Oil is the natural resource that very important for our daily life such as for fuel, electricity, as well as raw material for petrochemical and chemical industry. The demand of oil in the industry will increase, so oil production becomes very crucial in fulfilling the demand. Generally, oil production is classified into three stages, which are primary recovery, secondary recovery, and tertiary recovery. Tertiary recovery, so called enhanced oil recovery (EOR), is very important nowadays in order to increase the oil recovery from wells or oil fields. One of the popular methods in EOR is chemical EOR with benefit of relatively high oil recovery, however, the use of the method is still insignificant around 10.89% compared with the two methods. The oil recovery in tertiary recovery or enhanced oil recovery can recover oil between 10-30% of oil in place (OOIP). Specifically, tertiary recovery itself is the process to obtain the oil that is trapped in the rock using the material that is not contained in the well. Enhanced oil recovery classification is generally shown in Figure 1 below.

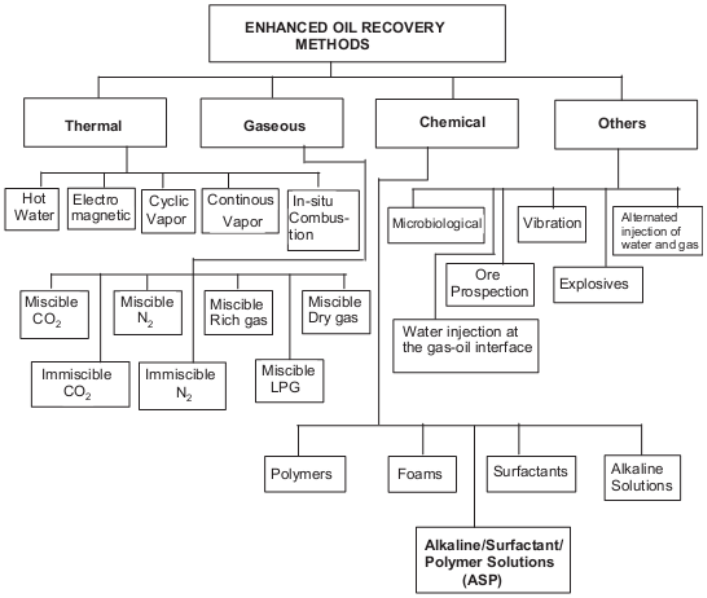

Figure 1. Enhanced Oil Recovery Classification (modified after Olajire, 2014)

One of the most effective EOR methods is known as Alkaline-Surfactant-Polymer Flooding, because it has the synergy between solution mixture from alkaline, surfactant, and polymer. Furthermore, polymer can increase the viscosity of the solution, so mobility ratio of the injected solution decreases significantly hence the oil recovery will increase. One of an alternative popular polymer is hydrolyzed polyacrylamide (HPAM), synthesized using hydrolysis of polyacrylamide, while polyacrylamide come from polymerization of acrylamide monomer. Polymerization method to produce HPAM applies aqueous solution polymerization in order to obtain very high molecular weight for EOR. The application of biodegradable surfactant (anionic type) is very good alternative to petroleum based one considering environmentally friendly aspect in ASP. The biodegradable surfactant was synthesized from sulphonation of fatty acid methyl ester (FAME), produced from methanolysis of Palm Kernel Oil and fractionation of its FAME with C16 and C20 FAME cut.

The objective of this paper is to characterize and discuss the effect of hydrolyzed polyacrylamide (HPAM) and biodegradable surfactant formulated for the alkaline-surfactant-polymer (ASP) Flooding in Enhanced Oil Recovery (EOR). The addition of surfactant is to reduce surface tension and change the wettability so it can reduce capillarity tension in the rock. Further, the study will compare oil recovery using ASP flooding compared to SP flooding or Polymer flooding, respectively.

2. Experimental

2.1 HPAM Formulation

HPAM formulation was started by adding acrylamide (13.94 g) and sodium carbonate (6.24 g) to aqua dm (200 mL) in a beaker. The solution is then purged by nitrogen for about 30 minutes. After the purging had been completed, potassium persulphate (0.2 g) was added into the solution as an initiator. The temperature reaction was controlled at 80 ^{o}C and stirred for 2 hours in nitrogen atmosphere. After that, precipitation of HPAM was carried out by adding methanol and followed by drying the precipitate in the oven at around 50 ^{o}C for about 1 hour.

2.2 MES Formulation

The formulation was aimed to calculate composition to produce surfactant. Methyl ester (0.35 mol) was filled into 500 ml three-neck flask and then sulfuric acid (0.39 mol) was fed drop by drop into the

flask. The solution was mixed and stirred using magnetic stirrer and maintained at temperature of 65 ^{o}C for about 1.5 hour. The flask temperature was slowly decreased to 50 ^{o}C, and then methanol 40%-w/w was added into the mixture. NaOH 30%-w/w was added for controlling pH between 5 to 6.

2.3 Phase Behaviour Test

The test is to determine the optimum composition of ASP mixture. Certain volume of ASP was filled into a 100 ml beaker glass. Diesel oil was added to the beaker and then the solution was mixed until homogenous solution was achieved for testing the phase behavior. The mixed solution was poured into a vessel and the vessel was covered up for about 60 minutes. The micro-emulsion formulation was checked and then the composition of ASP was determined with the optimum micro-emulsion solution. The optimum composition was determined by the highest volume of micro-emulsion occurred during addition of ASP into the oil-water mixture as visual examination showing three-phase behavior.

2.4 Viscosity Test

Viscosity test of injection solution was carried out using Brookfield Viscometer by setting the viscometer into zero (Autozeroing viscometer). The injection solution was placed into a 500 ml beaker and ready for testing in the Brookfield Viscometer.

2.5 Core Flooding Test

The core flooding test was shown in Figure 2 below. The core sandstone with the proportion of 35% quartz sand and 65% cement (???) was prepared and the core was heated in the oven for about one day and then its weight was recorded. The core was saturated with oil SO IT WAS NOT PRESATURATED WITH WATER? for 8 hours and the core weight was measured after being saturated by oil. The saturated core was placed into the holder and the injection solution sample was flowed into the core by turning on the pump in the storage vessel. The oil recovery (OOIP) collected in the flask was determined after flooding test had been completed.

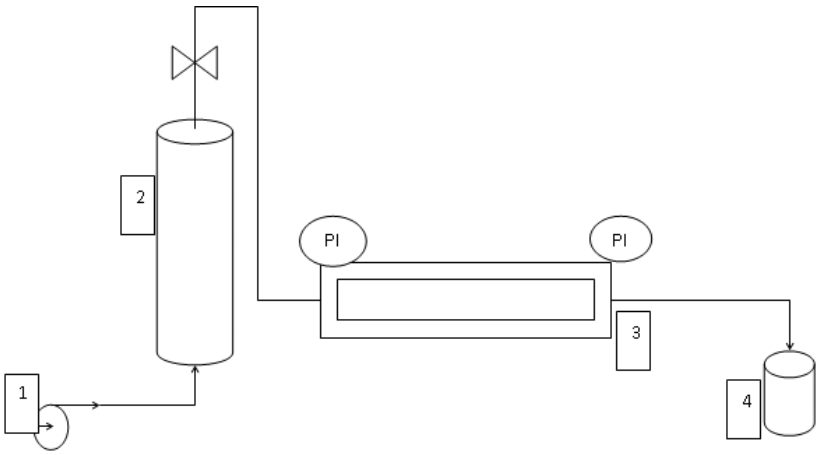

Note: 1. Pump; 2. Storage vessel; 3. Core holder; 4. Measuring glass

Figure 2. Schematic Diagram for core flooding test

3. Results and discussion

3.1 HPAM and MES Synthesis

Table 1 shows results of various HPAM produced from hydrolysis of PAM. The molecular weight of HPAM-1 was measured to be 2.77 x 10^7 dalton (g/mol) at temperature 80 ^oC using Mark-Houwing correlation. The average molecular weight of polymer for EOR is usually in the range of $2x10^7$ to $1x10^8$ dalton for EOR (Sorbie, 1999). The HPAM-2 has lower molecular weight (10.5 x 10^6) despite the same temperature condition, because in this HPAM-2 synthesis addition of initiator was done before conducting nitrogen purging. Hence, this made the oxygen still trapped in the solution hindering termination process during growing of polymerization chain reaction. HPAM-3 has the lowest molecular weight. For HPAM-3, the temperature of production was quite high, i.e., 95 ^oC, which showed the increase of temperature result in decrease of degree of polymerization during synthesis of HPAM, so the molecular weight obtained was lower, 2.1 x 10^6 dalton compared with HPAM-1.

Table 1 Molecular weight of HPAM polymers

Polymers	Molecular Weight (Dalton)
HPAM-1 (80^oC)	27.7 x 10^6
HPAM-2 (80^oC)	10.5 x 10^6
HPAM-3 (95^oC)	2.1 x 10^6

Note: HPAM-2 using initiator fed before nitrogen purging

Surfactant formulation was validated using the analysis of acid number and surfactant screening test. Surfactant screening test is being used to check the criteria in EOR with phase behavior and core flooding test. Acid number test is the total amount of mass KOH in mg used to neutralize 1 g fatty acid in sample. In MES reaction the methyl ester can be hydrolyzed into fatty acid and produce carboxylate sulphonate as a product. Hydrolysis and side product cause the acid number to increase. Surfactant that was produced had acid number below 1%. As the acid number of MES quite low, most of the products obtained in these experiments were MES's.

3.2 Effect of Alkaline, Surfactant, and Polymer

In polymer flooding, the increase of viscosity in injection solution can increase the flood efficiency so it can produce more oil recovery. When the viscosity increases, the risk of fingering in reservoir decreases, so it causes the flood efficiency to increase. Based on flow equation, when water viscosity is increased by polymer, shown in Figure 2, it will reduce the value of the water cut. The addition of polymer also decreases the relative permeability of water. The increase of viscosity in injection solution with increasing HPAM and decrease of water relative permeability will reduce the mobility ratio of water to oil in the reservoir. Hence, the decrease of mobility ratio will increase the oil recovery.

The decrease of polymer viscosity was affected by salt effect phenomena by alkaline as shown in Figure 4. The viscosity decrease is expected when the polymer is injected into the well. So, polymer viscosity will be relatively low at the injection start up, because of the presence of alkaline. However, the alkaline will be slowly consumed by water formation and rocks, so the viscosity of polymer will then increase step by step. Further, alkaline can decrease the adsorption of surfactant at the surface, hence it make the surfactant use more efficient.

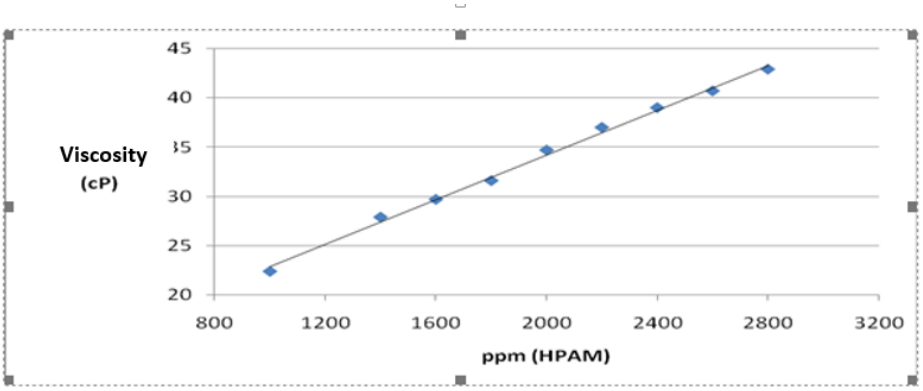

Figure 3. Effect of HPAM Concentration in the Viscosity of the Injection Fluid

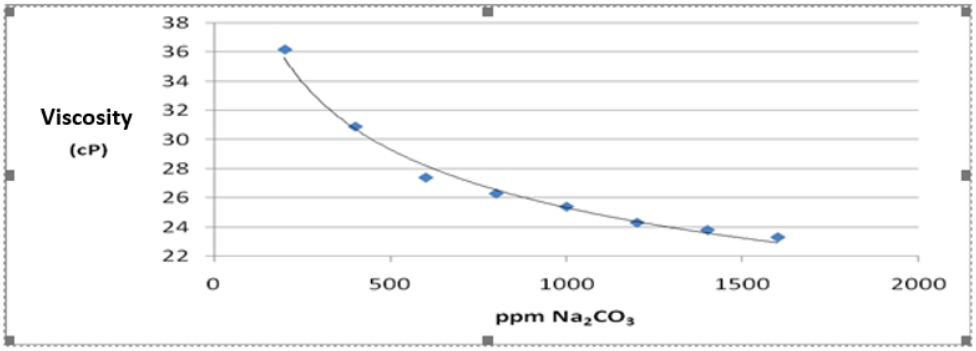

Figure 4. Effect of Alkaline to Viscosity in Injection Fluid

3.3. Phase behavior analysis

Figure 5 and 6 show the surfactant and oil that produced micro-emulsion that was separated into two phases. The micro-emulsion occurred at the optimum MES concentration of 0.5%, with the highest volume of the micro-emulsion. The effect of MES to phase behavior increases with increasing amount of MES, and then decreases after a certain amount producing three phases of mixture. It is due to the fact that surfactant reaches the critical micelles concentration (CMC), hence beyond the CMC, more surfactant soluble in bulk liquid would not decrease the surface tension anymore (Sheng, 2011).

Figure 5. Phase behavior analysis with different composition of MES 0.1%; 0.2%; 0.3%; 0.4% (from right to left, in %-w)

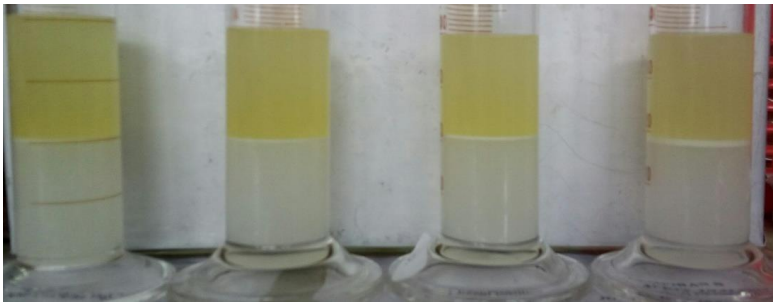

Figure 6. Phase behavior analysis with different composition of MES 0.5%; 0.6%; 0.7%; 0.8% MES (from right to left, in %-w)

3.4 Core Flooding Test

Results of core flooding test are shown in Table 2. Note that samples 1, 2, and 3 are only polymer flooding, surfactant flooding and SP flooding, respectively. Further, samples 4 and 5, were injected with similar concentration of MES and Na_2CO_3, while sample 4 has lower concentration of HPAM compared to sample 5. It can be seen that the ASP flooding increased the oil recovery. Oil recovery in EOR is usually around 10% to 30% OOIP, while the result of ASP showed comparable results, with OOIP between 12.8% to 23.5%. From all the samples, sample 5, ASP Flooding with large amount of polymer, has the highest OOIP. Further, the addition of alkaline with higher amount of polymer in the injection fluid produced higher oil recovery. This is because the increase of polymer concentration would then increase the viscosity of injection fluid and better sweep oil in the core. The highest oil recovery from ASP flooding has resulted in 23.53% of original oil in place (OOIP).

Table 2: Comparison of OOIP for Polymer, Surfactant, ASP flooding test

Sampel	Injection Fluid	% OOIP	Pressure of injection(psig)
1	HPAM 2800 ppm	14,89%	100
2	MES 0,5%	14,89%	27
3	HPAM 2800 ppm, MES 0,5%	17,65%	82
4	HPAM 2800 ppm, MES 0,5%, Na_2CO_3 200 ppm	23,53%	100
5	HPAM 1000 ppm, MES 0,5%, Na_2CO_3 200 ppm	12,82%	52

Note: MES and Na_2CO_3 in %-wt

With regard to core flooding analysis, it shows that ASP flooding produced the highest oil recovery compared to SP flooding or polymer flooding which give promising application in the field for EOR.

4. Conclusion

The synthesized HPAM has the molecular weight of 27.7 x 10^6 dalton, which is suitable for EOR application and has been tested for phase behavior and further for ASP flooding. Reaction temperature of HPAM affected the molecular weight of the product. The increase of HPAM concentration apparently increased the sweep efficiency and then improve the oil recovery. Alkaline decrease the viscosity of injection fluid and it is useful during fluid injection start up so it can flow easier into the reservoir. The effect of MES concentration in phase behavior increased and then decreased after reaching the CMC. Core flooding analysis showed that ASP flooding gave higher oil recovery compared to SP flooding or polymer flooding. The highest oil recovery from ASP flooding has resulted in 23.53% of original oil in place (OOIP).

Acknowledgment

The authors gratefully acknowledge the funding from the Institute of Technology Bandung through 2017 Research Group Funding.

References

1. Al Adasani, A.; Baojun B., Analysis of EOR Project and Updated Screening Criteria. Elsevier (2011)
2. Ahmad, R., Ibrahim, Z., et al. Synthesis of High Molecular Weight Partially Hydrolyzed Polyacrylamide and Investigation on its Properties, Polymer Science, Iran, 2005
3. Buckley, S.E.; Leverett, M.C., Mechanism of Fluid Displacements in Sands. Trans. AIME 146 (1942), 107-116.
4. Da Silva I., Lucas, et al. Study of Conditions for Polyacrylamide Use in Petroleum Reservoir: Physical Flow Simulation in Porous Media. Vol.4, No. , (2010)
5. Speight, J.G, Extra-heavy Oil Upgrading Technologies. Gulf Professional Publishing (2013)
6. Sheng, J.S., Enhanced Oil Recovery Field Case Studies. Elsevier (2013)
7. Klein, J; Conrad, K.D., Molecular Weight Determination of Poly(acry1amide) and Poly(acry1amide-co-sodium acrylate). Macromol. Chem. (1978), 1635-1638.
8. Kulicke, W.M., Kniewske, et al. Preparation, Characterization, Solution Properties and Rheological Behavior of Polyacrylamide. Prog. Polym. Sci. (1982). 373-468.
9. Koottungal, L., Worldwide EOR Survey. The Oil and Gas Journal 108 (14),(2010), 41–53.
10. Luo, J.H.; Bu, R.Y., et al. Properties of KYPAM, A Salinity-Resistant Polymer Used in EOR. Oilfield Chem. 19 (2002)
11. McCain, W., The Properties of Petroleum Fluids, PennWell Publication, USA, 1990
12. Moms, J.D.; Penzenstadler, R.J., Acrylamide Polymers. In: Kirk Othmer Encyclopedia of Chemical Technology, Vol. 1. John Wiley and Sons, New York, 1978, 312-330.
13. Sheng, J.J., Modern Chemical Enhanced Oil Recovery: Theory and Practice. Elsevier, Burlington, MA, 2011
14. Supriningsih, D., Pembuatan Metil Ester Sulfonat (MES) Sebagai Surfaktan Untuk Enhanced Oil Recovery (EOR). Jakarta: Universitas Indonesia. 2010
15. Wang, D.M., Cheng, J.C., et al. Viscous-elastic Fluids can Mobilize Oil Remaining After Water-flood by Force Parallel to The Oil Water Interface, Paper SPE 72123 SPE Asia Pacific Improved Oil Recovery Conference, Kuala Lumpur, Malaysia, 2001
16. Wang, D.M., Han, P., et al. Sweep Improvement Options for The Daqing Oil Field, Paper SPE 99441 SPE/DOE Symposium on Improved Oil Recovery (2006)
17. Wei, S.Y., Anthony, T.C., et al. Polyacrylamide, Handbook of Petroleum Exploration and Production.Elsevier. (1989), 189-218
18. Witheford, J.M., Pellon, J.J., et al. Preparation of Aqueous Acrylamide Polymer Solutions from Polymer Gels for Enhanced Oil Recovery. US.Patent. No. 4,605,689 (1986)
19. Yanuar, L., Surfaktan MES (Metil Ester Sulfonat) untuk EOR (Enhanced Oil Recovery). Bandung: Institute of Technology Bandung. 2010.

Influence of Sulphide Loading to Biological Sulphur Recovery Performance Using *Thiobacillus consortium*

Ardiyan Harimawan [1*], Antonius Indarto [1], Ronny Purwadi [1], Andre Hendrawan [1,] and Reynard [1]

[1]*Department of Chemical Engineering, Bandung Institute of Technology, Ganesa, Bandung 40132, Indonesia*

** Corresponding Author's E-mail ardiyan@che.itb.ac.id*

Abstract

Conventional sulphur recovery process like Claus and redox process cannot be efficiently and economically performed to process Indonesian natural gas which contains low hydrogen sulphide. Biological sulphur recovery is the novel economic process which has been used to convert low amount of H_2S contained in Indonesian natural gas. Experiment conducted to determine the effect of sulphide loading parameter, consisted of sulphide concentration and dilution rate, to biological sulphur recovery performance. Experiment done by using the laboratory scale of biological sulphur recovery unit (BSRU) and *Thiobacillus* consortium by applying parameter variation at loading sulphide concentration (68, 136 and 204 ppm) and dilution rate (0.08, 0.12 and 0.20/h). Process parameter including sulphide concentration, biomass and redox potential along the experiment were observed. The highest conversion attained at sulphide feed concentration 136 ppm and dilution rate 0.08/h.

1. Introduction

Natural gas is the mixture gas of light hydrocarbon which formed through creatures decomposition with methane (CH_4) as the major component. Natural gas can be converted to chemical and energy platforms. However, raw natural gas contains impurities which is sour gas with H_2S as the main component. Sour gas must be removed from natural gas to meet the safety and product requirements.

Until then, sour gas removal process done through the sulphur recovery process, for example Claus or liquid redox processes. Those conventional sulphur recovery methods possess many disadvantages. Claus process needs a lot of oxidation energy so it is not efficient to be done using Indonesian natural gas which contain low H_2S as the feedstock. On other hands, liquid redox process needs large amount of chelating agents, implicating high operation costs.

The novel sulphur recovery process which is more efficient and cheaper is through biological sulphur recovery unit (BSRU). Biological H_2S removal utilizes sulphur oxidizing bacteria (SOB) in converting sulphide to elemental sulphur. This technology has been commercially operated and chance to substitute the existing sulphur recovery technology. Yet, there is still limited study of the process behaviour. Hence, the behaviour of BSRU process parameter need to be studied. In this study, change at loading parameter including sulphide concentration and dilution rate done and the change of process performance was observed.

2. Material and Methods

2.1 Media

The composition of media is given (Table 1).

Table 1. Media composition

Components	Feed (per liter)	Inoculum (per liter)	Settler (per liter)
$NaHCO_3$	15.12 g	15.12 g	15.12 g
Na_2CO_3	1.12 g	1.12 g	1.12 g
Nutrimix	5 mL	5 mL	5 mL
Na_2S	(depends on level)*	1.05 g (136 ppm)	-

*see Table 2.

2.2 Bioreactor

The main apparatus used in this work is a laboratory scale BSRU consisted of feed tank, peristaltic pump, bioreactor, air sparger, settler and effluent tank. The flow diagram of the equipment is given (Fig. 1).

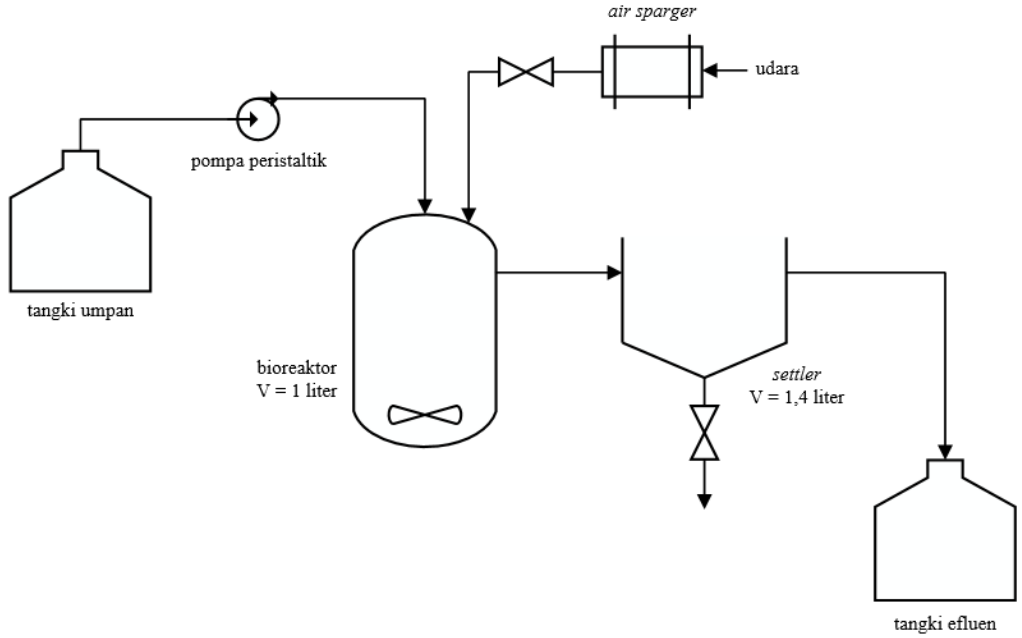

Fig. 1. Laboratory scale BSRU diagram

Thiobacillus culture grown in 2 L flask (working volume 1 L) contains mixture of medium described in Table 1 (500 mL) with sulphide concentration 136 ppm and culture (500 mL). The inoculum was placed in shaker incubator at 27°C and 150 rpm for 4 h. Then, inoculum was poured into the 1,4 L bioreactor. Settler solution 1,4 L poured into the settler. Feed was introduced into the bioreactor using a peristaltic pump (Omega Instruments). Flow rate is set as the variation of dilution rate.

Samples (6 mL each) were obtained from the bioreactor and settler effluent at each sampling periods. Measurements of pH, DO and redox potential at the sample done by using pH-meter (Martini Instruments Mi106), DO-meter (Lutron DO-5509) and ORP-meter (Hanna Instruments HI198121). Sulphur sample obtained at the end of the run through the sampling point located at the bottom of settler.

2.3 MLSS

MLSS measurements done through dry weight measurement method. First, the 15 mL falcon tubes weighed using mass balance. 6 mL of sample poured to falcon tube. Sample centrifugated at rotation rate 6000 rpm and temperature 4°C in 15 minutes. After the sample is centrifuged, the supernatant is separated from the biomass. The biomass is stored in a 100°C incubator for 24 h[1]. After being stored, the biomass weight is measured again.

2.4 Sulphur Components Analysis

Sulphide and sulphate analyzed respectively through iodometry and turbidimetry method based on APHA[2]. Settled elemental sulphur obtained through the settler sampling valve and stored at Eppendorf tube. The sulphur was left settled for 15 minutes. After 15 minutes passed, the percentage of sulphur can be determined visually. The existence and type of elemental sulphur was determined through X-ray diffraction (XRD) method.

2.5 Experiment Levels

Parameters which were varied during the experiment include loading sulphide concentration and dilution rate. The levels of each factors are given at Table 2.

Table 2. Experiment levels

Run	Feed Sulphide Concentration (ppm)	Dilution Rate (h^{-1})
1	136	0.12
2	204	0.12
3	68	0.12
4	136	0.20
5	136	0.08

3. Results and Discussion

3.1 Sulphide and Cell Concentration

Biomass concentration is related to sulphide concentration. Sulphide as the limiting substrate affect the change of specific growth rates[3]. Change of the growth rates leads to changes of cell concentration. Cell concentration is increased due to the cells growth. The decrease of cell concentration is caused by growth barriers so carried by effluent flow. The increase of sulphide concentration is only caused by substrate introduced to the bioreactor. The sulphide decrease is caused by sulphide utilization and conversion to another metabolite products. The biomass and sulphide concentration throughout the operation period at each run is given at Fig. 2 and 3. Sulphide conversion at each run is given at Table 3.

The feed sulphide concentration of 136 ppm gives the highest sulphide conversion. The conversion decrease at other feeding concentration is due to the decrease of cell concentration in the bioreactor, which implicate to lower substrate consumption rate accompanied by accumulation of sulphide. At low sulphide concentration (68 ppm), cells growth tends to be slower due to lower energy availability and metabolic stress (the stress mechanism described in section 3.4). On the other hand, higher concentration of substrate (204 ppm) leads to cell-growth repression due to toxicity of sulphide.

Low dilution rate (0.08/h) give chances for cells to utilize sulphide[4]. Thus, low dilution rates provide high sulphide conversion. On the other hand, high dilution rate (0.20/h) leads to a decrease in sulphide conversion as the cell concentration decreases throughout the process.

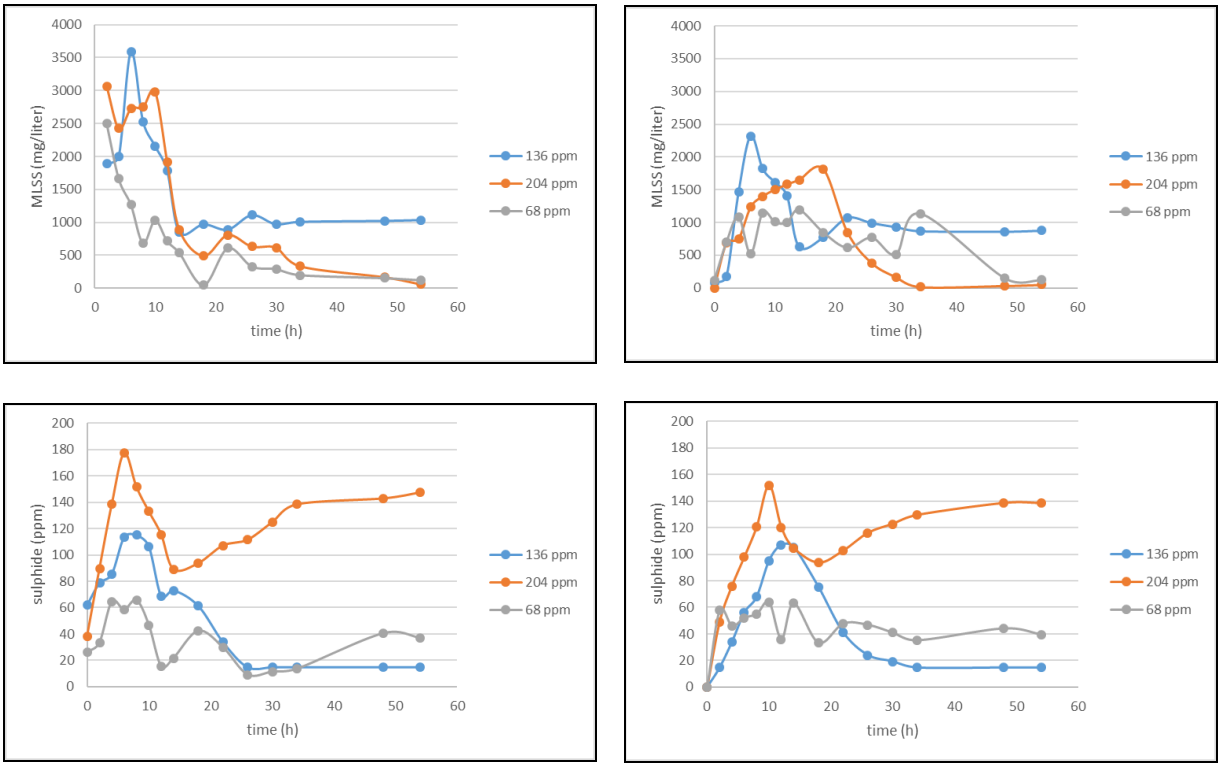

(a) (b)

Fig. 2. Biomass and sulphide concentration throughout the operation period at (a) bioreactor and (b) settler at different feed sulphide concentration at dilution rate 0,12/h

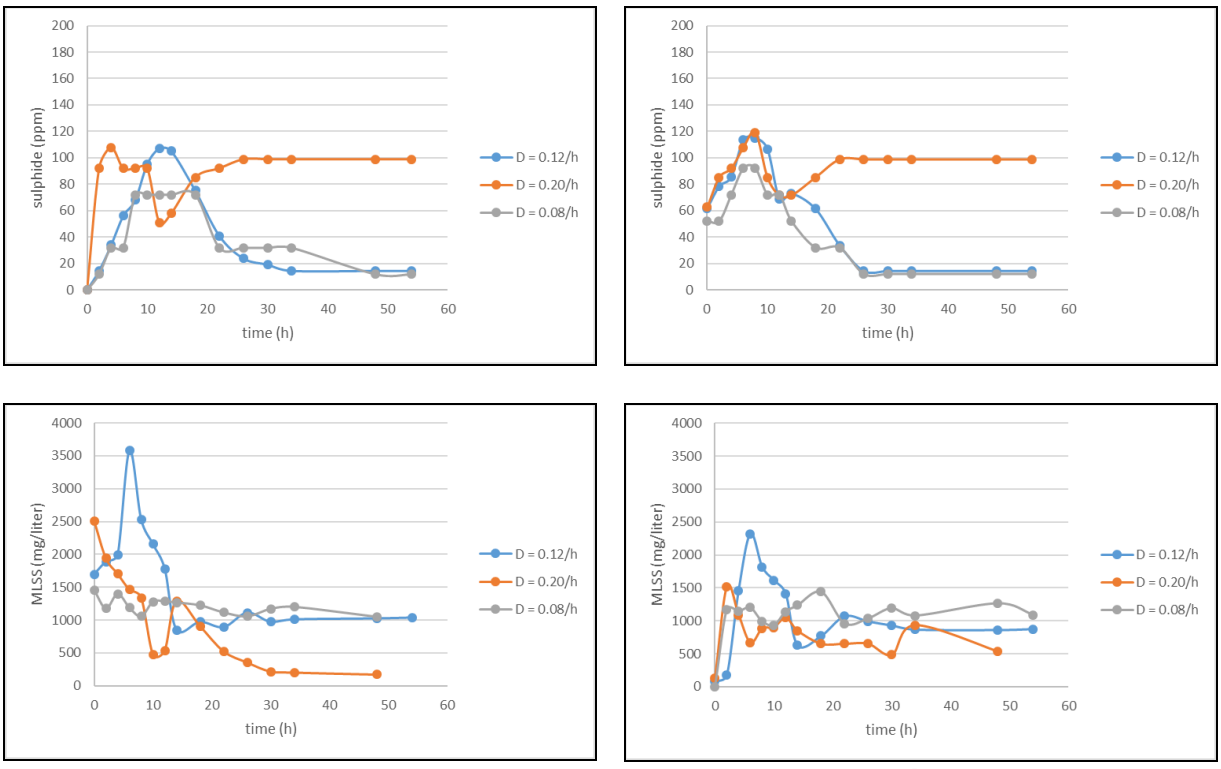

(a) (b)

Fig. 3. Biomass and sulphide concentration throughout the operation period at (a) bioreactor and (b) settler at different dilution rate at feed sulphide concentration 136 ppm

3.2 Sulphur

Through the settling test, the percentage of settling sulphur is 50% at low loading rate and 70% at high loading rate. This is in accordance with the research conducted by Jansenn et al.[5] which obtained the result that the sulphur ratio decreased at the loading rate less than 13 mg/(L·h). The increase of settling ratio at higher loading rate (70%) is due to two factors: feed sulphide concentration and dilution rate. High concentration of sulphide leads to higher concentration of sulphur products. The sulphur is attached extracellularly on the surface of bacteria[6] so that sulphur easily settled.

Table 4. Percentage of settled sulphur at different loading parameter

Sulphide Concentration (ppm)	Dilution Rate (h^{-1})	Loading Rate (mg/L·h)	Sulphur Percentage (%)
136	0.12	15.8	70
204	0.12	23.8	70
68	0.12	8.01	50
136	0.20	27.1	70
136	0.08	10.8	50

At fairly high loading rate, most of the viable cells are attached to the secreted sulphur particles. Sulphur aggregates can be seen on the settler due to the low shear rate condition that allows the aggregation. High levels of sulphide react with the elemental sulphur to form polysulphide. The polysulphide is soluble in water thus diminishing amount of observed sulphur.

3.3 Sulphate

Sulphate formed at each of runs. The percentage of sulphate formed is given at Table 5. Sulphate is produced at 5-25% of converted sulphide. The formation of the sulphate is triggered by the presence of free oxygen on the fermentation broth surface during the operation. Oxygen reacts excessively with the sulphides on the broth surface to form sulphate. This can be proved through the molar percentage of oxygen and sulphide at observed sulphide concentration (Fig. 4). The percentage value is above the unity so the sulphate formation occured[7].

Table 5. Sulphate percentage at each of runs

Feed Sulphide Concentration (mg/L)	Dilution Rate (h^{-1})	Loading Rate (mg/h)	Converted Sulphide (mg/L)	Sulphate (mg/L)	Sulphate Percentage (%)
136	0.12	15.8	119.8	29.9	25.0
204	0.12	23.8	68.57	7.97	11.6
68	0.12	8.01	27.18	3.29	12.1
136	0.20	27.1	34.23	2.74	8.0
136	0.08	10.8	123.9	6.20	5.0

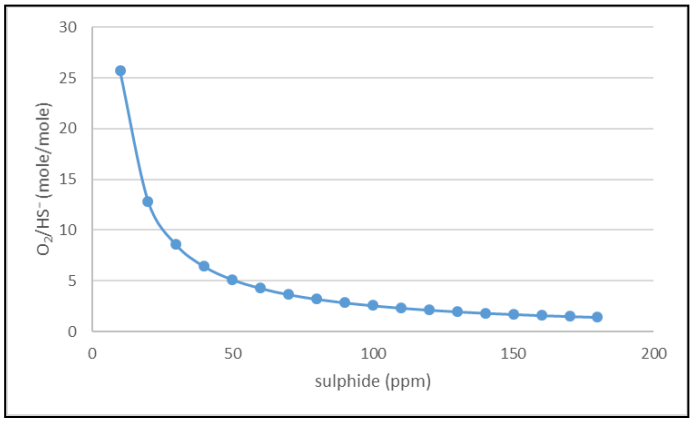

Fig. 4. Oxygen and sulphide molar percentage at the range of sulphide concentration

3.4 Redox Potential

Redox potential is a parameter that sensitive to the change of sulphide concentration[8]. Steady redox potential at each run is about −450 mV. The steady state condition illustrate the stability of cellular metabolism. Redox potential profile throughout the operation is given at Fig. 5.

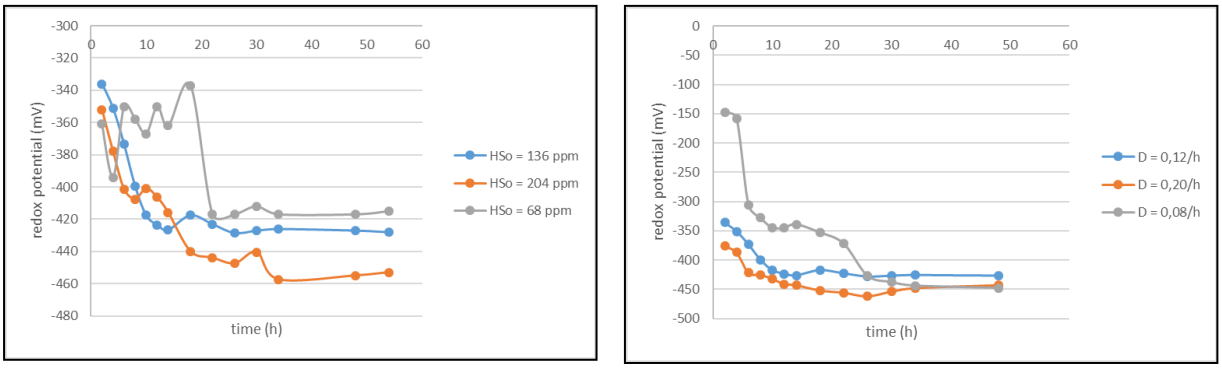

(a) (b)

Fig. 5. Redox potential throughout the period of operation at (a) different loading sulphide concentration and (b) different dilution rate

Cells undergo stress condition whenever changes of medium condition such as substrate concentration occurs suddenly. Metabolic disorders by low energy input cause low sulphide utilization resulting in sulphide accumulation in the fermentation broth. Nevertheless, the accumulation sulphides increase the rate of sulphide utilization through cysteine metabolic pathways[9] as shown at Fig. 6.

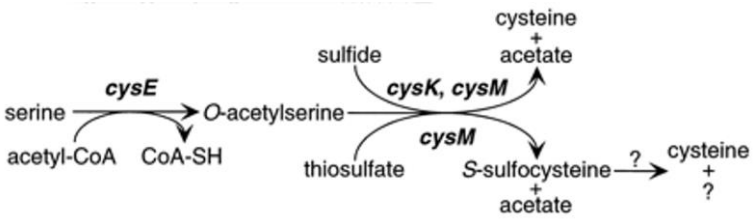

Fig. 6. Cysteine metabolism pathway
(Source: Kitabatake, 2000)

Cystein can induce the formation of reactive oxygen species (ROS) which is both radical and toxic. The anti-stress mechanism in the cells work through the reaction between cysteine and GSH forming a protein that released out of the cells. The presence of these proteins increases the redox potential of fermentation broth[10], as the profile seen in low concentration sulphide feed (68 ppm).

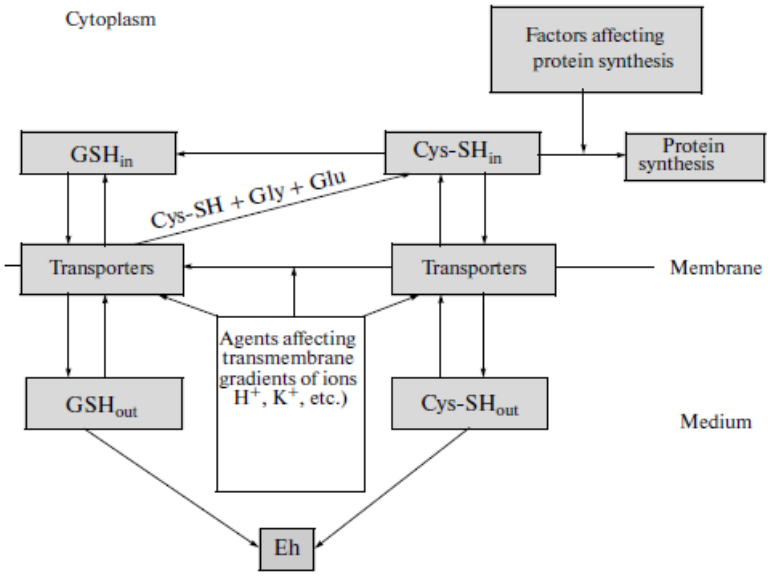

Fig. 7. Anti-stress mechanism in bacteria
(Source: Oktyabrskii and Smirnov, 2011)

Steady redox potentials (Table 6) have a linear relationship to the loading sulphide concentration because the redox potential is affected by substrate concentration that can be oxidized or reduced, pH, and DO. pH and DO were kept constant during experiments so the redox potential was only influenced by feed sulphide concentration. This is in accordance with Janssen et al.[8], Khanal et al.[11] and Krishnakumar et al.[12].

Table 6. Steady redox potential at each run

Sulphide Concentration (ppm)	Dilution Rate (h^{-1})	Loading Rate (mg/L·h)	Steady Redox Potential (mV)
136	0.12	15.8	−427
208	0.12	23.8	−455
68	0.12	8.01	−415
136	0.20	27.1	−445
136	0.08	10.8	−446

4. Conclusions

The highest sulphide conversion was obtained at sulphide concentration of 136 ppm with dilution rate of 0.12/h and 0.08/h. The percentage of settled sulphur is 70% at the loading rate more than 13 mg/h which indicates that the physical and chemical properties of biosulphur are sufficient to create aggregated conditions. Small amount (less than 30%) of sulphate formed compared with the overall sulphide conversion due to oxygen limiting condition that decrease the sulphate-forming reaction rate through the thiosulphate pathway either biologically or chemically.

Acknowledgements

Acknowledgements given to Mr. Hilman Hilmawan who had helped at planning the experiment. This work was supported by Pertamina EP whom had sent the consortium culture and Nutrimix.

References

1. Schedel M, Trüper HG, Anaerobic oxidation of thiosulfate and elemental sulphur in *Thiobacillus denitrificans*. *Archives of Microbiology*; 124: 205-210(1980).
2. APHA, *Standards Methods for the Examination of Water and Wastewater (20nd Ed.)*, 1999: London.
3. Shuler ML, Kargi F, *Bioprocess Engineering: Basic Concepts (2nd Ed.)*, 2002: New Jersey.
4. Thani A, Lin YH, et al. Variation of fermentation redox potential during cell-recycling continuous ethanol operation. *Journal of Biotechnology*; 239: 68-75(2016).
5. Janssen A, de Keizer A, et al. Surface characteristics and aggregation of microbiological-ly produced sulphur particles in relation to the process conditions. *Colloids and Surfaces B: Biointerfaces*; 6: 115-129(1996).
6. Janssen AJH, Ruitenberg R, et al. Industrial applications of new sulphur biotechnology, *Water Science Technology*; 44: 85-90(2002).
7. Janssen AJH, Sleyster R, et al. Biological sulphide oxidation in a fed-batch reactor. *Biotechnology and Bioengineering*; 47: 327-333(1995).
8. Janssen AJH, Meijer S, et al. Application of the redox potential for controling a sulfide oxidizing bioreactor. *Biotechnology and Bioengineering*; 60: 147-155(1998).
9. Kitabatake M, So WH, et al. Cysteine biosynthesis pathway in the archaeon *Methanosarcina barkeri* encoded by acquired bacterial genes? *Journal of Bacteriology*; 182: 143-145(2000).
10. Oktyabrskii ON, Smirnova GV, Redox potential changes in bacterial cultures under stress conditions. *Microbiology*; 81: 131-142(2012).
11. Khanal SK, Ju-Chang H, ORP-based oxygenation for sulfide control in anaerobic treatment of high-sulfate water. *Water Resource*; 37: 2053-2062(2003).
12. Khrisnakumar B, Majumdar S, et al. Treatment of sulphide containing wastewater with sulphur recovery in a novel reverse fluidized loop reactor (RFLR). *Water Resource*; 39: 639-647(2005).

Flow Rate Effect on Aluminum Corrosion in Citric Acid Solution

Ferdyan Ihza Akbar[1,*], Isdiriayani Nurdin[1], Hary Devianto[1], Pramujo Widiatmoko[1], Tiara Calista Shandy[1]

[1]*Department of Chemical Engineering, Institut Teknologi Bandung, Jalan Ganeca 10, 40135, Indonesia*

** Corresponding Author's E-mail akbar.ferdyanihza@gmail.com*

Abstract

Citric acid is a carboxylic acid that is widely used as an additive in the food and beverage industries. Aluminum is often used as a beverage packaging and process equipment due to its high thermal conductivity, lightweight, high strength, and low production costs. This study aims to characterize aluminum corrosion behavior in flowing citric acid solution. The corrosion rate was measured by using Rotating Disk Electrode (RDE) and potentiostat. Citric acid concentration of 2%, 3.5% and 5%-weight were used with RDE rotation speed varies at 400, 900, and 2000 rpm. Corrosion mechanism was predicted by using cyclic voltammetry (CV). X-ray Diffraction (XRD) and Scanning Electron Microscopy (SEM) were carried out to evaluate corrosion product. Cyclic Voltammogram showed that aluminum corrosion reaction in citric acid solution is irreversible with single oxidation and reduction step. XRD and SEM results identified the corros ion product as Al_2O_3. Experiment results showed that aluminum corrosion rate increased along with rising rotation speed. Curve of i_L vs $\omega^{1/2}$ in 3.5% citric acid solution showed linear behavior so that it followed Koutecky-Levich Equation. On the other hand, nonlinear behavior was shown in 5% citric acid solution which probably occurred due to viscosity and diffusivity change. Concentration rise from 3,5% to 5% has reduced corrosion rate due to aluminum passivation. In citric acid 2%, did not show limitting current which means that which means that corrosion reaction was not controlled by mass transfer.

1. Introduction

In food and beverages industry, process equipment and packaging are the most contacted element with the process material. Equipment and packaging material selection is an important aspect to ensure food safety within the whole process. Food industry commonly uses metal as equipment material due to its high thermal conductivity and strength. Interaction between process equipment and process fluid is high potential to cause equipment failure due to corrosion. Corrosion on equipment and packaging is widely caused by many factors such as pH, dissolved oxygen, temperature, and contact duration.

Aluminum is a widely used material as process equipment or even packaging due to its light weight, cheap, and strong behaviour. Research regarding corrosion resistance of aluminum in static citric acid solution had already been done. However, quantiative data about aluminum corrosion resistance in dynamic citric acid solution as representative of process dynamic has not been conducted.

This study aims to determine corrosion characteristic on aluminium in moving citric acid solution. This research was done in a scope of determining the working electrode rotating speed and citric acid solution concentration effect on mass transfer controlled corrosion rate. The experiment run was all conducted in ambient temperature and pressure. This research

benefit is to earn corrosivity data of aluminum corrosion in dynamic citric acid solution so that this data could possibly be referred for considering aluminum as selected material in food industry.

2. Experimental

Aluminium corrosion character in flowing citric acid solution was determined following some systematic experiments as shown in following figure.

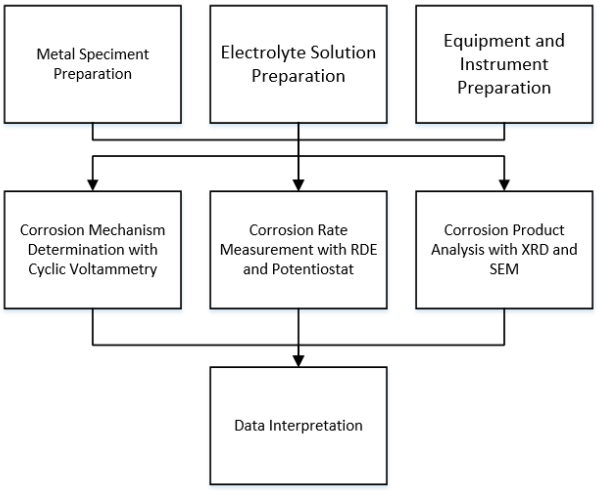

Fig. 1. Experimental Scheme

Citric acid solution was made by dissolving citric acid powder into aqua dm. Salt bridge was prepared from a saturated KCl solution in form of gel. Working electrode was constructed by shaping aluminum rod into small required speciment in 3 mm diameter. Pt-Ir spiral wire (diameter = 8 mm) was used as counter electrode. Reference electrode used was Saturated Calomel Electrode (SCE) which was immersed in saturated KCl solution and then connected to polarization cell with salt bridge. Main equipment used in this experiment was BASi RDE-2 as electrode rotation instrument and Gamry Potentiostat as cell polarization instrument. Potential scanning and electric current data acquisition were conducted using a personal computer which connected to potentiostat. Instrument configuration of this experiment is shown in Fig. 2.

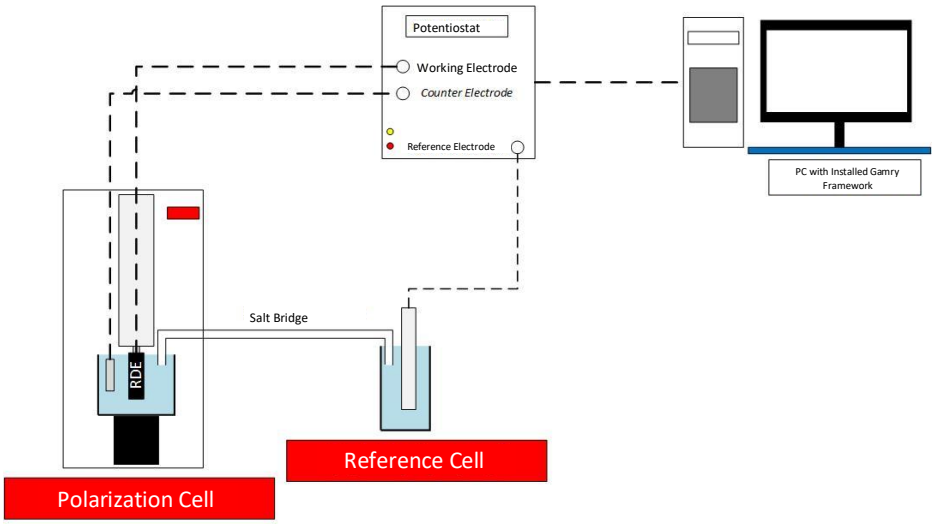

Fig. 2. Experimental Instruments Configuration

Corrosion product analysis was conducted by cutting aluminum plate into 2 cm x 3 cm x 0.2 cm and was then immersed in 5%-w/v citric acid solution.

3. Results and Discussion

This research's scopes were measuring corrosion rate of aluminum in flowing citric acid solution including prediction of its corrosion mechanism. Before conducting the experiment series, aluminum alloy is analyzed by using OES (Optical Emission Spectroscopy). After comparing the analysis result to Vargel (1979), the aluminum used in this experiment was 6000 series (Al-Mg-Si). Corrosion rate was measured within varied flow rate and citric acid solution concentration. Corrosion mechanism was predicted by interpreting cyclic voltammogram and corrosion product analysis.

3.1. Corrosion Rate Measurement

Corrosion rate of aluminum in citric acid solution was calculated by using Faraday's Law within following equation.

$$r = \frac{ia}{nF} \tag{1}$$

3.1.1 Flow Rate Effect on Aluminum Corrosion

Aluminum polarization in citric acid solution of 2%-w/v was not resulting limitting current within varied rorating speed of RDE. This indicated that aluminum corrosion in 2%-w/v citric acid solution was still controlled by charge transfer. Fig. 3 showed flow rate effect on earned limitting current within 3.5%-w/v and 5%-w/v citric acid solution.

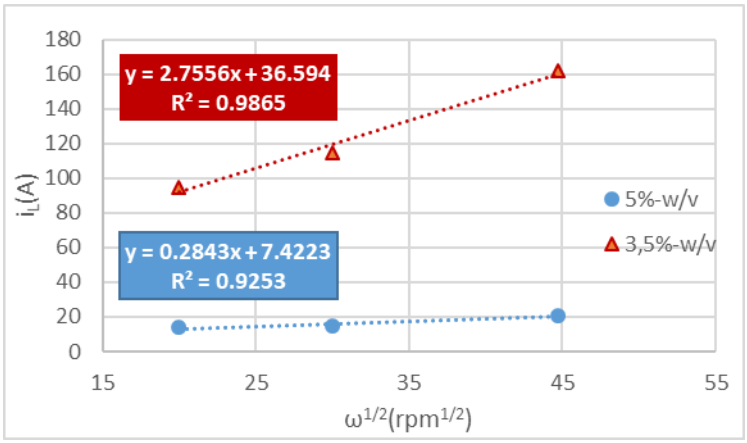

Fig. 3. Flow rate effect on limitting current

Flow rate rise didn't affect significant limitting current alteration at 5%-w/v citric acid solution. On the other hand, limitting current rise occurred significantly at 3.5%-w/v citric acid solution from 900 rpm to 2000 rpm rotation speed. Limitting current rise as rotation speed was increased happened due to thinning effect on diffusion layer where concentration gradient between bulk phase and electrode surface phase is located (Jones, 1996). Cited from Copson (1960), thinner difussion layer would ease the H^+ ion to reach metal surface, thus corrosion rate would rise. This phenomenon is also aligned with Fick's Law which stated that thinner diffusion layer will shorten the mass transfer distance so that mass transfer rate will rise. Table 1 shows that corrosion rate calculated by using limitting current value.

Table 1. Aluminum corrosion rate (mm/yr) in 3.5%-w/v and 5%-w/v citric acid solution.

	3,5%-w/v		5%-w/v	
Rotation Speed (rpm)	Limitting Current (µA)	Corrosion Rate (mm/tahun)	Limitting Current (µA)	Corrosion Rate (mm/tahun)
2000	161.689	24.86	20.601	3.167
900	114.664	17.63	14.797	2.275
400	94.444	14.52	13.794	2.121

Aluminum corrosion behaviour in flowing citric acid solution could be predicted with Koutecky-Levich model which correlates root of rotating speed ($\omega^{1/2}$) with limitting current (i_L) as shown in following equation.

$$i_L = 0.62nFAD^{\frac{2}{3}}\nu^{-\frac{1}{6}}Co^{*}\omega^{\frac{1}{2}} \quad (1)$$

Fig. 3 shows a trendline with non-zero intercept which contradictory with Koutecky-Levich correlation. According to Traimer et. al. (2001), non-zero intercept is the mathematical parameter of charge transfer control. Cited from Bard and Faulkner (2001), intercept value also shows that the happening mass transfer could sustain the concentration at the metal

surface close to the bulk phase, thus the measured current is also controlled by charge transfer phenomenon. This situation reinforced the fact that no limitting current was observed during corrosion rate measurement in 2%-w/v citric acid solution

Limitting current correlation to rotation speed shows lower linearity on 5%-w/v compared to 3.5%-w/v. It could be predicted that there was diffusivity and viscosity alteration during the rotation so that aluminum corrosion in 5%-w/v was more deviated from Koutecky-Levich equation.

3.1.2 Concentration Effect on Aluminium Corrosion in Citric Acid Solution

Aluminum corrosion rate in 5%-w/v citric acid solution was lower that 3.5%-w/v. This phenomenon was triggered by passive layer formation. Cited from Bard and Faulkner (2001), cathodic species concentration rise changes the polarization curve of the half-cell reaction. The citric acid solutio of 2%-w/v and 3.5%-w/v were not yet entered the passive potential range. While measurement was conducted in 5%-w/v, corrosion current was getting lower significantly as the result of the system had entered the passive region.

Corrosion rate measurement with RDE-Potentiostat showed that all of corrosion rates were categorized as severe corrosion as their values were above 1.270 mm/yr (NACE, 1984). This condition indicates that aluminum 6000 series is not suitable for equipment material that processes flowing citric acid solution at transition to turbulent regime.

Prediction of Aluminium Corrosion Mechanism in Citric Acid Solution

Corrosion mechanism was predicted by using cyclic voltammetry method. Informations gained from this method were reaction reversibility, corrosion product stability, and number of reaction step (Bard & Faulkner, 2001). Based on experiment results, aluminum corrosion in citric acid solution was characterized as reversible if only anodic and cathodic peak potential difference is ($E_{pa} - E_{pc} \leq 0.118/n$) ≈ 0.039 volt. Corrosion product were categorized stable if only the ratio of anodic and cathodic peak current is (i_{pa}/i_{pc}) ≈ 1. The amount of reaction step is shown from the number of peak formed in the voltammogram. Voltammogram resulted from the experiment is shown in Fig. 4.

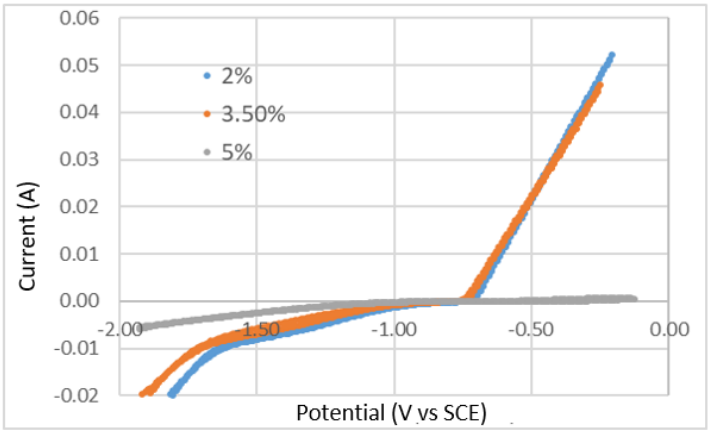

Fig. 4. Voltammogram of Aluminium Corrosion in Citric Acid Solution of 2%-w/v, 3.5%-w/v, and 5%-w/v.

Voltammogram at 2%-w/v is nearly identical to 3.5%-w/v. However at 5%-w/v, voltammogram shows a moderate trend. This condition happened due to passivation formation as Al_2O_3. Voltammogram obtained from the experiment is not showing any certain peak neither at cathodic nor anodic side. Therefore, the peak was assumed only one peak each. Peak potential values were estimated from the point where the curve exactly went rise (anodic) or low (cathodic). On the other hand, current peaks were estimated at 200 mV potential from each peak. Corrosion mechanism calculation result is shown at Table 2.

Table 2. Hasil perhitungan selisih potensial dan perbandingan arus antara puncak anodik dan katodik

Konsentrasi	ΔE_P (volt)	i_{pa}/i_{pc} (A)
2%-w/v	0,1554	4,629
3,5%-w/v	0,2199	12,45
5%-w/v	0,5097	0,8000

According to cyclic voltammetry result shown at table 2, aluminum corrosion in citric acid solution was categorized irreversible and it happened in one step of reaction each. The voltammogram also showed that the corrosion product was in unstable form. Fig. 5 shows the detailed view of voltammogram of aluminium corrosion in 5%-w/v citric acid solution.

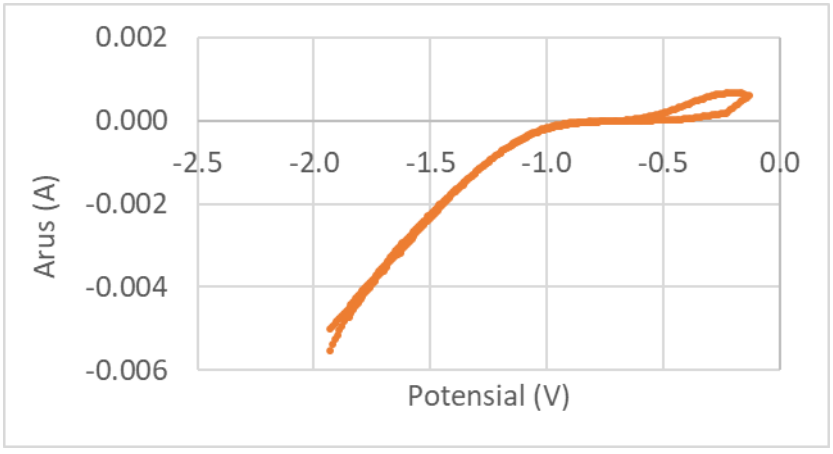

Fig. 5. Voltammogram of aluminum corrosion mechanism in 5%-w/v citric acid solution.

Fig. 5. shows that there is hysteresis phenomenon on anodic side in the voltammogram. Hysteresis shows that there was pitting corrosion phenomoneon during the experiment run

(Deyab & Keera, 2012). Pitting corrosion is also possible to occurred as the result of imperfect passive layer formation.

3.2 Corrosion Product Analysis

Corrosion produc analysis was conducted by immersing aluminum plate in 5%-w/v citric acid solution for 7 days. Surface condition after immersing is shown at Fig. 6.

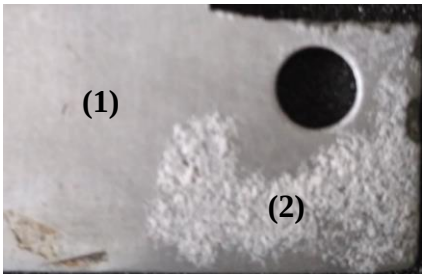

Fig. 6. Aluminum plate sample after immering in 5%-w/v citric acid solution for 7 days.

After immersing, aluminum plate was rinsed with aqua dm and then ethanol. After drying, aluminum plate sample was then analyzed with X-ray Diffraction (XRD). Corrosion product was analyzed at Bandung Center of Geological Survey. Diffractoram is shown in Fig. 7.

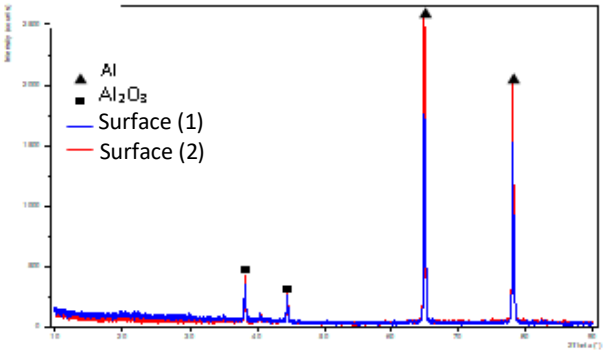

Fig. 7. Diffractogram of corrosion product of aluminum in 5%-w/v citric acid solution.

The blue diffractogram at Fig. 7 shows the XRD analysis on the smooth aluminum surface and the red one is the rough surface. After superpositioning, the diffractogram results coincided each other so that it indicated same oxide layer was formed on the surface. Diffractogram peak was then matched with the database from Bandung Center of Geologial Survey. XRD result shows that the layer formed on the aluminum sample was aluminum oxide (Al_2O_3). Rough crystal formed on the surface was then analyzed using Scanning Electrone Microscope (SEM) to obtain the exact information regarding the component inside it. SEM analysis was conducted in Bandung Center of Geological Survey for both rough surface and smooth surface. SEM result images are show at Fig. 8.

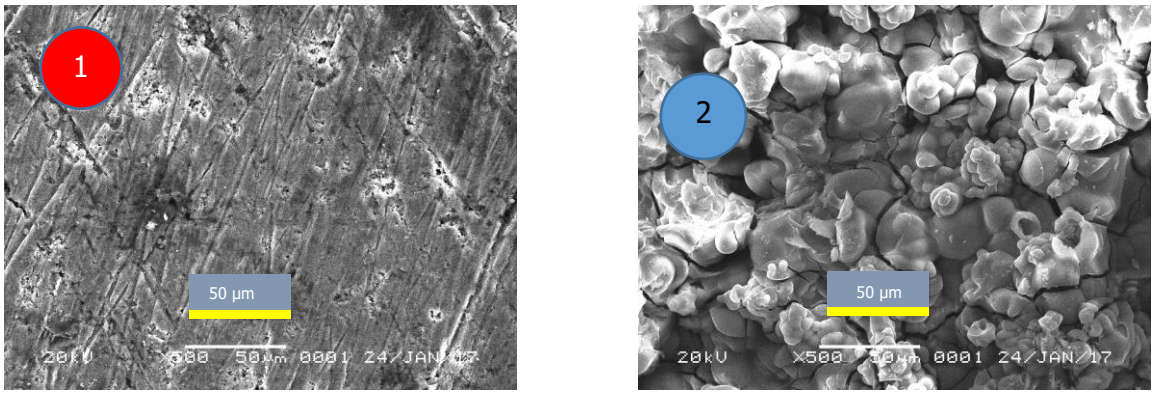

Fig. 8. SEM analysis result on smooth (1) and rough (2) surface of aluminum after immersion

SEM analysis also showed that immersed aluminum surface was covered with Al_2O_3 on both rough surface and smooth surface. Macroscopically, these shape difference seemed unobservable. However, Al_2O_3 surface on rough surface was on random shape which indicated that there was imperfect passive layer formation which led pitting corrosion

Referring to all corrosion mechanism analysis, aluminum corrosion reaction in citric acid solution was predicted as shown in the following equation.

$$\text{Cathodic Reaction} \quad : 2H^+ + 2e^- \rightarrow H_{2(g)} \tag{2}$$

$$\text{Anodic Reaction} \quad : Al \rightarrow Al^{3+} + 3e^- \tag{3}$$

Anodic reaction in form of Al^{3+} would form the corrosion product of $Al(OH)_3$. While the alumminum was dried after rinsing, $Al(OH)_3$ would undergo dehydration process which formed Al_2O_3. Overall all reaction of corrosion product of aluminum in citric acid solution is shown in the following equation.

$$Al^{3+} + H_2O \rightarrow Al(OH)_3 + 3H^+ \tag{4}$$

$$2Al(OH)_3 \rightarrow Al_2O_3 + 3H_2O \tag{5}$$

5. Conclusion

The research process concludes that aluminum was corroded irreversibly in citric acid solution with one step each on anodic and cathodic side. Corrosion product resulted from the process was unstable Al_2O_3. Citric acid solution flow rate rise would cause aluminum corrosion rate. Concentration rise from 2%-w/v to 3.5%-w/v would rise the corrosion rate and went lower while the concentration was raised to 5%-w/v due to passivation. Based on all of measurements and analysis, aluminum corrosion rate in citric acid solution that flowed from transition to turbulent superturbulent region was categorized severe.Therfore, it could be concluded that aluminum 6000 series is not recommended to be utilized as food industry process equipment that handles citric acid solution based material.

References

1. Apelblat, A., Citric Acid. Springer International Publishing, Switzerland, 2014.
2. Ashurst, P. R., Chemistry and Technology of Soft Drinks and Fruit Juices, 2nd Ed., Blackwell Publishing Ltd., Great Britain, 2005.
3. Bard, A. J., & Faulkner, L. R., Electrochemical Methods: Fundamentals and Applications, John Wiley & Sons, Inc., New York, 2001.
4. Bioanalytical Systems, Inc., Instruction Manual Rotating Disk Electrode. West Lafayette, 2000.
5. Callister, W. D.; Rethwisch, D. G., Materials Science and Engineering: An Introduction, 9th Ed., Wiley, Hoboken, 2014.
6. CIEC Promoting Science at the University of York, Biotechnology in the Chemical Industry, accessed from The Essential Chemical Indutry online: www.essentialchemicalindustry.org, 2013.
7. Craig, B. D., & Anderson, D. B., Handbook of Corrosion Data. ASM lnternational, United States of America, 2002.
8. Daniel, M., Medicinal Plants Chemistry and Properties, Science Publishers, USA, 2006.
9. Davis, J. R., Corrosion: Understanding the Basics, ASM International, Ohio, 2000.
10. Deyab, M. A., & Keera, S. T., Cyclic voltammetric studies of carbon steel corrosion in chloride-formation water solution and effect of some inorganic salts, *Egyptian Journal of Petroleum 21* (2012) 31-36.
11. Fachruddin, I. L., Membuat Aneka Sari Buah, Penerbit Kanisius, Yogyakarta, 2002.
12. Fontana, M. G., Corrosion Engineering, 3rd Ed., McGraw-Hill, Singapura, 1987.
13. Formica, J. Chapter 18: X-Ray Diffraction, dalam F. Settle, Handbook of Instrumental Techniques for Analytical Chemistry (hal. 339-342). Prentice-Hall PTR, New Jersey, 2011.
14. Ghali, E. Aluminum and Aluminum Alloys .BR. W. *Revie, Uhlig's Corrosion Handbook* (hal. 715-744). John Wiley & Sons, Inc., New Jersey, 2011.
15. Jamaati, R.; Toroghinejad, M. R.; Najafizadeh, A., Application of anodizing and CAR processes for manufacturing Al/Al2O3 composite, Materials Science and Engineering A 527 (2010) 3857–3863.
16. Jones, D. A. Principles and Prevention of Corrosion", Prentice-Hall International (UK), London, 1996.
17. Kementerian Kesehatan Republik Indonesia (Kemenkes RI), Bahan tambahan Pangan, PERMENKES RI No. 33 tahun 2012.
18. Solmaz, R. dkk., Citric Acid as Natural Corrosion Inhibitor for Aluminium Protection, Maney, 43 (2007), 190.
19. Khachatourians, G. G.; Arora, D. K., Applied Mycology and Biotechnology, Volume I: Agriculture and Food Production, Elsevier, Amsterdam, 2001.
20. Lopez-Garcia, R., Citric Acid, dalam Kirk-Othmer, Kirk-Othmer Encyclopedia of Chemical Technology (hal. 1-25). John Wiley and Sons, Inc., 2010.
21. Max, B.; Salgado, J. M.; Rodríguez, N.; Cortés, S.; Converti, A.; Domínguez, J. M.,
22. Biotechnological production of citric acid, Brazilian Journal of Microbiology, 41 (2010), 862-875.
23. National Center for Biotechnology Information, Citric Acid, Diakses 4 Maret 2016, dari Pub Chem Open Chemistry Database: https://pubchem.ncbi.nlm.nih.gov/compound/311
24. Nikolic, J.; Expósito, E.; Iniesta, J.; González-Garcia, J.; Montiel, V., "Theoretical Concepts and Applications of a Rotating Disk Electrode", J. Chem. Educ. (2000), 1191.
25. Perez, N., Electrochemistry and Corrosion Science, Kluwer Academic Publishers, Boston, 2004.

26. Prasetya, A. Y.; Nurdin, I., "Korosi Aluminium dalam Larutan Asam Sitrat", Jurnal Teknik Kimia Indonesia 11 (2012) 116-123.
27. Roberge, P. R. *Handbook of Corrosion Engineering*, McGraw-Hill, Hightstown, 2000.
28. Robertson, G. L., Food Packaging: Principles and Practice, 3rd Ed., CRC Press, Boca Raton, 2012.
29. Shreir, L.; Jarman, R.; Burstein, G., Corrosion Volume 1: Metal/Environment Reactions 3rd Ed., Butterworth-Heinemann, Oxford, 2000.
30. Talbot, D.; Talbot, J., Corrosion Science and Technology CRC Press LLC, Florida, 1998.
31. Treimer, S., Tang, A., & Johnson, D. C., A Consideration of the Application of Koutecky-Levich Plots in the Diagnoses of Charge-Transfer Mechanisms at Rotated Disk Electrode, WIley-VCH, Ames, 2001.
32. Waseda, Y.; Matsubara, E.; Shinoda, K., X-ray Diffraction Crystallography: Introduction, Examples and Solved Problems, 1st Ed., Springer-Verlag Berlin Heidelberg, 2011.
33. Vargel, C., Le comportement de l'aluminium et de ses alliages, Dunod, Paris, 1979.

Data Reconciliation for Modelling and Troubleshooting of Ammonia Synthesis Reactor

Tri Partono Adhi[1*], Untoro Eko Saputro[1]

[1]*Department of Chemical Engineering, Institut Teknologi Bandung, Jl. Ganesha 10, Bandung 40132, Indonesia*

** Corresponding Author's E-mail tpadhi@che.itb.ac.id*

Abstract

Data reconciliation (DR) could provide efficiency analysis, condition monitoring & operation optimization or troubleshooting. DR techniques improve the accuracy of measurements using redundancies measurements of plant data. Bad plant data could lead wrong solution based on modelling and troubleshooting simulation. Gross error is one of causes of bad plant data, then it could be overcome by mass and energy balance through data reconciliation. DR also bring direct or indirect financial benefits by eliminate gross error measurements. This paper presents and demonstrates utilization of plant data to modelling and troubleshooting of ammonia synthesis reactor system using DR. Statistical analysis based on DR shows suitable model to define system condition. DR and gross error detection are simulated using Aspen HYSYS V8.8. Ammonia synthesis reactor system is assumed to consist of feed-effluent heat exchanger (FEHE) and single bed reactor. The result presents that bad plant data shows gross error measurements or system problems such as leakage in FEHE or channelling in reactor. Gross errors could be eliminate using DR by serial elimination strategy. DR also indicates appropriate model with plant data by simulation. The fitted model could provide the right troubleshooting solutions and avoid wrong solutions from system problems. So, DR brings outcomes as a time and financial benefits from troubleshooting of bad plant data in ammonia synthesis reactor.

Keywords: data reconciliation, gross error, plant data, reactor, troubleshooting

1. Introduction

Data reconciliation could help to improve the accuracy of online measurements with no extra requirement on equipment upgrading[1]. Accurate measurement also provides reliable plant data which could determine the effectiveness of plant performance for improvement strategies especially troubleshooting. If these data are not reliable, decisions might be made based on wrong assumptions and more harm than good may occur[1]. Data reconciliation and gross errors detection could provide efficiency analysis, condition monitoring and operation optimization[2]. Data reconciliation could bring time benefit especially for complex chemical process systems, such as ammonia reactor system which is consisted of feed-effluent heat exchanger (FEHE) and reactor by analyzing and optimizing plant data in this system.

Gross errors could appear because of the inaccurate of measurement devices or inadequate mathematical models which analyzed by data reconciliation. When a set of data is realistic, then the material and energy is almost balance. Imbalance material and energy might indicate gross errors in data[3].

Data reconciliation in process modelling require redundancy to guarantee available plant data between redundant and observable data. Redundancy could lead to discrepancy, and conflicted readings have to be reconciled. Basic issues are whether the estimation of an observed value can be improved by using the other measurements (redundancy), an unobserved value is estimable from the observed ones (determinability) and whether an

observed value is a gross error[4]. Data reconciliation could be best analysis method to indicate process condition and decide solution of the problems by comparing redundant and reconciled data and simulation. Data reconciliation modelling evaluate the system performance, obtain reconcile data (DR), or to optimize/troubleshoot the system by adjusting some parameters[5].

Data reconciliation modelling use mathematical process model which represent system condition. The suitable mathematical model is influenced by plant data which is analyzed by data reconciliation. The process model is a set of inequality and equality constraints and describes the fundamental relationship of process units, such as material and energy balances, rate equations and equilibrium relations[6]. Good plant data provides data redundancy to guarantee data availability. Redundancy could be used to determine the suitable mathematical model and improve the accuracy of plant data by reducing the effect of random errors. Data reconciliation use redundant data and adjust the redundant data according to their estimated standard deviations to obtain the estimation that satisfy system constraints[2]. Reconciled process data is used to specify the current status of the plant model and for estimation of the model parameters for plant-model matching[6].

Combined FEHE and ammonia reactor is one important system in ammonia plant. These plant data are usually provided in logbook and noted by operator, and it is also recorded in DCS system. These data are important to improve plant performance or solve plant problems, so accurate and reliable data are needed. Data reconciliation could provide simple way to monitoring and analyzing plant data, furthermore it could be used to troubleshoot the problems. Bad plant data without any reconciliation could trigger wrong troubleshooting solution eventually could harm plant and environment, moreover it could bring time and financial loss to apply that wrong solution. Gross errors are the main source of wrong solution without any data reconciliation. Gross errors are the data problems which frequently appear, so it is important to identify and isolate gross errors. Based on bad plant data which contain gross error data, the decrease plant performance could be identified, so the system could be overhauled to fix the performance. There may also be a possibility where the system is running well, but there are gross errors in these data because of human/operator errors, inaccurate measurement, or others problems.

This paper evaluates two main problems in FEHE and ammonia reactor system, they are the gross error problem which analyzed and eliminated by data reconciliation and the ammonia system problems which is indicated by the decreasing of outlet temperature. This paper presents and demonstrates a brief utilization of plant data to analyze and troubleshooting of FEHE and single bed ammonia synthesis reactor. Both problems are solved by data reconciliation based on mathematical process modelling by software and statistical analysis.

2. Methodology

Data reconciliation also adjusts process measurements with random errors by having them satisfy material and energy balance constraints and is a way to improve the quality of the measurements taken from a process via DCS or any other means of data collection[6]. The problem of data reconciliation in plant is to minimize an objective function, e.g. the sum of the squared adjusts pondered by their reciprocal variances, subject to linear or nonlinear restrictions (material balances)[7]. Steady state simulation packages equipped with optimization routines can be used to perform data reconciliation and obtain accurate results. This approach can be used to reconcile linear and nonlinear problems via the minimization of a weighted least squares objective function by varying appropriate flowsheet variables[8].So, data reconciliation problem simulation is defined as a nonlinear steady-state data by a least sum of square minimization problem as follows:

$$Q_{min} = \sum \left(\frac{x_i^m - x_i}{\sigma_i} \right)^2 \quad (1)$$

$$f(x_i, y_i) = 0 \quad (2)$$

Q_{min} is estimated covariance matrix of measured data; **x^m** is measured values; **x_i** is reconciled values of measured parameters; and **σ_i** represents the estimated error standard deviation. **f(x,y)** represents the steady state system constraint equations; **y_i** represents the calculated value for the unmeasured parameters.

Process simulators with optimization capabilities such as Aspen HYSYS can be used to carry out data reconciliation and parameter estimation[9]. Data reconciliation and gross error detection are simulated using Aspen HYSYS V8.8 to achieve efficient calculation including measurement design, gross error detection and elimination, errors propagation, as well as parameters estimation. Data and model are compared to determine an adequate model by formulation as follows:

$$Q_{min} \approx \chi^2_{crit}(v) \quad (3)$$

Q_{min} represents the random variables with distribution of **χ^2**, and **v** represents the degree of freedom. If Q_{min} is greater than critical value of distribution χ^2 (σ_c), it indicates that data and model are conflicted which could not be ignored (significant factor). The basis of design of ammonia reactor modeling in Aspen HYSYS uses kinetic data by Temkin equation. Ammonia synthesis is an exothermic reaction with kinetic equation which are defined by following equations:

$$N_{2\,(g)} + 3H_{2\,(g)} \leftrightarrow 2NH_{3\,(g)} \quad \Delta H = -92{,}22 \text{ kJ/mol} \quad (4)$$

$$r = k_1 p_{N_2} \frac{p_{H_2}^{1{,}79}}{p_{NH_3}^{-1{,}19}} - k_{-1} \frac{p_{NH_3}^{0{,}81}}{p_{H_2}^{-1{,}21}} \quad (5)$$

$$k_1 = 36421 \exp\left(\frac{-19484}{RT}\right) \quad (6)$$

$$k_{-1} = 3{,}4585.10^{14} \exp\left(\frac{-38119}{RT}\right) \quad (7)$$

Feed composition & condition is shown in table 1. Ammonia synthesis reactor is presented in table 1. Simulation in Aspen HYSYS V8.8 use Peng-Robinson Package, and ammonia reactor single bed is modelled by single adiabatic plug flow reactor.

Table 1. Composition and feed condition of reactor

Temperature (^oC)	437
Pressure (bar)	142.1
Flowrate (kg/h)	203422
Flowrate (kmol/h)	19440
Vapour Fraction	1.00
Composition (%-mol)	
N_2	17.77
H_2	63.77
NH_3	8.81
CH_4	4.82
Ar	4.82

Table 2. Composition and feed condition of reactor

Name	R-100
Volume reactor (m^3)	13.96
Length (m)	6
Diameter (m)	1.721
Void fraction	0.36
Type of reactor	Adiabatic Plug Flow Reactor

Data reconciliation is assumed as single jeopardy. It means that there are no two or more problems simultaneously or problems and gross errors which're occurred simultaneously. Others assumption is there is no channelling in ammonia reactor system based on scope of study which are gross error measurements and the decreasing of catalyst activity problem. Then, based on these data and assumptions, methodology is divided into 4 main steps, they are:

1. **Ideal modelling using Aspen HYSYS and operation/plant data collection.** This model is based on design data with standard deviation of measurement devices. Operational data is acquired from operator shift with redundancy data.
2. **Data analysis and gross error identification and isolation.** Data reconciliation use ideal model and operational/plant data to obtain reconciled data. Error from reconciled data and plant data is compared to standard deviation of measurement devices. If error is greater than standard deviation, gross error identification and isolation are next step to determine system condition.
3. **Troubleshooting with measured data which don't have gross errors.** If there are no gross errors, we generate new model which is appropriate to problem in system. Measured data will be checked with new model and produce reconciled data. If error is in standard deviation range and identical with new model, so system is experienced problem based on model.
4. **Decision making.** Based on data reconciliation and troubleshooting, solutions are given based on analysis. For example, catalyst regeneration if there is catalyst deactivation or instrumentation check and calibration if there is gross error. Detail methodology is shown in figure 1.

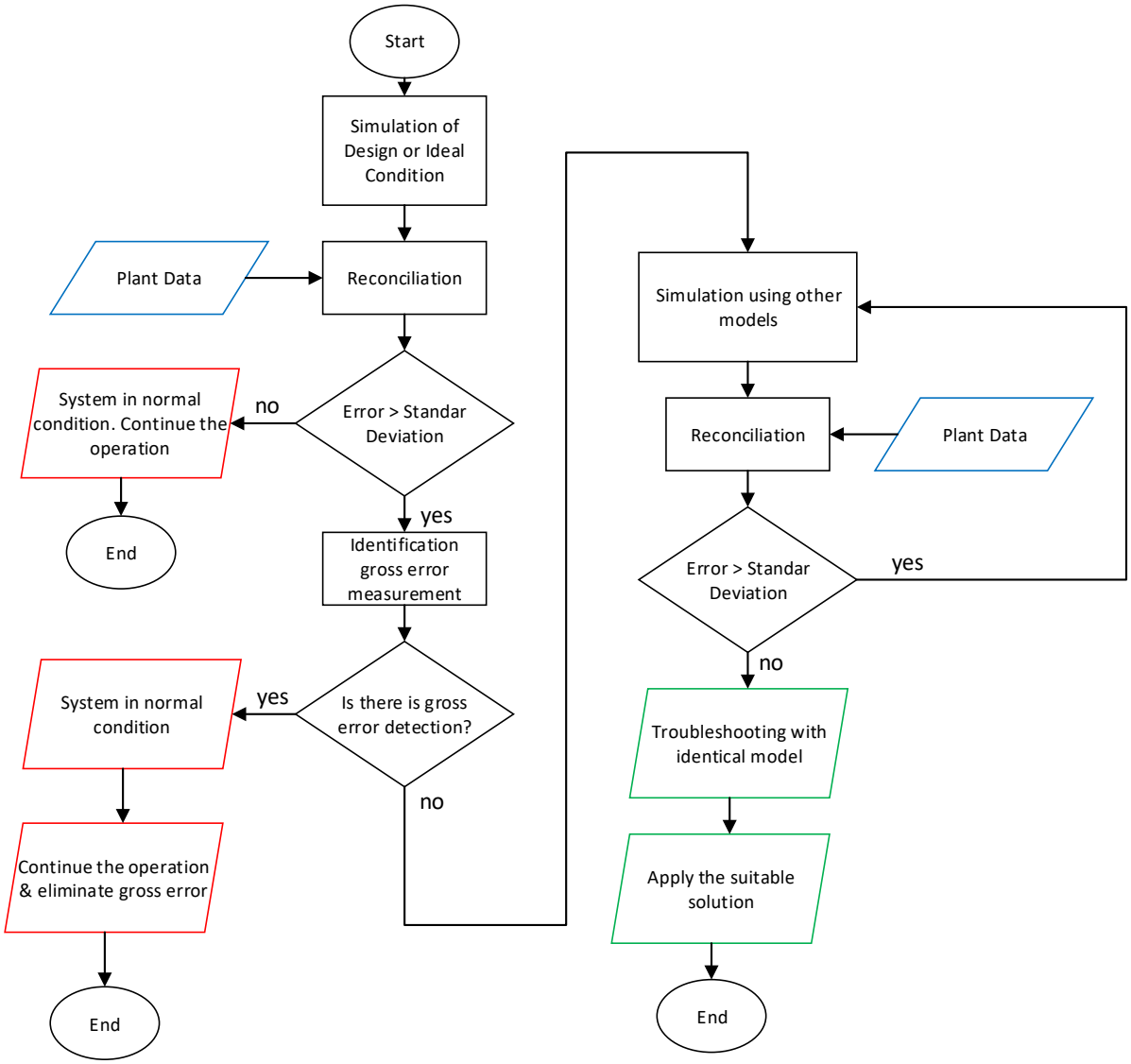

Figure 8. Methodology of simulation data reconciliation for troubleshooting

3. Result and Discussion

Based on design data of ammonia plant, ideal model is shown in figure 2. Result of streams inlet and outlet is presented in table 3. Specification of measurement devices in ammonia reactor system is also presented in table 4.

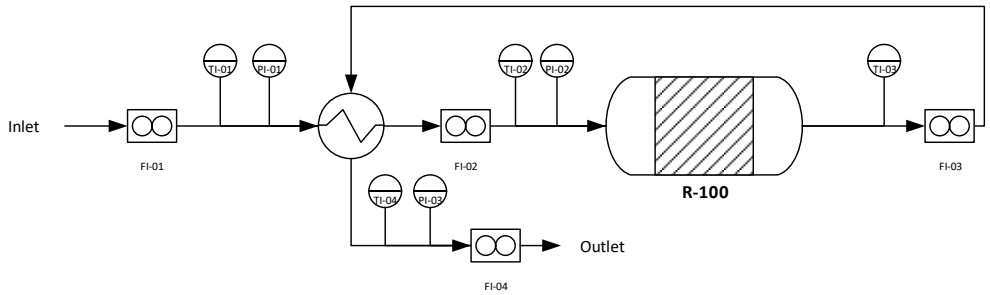

Figure 2. Ideal model of ammonia synthesis reactor

Table 3. Stream specification of ideal model reactor

Stream	Inlet	Outlet Reactor	Outlet HE
Temperature (°C)	437	493.5	356.6
Pressure (bar)	142.1	141.7	141.5
Flow (kg/h)	203422	203422	203422
Flow (kmol/h)	19440	187788	187788
Vapour fraction	1.00	1.00	1.00
Composition (%-mol)			
N_2	17.77	16.62	16.62
H_2	63.77	60.69	60.69
NH_3	8.81	12.70	12.70
CH_4	4.82	5.00	5.00
Ar	4.82	4.99	4.99

Table 4. Measurement devices specification of reactor system

Tag Number	Type	Unit	Min	Max	St. Dev.
FI-01 s.d. FI-04	Online analyser	(kg/h)	150000	250000	$\pm$ 100
TI-01 s.d. TI-04	Temperature indicator	(°C)	300	500	$\pm$ 1
PI-01 s.d. PI-04	Pressure Indicator	(bar)	125	150	$\pm$ 1

2.1 Data Reconciliation and Gross Error Detection

Hypothetical plant data are acquired as shown in table 5 with some redundancies. Based on these data, data reconciliation result from this plant data is shown in table 6.

Table 5. Plant data from ammonia synthesis reactor

Time	FI-01 (kg/h)	FI-02 (kg/h)	FI-03 (kg/h)	FI-04 (kg/h)	TI-01 (°C)	TI-02 (°C)	TI-03 (°C)	TI-04 (°C)	PI-01 (bar)	PI-02 (bar)	PI-03 (bar)	PI-04 (bar)
10	203421	203423	203431	203421	301	438.1	494	387	142.5	142	141.9	141.1
14	203427	203429	203471	203451	298.9	436.3	492.7	386	142.1	141.7	141.5	141.2

Table 6. Data reconciliation result before and after gross error elimination (GEE)

Case					Before GEE		After GEE	
Time	Tag	Plant data	Std. Dev.	Design Data	Reconciled Data	Error/Std. Dev. (%)	Reconciled Data	Error/Std. Dev. (%)
10	FI-01 (kg/h)	203421	100	203423	203423	1.56	203423	1.56
	FI-02 (kg/h)	203423	100	203423	203423	0.44	203423	0.44
	FI-03 (kg/h)	203431	100	203422	203422	8.73	203422	8.78
	FI-04 (kg/h)	203421	100	203422	203422	1.27	203422	1.22
	TI-01 (°C)	301	1.0	300	315.3	1426.65	300.0	100.00
	TI-02 (°C)	438.1	1.0	437	437.4	73.76	437.0	110.00
	TI-03 (°C)	494	1.0	493.5	494.8	75.31	494.4	39.06
	TI-04 (°C)	387	1.0	356.6	372.8	1419.49	357.5	2.95
14	FI-01 (kg/h)	203427	100	203423	203423	4.44	203423	4.44
	FI-02 (kg/h)	203429	100	203423	203423	6.44	203423	6.44
	FI-03 (kg/h)	203471	100	203422	203422	48.77	203423	48.78
	FI-04 (kg/h)	203451	100	203422	203422	28.77	203423	28.78
	TI-01 (°C)	298.9	1.0	300	313.8	1489.55	300	110.00
	TI-02 (°C)	436.3	1.0	437	436.1	18.68	437	70.00
	TI-03 (°C)	492.7	1.0	493.5	493.5	77.42	493.5	169.06
	TI-04 (°C)	386	1.0	356.6	371.3	1470.03	356.6	2.85
Q_{min} (Objective Function)						**845.77**		**8.02**
$\chi^2(v) = \sigma_c$						**27.60**		**27.60**

Based on table 6, measurement devices TI-01 and TI-04 has high error but others measurement devices still have tolerable error but TI-01 have similarity value with design data. TI-04 record higher temperature of outlet HE than temperature of design data. The hypothesis is there is gross error measurement in TI-04. Then, TI-04 measurement is ignored to identify and isolate the gross error by changing standard deviation to 1000. Data reconciliation after gross error elimination of FI-02 measurement is shown in table 7.

Data reconciliation could eliminate gross error which also could minimize objective function (Q_{min}) from 845.77 to 8.02. It indicates that there is gross error measurement in TI-04. So, there is no problem occurred in ammonia reactor based on this analysis because the error from data reconciliation of plant data after gross error elimination is still tolerable. Action required based on this analysis are instrument TI-04 overhaul and calibration, procedure checking of TI-04 measurement by operator (it could be human error, e.g. miss input from operator to logbook especially in TI-04).

2.2 Data Reconciliation Modelling and Troubleshooting

Outlet temperature and low conversion of ammonia system could indicate problem in the system. It could be caused by so many problems such as gross error measurement, leakage of FEHE or channeling in reactor. This system is single input and single output, so material in and out should be same. Leakage FEHE and channeling also provide identical mass balance without Channeling is also reasonable problem in bed reactor. Both problems could decrease temperature of outlet system. In this case, this system also has been analyzed has no problems in catalyst activity.

Data reconciliation modelling could analyze the model of system problems. Bad plant data were acquired as shown in table 7. It indicates that there were problems in the ammonia reactor because of temperature outlet drop. Based on this case, temperature measurements have two redundancies because each temperature inlet and outlet FEHE is known, so TI-02 and TI-04 could be calculated by model.

Table 7. Bad plant data of ammonia reactor

Tag	TI-01 (°C)	TI-02 (°C)	TI-03 (°C)	TI-04 (°C)	FI-01 (kg/h)	FI-02 (kg/h)	FI-03 (kg/h)	FI-04 (kg/h)
Design Data	300	437	493.5	356.6	203422.6	203422.6	203422.6	203422.6
Plant Data 1	300.5	437.5	490.2	353.1	203422.5	203422.6	203422.5	203422.7
Plant Data 2	299.8	436.8	490.6	353.9	203422.4	203422.3	203422.3	203422.3

Based on these plant data, the data reconciliation result (using Aspen HYSYS simulation) based on ideal model is shown in table 8. Gross errors should be detected in TI-03 and TI-04 because of gap between plant data and design data, then it proven by DR of ideal model. However, the plant data is actual and there is no gross error measurements after actual checking in field data. Moreover, it also could not explain the low conversion of reactor (drop ~7%). If there is no gross error measurement in plant data, the process model should be analysed because ideal model also shows a conflict between data and model which could not be ignored because $Qmin > \sigma_c$. First model which could be analysed in this case is leakage of FEHE. Leakage of FEHE could influence the outlet temperature and conversion of reactor because the mass flow loss in reactor and by pass flow in FEHE. Second model is channelling in reactor ammonia. Channelling also identified by low conversion in reactor and temperature

drop which has same typical condition with leakage of FEHE. Both of these model could be analysed by DR modelling which is shown in figure 3.

Table 8. Ideal model data reconciliation

Case					Before GEE		After GEE	
Time	Tag	Plant data	Std. Dev.	Design Data	Reconciled Data	Error/Std. Dev. (%)	Reconciled Data	Error/Std. Dev. (%)
10	FI-01 (kg/h)	203422.5	100	203423	203423	0.06	203423	0.06
	FI-02 (kg/h)	203422.6	100	203423	203423	0.04	203423	0.04
	FI-03 (kg/h)	203422.5	100	203422	203422	0.27	203422	0.27
	FI-04 (kg/h)	203422.7	100	203422	203422	0.47	203422	0.47
	TI-01 (°C)	300.5	1.0	300	299.6	93.48	300.5	0.00
	TI-02 (°C)	437.5	1.0	437	438.7	124.16	437.5	0.00
	TI-03 (°C)	480.8	1.0	493.5	493.5	329.61	493.5	0.33
	TI-04 (°C)	343.7	1.0	356.6	354.4	133.97	356.6	0.35
14	FI-01 (kg/h)	203422.3	100	203423	203423	0.26	203423	0.26
	FI-02 (kg/h)	203422.3	100	203423	203423	0.26	203423	0.26
	FI-03 (kg/h)	203422.3	100	203422	203422	0.01	203422	0.08
	FI-04 (kg/h)	203451	100	203422	203422	28.69	203422	28.78
	TI-01 (°C)	299.8	1.0	300	299.2	63.03	299.8	0.00
	TI-02 (°C)	436.8	1.0	437	437.8	102.64	436.8	0.00
	TI-03 (°C)	480.1	1.0	493.5	493.5	289.65	493.5	0.29
	TI-04 (°C)	343.2	1.0	356.6	355.0	106.21	356.6	0.27
Q_{min} (Objective Function)						**26.13**		**0.084**
$\chi^2(v) = \sigma_c$						**19.70**		**19.70**

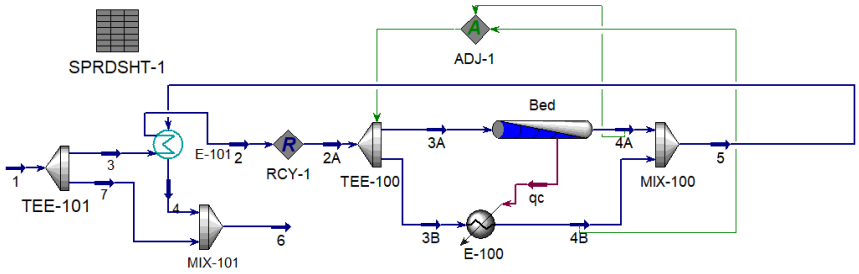

Fig.3. Modelling leakage of FEHE and reactor channelling in Aspen HYSYS

The DR result of leakage of FEHE model is presented in table 8, meanwhile the channelling reactor model DR result is shown in table 9. FEHE's leakage shown 7% leakage after DR, but channelling reactor model shown 8.8% channelling based on data fitting feature in simulation. FEHE's leakage also still has conflict between data and model because of Qmin > σ_c. In other hand, channelling reactor model shown appropriate mathematical process model without conflicting, it shown by value of Qmin < σ_c based on statistical analysis. So, the suitable

model indicates the process condition, it mean that there is channelling in ammonia reactor which is caused temperature drop and low conversion.

Table 9. Leakage of FEHE model data reconciliation

Time	Tag	Plant data	Std. Dev.	Reconciled Data	Design Data	Error/Std. Dev. (%)
10	FI-01 (kg/h)	203422.5	100	203423	203423	0.06
	FI-02 (kg/h)	203422.6	100	189183	203423	14239.62
	FI-03 (kg/h)	203422.5	100	188413	203422	15009.22
	FI-04 (kg/h)	203422.7	100	202653	203422	769.84
	TI-01 (ºC)	300.5	1.0	300.0	300	50.00
	TI-02 (ºC)	437.5	1.0	437.0	437	50.00
	TI-03 (ºC)	490.2	1.0	491.2	493.5	96.66
	TI-04 (ºC)	353.1	1.0	349.9	356.6	318.92
14	FI-01 (kg/h)	203422.3	100	203423	203423	0.26
	FI-02 (kg/h)	203422.3	100	189183	203423	14239.32
	FI-03 (kg/h)	203422.3	100	188413	203422	15009.02
	FI-04 (kg/h)	203451	100	202653	203422	798.14
	TI-01 (ºC)	299.8	1.0	300	300	356.34
	TI-02 (ºC)	436.8	1.0	437.0	437	20.00
	TI-03 (ºC)	490.6	1.0	491.2	493.5	56.66
	TI-04 (ºC)	353.9	1.0	349.9	356.6	398.92
	Q_{min} (Objective Function)					**85758**
	$\chi^2(v) = \sigma_c$					**19.70**

Table 106. Channelling reactor model data reconciliation

Time	Tag	Plant data	Std. Dev.	Reconciled Data	Design Data	Error/Std. Dev. (%)
10	FI-01 (kg/h)	203422.5	100	203422.6	203423	0.06
	FI-02 (kg/h)	203422.6	100	203422.6	203423	0.04
	FI-03 (kg/h)	203422.5	100	203422.2	203422	0.25
	FI-04 (kg/h)	203422.7	100	203422.2	203422	0.45
	TI-01 (ºC)	300.5	1.0	300.2	300	33.51
	TI-02 (ºC)	437.5	1.0	437.2	437	34.65
	TI-03 (ºC)	490.2	1.0	490.3	493.5	9.78
	TI-04 (ºC)	353.1	1.0	353.4	356.6	31.51
14	FI-01 (kg/h)	203422.3	100	203423	203423	0.26
	FI-02 (kg/h)	203422.3	100	203423	203423	0.26

FI-03 (kg/h)	203422.3	100	203422	203423	0.05
FI-04 (kg/h)	203451	100	203422	203423	28.75
TI-01 (°C)	299.8	1.0	300.2	300	38.49
TI-02 (°C)	436.8	1.0	437.1	437	26.44
TI-03 (°C)	490.6	1.0	490.3	493.5	30.22
TI-04 (°C)	353.9	1.0	353.5	356.6	37.34
Q_{min} (Objective Function)					**0.87**
$\chi^2(v) = \sigma_c$					**19.70**

Ensuring the DR analysis, case study is done to compare the DR and modelling. FEHE's leakage and channelling are identified using case study by adjusting leakage of FEHE and channelling (%) to analysed temperature outlet. The result of case study is shown in figure 4. The FEHE's leakage could achieve outlet temperature FEHE at 7% leakage, but it has different value at outlet temperature reactor and mass-flowrate at outlet reactor. Then, channelling satisfy all parameters in this condition at 8.8% channelling reactor. It also show channelling make conversion drop up to 6.7%. Then, it's also identical to plant data which show 7% conversion drop. So, the problem of this system is channelling of ammonia reactor at 8.8% channelling. Then, the troubleshooting solution should be repair the channelling problem by readjusting packing bed, using distributor, or analysing residence time distribution to solve channelling problem.

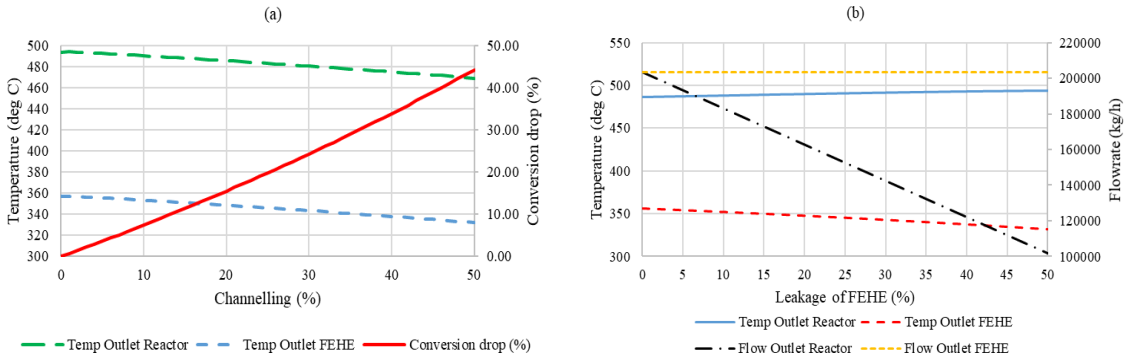

Fig.4. Case study result using Aspen HYSYS V8.8 for (a) Channelling reactor case & (b) Leakage of FEHE case

4. Conclusions

Data reconciliation are valuable techniques to improve the reliability of plant data, especially for troubleshooting purpose. It adjusts the process data to satisfy the constraints of the system model to define current status and condition of the plant model. Redundancy measurement guarantee data reconciliation using Aspen HYSYS V8.8 simulations. In this study, bad plant data in ammonia system reactor could be analyzed using data reconciliation based on gross error measurements, leakage of FEHE or reactor channeling. Bad plant data are fitted with simulation model then gross errors are identified and eliminated to see current status of plant. Appropriate process model present current condition and problems. This study compares FEHE's leakage and reactor channeling with statistical analysis and case study feature. This study proves simple and fast troubleshooting solutions and may result in operational and financial benefits by avoiding wrong actions or solutions due to unreliable data processed.

Acknowledgements

The authors gratefully acknowledge the support by Institut Teknologi Bandung, Department of Chemical Engineering especially Laboratory of Process Equipment and Process Simulation

References

1. Sisi Guo, Pei Liu, et al. Data Reconciliation for the Overall Thermal System of a Steam Turbine Power Plant. *Applied Energy*; Volume **165**, 1037-1051(2016)
2. Xiaolong Jiang, Pei Liu, et al. Data Reconciliation and Gross Error Detection for Operational Data in Power Plant. *Energy*; Volume **75**, 14-23 (2014)
3. Vincent S. Verneuil, Pin Yang, et al. Banish Bad Plant Data. *Chemical Engineering Progress*; October 1992 (45-51)
4. Ricardo Maronna & Jorge Arcas**.** Data Reconciliation and Gross Error Diagnosis Based on Regression. *Computers and Chemical Engineering*; **33** : 65-71 (2009)
5. Humaad Ijaz, Uma M.K. Ati, et al. Heat Exchanger Network Simulation, Data Reconcilation & Optimization. *Applied Thermal Engineering*; **52** : 328 – 335 (2013)
6. Derya B. Ozyurt & Ralph B. Pike**.** Theory and Practice of Simultaneous Data Reconciliation and Gross Error Detection for Chemical Processes. *Computers and Chemical Engineering*; **28** : 381 – 402 (2004)
7. Jose Placido, Alexandre A. Campos, et al. Data Reconciliation Practice at a Petroleum Refinery Company in Brazil. *10th International Symposium on Process System Engineering – PSE2009*; 777-782 (2009)
8. M. Piccolo & P.L. Douglas. Data Reconciliation Using AspenPlus, *Asia-Pasific Journal of Chemcial Engineering*; Volume **4** Issue 3-4 157-182 (1996)
9. Ahmad Rafiee, & Flor Behrouzshad. Data Reconciliation with Application to a Natural Gas Processing Plant. *Journal of Natural Gas Science and Engineering* **31** : 538 – 545 (2016)
10. Joao S. Albuquerque, & Lorenz T. Biegler. Data Reconciliation and Gross Error Detection for Dynamic System. *Process System Engineering;* AIChE Journal Vol. **42,** No. **10** 2841–2856 (1996).

Simulation of three phase reactor hydrodeoxygenation RPO to Green Diesel in industrial scale Adiabatic Fixed Bed Reactor

Affandry Taufik, IGBN Makertihartha*, and Subagjo

Department of Chemical Engineering
Institut Teknologi Bandung, Bandung 40132 Indonesia

* *Corresponding Author's E-mail makertia@che.itb.ac.id*

Abstract

Three phase reactor model for describing Hydrodeoxygenation (HDO) reaction to convert Refined Palm Oil (RPO) toward Green Diesel range hydrocarbons was simulated. The simulation carried out as industrial scale of adiabatic fixed bed reactor to figure out the behavior and effect of varied operating conditions such as inlet tempeature (T_{in}), Liquid Hourly Space Velocity (LHSV) and ratio of hydrocarbons to triglycerides (HC/TG). T_{in} was varied from 553 K to 633 K, LHSV was varied from 1 to 2.5 h^{-1}, rasio HC/TG was varied 3-5:1. HDO reaction rate of RPO was represented by the HDO rate of oleic acid. The highest green diesel production was found at 2.5 h^{-1}, 603 K and HC/TG ratio 5:1.

1. Introduction

Nowdays, many countries trying to switch their energy needs from crude oil based into renewable based fuel. In 2016, Indonesia imported 20,7 million tons crude oil[1]. Meanwhile, Indonesia is the largest crude palm oil producer in the world which produced 34,5 million tons palm oil and palm kernel oil at 2016 [2]. It can be converted into 29,5 million tons of fuel approximately which may fulfill Indonesian crude oil need. Therefore, Indonesia should develop technology to convert palm oil into fuel. Palm oil contains triglycerides which can be converted to biohydrocarbon in diesel range called green diesel[3]. The best invented technology is hydrodeoxygenation (HDO)[4]. Hydrodeoxygenation is a catalytic process to remove oxygen from triglycerides using hydrogen[5]. The product of this process are hydrocarbons which can blend with conventional oil without limitation.

UOP and Neste Oil have built and commercialized their HDO processes, which are Ecofining™[6] and NexBTL®[7] respectively. The first stage of those processes is HDO, then followed by isomerisation to impove product quality. Both processes using wide range lipid from animals and plants as feeds. Simulation should be conducted to understand operation conditions effect on reactor performance before being applied at industrial reactor. There is no simulation to exhibit the effect of operation conditions on HDO reactor performance in industrial scale using palm oil as feed. Subramanyam simulated HDO reactor using bio-oil as feed trough laboratory scale reactor and studied the effect of WHSV, temperature and pressure[8]. Simulation of HDO reactor also studied by Kilpiö[9] which focused to study the activity and deactivation in bed using stearic acid as feed. This work was conducted to determine the effect of operation condition such as inlet temperature (T_{in}), hydrocarbon to triglycerides ratio (HC/TG) and Liquid Hourly Space Velocity (LHSV). The feed used in this study was triglycerides from Refined Palm Oil (RPO).

2. Three phases reactor modelling

The strategy to build mathematical model of HDO palm oil are :

1. Define the system of chemical reaction.
2. Determine the reaction rate.
3. Select the reactor model.
4. Estimate the transport and thermophysical parameters.
5. Formulate equations and parameters.
6. Apply mathematical models into simulation using Matlab 2015b.

2.1 System of chemical reaction

HDO reaction of triglycerides is highly exothermic. All HDO process licensor use recycled hydrocarbons product from reactor effluent to avoid high temperature rising along bed. Those hydrocarbons introduced together with triglycerides. It not only used to avoid temperature rise but also to increase hydrogen solubility in liquid phase. Hydogen solubility is the key of HDO process. High HC/TG ratio increases hydrogen solubility but reduces the conversion. The variations studied in this article were T_{in} 553. 573, 603 and 633 K. LHSV 1, 1,5 , 2 and 2,5 h^{-1}. HC/TG ratio 3:1, 4:1 and 5:1. Mass flow 59,9 tons/hour, bed diameter and length were 263 cm and 465 cm and constant pressure 60 bar.

Since RPO consists of various types of triglycerides in some fractions, those triglycerides were simplified as single component and noted as TG at this work. The product of this reaction also consists of various types of hydrocarbons in diesel range which have some fractions. Simplified form of those hydrocarbons as single component named HC. Various types of triglycerides and hydrocarbons in RPO and HC shown in Table.1. HDO reaction of triglycerides then simplified as a single reaction shown in Eq.1. Simulation was conducted in fixed dimension and fixed configuration reactor. HDO reactor was single bed reactor. Reactor dimension were 465 cm and 265 cm for length and diameter respectively.

$$1\ TG + 16\ H_2 \rightarrow 3\ HC + 1\ C_3H_8 + 6\ H_2O\ ; H_{298} = -539 \frac{kJ}{mol} \quad (1)$$

Table 1. TG and HC Components

TG[18]		HC	
Components	Fractions	Components	Fractions
PMP	0.004	Tetradecane	0.03
PPP	0.067	Hexadecane	0.39
PPO	0.294	Octadecane	0.57
SPO	0.05	Abreviation of esters in triglycerides:	
OOS	0.026	M = Miristic	
PPLi	0.084	P = Palmitic	
POO	0.239	S = Stearic	
POLi	0.118	O = Oleic	
PliLi	0.014	Li = Linoleic	
OOO	0.061		

2.2 Rate of chemical reaction

The rate of chemical reaction used in this simulation was the rate equation of HDO oleic acid proposed by Kumar[10]. HDO oleic acid could represent HDO of RPO since oleic acid is the largest fraction of RPO. The equation rate of HDO oleic acid is:

$$r_{HDO} = 3{,}97 \times 10^{12} \exp\left(\frac{-130700}{RT}\right) \times C_{OA} \quad (2)$$

2.3 Reactor model selection

Adiabatic fixed bed reactor commonly used in industrial scale. In this study, three phases heterogeneous model was selected because that model describes real phenomena in reactor and operated in adiabatic condition. The partial volume of three phases model shown on Fig.1. Mathematical model of fixed bed three phases reactor which has been derived by Korsten[11] used in this study. The following assumptions were used to derived mass and energy balance assumptions :

1. Velocity of gas and liquid was constant along reactor.
2. There were no radial temperature and concentration diffusion.
3. Catalyst activity did not change with the time.
4. Vaporisation and condensation were neglected.
5. The reactor was operated in steady state condition.
6. Chemical reaction only took place on catalyst surface.
7. Catalyst effectiveness was high.
8. Interparticle and interphase heat transfers of three phases catalyst-liquid-gas were high.

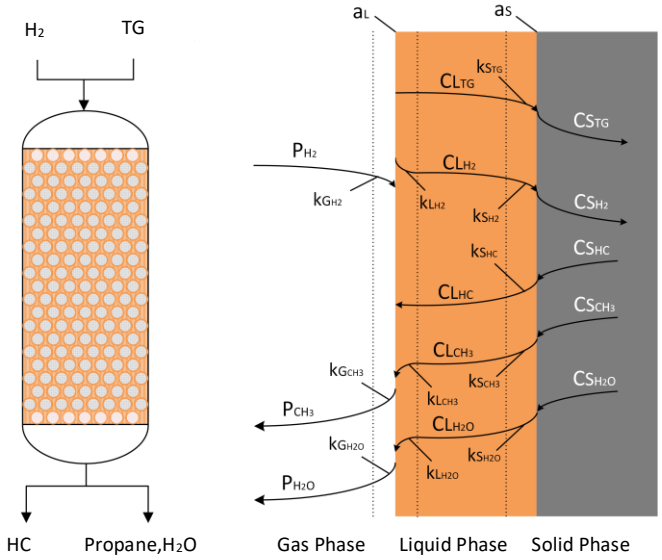

Figure 9. Three phases heterogeneous model reactor

There were five involved components in reactor model. Gaseous components were hydrogen, propane and water existed in gas, liquid and solid phases (catalyst). Liquid components were TG and HC only existed in liquid and solid phases. All components existed

in solid phase. Concentration of each components in each phases depended on mass transfer coefficients between those phases.

Mass balance of gaseous components in gas phase :

Components	Mass balance equation
Hydrogen	$\frac{u_G}{RT^G}\frac{dP^G_{H_2}}{dz} = k^L_{H_2} a_L \left(C^G_{H_2} - C^L_{H_2}\right)$
Propane	$\frac{u_G}{RT_G}\frac{dP^G_{CH_3}}{dz} = k^L_{CH_3} a_L \left(C^G_{CH_3} - C^L_{CH_3}\right)$
Water	$\frac{u_G}{RT_G}\frac{dP^G_{H2O}}{dz} = k^L_{H2O} a_L \left(C^G_{H2O} - C^L_{H2O}\right)$

Mass balance of gaseous components in liquid phase :

Components	Mass balance equation
Hydrogen	$u_L \frac{dC^L_{H_2}}{dz} = k^L_{H_2} a_L \left(C^G_{H_2} - C^L_{H_2}\right) - k^S_{H_2} a_S \left(C^L_{H_2} - C^S_{H_2}\right)$
Propane	$u_L \frac{dC^L_{CH_3}}{dz} = k^L_{CH_3} a_L \left(C^L_{CH_3} - C^L_{CH_3}\right) - k^S_{CH_3} a_S \left(C^L_{CH_3} - C^S_{CH_3}\right)$
Water	$u_L \frac{dC^G_{H2O}}{dz} = k^L_{H2O} a_L \left(C^G_{H2O} - C^L_{H2O}\right) - k^S_{H2O} a_S \left(C^L_{H2O} - C^S_{H2O}\right)$

Mass balance of liquid components in liquid phase :

Components	Mass balance equation
TG	$u_L \frac{dC^L_{TG}}{dz} = -k^S_{TG} a_S \left(C^L_{TG} - C^S_{TG}\right)$
HC	$u_L \frac{dC^L_{HC}}{dz} = -k^S_{HC} a_S \left(C^L_{HC} - C^S_{HC}\right)$

Mass balance all components in solid phase

Components	Mass balance equation
Hydrogen	$k^S_{H_2} a_S \left(C^L_{H_2} - C^S_{H_2}\right) = -16 r_{HDO}(C^S, T^S)$
Propane	$k^S_{CH_3} a_S \left(C^L_{CH_3} - C^S_{CH_3}\right) = 1 r_{HDO}(C^S, T^S)$
Water	$k^S_{H_2O} a_S \left(C^L_{H_2O} - C^S_{H_2O}\right) = 6 r_{HDO}(C^S, T^S)$
TG	$k^S_{TG} a_S \left(C^L_{TG} - C^S_{TG}\right) = -r_{HDO}(C^S, T^S)$
HC	$k^S_{HC} a_S \left(C^L_{HC} - C^S_{HC}\right) = 3 r_{HDO}(C^S, T^S)$

2.4 Transport and thermophysical parameters

All needed equations to estimate transport and thermophysical parameters are attached as supplementary data.

3. Reactor performance and simulation

3.1 Alteration of hydrogen concentration along reactor

Inlet temperature has great effect on hydrogen solubility into the liquid phase. Higher T_{in} increases hydrogen equilbrium concentration at interphase layer due to henry constant of hydrogen decreasing at liquid phase. Profile hydrogen, gas product, conversion and temperature for varied T_{in} carried out in at LHSV 1 h^{-1}, HC/TG 4:1.

3.2 Concentration of hydrogen at gas-liquid interphase

Hydrogen concentration at interface layer exhibits decline trend along lowered temperature due to hydrogen consumption by the reaction and also increment of hydrogen solubility at liquid phase. Fig. 2 showed decreased of hydrogen concentration on interphase of gaseous and liquid phase higher in inlet temperature 633 K compared with decreased of hydrogen concentration in 603, 573, 553 K. The higher temperature of liquid phase, the lower Henry's constant so that higher hydrogen solubility.

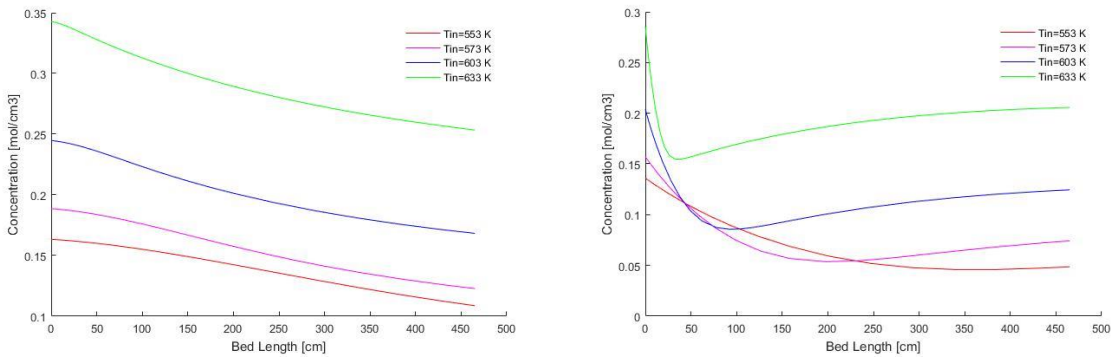

Figure 2. Hydrogen concentration at gas (left) and liquid interphase (right)

3.3 Concentration of hydrogen in liquid phase

Fig. 2 showed hydrogen concentration in liquid phase decreased significantly at the beginning of entry of the reactor bed. At T_{in} 553 K, hydrogen concentration decreased along the reactor. This was due to consumption hydrogen concentration along the reactor, in line with the curve of triglyceride consumption decreased along the reactor in T_{in} 553 K. At T_{in} above 553 K, hydrogen concentration decreased at a certain length of reactor and then increased gradually. Steep decreased of hydrogen concentration denoted biggest rate reaction affect of overall conversion of triglyceride so the hydrogen concentration in liquid phase gained along the reactor.

3.4 Alteration of TG concentration in liquid phase

The rose of the temperature would have accelerated TG consumption along the reactor. At 553 K T_{in}, TG concentration is 0.0027 mol/cm^3 and conversion is 70%. At T_{in} 573, 603 and 633 K, TG have been perfectly converted at 450, 125 and 50 cm. Fig. 3 show profile TG consumtion along reactor bed.

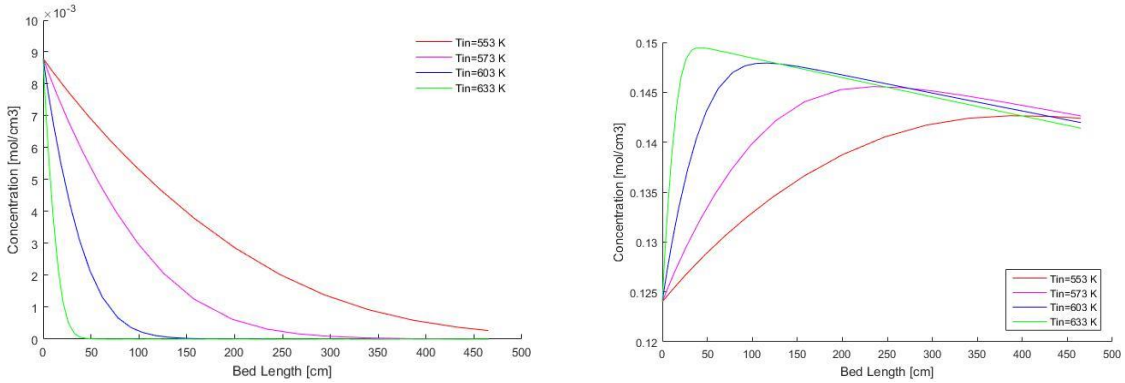

Figure 3. Concentration of TG (left) and HC (right) in liquid phase

3.5 Concentration of HC in liquid phase

Higher T_{in} would accelerated generation rate of HC in liquid phase. HC concentration increases very quickly at the beginning of the bed and then lowered as the result of liquid volume expansion. T_{in} 633 K give higher HC concentration rise than other temperatures. Fig.3 showed profile production of HC along reactor bed.

3.6 Alteration of gaseous product concentration in gas phase

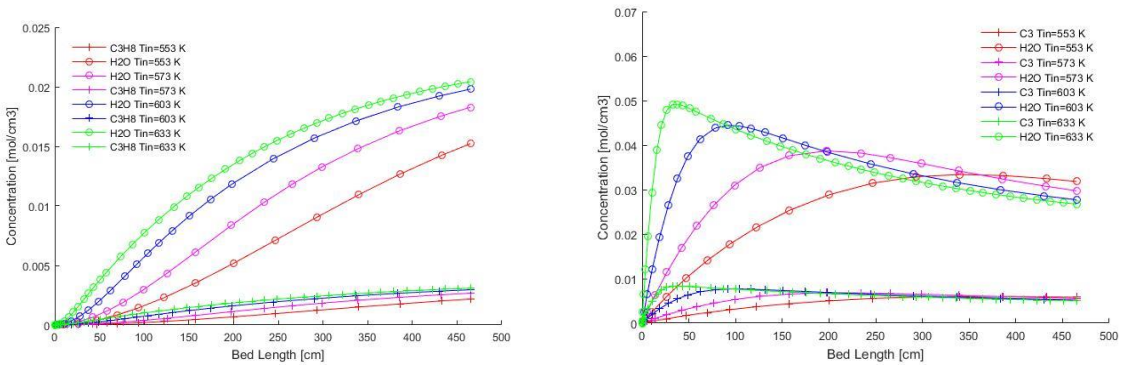

Figure 4. Propane and water concentration at gas (left) and liquid interphase (right)

Fig.4 showed increasing of solubility concentration of gas product (propane and water) in gaseous phase was smaller at the end of the bed due to temperature rose along the bed. Reduced solubility in the gaseous phase due to rising temperatures along the reactor caused more gas products moved from the liquid phase to the gas phase, so that the concentration of gas products in the gas phase increases along the bed. The highest product concentration in gaseous phase was occur in T_{in} 633 K and the lowest one when T_{in} 553 K.

3.7 Alteration of gaseous product concentration in liquid phase

Concentration of propane and water tended to increase at the start of the bed then decreased gradually and showed on Fig.4. Concentration of gas product significant increased at the start of the bed due to the magnitude of the reaction rate at the start of the bed, then decreased gradually in line with the reduced reaction rate along the bed. Increasing T_{in} would enhance reaction rate and production of propane and water in liquid phase. Liquid phase temperature that was increased along the reactor would decreased propane and water solubility in liquid

phase, as a result propane and water concentration at the end of the bed smaller than propane and water concentration at the start of the bed.

3.8 Effect of inlet temperature (T_{in})

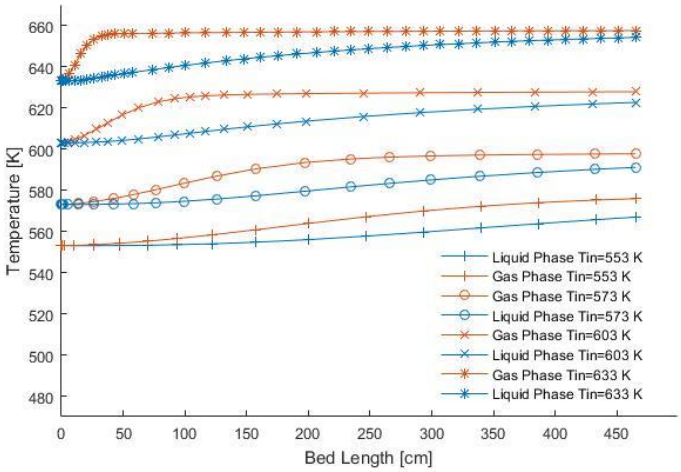

Figure 5. Profile temperature along reactor bed

Typical temperature profile for adiabatic and irreversible reaction always increase along the bed. Temperature rising is always maintained in order to avoid cracking of the product. Fig.5 shows temperature profile increased along the reactor in various T_{in}. The higher Inlet temperature would increase temperature due to rose of reaction rate. When T_{in} 533 K, the temperature increased 11 K in the liquid phase, also in T_{in} 573 K showed temperature increased 22 K in liquid phase. However, when T_{in} 633 K temperature increased only 22,5 K while in T_{in} 603 K temperature increased 23 K. This was because the reaction heat at 633 K converted triglycerides so rapidly that the liquid phase heat capacity falls close to the hydrocarbon heat capacity. Heat capacity of hydrocarbon that was increased very fast, accelerated heat transferred form liquid phase to gaseous phase, resulted temperature increased on gaseous phase in 633 K faster than temperature increased on gaseous phase in lower temperature.

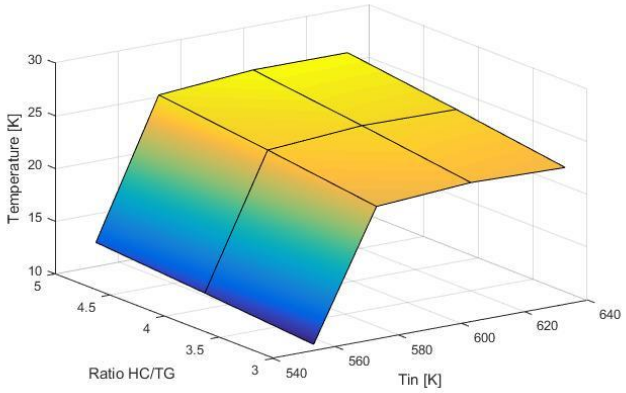

Figure 6. Effect of T_{in} and HC/TG ratio to temperature rise along reactor bed

T_{in} and HC/TG ratio affect on temperature increased showed in Fig 6. The lowest temperature increase was 10,6 K in T_{in} 553 K with HC/TG ratio 3:1 h^{-1} and the highest one is

25,8 K in T_{in} 603 K with HC/TG ratio 5:1 h^{-1}. On low HC/TG ratio (3:1), temperature rise smaller than tempearature rise when operated at HC/TG ratio 4:1 and 5:1. This was caused by enormity of HC/TG ratio that would increase hydrogen solubility in liquid phase where Henry's constant of hydrocarbon smaller than Henry's constant of triglyceride. Low hydrogen concentration would bound reaction thereby limited the heat released in the reaction.

3.9 Effect of T_{in} to conversion

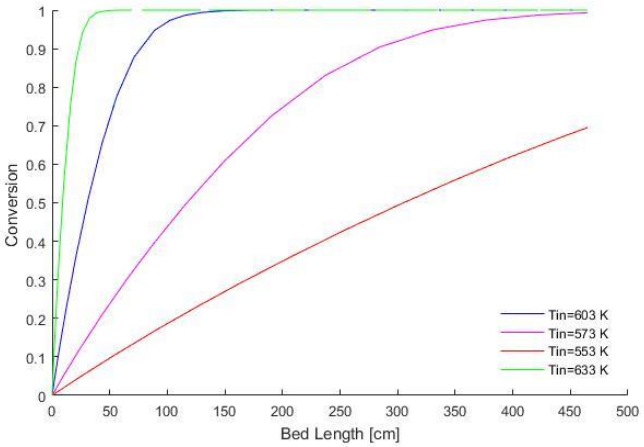

Figure 7. Profile conversion for various T_{in}

Increasing temperature always increase the reaction rate and increase the conversion. Conversion profiles on various T_{in} are showed in Fig.7. In the same LHSV, the bigger T_{in}, the greater T_{in} would increase the reaction rate and conversion. The maximum conversion that can be reached at the end of the bed for T_{in} 553 K is about 70%. At higher T_{in}, 100% conversion achieved at shorter reactor length.

3.10 Effect LHSV and T_{in} over conversion

An increase in inlet temperature would increase the conversion. The effect of LHSV and T_{in} to conversion shown on Fig.8 .The lowest conversion was in T_{in}553 K and LHSV 2.5 h^{-1} with conversion 33%. A 100% conversion had been achieved on T_{in} 603 K with LHSV 1 h^{-1}. LHSV increments would minimize conversions. Small LHSV required a lower T_{in} to achieve maximum conversion. In contrast, to large LHSV, higher T_{in} is required to achieve maximum conversion.

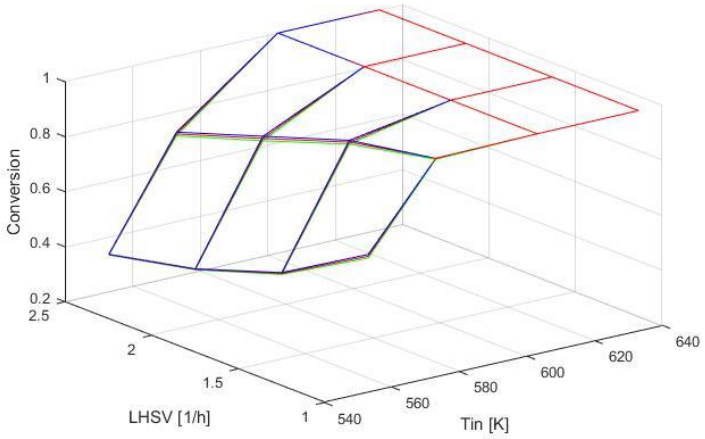

Figure 8. Effect of LHSV and T_{in} on conversion

The smallest conversion was found in LHSV is 2.5 h^{-1} and T_{in} 553 K is 33%. At maximum LHSC 2.5 h^{-1}, 100% conversion is obtained at temperature 633 K. While at the lowest LHSV was 1 h^{-1}, 100% conversion is obtained at temperature 573 K. At T_{in} 603 K, conversion has reached 100% conversion for all LHSV.

4. Conclusion

Three phases reactor model was succesfully employed in this work to predict the behavior of hydrogen consumption, green diesel production and temperature rising of HDO reactor to convert RPO to green diesel. According to the simulations results the following conclusions can be pointed out:

1. Higher T_{in} increases conversion and bed temperature. T_{in} 633 K exhibits highest temperature rise and maximum conversion which is 100% was reached for all LHSV at 603 K.
2. Higher LHSV needs higher T_{in} to get maximum conversion. At highest LHSV (2.5 h^{-1}), reactor must be operated at 603 K to get maximum conversion. While at lowest LHSV (1 h^{-1}), reactor must be operated at 573 K.
3. Higher HC/TG increases hydrogen solubility, temperature and conversion. HC/TG 5:1 gives highest conversion.

Acknowledgment

The authors thank to people who worked in Laboratory of Chemical Reaction and Catalysis for their support.

References

1. Bumi, D. J. M. dan G. & Mineral, K. E. dan S. D. Data Grafis Impor Minyak Mentah & Kondensat. (2017). Available at: http://statistik.migas.esdm.go.id/index.php?r=rekapImporMinyakMentah/index. (Accessed: 7th March 2017)
2. GAPKI, G. P. K. S. I. Refleksi Industri Kelapa Sawit 2016 & Prospek 2017. (2017). Available at: https://gapki.id/refleksi-industri-kelapa-sawit-2016-prospek-2017/. (Accessed: 3rd March 2017)
3. Soerawidjaja, T. H. Kuliah Inaugurasi Judul : Energi : Sang Sumber Daya Induk Energi : Sang Sumber Daya Induk. (2013).

4. Santikunaporn, M. & Danphitak, S. Hydrodeoxygenation of Linoleic Acid on Ni-Mo Catalyst. *Thammasat Int. J. Sci. Technol.* 15, 1–6 (2010).
5. Dickerson, T. & Soria, J. Catalytic fast pyrolysis: A review. *Energies* 6, 514–538 (2013).
6. Lehmus, P. Large scale chemical conversion of oils and residues in Rotterdam. in *European Biofuels Technology Platform - 6th Stakeholder Plenary meeting* 26 (2014).
7. UOP, H. Honeywell Green Diesel™. Available at: https://www.uop.com/processing-solutions/renewables/green-diesel/. (Accessed: 24th March 2017)
8. Subramanyam, M. D., Gollakota, A. R. K, et al. CFD Simulations of Catalytic Hydrodeoxygenation of Bio-oil using Pt/Al2O3 in a Fixed Bed Reactor. *RSC Adv.* (2015).
9. Kilpiö, T., Mäki-Arvela, P., Salmi, T. & Murzin, D. Y. in *Multiphase Catalytic Reactors* (eds. Önsan, Z. & Avci, A. K.) 365–376 (John Wiley and Sons, 2016).
10. Kumar, P., Yenumala, S. R., et al. Kinetics of hydrodeoxygenation of stearic acid using supported nickel catalysts: Effects of supports. *Appl. Catal. A Gen.* 471, 28–38 (2014).
11. Mederos, F. S. & Ancheyta, J. Mathematical modeling and simulation of hydrotreating reactors: Cocurrent versus countercurrent operations. *Appl. Catal. A Gen.* 332, 8–21 (2007).

Suplementary

Parameters	Corelation	Reference
Gas-liquid mass transfer coefficient	$\frac{k_i^L a_L}{D_i^L} = 7\left(\frac{G_L}{\mu_L}\right)^{0.4}\left(\frac{\mu_L}{\rho_L D_i^L}\right)^{\frac{1}{2}}$	Goto & Smith[15]
Liquid-solid mass transfer coefficient	$\frac{k_i^S}{D_i^L a_S} = 1.8\left(\frac{G_L}{a_S \mu_L}\right)^{1/2}\left(\frac{\mu_L}{\rho_L D_i^L}\right)^{1/3}$	Korsten & Hoffmann[12]
Molecular diffusity	$D_{AB} = 8.93 \times 10^{-3}\frac{V_B^{0.267}}{V_A^{0.433}}\frac{T}{\eta_B}$	Poling [16]
Henry constant	$H = H_0 \exp\left(\frac{-\Delta E}{RT}\right)$	Fillion & Morsi[17]
Viscosity TG	$\ln v = A + \frac{B}{T} + \frac{C}{T^2}$	Azian[18].
Viscosity HC	$og(\mu + 0.8) = 100(0.01T)^b$	Mehrotra[19]
Density TG	$\rho = \frac{(\sum x_i MW_i)}{\left(\sum \frac{x_i T_{ci}}{P_{ci}}\right)(\sum x_i Z_{ri})^{\left[1+(1-T_r)^{\frac{2}{7}}\right]}} + F_C$	Halvorsen dkk[20]
Heat capacity TG	$C_{p,i}(T) = A_{1,i} + A_{2,i}T$	Zong[21]
Heat capacity HC	$\Delta c_i = a_i + b_i\frac{T}{100} + d_i\left(\frac{T}{100}\right)^2$	Ruzicka & Domalski[22]
Enthalpy of formation TG	$\Delta H°_{f,mix} = \sum\frac{1}{3}\Delta H°_{f,i}$	Zong[21]

Dynamic Study of Feed-Effluent Heat Exchanger Addition on Double Bed Reactor Configuration of Exothermic Reaction within Varied Bed Volume Distribution

Tri Partono Adhi[1,*], Ferdyan Ihza Akbar[1]

[1]*Department of Chemical Engineering, Institut Teknologi Bandung, Jalan Ganeca 10, 40135, Indonesia*

* *Corresponding Author's E-mail: tpadhi@che.itb.ac.id*

Abstract

Exothermic reaction is a common reaction in chemical industry Feed-Effluent Heat Exchanger (FEHE) is commonly added to increase thermal efficiency. In this study, ammonia synthesis was chosen due to its wide utilization and its high feed temperature requirement to start the reaction so that FEHE will be perfectly placed at ammonia plant. However, FEHE could lead the process to experience unstable phenomenon called hysteresis due to its interaction between equipments as one steady state parameter. Hysteresis phenomenon may result hazard and asset losses such as explosion and loosing material integrity. The benefit of using double bed reactor configuration is its capability to use several design parameters as variation to overcome hysteresis. In this study, bed volume distribution was chosen to be that varied parameter. This study aims to determine how bed volume distribution affects hysteresis zone in ammonia reactor by utilizing Aspen Hysys® V8.8 as simulation tool. Simulation showed that lower 1st bed volume (V1) would narrow hysteresis zone yet decrease the ignition temperature and increased extinction temperature that lower the conversion. Conversion profile showed that V1=5 m^3 got the highest conversion for system with 0.5 quenching ratio while total volume was 30 m^3. However, the feed temperature was fallen at hysteresis zone. Dynamic simulation showed that highest conversion feed temperature (17.73%ΔTf above extinct temperature) was still able to preserve stability with descending temperature approach. Hysteresis itself started to occur at 2.9%ΔTf above extinct temperature

1. Introduction

Exothermic reaction is one of widely known reaction that is applied in many chemical plant. One of widely used exothermic reaction is ammonia synthesis which is one of important industrial commodity due to its wide utilization as chemical product precursor such as urea, nitric acid, and etc. In reactor configuration for exothermic reaction, Feed-Effluent Heat Exchanger (FEHE) is commonly used that aims to exchange heat between reactor effluent and reactor feed as shown in Fig. 1.

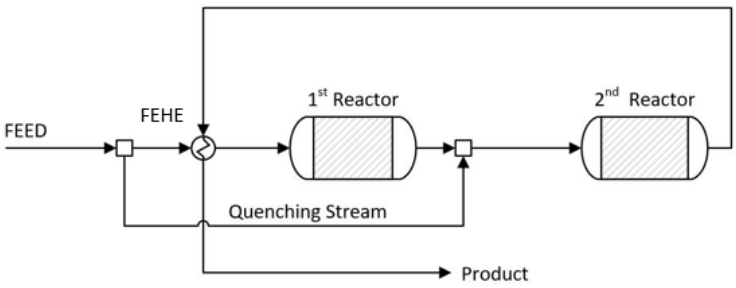

Fig. 1. Ammonia reactor system configuration

Such heat integration system would reduce utility requirement and increase thermal efficiency. However, the integration system could possibly lead the process system to experience significant temperature oscillation as shown in Fig. 2. Oscillations occur as the result of two or more processes that are coupled together with each other [1,7]. In this case, reactors performance is closely related to how the FEHE performs. As the result, reactor possibly undergoes a phenomenon while same operating condition could produce several steady state outputs that lead the process to oscillate[1,6]. This condition could cause several hazards for the equipment material and even operational staff [4,5]. Hazards that occurred could dangerously result disasters such as explosion or poisoneous chemical leakage which causing economic losses.

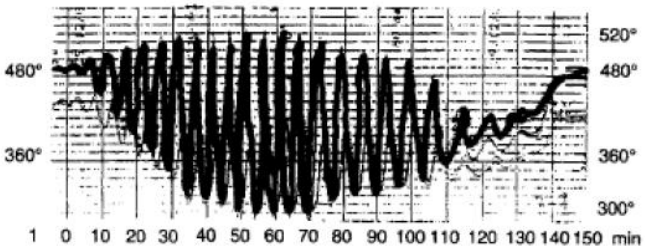

Fig. 2. Hysteresis phenomenon on industrial scale ammonia reactor. [3]

Hysteresis area could be predicted by plotting one of steady state parameter such (T outlet) as result of T feed input as shown in Fig. 3.

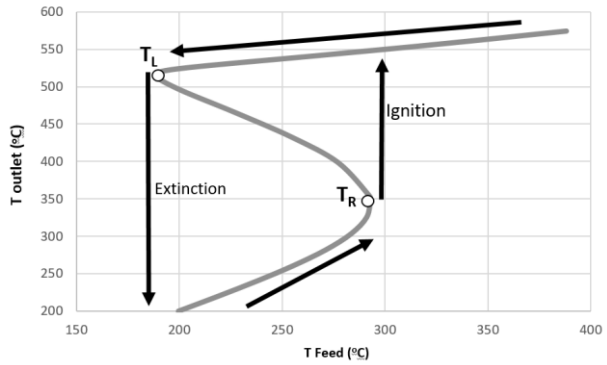

Fig. 3. Curve plot to determine hysteresis zone

The 'S' curve produced showed that within range of T_L and T_R (ΔT_f), each T feed input will result several values of T outlet. Therefore, there will be possibility for the process to experience oscillation while entering this region.

Some efforts to deal with this condition could be done by changing other supporting operation parameter for double bed system such as adding trim heat exchanger, changing the quenching ratio or bed volume distribution. Therefore, this study would show parametric review and simulation regarding actions to overcome and reduce hysteresis phenomenon by choosing bed volume distribution as varied parameter. As the bed volume distribution were evaluated, conversion profile was also analyzed to determine the temperature at particular bed volume distribution to produce optimum reactant conversion. As the matter of limitting the problem, this review focused on observing feed temperature, outlet reactor temperature, quenching ratio, reactant conversion, and starting hysteresis temperature.

2. Methods

This review chose ammonia synthesis reaction as simulation case base. Aspen Hysys® V8.8 were used to act as an assistive tools for simulating the dynamic behaviour resulted from altered parameter value. Simulation configuration is shown in Fig. 4.

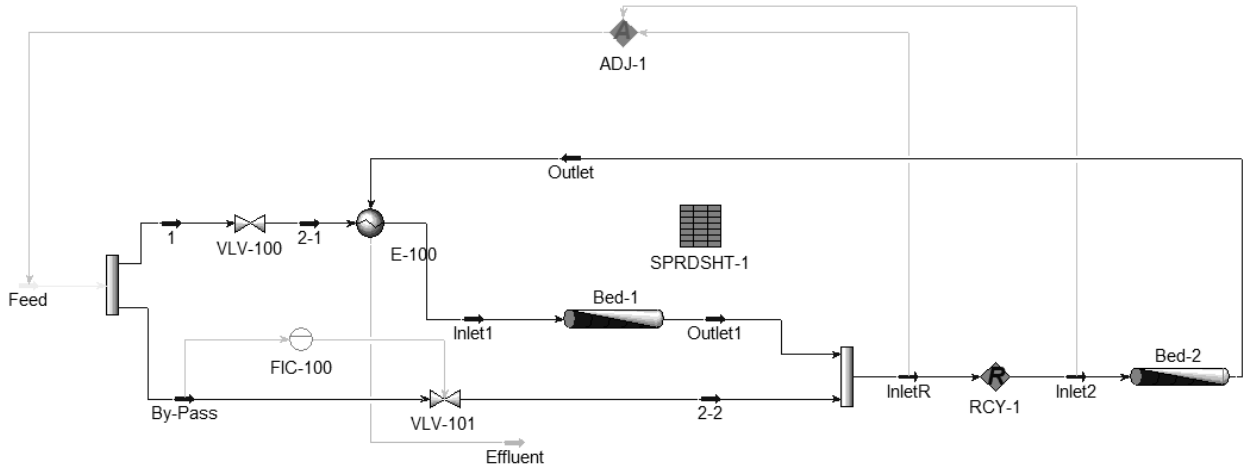

Fig. 4. Simulation Configuration

Fluid package used in the simulation was Peng-Robinson. Ammonia reaction kinetics behaviour for calculation was based on following equation[2] .

$$N_2 + H_2 \leftrightarrow NH_3 \tag{1}$$

$$r = 23.618 \exp\left(-\frac{87{,}090}{RT}\right)\frac{P_{N2}P_{H2}^{1.5}}{P_{NH3}} - 3.39\text{x}10^{13} \exp\left(-\frac{198{,}460}{RT}\right)\frac{P_{NH3}}{P_{H2}^{1.5}} \tag{2}$$

Plug Flow Reactor (PFR) with total volume 30 m^3 was used in the simulation. Feed mole flow for each component N_2, H_2, and NH_3 are respectively 6,752.36 kmol/hr; 20,254.28 kmol/hr; and 1,175.18 kmol/hr. Quenching process was simulated by using splitter and mixer features of Aspen Hysys® V8.8. Quenching ratio was assumed 0.5 during the bed volume distribution simulation. FEHE simulation was conducted with steady-state-rating mode and sized rigorously by using interactive mode to obtain certain characteristic on heat transfer. FEHE specification sheet is shown in Table 1.

Table 1. FEHE Specification Sheet.

Specification	**Value**	**Specification**	**Value**
TEMA	AEL	Shell Diameter (mm)	818.85
Number of Shell per Pass	1	Number of Tube per Shell	872
Number of Shell in Series	1	Tube Pitch (mm)	23.81
Number of Shell in Parallel	2	Tube Layout Angle	Triangluar (30º)
Tube Passes per Shell	1	Shell Fouling Factor (˚C m2/kJ)	0.000028
Orientation	Horizontal	Baffle Type	Single
First tube pass flow direction	Counter	Baffle Orientation	Horizontal
Elevation	0	Baffle Cut (%Height)	20.00
Shell HT coeff. (kJ/m^2˚C)	8908	Baffle Spacing (mm)	800.00
Tube HT coeff. (kJ/m^2˚C)	12304	Tube OD (mm)	19.050
Overall U (kJ/m^2˚C)	2604	Tube ID (mm)	10.668
Overall UA (kJ/m^2˚C)	101900	Tube Thickness (mm)	4.191
Shell pressure drop (bar)	0.5855	Tube Length (m)	3.750
Tube pressure drop (bar)	0.1386	Tube Fouling Factor (˚C m2/kJ)	0.000028
Heat transfer area per shell (m^2)	195.7	Themal cond. (W/mK)	45
Tube volume per shell (m^3)	0.2923	Wall Heat Capacity Coeff. (kJ/kg C)	0.473
Shell volume per shell (m^3)	1.043	Wall Density (kg/m3)	7801

Hysteresis zone identification was conducted by using Adjust feature on Aspen Hysys® V8.8. This process was done by varying the 2nd reactor inlet temperature to adjust the feed temperature on each quenching ratio. This attempt eventually would result a plot of T Feed vs T Outlet correlation to identify hysteresis zone. Reactant conversion was then identified by using Case Study feature on Aspen Hysys® V8.8. This study was done by varying feed temperature on each quenching ratio or bed volume distribution and observing the mole flow of the ammonia in the outlet stream. At the end, Aspen Hysys® V8.8 Dynamic feature was conducted to observe the process dynamic behaviour at quenching ratio which resulted highest reactant conversion. Eventually, dynamic observation was used to determine starting temperature of oscillation as the percentage of ΔT_f. Dynamic simulation was also used to determine process stability while feed temperature was set at value that resulted highest conversion in chosen quenching ratio.

3. Results and Discussion

As in the single bed configuration, unstable process is also possible to occur due to FEHE utilization. Identified instability zone study resulted from varied bed volume distribution of double bed reactor would be explained in the following section.

3.1 Hysteresis Zone Alteration Due to Varied Bed Volume Distribution

Fig. 5 shows that generally higher quenching ratio would lead to more narrow hysteresis but higher extinct temperature.

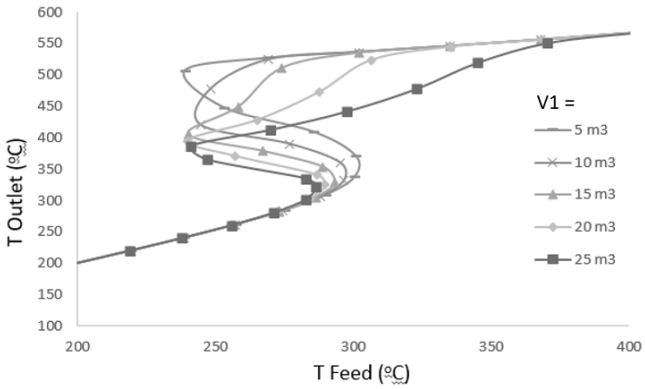

Fig. 5. Hysteresis zone alteration on varied bed volume distribution

Higher extinct temperature is possible to lead the reaction to be easily extincted and it further would result lower reactant conversion. 1st bed volume (V1) was varied at 5, 10, 15, 20, and 25 m^3 with total bed volume of 30 m^3. Hysteresis zone experienced narrowing process to center part of the curve as the ignition temperature lowered and extinct temperature raised. Reactant conversion was then evaluated for each bed volume distribution to obtain additional information regarding to determine the best stable condition to proceed the process. Reactant conversion was then evaluated from each quenching ratio at steady state simulation as shown in Fig. 6.

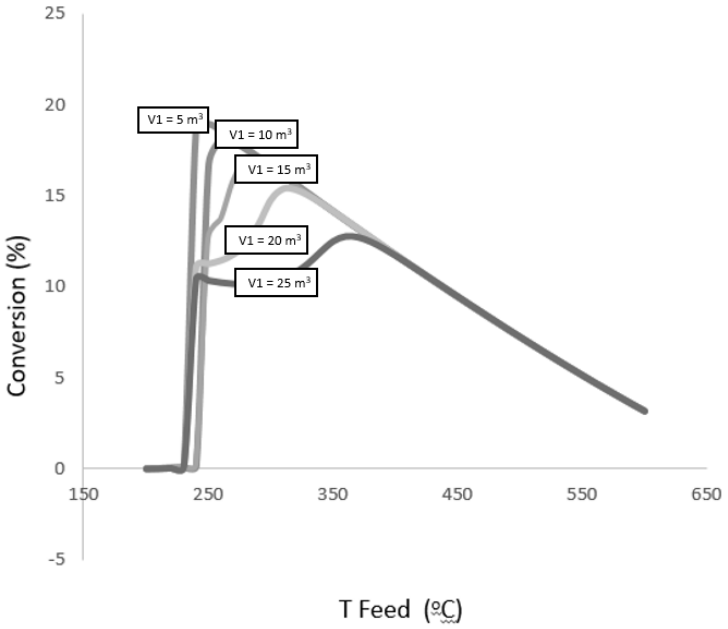

Fig. 6. Conversion profile on varied quenching ratio with 1st bed volume = 20 m^3

Fig. 6 shows that generally lower V1 will increase the conversion and it shows highest overall conversion profile is 18.93% at V1 = 5 m^3. Highest conversion was obtained at T feed = 250ºC which was 18.93%. However, this temperature was located inside the hysteresis zone and was close to the extinct temperature V1 = 5 m^3 which was 239ºC. Therefore, dynamic simulation was then conducted to determine the stability behaviour at 250ºC so information regarding stability at highest conversion operation could be obtained.

3.2 Dynamic Simulation

In this section, Aspen Hysys® V8.8 Dynamic Mode feature was utilized to identify stable/unstable behaviour in real time. From Fig. 5, we know that extinct temperature is 239˚C at V1 = 5 m^3. Hence, utilizing Dynamic Mode could possibly show minimum temperature to start hysteresis (as function of ΔT_f = 62.013^{0}C) before the oscillation extinct the reaction. Dynamic Mode (Fig. 7) was started at 200ºC far below the ignition temperature. From Fig. 5, ignition temperature was at 310ºC. Therefore, the feed temperature was then set 310ºC to ignite the reaction. After obtaining stable outlet temperature, feed temperature was then lowered ramply to 241ºC. At this point, the outlet temperature was still stable. Feed temperature was then lowered ramply by 0.1ºC to final value 240.8. At this point, dynamic simulation showed oscillation has occurred. This condition means that at V1 = 5 m^3 and 0.5 quenching ratio, hysteresis mathematically will start approximately at:

$$T\ feed\ hysteresis = T\ extinction + 2.9\%\ (\Delta T_f) \quad (3)$$

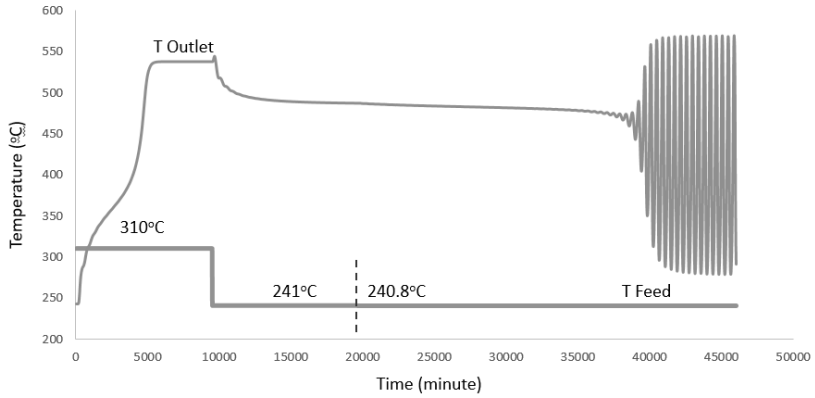

Fig. 7. Minimum hysteresis temperature determination at V1 = 5 m^3

Highest conversion while applying 0.2 quenching ratio and bed volume distribution 2:1 was obtained at 190˚C. Mathematically this point was formulated as:

$$T\,feed\,highest\,conversion = T\,feed\,extinction + 17.73\%\,(\Delta T_f) \quad (4)$$

Therefore, this feed temperature was tested in Dynamic Mode to measure whether the highest conversion could be achieved stably. Result is shown in Fig. 8. Referring to Fig. 8, we are able to conclude that highest conversion of the reaction (at V1 = 5 m^3 & 0.5 quenching ratio) could be achieved stably.

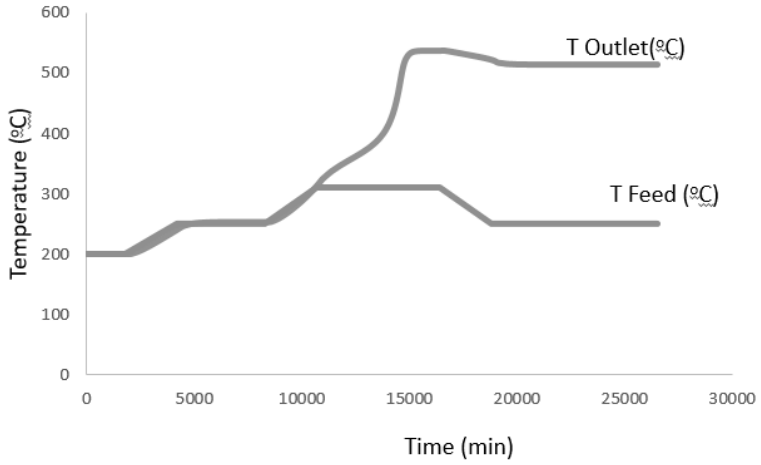

Fig. 8. Stability identification at highest conversion feed temperature (190˚C)

4. Conclusion

Bed volume distribution is one of factor that possible to affect how wide the hysteresis area is while plotting T outlet vs T feed. Higher V1 showed narrowing hysteresis yet increase the extinct temperature that could lower the conversion. Highest conversion was obtained at V1 = 5 m^3 (0.5 quenching ratio) with T feed = 250˚C which entering the hysteresis zone. However, this condition was chosen to be analyzed more in the Dynamic Mode to determine whether 250˚C would already triggered the oscillation. Dynamic Mode showed that oscillation started at 240.8˚C and further extinct the reaction. The highest conversion feed temperature was then tested in Dynamic Mode and resulted stable operation. Therefore, while using 1st bed volume at 5 m^3 (total volume = 30 m^3) and 0.5 quenching ratio, ammonia reaction highest conversion of 18.93% is still able to be obtained at stable operation.

Acknowledgement

The authors gratefully acknowledge the support by Institut Teknologi Bandung, Department of Chemical Engineering especially Laboratory of Process Equipment and Process Simulation

References

1. B. A. Finlayson, *Hysteresis and Multiplicity in Wall-Catalyzed Reactors*, ACS Symposium Series, **65**, 1 (1978)
2. G. R. Setyadi & T. P. Adhi, *Dynamic Simulation Adiabatic Extothermal Reactor with addition of FEHE,* ITB Chemical Engineering Department (2005)
3. J. C. Morud & S. Skogestad, *Analysis of Instability in an Industrial Ammonia Reactor,* AIChE.J, **44**, 888-895 (1988)
4. J.R. Rouse & C. Hyde, *A Comparison of Simple Methods to Incorporate Material Temperature Dependency in the Green's Function Method for Estimating Transient Thermal Stresses in Thick-Walled Power Plant Components,* MDPI, 1, (2015)
5. P. Laššak, J. Labovský, et al. *Influence of parameter uncertainty on modeling of industrial ammonia reactor for safety and operability analysis,* **23,** 280 – 288 (2010).
6. R. K. Herz, *Chemical Reaction Engineering-Part 15-CSTR Thermal Effects, SS + Dynamic*, University of California San Diego, **15,** 5 (2015)
7. R. K. Herz, *Chemical Reaction Engineering-Part 15-CSTR Thermal Effects, SS + Dynamic*, University of California San Diego, **15,** 7 (2015)

Evaluation of Solid State Fermentation and Conventional Oven Drying for Development of Microbial Starter for Fermented Cassava Flour Production

Khairul Hadi B, Ricky, Corwin Rudly and Made Tri Ari Penia Kresnowati*

Microbiology and Bioprocess Technology Laboratory, Chemical Engineering, Faculty of Industrial Technology, Institut Teknologi Bandung, Jl. Ganesha 10 Bandung 40132, Indonesia

** Corresponding Author's E-mail: kresnowati@che.itb.ac.id*

Abstract

Prior fermentation has been shown to improve the properties of the produced cassava flour, such as neutral colour, aroma as well as lower cyanogenic content. Correspondingly, the availability and accessibility of practical and easy to use microbial starter is important for the production of fermented cassava flour (fercaf). This paper described the evaluation of solid state fermentation and conventional oven drying, as a simple and economical method, for preparing microbial starter used for fercaf production. The microbes are cultivated in solid state substrate of fercaf flour, latter it will role as preservation support. Other microbial preservation methods i.e. spray drying and freeze drying were also tested for comparison. Of the three species in the microbial starter for fercaf production, *Aspergillus oryzae* and *Bacillus subtilis* were shown to stable during storage at room temperature and at week 4 the viabilities were 130 and 88.9% of its original concentration respectively. On the other hand this method was not shown to work well for *Lactobacillus plantarum* such that, the cell viability was shown to decrease significantly to 0.8% at week 3. Overall, the proposed method provided better cell viability compare to freeze drying or spray drying method.

Keyword: microbial preservation, cell viability, microbial starter, conventional oven drying, freeze drying, spray drying

1. Introduction

Cassava (*Manihot esculenta*) is one of the staple foods abundantly available in Indonesia. It is easy to be cultivated in tropical-subtropical regions with low demand for nutrients [1]. However the use of cassava in food derivative products i.e. bakery, noodle and biscuits is still limited because of its unique physical characteristics and pasting properties. Moreover raw cassava normally contains high cyanogenic substances which naturally act as mechanism of self-protection: cyanogens level in cassava leaves are in the range of 200-1,300 mg CN equivalents/kg dry weight and in cassava roots are in the range of 10-500 mg CN equivalents/kg dry weight. The cyanogenic content is higher than the maximum levels recommended for foods by the FAO, that is10 mg CN equivalents/kg dry weight [2]. On the other hand cassava is gluten-free staple; therefore gluten intolerant people can consume it safely. In order to extend its potential utilizations, the properties of cassava flour need to be modified: the protein content and starch structure should be improved and altered.

Fermentation of cassava, prior to its milling, has been shown to improve the properties of the produced cassava flour [3,4]. The product is known as modified cassava flour (Mocaf) or fermented cassava flour (Fercaf). Throughout the fermentation the activity of microorganism causes the hydrolysis of fiber and starch, induces the decrease of cyanogenic content of cassava. Overall, the process provides better organoleptic attributes such as neutralize aroma and texture as well as improve the whiteness[3,5-7]. In some cases, fermentation may also increase the nutritive value of the produced flour which is represented by the protein content of the flour.

The quality of flour is influenced by the microorganism involved in the fermentation [8]. Commonly, inoculum is prepared prior to the main fermentation of fermented cassava flour production process. In general the inoculum used is called as starter. However, conventional inoculum preparation is laborious and time consuming. It is not practical to be applied at home and small industries. In order to attain practical way in starter preparation: easy to store, preserve and transport, an instant starter should be developed. Starter containing particular species of microorganisms, each with certain amount of cell viability will provide the desired quality of fermented cassava flour.

There were some common methods used in microbial preservation i.e. spray-drying, freeze-drying and freezing and frozen storage [9]. Spray-drying method has been used in yeast and negative gram bacteria preservation successfully [10]. Freeze-drying or lyophilization method requires cryoprotective agent to protect the cell from osmotic lysis. It has been applied in developing yoghurt starter [11]. The main disadvantage of both methods is the high equipment cost and energy demand making it uneconomical to be applied in small industries. Conventional drying is a simple method which can be performed at mild condition close to room temperature thus it requires less energy than others. However it will work on spore production or formation microorganism such as filamentous fungi and bacillus and form undesired rhological properties of the dried cultures [12].

Research and development of instant starter particularly in food and beverages application has been started since the last decades. The utilization of solid-state fermentation in enhancing protein and nutrient values on cassava has been studied over decade. *A.niger* was utilized to enhance the protein content in cassava and used various nitrogen sources in solid-state fermentation [13]. Cassava was also fermented by *S.cereviceae* in order to enhance nutritive values [14]. While *B.subtilis, L.plantarum* and *S.cereviceae* were applied to solid substrate of feed-grade soybean meal and wheat bran [15], those studies were proposed to provide protein rich animal feed with non-aseptic condition.

It is the aim of this research, to evaluate to application of solid state fermentation and conventional oven drying for preparing microbial starter used for fercaf production. The advantages of low water usage and energy cost in drying would provide the best method in instant starter preparation in this study. Moreover the development of an instant fercaf starter of the specified microorganism hopefully would foster domestic production and create a new food-biotech industry in Indonesia.

2. Experimental

2.1. Microbial culture preparation

The microorganism used were *Aspergillus oryzae* ITBCC L24, *Bacillus subtilis* ITBCC B128 and *Lactobacillus plantarum* ITBCC B188, which are obtained from Laboratory of Microbiology and Bioprocess Technology of Chemical Engineering, Institut Teknologi Bandung. The microorganisms were cultured in a submerged fermentation of 50 mL working volume in 250 mL flask using potatoes dextrose broth, nutrient broth and MRS broth as media for *A.oryzae*, *B.subtilis* and *L.plantarum* respectively. The bacteria were cultivated for 24 h, while the mold for 4 d before further used [16].

2.2. Solid state fermentation and immobilization on support

Cell immobilization were carried out during the solid substrate/support fermentation, 20 g of fercaf was added aseptically into each of microbial culture at its stationary growth phase. The mixture formed semi-solid or slurry phase then were subjected to incubation for two days for *B.subtilis* and *L.plantarum* and four to five days for *A.oryzae* until the spore produced.

2.3. Conventional drying

After period of incubation, each of culture mixture was spread in a tray and then covered by sterile muslin cloth, in order to avoid for contamination but allow water vapor to escape. The container then was placed in an oven which was preset at temperature about 32^{o}C for 4-5 days.

2.4. Spray drying

The spray dryer apparatus used was EYELA-SD having two-way nozzle atomizer with operational pressure range between 0.8-1.2 kg/cm^2. The flowed air operated at 80^{o}C, on suction mode and flow rate at 0.5 m^3/min. The configuration of flowing air was co-current and the feed flow rate was set at 250 mL/h, the feed suspension was prepared by added the 5% carrier w/v to the liquid culture. The dry product was collected at single cyclone separator and stored at petri disk at room temperature.

2.5. Freeze drying

The suspension with the amount of 5 mL was added in 15 mL capacity of vial, the bottles were covered by perforated parafilm, and then five bottles were placed in freeze dryer. All of the suspensions were prepared as same as spray-drying methods except *A.oryzae* culture. In this method, the mold suspension was consisting of spore extracted from agar slant, 0.85% (w/v) NaCl, and 0.1% (v/v) Tween 80 both of them were analytical grade and 5% fercaf (w/v) in 200 mL sterile demineralized water aseptically. The equipment used was ALPHA1-2 LDPlus. The suspensions were initially frozen and then dried at 0.07 mbar and -50^{o}C for three days. Finally the product was stored at room temperature.

2.6. Cell viability quantification

Cell concentration in the dried starter sample was analyzed using total plate count (TPC) methods. Specific agar medium was used for each species: d-mannitol-yolk polymixin, MRS and potatoes dextrose for *B.subtilis*, *L.plantarum* and *A.oryzae*, respectively. The wet solid colony before drying was used as the basis for viability quantification, and the viability will be expressed as:

$$\%Viability = \frac{N_i}{N_j} 100\% \quad (1)$$

In which N_i is the initial cell concentration, when solid state fermentation was completed prior to drying. The colony number would be counted at the time when the drying was completed (N_0), then at the next first (N_1), second (N_2), third (N_3) and fourth (N_4) week storage period at room temperature.

2.7. Fermentation

The prepared starter was then tested in cassava chips fermentation for fercaf production. A specific amount of each starter containing 10^7 cfu/mL for the bacteria and 10^4 spore/mL for the mold corresponding to 3 g for *B.subtilis*, 1 g for *A.oryzae*, respectively of instant starter, were used in 2 kg cassava chip fermentation in a batch reactor, (Soil Aquifer Treatment) sat water to fresh cassava ratio was at 8 L/kg [16]. Prior to fermentation, the inoculum was prepared by using 24 h acclimated each instant starter in each 500 mL working volume containing 50 g cassava chip. The fermentation was carried out in a batch reactor at 34^{o}C for 16 h, with 4 h time interval for observation of number of colony in broth fermentation.

2.8. Statistical analysis

The experiments were conducted in duplicate and the one-way analysis of variance was applied to the result of cell viabilities during storage.

3. Results and Discussions

3.1. Conventional Oven Drying Performance for Microbial Cell Preservation

Cell concentrations in the liquid cultures were analyzed to be 1.1 x10^7, 4.8 x10^6 and 1.2 x10^4 cfu/mL subsequently for *B.subtilis*, *L.plantarum* and *A.oryzae*. It was expected that microbial cell would grow further when these cultures were transferred to the solid media and cultivated further as solid state fermentation. As was expected the concentration of *B.subtilis* and *A.oryzae* were measured to be (1.0±0.9) x10^8 and (7.4±0.0) x10^7 cfu/g, respectively, at the end of solid state fermentation. On the other hand, the concentration of *L.plantarum* was measured to be very low. It was not surprising

because *L.plantarum* is not spore-forming bacteria and can only sustain in the present of free water. The spore-forming lactobacillus is commonly known as sporolactobacillus [17].

After drying was performed, the dry solid obtained was around about 15 g for each sample. The TPC analysis gave cell concentration of (1.19±1.6) $x10^9$ and (1.7±0.0) $x10^8$ cfu/g, respectively for *B.subtilis* and *A.oryzae*. The corresponding conventional oven drying performance in cell preservation, which was parameterized as the ratio of cell viability after and before the drying process are presented in Table 1.

Table 1. Conventional Oven Drying Performance for Microbial Cell Preservation

Microorganisms	**Cell viability ratio**
Aspergillus oryzae ITBCC L24	1.22±0.39
Bacillus subtilis ITBCC B128	1.68±1.62
Lactobacillus plantarum ITBCC B188	$(0.87±1.2)x10^{-2}$

According to Table 1., the cell viability for both *A.oryzae* and *B.subtilis* close to one means that there were less decay or death cell during the drying process. On the other hand *L.plantarum* gave ratio close to zero means that there was less cell remain after the drying process, the variability showed were almost comparable to the mean values, that was because a certain parameter in incubation and drying process i.e. the thickness of the layer spread was not maintain, this would be a new consideration in future research. The preservation using spray-drying methods was only viable for *B.subtilis* and *L.plantarum* using fercaf and low-fat milk as a carrier, respectively. The filament physiology of mold inhibits the atomization process during the drying. Therefore the method was not applicable to *A.oryzae*. After the spray-drying process the cell viability ratio were measured to be 2.37 $x10^{-3}$ and 0.207 for *B.subtilis* and *L.plantarum* respectively. In freeze-drying method, *B.subtilis* with fercaf carrier showed comparable cell viability, 7.7 $x10^{-2}$ to the one with dextrin which was about 9.3 $x10^{-2}$. On the other hand, *L.plantarum* was showing the most prominent result than others, it was measured to be 0.77. The results obtained by using both spray-drying and freeze drying methods were similar to another reference which was applying these method for three kinds of lactic acid bacteria[18]. The cell viability ratio given by *A.oryzae* in this method was, 0.299 after the drying process.

Another study was also conducted by using of vacuum drying method in unpublished research article. The results showed that those three microorganisms had cell viability ratio lower than 0.1 after drying process at 55ºC in vacuum condition. All of methods applied provided large variation in results which depend on microorganism, the temperature and time course of the processes.

3.2. Cell viability during storage

Each of preserved microorganisms obtained from different method was stored at room temperature. Then the viability was observed weekly during the period of storage. The results are provided in Fig. 2.

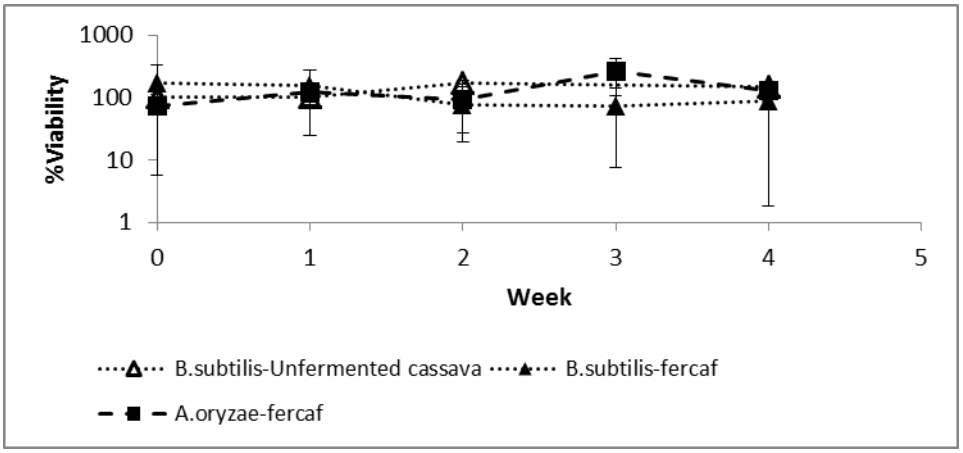

(a)

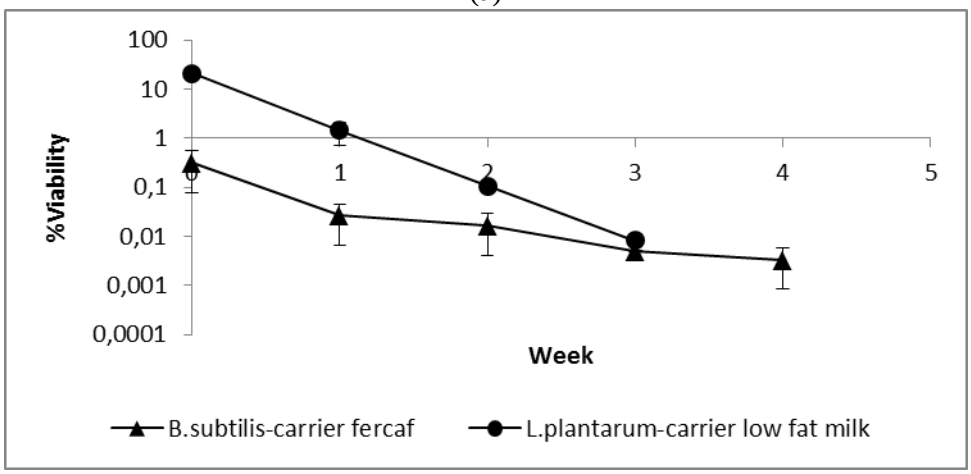

(b)

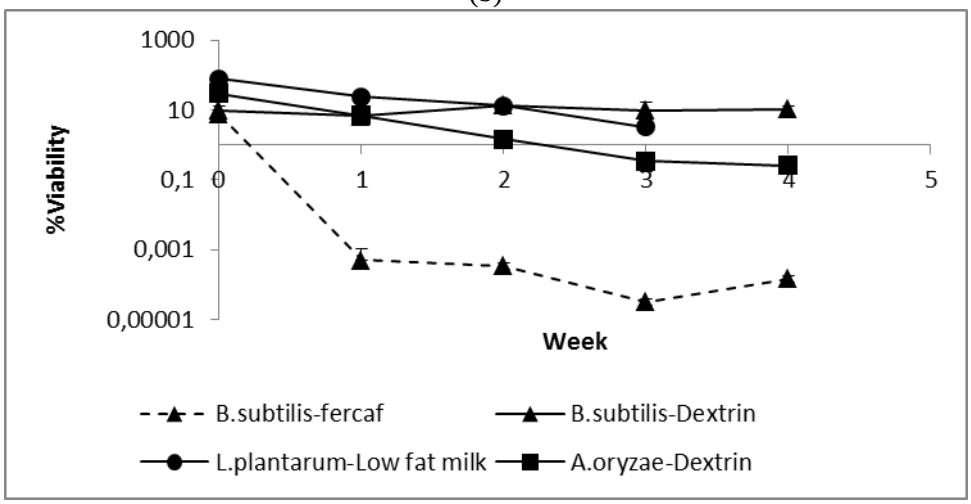

(c)

Fig. 1. The percentage viability of microorganism during storage period a) Conventional drying b) Spray drying and c) Freeze drying

The one-way ANOVA test resulted that there is no significant different ($p>0.05$) on viability between the trend of viability of *B.subtilis* and *A.oryzae* during period of storage. The obtained values were around 100%, or in another word similar to the number of colony obtained after incubation (solid-state fermentation) prior to drying. Two way ANOVA test was also conducted for *B.subtilis*, besides provided the effect of time course of storage, the test was also applied to the carrier utilized i.e. fercaf and unfermented dried cassava. The unfermented dried cassava flour also was used as a

support/solid substrate, and fig. 1 shows that there is no significant different ($p>0.05$) with the one using residual fercaf. Then it is recommended that utilizing un-passed screen fercaf will be the best way to maximize the whole utilization of fercaf flour.

The spray-drying provided the bacterial viability at 0.31±0.23 and 20.7±5.0 % for *B.subtilis* and *L.plantarum* respectively. There were significant ($p<0.05$) decrease in viability during 4 weeks storage, which were 0.001 and 0.008 % for *B.subtilis* and *L.plantarum* respectively. On the other hand, the freeze drying preservation on *B.subtilis* showed stable viability during 4 weeks observation at room temperature by using dextrin as a carrier, the value were sticking around 10%. The assessment on *L.plantarum* by using low-fat milk resulted that the viability after drying was 70% from prior to drying and at week third it decreased to 3.25 %. The result for *A.oryzae* gave 30% viability after drying was completed and only 2.0 % remained at week fourth.

3.3. Evaluation of instant starter for fermentation of cassava chips

The instant starter prepared by conventional oven drying was further evaluated in real fermentation of cassava chips for fercaf production. Because the proposed method cannot produce good quality of dry L.plantarum starter, conventional method of *L.plantarum* inoculum preparation method was applied. The fermentation process was followed by measuring cell concentration during the fermentation.

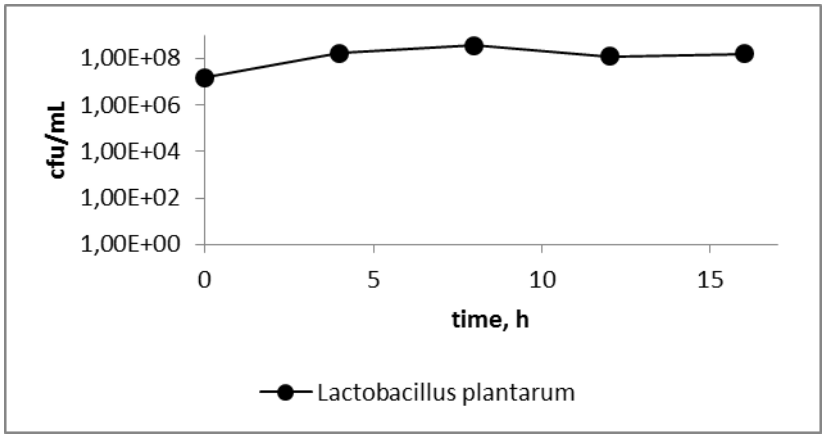

(a)

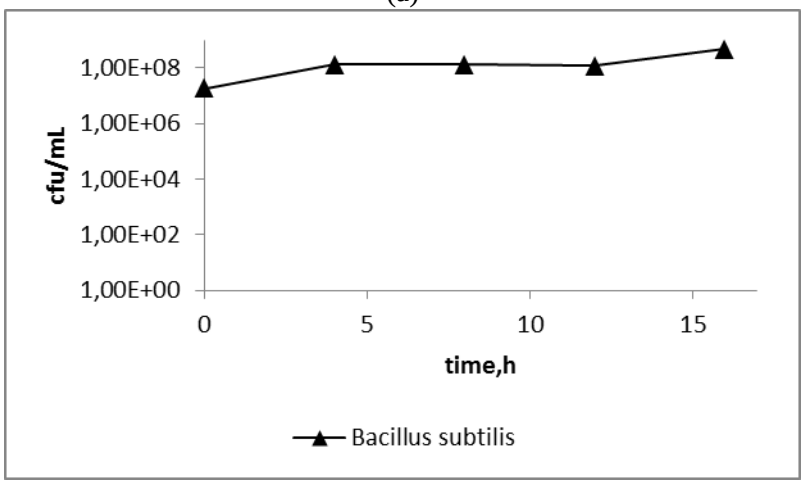

(b)

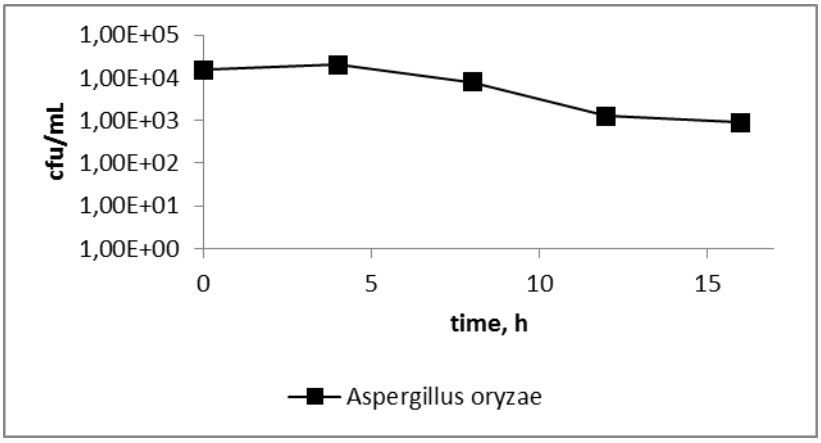

(c)

Fig. 2. The number of colony for each species a) *L.plantarum* b) *B.subtilis* c) *A.oryzae*

The result showed that *B.subtilis* and *L.plantarum* grew well during the fermentation. Similar trend was observed when conventional inoculum preparation method was applied [16]. Different trend was observed for *A.oryzae*. The cell concentration was observed to increase during the first four hours observation, but gradually decreased afterwards. This might be cause by the tendency of this fungus to grow on the surface of cassava chips, whereas samples for TPC analysis were taken from the fermentation broth.

At the end of the fermentation process, the broth's pH was observed to decrease from 5.5 to 4.0. This indicated the production of organic acid which also showed that fermentation proceeded. For comparison, control fermentation without starter addition, which is commonly known as retting process, was also conducted during the same time and the broth's pH was still closed to the initial pH. From the physical appearance, the chips produced from fermentation process gave more neutral aroma and whiter in color, compared to the chips produced from the retting process.

Overall, these growth profiles indicated that the fermentation process occurred and had been influenced by the presence of the microorganism from the starter. Drying process also will give more advantages when conducted in more simple method and equipment, for the large scale in the future production, even by using room temperature oven, the cost of scale up of unit operation will be the main consideration, thus the sun drying method would be a better alternative choice, however the consideration will be changed to the aseptic requirement to avoid the contamination.

Conclusion

The research showed that the conventional drying method combined with semi-solid fermentation could produce good quality of dried instant starter. The viability of both *B.subtilis* and *A.oryzae* starter were quite stable during the drying process and further during the storage at room temperature. These starters also gave good performance when were applied in cassava chips fermentation for fercaf production. The quality of the product, simplicity of process as well as its cost efficiency made this method an interesting alternative for producing instant starter for fercaf production. This method, however, could not be applied for preparation of *L.plantarum* instant starter.

Acknowledgement

This research was funded by the Ministry of Research, Technology and Higher Education under Development of Industrial Technology Program (PPTI) scheme entitled 'Development of Semi Continuous Fermented Cassava Flour Production Process at Pilot Scale'.

References

(1) Stupak, M., Vanderschure, H., Gruissem, W., Zhang, P. Biotechnological approaches to cassava protein improvement. *Trends in Food Science & Technology*: 10(2006).
(2) Siritunga, D., Sayre, R. Engineering cyanogen synthesis and turnover in cassava (*Manihot esculenta*). *Plant Molecular Biology*; 56(4): 661-669(2004).
(3) Kresnowati, M. T. A. P., Bindar, Y., Aliwarga, L., Lestari, D., Prasetya, N., Tanujaya, A. R. Effects of Retting Media Circulation and Temperature on the Fermentation Process in Soft-Texture and Low Cyanogenic Content Cassava Flour Production. *AJChE 2014*; 14(2): 67-76(2014).
(4) Meitha, A., Bindar, Y., Kresnowati, M. T. A. P. Effects of Cassava Chips Fermentation Conditions on The Produced Flour Properties. *Asean Journal of Chemical Engineering*; 16(1)(2016).
(5) Daubresse, P., Ntibashirwa, S., Gheysen, A., Meyer, J. A. A Process for Protein Enrichment of Cassava by Solid Substrate Fermentation in Rural Conditions. *Biotechnology and Bioengineering*; XXIX: 962-968(1987).
(6) Akindahunsi, A. A., Oboh, G. Effect of Fungi Fermentation on Organoleptic Properties, Energy Content and In-Vitro Multienzyme digestibility of Cassava Products (Flour & Gari). *Nutritional Heatlh*; 17(2): 335-342(2003).
(7) Gunawan, S., Widjaja, T., Zullaikah, S., L., I., Aparamarta, H. W.; Prasetyoko, D. Effect of Fermenting Cassava with Lactobacillus plantarum, Saccharomyces cereviseae, and Rhizopus oryzae on the Chemical Composition of Their Flour. . *International Food Research Journal*; 22(3): 1280-1287(2015).
(8) Kresnowati, M. T. A. P., Listianingrum, Zaenudin, A., Trihatmoko, K. The effect of microbial starter composition on cassava chips fermentation for the production of fermented cassava flour. In *International Conference of Chemical and Material Engineering(ICCME) 2015*; American Institute of Physics, 2015; Vol. 1699; pp 1-6.
(9) Alonso, S.: Novel Food Fermentation Technologies. In *Novel Preservation Techniques for Microbial Cultures*; V., G., Barbosa-Cánovas, Eds.; Springer International Publishing Switzerland: Switzerland, 2016.
(10) Peighambardous, S. H., Tafti, A. G., Hesari, J. Application of spray-drying for preservation of lactic acid starter cultures: a review. *Trends in Food Science & Technology*; 22: 215-224(2011).
(11) Morgan, C. A., Herman, N., White, P. A. Preservation of micro-organisms by drying: A review. *Journal of Microbiological Methods* 66: 183-193(2006).
(12) Tsaousi, K., Velli, A., Akarepis, F., Bosnea, L., Drouza, C., Koutinas, A. A., Bekatorou, A. Low-Temperature Winemaking by Thermally Dried Immobilized Yeast on Delignified Brewer's Spent Grains. *Food Technol. Biotechnol.*; 49(3): 379-384(2011).
(13) Noomhorm, A., Ilangantileke, S., Bautista, M. B. Factors in the Protein Enrichment of Cassava by Solid State Fermentation. *J Sci Food Agri*; 58: 117-123(1998).
(14) Boonnop, K., Wanapat, M., Nontaso, N., Wanapat, S. Enriching Nutritive Value of Cassava Root by Yeast Fermentation. *Sci. Agric. (Piracicaba, Braz.)*; 66(September/October): 629-633(2009).
(15) Ying, W., Zhu, R., Lu, W., Gong, L. A new strategy to apply *Bacillus subtilis* MA139 for the production of solid-state fermentation feed. *Letters in Applied Microbiology*; 49: 229-234(2009).
(16) Listianingrum, Trihatmoko, K., Zaenudin, A., Kresnowati, M. T. A. P. The Effect of Microbial Starter Composition on Pasting Properties of Fermented Cassava Flour. *The 22nd Regional Symposium on Chemical Engineering: RSCE 2015*; (2015).
(17) Fujita, R., Mochida, K., Kato, Y., Goto, K. Sporolactobacillus putidus sp. nov., an endospore-forming lactic acid bacterium isolated from spoiled orange juice. *International Journal of Systematic and Evolutionary Microbiology*; 60: 1499-1503(2010).
(18) To, B. C. S., Etzel, M. R. Spray Drying, Freeze Drying, or Freezing of Three Different Lactic Acid Bacteria Species. *Journal of Food Science*; 62(3): 576-579(1997).

Optimization of OPEFB Hydrothermal Pre-treatment for Xylitol Production

Diah Meilany-[1,2], MTAP Kresnowati[2*], Tjandra Setiadi[2,3]

[1]Chemical Engineering, Politeknik Negeri Malang, Jl. Sukarno Hatta No 9, Malang 65141, Indonesia
[2]Chemical Engineering, Institut Teknologi Bandung, Jl. Ganesha no 10, Bandung 40132, Indonesia
[3]Center for Environmental Studies (PSLH), Institut Teknologi Bandung, Jl. Sangkuriang 42A, Bandung 40135, Indonesia

** Corresponding Author's E-mail kresnowati@che.itb.ac.id*

Extended Abstract

Oil palm empty fruit bunch (OPEFB) is one of the industrial waste from palm oil industry that is available in huge quantities in Indonesia. On the other hand, OPEFB is a lignocellulosic biomass which component is hemicellulose with xylan as the main component. This could be further used for xylitol production via fermentation.

Xylitol is known as a substitute sugar mainly consumed by the diabetic patient since it has the same sweetness as sucrose yet much lower calorific value. Xylitol is produced by hydrogenation reaction of xylose as reactant that is converting aldehyde (xylose) into alcohol (xylitol) using Ni catalyst. Another way to produce xylitol is by fermentation performed by microbes such as yeast or fungi. This process is moderate and known as a green technology.

Xylose, the substance needed to produce xylitol, is a pentose with an aldehyde as a functional group. It is derived from hemicellulose, a part of lignocellulosic biomass, which consists of cellulose, hemicellulose, and lignin. Xylose as the substrate of fermentation is produced from hydrolysis of hemicellulose, which can be enzymatic. The most important thing is that enzyme is hindered by macro and microstructure of biomass component especially by lignin which is a bulky polymer.

There have been many attempts made to reduce the effect of lignin existence by pretreating lignocellulosic biomass. One of them is hydrothermal pre-treatment process which uses high-temperature water (>110°C) in a certain period of time. This research aimed to perform some optimization schemes that were maximizing xylose in OPEFB pre-treated solid, maximizing xylose in both OPEFB pre-treated solid and liquid, maximizing xylose in both OPEFB pre-treated solid and liquid, and simultaneously minimizing glucose in OPEFB pre-treated solid and liquid. The last optimization scheme was also aimed to know the obtained ratio of glucose to xylose and check whether it can fit well with the constraint of xylitol fermentation. The optimization results are summarized in table 1.

Table 7 Summary of hydrothermal pre-treatment optimization scheme

No.	Optimization scheme	Hydrothermal pretreatment condition			Xylose recovery
		Solid loading [%]	Temperature [°C]	Pretreatment time [minutes]	
1.	Maximizing xylose recovery in OPEFB pre-treated solid	7,2%	164	48,2	0,096 g/g OPEFB
2.	Maximizing xylose recovery in OPEFB pre-treated solid and liquid	5%	163	60	0,12 g/g OPEFB
3.	Maximizing xylose recovery in OPEFB pre-treated solid, liquid, and minimizing glucose in OPEFB pre-treated solid and liquid	13,5%	158	60	0,11 g/g OPEFB

The ratio of glucose to xylose at the calculated optimum condition was 1:1.1. This ratio cannot fulfill the result of previous work that stated the optimum ratio of glucose to xylose in xylitol fermentation was 25%.

As can be seen in table 1, the optimum condition of pretreatment process calculated for three different optimization goals in term of solid loading, temperature and time were almost alike. There is a little difference in temperature between the first and the second scheme and also a little difference in time between the second and the third scheme. SL and time showed the more significant effect on glucose recovery than on xylose recovery. This condition led to a shift of the optimum value of SL and time on the additional goal of minimizing glucose recovery. Temperature effect on xylose recovery gave a maximum value of xylose recovery so it can stand on almost the same value through three different schemes.

Keywords: OPEFB, hydrothermal pre-treatment, temperature, time, solid loading

Factorial Design Analysis applied to Bleaching of Rice Bran Oil

I Dewa Gede Arsa Putrawan[1,*], Rika Suryati[2], and Adrian Setyadi[2]

[1]*Research Group on Chemical Product Design and Development,*
[2]*Study Program of Chemical Engineering,*
Faculty of Industrial Technology, Institut Teknologi Bandung
Jalan Ganesha 10, Bandung 40132, Indonesia

** Corresponding Author's E-mail idewa@che.itb.ac.id*

Abstract
Rice bran contains edible oil which is rich in anti oxidants but, however, it has problems during storage, due to the activity of lipase enzyme. The most popular stabilization method is extrusion cooking. The extrusion cooking of rice bran, however, results in dark oil. This research is aimed to study the bleaching of rice bran oil from extrusion cooked rice bran. The experiments were carried by a full 2k factorial design with bleaching earth-to-oil ratio, temperature, and time as factors. The color of rice bran oil was measured by spectrophotometer. It was found that all main factors have significant effects on the color of rice bran oil. Among the interaction factors, only the interaction between temperature and bleaching earth-to-oil ratio has significant effect. The best result was obtained at temperature of 110°C, time of 30 minutes, and bleaching earth-to-oil ratio of 10%. In addition, rice bran oil de-acidified by solvent extraction was found to be more difficult to bleach than that by neutralization.

1. Introduction

Rice bran is a byproduct of rice milling. Rice mills generally separate rice into three fractions, i.e., white rice, rice husk, and rice bran. These fractions contribute about 70%, 20%, and 10%, respectively, of rice weight. Rice bran consists of 15~18% fat/oil, 0.4~1.5% wax, 5~8% protein, 40~50% soluble carbohydrate, and 5~8% fiber[1,2]. Rice bran oil is a healthy edible oil, containing vitamins, antioxidants, nutrients and trans fat free. It can help lower cholesterol, fight diseases, enhance the immune system, fight free radicals and more. Rice bran oil is vastly superior to traditional cooking oils and can be considered a nutraceutical (food as medicine) oil that is perfect for healthy cooking needs. The unique components, such as oryzanol or tocotrienol, have been drawing people's attention. Numerous studies show rice bran oil reduces the harmful cholesterol (LDL) without reducing good cholesterol (HDL). In those studies, oryzanol is reported as the key element responsible for that function[3]. Tocotrienol, on the other hand, is highlighted as the most precious and powerful vitamin E existing in nature and is said to have an anti-cancer effect[3]. It has been suggested to suppress production of reactive oxygen species more efficiently than tocopherols. As a vitamin-E source, rice bran oil is rich not only in alpha tocopherol but also has the highest amount of tocotrienol in liquid form vegetable oils.

Indonesia is the third largest rice producer in the world after China and India. The annual rice production of Indonesia achieved 50-60 million tones. This means that Indonesia produces rice bran of 5-6 million tons per year. However, it is not utilized for edible oil production. Rice bran is generally utilized for animal feeds and sometimes left near rice millers as waste. In certain countries, notably India, China, and Japan, however, rice bran oil makes a significant contribution to the edible oil supply.

It is well known that raw rice bran contains an extremely active lipolitic enzyme (lipase) which hydrolyses the triglycerides and releases free fatty acids. The major impediment to the development of rice bran oil industries in Indonesia has been the high free fatty acid content

of the extracted oil due to the action of this enzyme. Lipase mixes with rice bran after milling and become very active on contact with air. High free fatty acids are not acceptable for edible oil refining since removal of the acidity leads to considerable losses of neutral oil. Free fatty acid levels can rise to 20 per cent in a matter of days[4]. Without stabilization process, storage of several days causes the extraction of rice bran oil becomes uneconomic.

One of popular stabilization methods is extrusion cooking. Stabilization of rice bran by extrusion cooking results in dark crude rice bran oil. The bleaching of rice bran oil becomes more difficult compared to other edible oils. Bleaching of edible oils is usually done by adsorption using bleaching earth. The bleaching performance of a bleaching earth is influenced by the quality of oil, bleaching earth-to-oil ratio, temperature, and time. In addition, the darkness of rice bran oil from extrusion cooked rice bran was affected by cooking condition, quality of rice bran, and perhaps the variety of rice. Although numerous researches on rice bran oil have been published, experimental results on bleaching of rice bran oil are limited. O'Brien et al[5] found the best bleaching condition at temperature range of 70 to 110°C and time range of 15 to 30 minutes. Caustic refining was found to give lighter rice bran oil compared to solvent refining and steam refining[6]. Treating rice bran oil miscella by silica gel was found to improve oil color but the slow flow rate of miscella through silica gel bed was found to be a problem[7]. Sayre et al[8] found that the extrusion of rice bran at 130°C did not affect the bleached oil color using acid activated clay. Strieder et al[9] studied bleaching in combination with winterization and found that the use of 1% (w/w) of adsorbent in relation to the mass of oil and 8% (w/w) activated carbon in relation to the total mass of adsorbent were the best conditions, which resulted in a removal of 83% of primary oxidation products and of 57% of carotenoids content. A comprehensive study on the effects of bleaching operation has not been done.

This research is aimed to study the bleaching of rice bran oil from extrusion cooked rice bran by 2^k factorial design. Bleaching earth-to-oil, temperature, and time are selected as experimental factors. The color of rice bran oil was measured by spectrophotometer. Recently, solvent extraction was found to be promising as a substitute for neutralization in removing the free fatty acid content of rice bran oil. This research, therefore, is also proposed to compare the bleaching of rice bran oils from solvent refining and neutralization.

2. Experiment

2.1 Materials

Freshly milled raw rice bran, containing an average of 12% oil and moisture of 14%, was obtained from a local rice mill. The rice bran was collected within one hour after milling. Normal hexane of technical grade was used for extracting rice bran oil. The bleaching earth used was an optimum proprietary product of a bleaching earth corporate in West Java, Indonesia. Methanol and caustic soda was used for removing free fatty acid by solvent extraction and neutralization, respectively. All chemical utilized for analysis were of pure grade.

The rice bran accepted was first cooked using an extrusion cooker with 3 dies (3 mm ID x 25 mm length opening), which was designed according to a previous literature[10]. The raw bran was fed directly into the extruder. Our previous result showed that the heat developed was sufficient to achieve a cooking temperature of 110 to 130°C[11]. The extruded hot bran was cooled in a sieve wire-air cooler to 40°C. Moisture contents of the sample brans were adjusted by conditioning in an atmosphere, and samples were then packed in polyethylene bags to prevent moisture adsorption until extraction were completed. The extruded rice bran was then contacted with normal hexane in an extractor of 50 liters capacity to extract rice bran oil. Normal hexane was removed by distillation under vaccuum to obtain crude rice bran oil. The crude rice bran oil was dewaxed and degummed by aqueous calcium chloride, settling and centrifugation. Free fatty acids were removed from dewaxed rice bran oil by two methods,

i.e, solvent extraction using methanol and neutralization using caustic soda. Bleaching experiments were carried in a stirred glass using 30 grams of rice bran oil. The experiments were design using a full 2^k factorial design. Three factors were studied, i.e., bleaching earth-to-oil ratio, temperature, and time as main factors. Activated carbon, 5% of bleaching earth, was also added in all bleaching runs. Table 1 shows the levels used.

Oil color was measured by a spectrophotometer (an HP 8452A model) with automatic wave length scanning and recording. Cuvettes with 1 cm light path were used and absorbance at wave lengths of 190-800 nm was recorded.

Table 1: Factor levels.

Factor	Level	
	-1	+1
Bleaching earth-to-oil ratio (%)	1	10
Temperature (^oC)	70	110
Time (minute)	15	30

3. Results and Discussion

3.1 Interpretation of absorbance curve

Fig. 1 shows typical spectra of rice bran oils, before and after bleaching, in which free fatty acids were removed by neutralization. Two spectra for bleached rice bran oils represent the best and the worst bleaching, respectively. The spectra of neutral rice bran oil exhibits maxima at 496, 538, 560, 610, and 672 nm. The absorbance peaks at 538, 610, and 672 nm are characteristics of red, blue, and green respectively. As can be seen, these three peaks were removed after bleaching at the best condition but just shortened after bleaching at the worst condition. In other words, the performance of bleaching depends on bleaching condition.

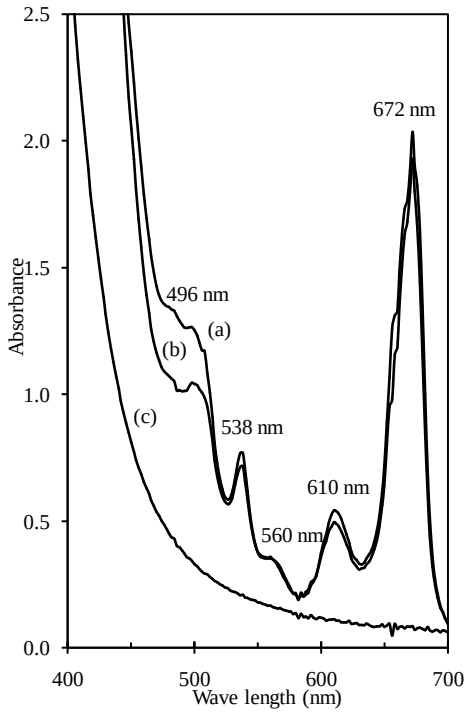

Figure 1: Spectra of rice bran oils (a) after neutralization, (b) after bleaching at %BE = 1%, T = 70 °C, t = 30 min, and (c) after bleaching at %BE = 10%, T = 110 °C, t = 30 min.

3.2. Removal of free fatty acid

As noted previously, bleaching was done after de-acidification. Neutralization by caustic soda is conventionally applied and solvent extraction by alcohol is recently considered as a promising substitute for neutralization[12,13]. Both methods were applied here to study their effects on the bleaching performance. The acid number of crude rice bran oil was 30.0 mg KOH/g. Neutralization was carried in the excess caustic soda of 1% resulting neutral oil with acid number of 2.6 mg KOH/g. The alcohol selected as solvent is methanol. Six stages of extraction reduce the acid number of oil to only 9.1 mg KOH/g.

Fig. 2 shows the spectra of oils before and after bleaching for both de-acidification methods. The absorbance peaks of bleached oil from neutralization are lower than those of oil from solvent extraction. Previously, Kim et al[6] also found that solvent extraction darkened rice bran oil. In this study, it was also found by visual that the crude rice bran oil de-acidified by neutralization was lighter than that by solvent extraction. It means that neutralization not only remove free fatty acids but also decolorized rice bran oil. It is due to the formation of soap in neutralization which could adsorb colors although the adsorption is not as good as bleaching earth. On the other hand, solvent extraction merely reduced free fatty acid content and could not reduce the color. As can be seen, the absorption spectra of crude rice bran oil is not significantly different to that after solvent extraction. Moreover, the free fatty acid content of rice bran oil could not be reduced to a value lower than 9.1 mg KOH/g. The free fatty acid left is known to add difficulty in bleaching process.

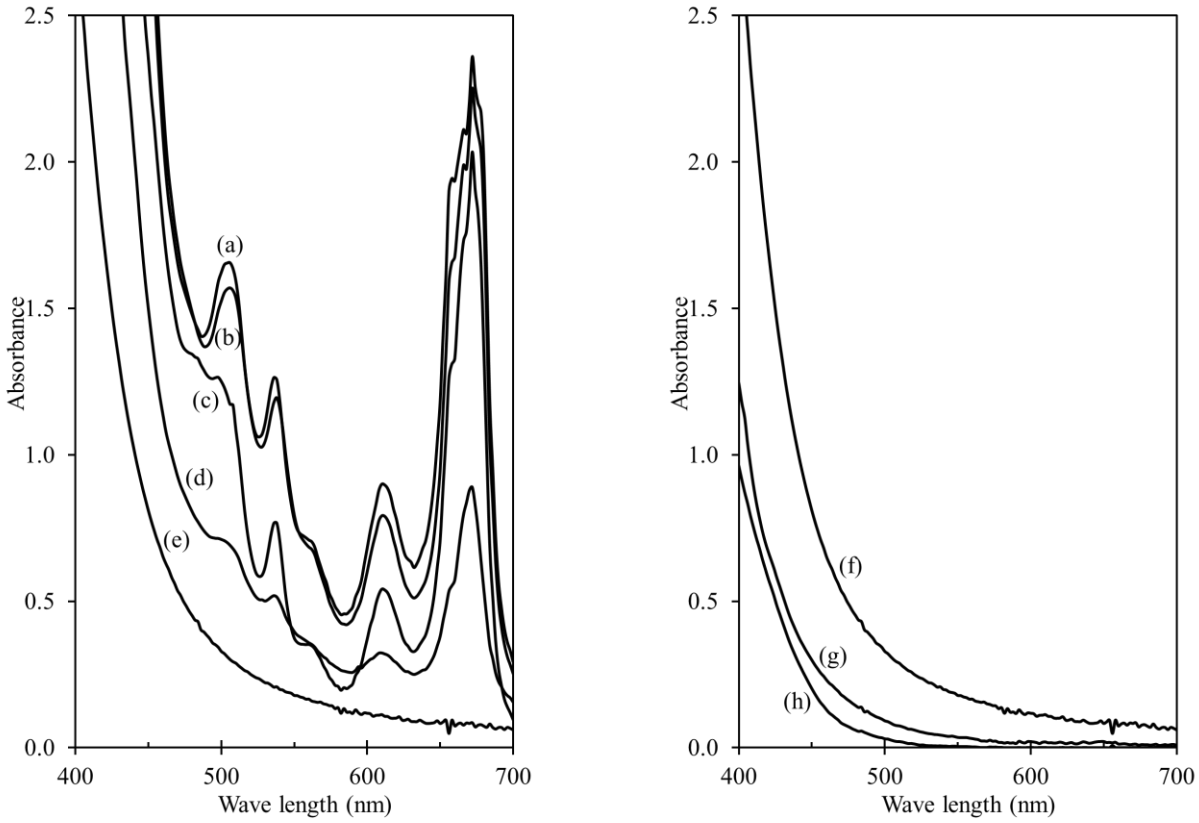

Figure 2: Spectra of rice bran oils (a) crude, (b) after extraction, (c) after neutralization, (d) after extraction and bleaching, (e) after neutralization and bleaching, (f) maximum bleached rice bran oil of this study, (g) commercial bulk refined palm oil, and (h) imported refined rice bran oil.

3.3. Analysis of factorial design

A guideline to convert absorbance spectra to bleaching performance was not found. Visual observation, however, showed that the lower the sum of absorbance peaks at the red, blue, and green color characteristics, i.e., 538, 610, and 672 nm, respectively, the lighter the oil color. The sum of the absorbance peaks at these three wave lengths was selected as a response.

Table 2: Measured responses.

Run	X_1	X_2	X_3	X_1X_2	X_1X_3	X_2X_3	$X_1X_2X_3$	Response			
	%BE	T	t	%BE·T	%BE·t	T·t	%BE·T·t	Y1	Y2	Y_{ave}	σ
1	-1	-1	-1	1	1	1	-1	3.033	3.243	3.13	0.1
2	-1	-1	1	1	-1	-1	1	3.153	3.126	3.14	0.0
3	-1	1	-1	-1	1	-1	1	2.348	2.231	2.29	0.0
4	-1	1	1	-1	-1	1	-1	2.533	2.762	2.64	0.1
5	1	-1	-1	-1	-1	1	1	0.616	0.666	0.20	0.0
6	1	-1	1	-1	1	-1	-1	0.664	0.549	0.25	0.0
7	1	1	-1	1	-1	-1	-1	0.528	0.140	0.12	0.2
8	1	1	1	1	1	1	1	0.389	0.468	0.40	0.0
∑ (-)	11.22	6.74	5.76	5.40	6.12	5.81	6.17				
∑ (+)	0.99	5.47	6.45	6.81	6.09	6.40	6.04				
Effect	-5.11	-0.63	0.34	0.71	-0.02	0.29	-0.06				
Coefficient	-2.56	-0.32	0.17	0.35	-0.01	0.15	-0.03				
										Average:	1.53	0.1

Table 2 also shows the effects of main factors and interaction factors including the standard deviation. In general, the relation between response and all factors is given below:

$$Y = \beta_o + \beta_1 \cdot X_1 + \beta_2 \cdot X_2 + \beta_3 \cdot X_3 + \beta_{12} \cdot X_1 \cdot X_2 + \beta_{13} \cdot X_1 \cdot X_3 + \beta_{23} \cdot X_2 \cdot X_3 + \beta_{123} \cdot X_1 \cdot X_2 \cdot X_3 \quad (1)$$

where Y is response, X_1 is bleaching earth-to-oil ratio (%BE), X_2 is temperature (T), and X_3 is time (t). Considering the effects shown in Table 2, the relation between color, bleaching earth-to-oil ratio, temperature and time can be expressed as follows:

$$Y = 1.54 - 2.56 \cdot \%BE - 0.32 \cdot T + 0.17 \cdot t + 0.35 \cdot \%BE \cdot T - 0.01 \cdot \%BE \cdot t + 0.15 \cdot T \cdot t + 0.03\% \cdot BE \cdot T \cdot t \quad (2)$$

The confidence interval for the coefficients in the above equation can be expressed by the following equation:

$$CI\ (\beta_i) = \beta_i \pm t_{\alpha,n-1} \cdot s/\sqrt{(n)} \quad (3)$$

where β_i is the nominal value of i^{th} coefficient, $t_{\alpha,n-1}$ is t value from the student's t distribution at significance level of α and degree of freedom n-1, n is number of data, and s is standard deviation. If the limits of confidence interval of a coefficient have different signs, the effect of corresponding factor is not significant. The standard deviation found in this study was 0.11. At the confidence level of 95% and number of data of 8, the student's t value was found to be 2.84. The confidence intervals of the coefficients can be expressed as:

$$CI\ (\beta i) = \beta i \pm 0{,}11 \quad (4)$$

Considering the confidence interval of each coefficient, it can be convinced that the two interaction factors between bleaching earth-to-oil ratio and time, between temperature and time, and the three interaction factors have no significant effects on the response. In contrast, all main factors and the interaction factor between bleaching earth-to-oil ratio and temperature have significant effect. The

relation between color, bleaching earth-to-oil ratio, temperature and time, therefore, can be simplified as follows:

$$Y = 1.53 - 2.36 \cdot \%BE - 0.32 \cdot T + 0.17 \cdot t + 0.35 \cdot \%BE \cdot T \quad (5)$$

3.4 Comparison to commercial edible oil

Fig. 2 also compares the spectra of rice bran oil bleached in this study and that of commercial edible oils. Two commercial oils were included, one is a local bulk refined palm oil and one is an imported refined rice bran oil. Commercial oils are lighter than the bleached oils of this study. Even the best bleached oil is still darker than both commercial oils. Visual observation also showed that both commercial oils are lighter than the bleached oils of this study. The optimum grade of the bleaching earth used could not bleach as light as the commercial oils.

4. Conclusions

The effects of bleaching earth-to-oil ratio, bleaching temperature and bleaching time in bleaching of rice bran oil extracted from extrusion cooked rice bran have been studied using a full 2^k factorial design in which bleaching earth-to-oil ratio, bleaching temperature and bleaching time were selected as factors. It was found that all main factors have significant effects on the color of bleached oils. Among two and three interaction factors, however, only the interaction factor between bleaching earth-to-oil ratio and temperature has significant effect. The best bleached oil was obtained at bleaching earth-to-oil ratio of 10%, bleaching temperature of 110 ^oC and bleaching time 30 minutes. However, the bleached oil was not as light as the commercial edible oils. It was also found that rice bran oil pretreated by solvent extraction was more difficult to bleach than that pretreated by neutralization

References

1. Luh, B. S., Rice: production and utilization. AVI Publishing Co., Westport, Connecticut (1980).
2. Salunke, D. K., Chavan, J. K., et al. World oil seeds: chemistry, technology, and utilization. Van Nostrand Reinhold, New York (1992).
3. Sugano, M., Tsuji, E., Rice Bran Oil and Cholesterol Metabolism. Journal of Nutrition; 127: 521-523 (1997).
4. Loeb, J. R., Morris, N. J., et al. Rice Bran Oil: Storage of Bran as It Affects Hydrolysis of the Oil. Journal of American Oil Chemists Society; 26: 738-743 (1949).
5. O'Brien, R. D., Walter E. Farr, et al. Introduction to Fats and Oils Technology. 2nd ed. USA: AOCS Press (2000).
6. Kim, S. K., Kim, C. J., et al. Effect of Caustic Refining, Solvent Refining and Steam Refining on the Deacidification and Color of Rice Bran Oil. Journal of American Oil Chemists Society; 62: 1492-1495 (1985).
7. Krishna, A. G. G., A Method for Bleaching Rice Bran Oil with Silica Gel. Journal of American Oil Chemists Society; 69: 1257-1259 (1992).
8. Sayre, R. N., Nayyar, D. K., et al. Extraction and Refining of Edible Oil from Extrusion-Stabilized Rice Bran. Journal of American Oil Chemists Society; 62: 1040-1043 (1985).
9. Strieder, M. M., Pinheiro, C. P., et al. Bleaching optimization and winterization step evaluation in the refinement of rice bran oil. Separation and Purification Technology; 175: 72-78 (2017).
10. Kim, S. K., Byun, S. M., Cheigh, H. S., Yoon, S. H., Optimization of Extrusion Rice Bran Stabilization Process. Journal of Food Science; 52: 1355-1357, 1366 (1987).
11. Busro, R. and Hariman, BS Thesis, Stabilization of Rice Bran by Extrusion Cooking. Chemical Engineering ITB (2006).

12. Rodrigues, C. E. C., Gonçalves, C. B., et al. Deacidification of Rice Bran Oil by Liquid-liquid Extraction using a Renewable Solvent. Separation and Purification Technology; 132: 84-92 (2014).
13. Gonçalves, C. B., Rodrigues, C. E. C., et al. Deacidification of Palm Oil by Solvent Extraction. Separation and Purification Technology; 160: 106-111 (2016).

Utilization of Rice Husk as Bioanoda in Microbial Desalination Cell System using Leachate as Substrate

Pratiwi Rostiningtyas Lusiono[1], Tania Surya Utami[1]*, Rita Arbianti[1]

Chemical Engineering Departement, Faculty of Engineering, Universitas Indonesia, Depok 16424, Indonesia

** Corresponding Author's E-mail: nana@che.ui.ac.id*

Abstract
Microbial Desalination Cell (MDC) is a bioelectrochemical development system of Microbial Fuel Cell (MFC), which has the ability to desalinate water while producing electricity using ecoelectrogenic bacteria. The price of materials used as an electrode at MDC is quite expensive so it will be a hindrance to large-scale applications. The use of charcoal as an MDC electrode is very potential to reduce the cost of assembling MDC and charcoal is also more environmentally friendly because it is not toxic and can be disposed of without special treatment. The rice husk has a considerable carbon source and can be developed as an electrode material. In addition to electrodes, the pH imbalance between chamber has always been an obstacle to the MDC system and some approaches have an impact on increasing the cost of capital and operating costs. To answer the problem, in this study leachate and sodium percarbonate(SP) used as natural buffered electrolyte because both have bicarbonate buffer system. This study result four variants concentration of sodium percarbonate were tested and the best desalination performance with catholyte Sodium Perkarbonate was obtained at a concentration of 0.1 M (% Salt Removal = 14.36%). Performance of sodium percarbonate as catholyte was also compared with commercial catholyte buffer phosphate. MDC with concentration of sodium percarbonate as catholyte gave the best desalination performance (% Salt Removal = 14,36%)

1. Introduction

MDC (Microbial Desalination Cell), is a bioelectrochemical development system of Microbial Fuel Cell (MFC), which has the ability to desalinate water while producing electricity using ecoelectrogenic bacteria that produce electrical energy[1], thus requiring no energy.

Desalination can occur because the salt ions in the desalination chamber move to the anode chamber and the cathode chamber through Ion Exchange Membranes (IEM) to balance the charge due to proton accumulation on the anode chamber and proton consumption on the cathode chamber [10].

The anode used is the biological charcoal from the rice husk. Rice husk is the rest of the rice mill, which is currently not optimally utilized. The use of rice husk is currently limited to fuel for the manufacture of bricks and crackers. Rice husk consists of organic elements such as cellulose 33.71%, hemicellulose 17.71%, and lignin 35.53%[11]. Rice husk also contains inorganic elements, in the form of ash with the main content is silica 94-96%. In addition, there are also other components such as Potassium, Calcium, Iron, Phosphate, and Magnesium[3].

Charcoal will be coated on a stainless steel mesh that acts as an electron collector[15]. The use of charcoal electrodes in addition to the cheap price, also because it can support the formation

of a biofilm faster on the surface of the electrode in the anode chamber. The biofilm formed may act as an anode catalyst and assist in increasing the resulting current.

The anolyte used is leachate water, which is garbage recharge water, coming from inlet of Waste Water Treatment Plant (IPAS) III at BantarGebang. The reason for using leachate water is the greater the quantity and pollution caused.

Potential testing of leachate and rice husk rice in the MDC process is done by identifying the concentration of salt in desalination water.

2. Methodology

2.1 MDC Configuration

MDC reactor consist of three chambers : the anode chamber, desalination chamber, and cathode chamber. The anode chamber and desalination chamber was separated by Anion Exchange Membrane (AEM, AMI-7001, Membrane International, Inc), while the desalination chamber and cathode chamber was separated by Cation Exchange Membrane (CEM, CMI-7000, Membrane International, Inc).

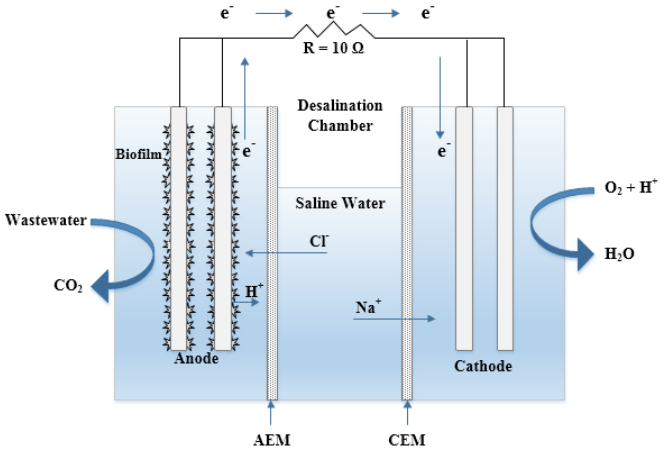

Fig 10. MDC Scheme

The ratio of the anode chamber : desalination chamber : and cathode chamber was 4 : 1: 2,[14] with the actual volume of 400 ml : 100 ml : 200 ml.Two rice husk charcoal electrode were used as the anode. Rice husk charcoal will be coated on stainless steel mesh that serves as gatherer of electrons[15]. The cathode used was two fiber bundles of carbon fiber cloth. The anode and cathode were connected by copper wire with external resistance of 10 Ω.

2.2 Rice Husk Electrode Preparation

Stainless steel 20 mesh is used to facilitate the coating and as a collector of electricity. Rice husk charcoal mixed polivynyl alcohol (PVA) solution with comparison charcoal : PVA (4:1(b/b)), to form a paste of charcoal. Stainless steel mesh coated with charcoal paste horizontally[12], then dried at room temperature for ±24 h. To remove metal contaminants and inorganic compounds, bioelectrode were immersed in 0.1 HCl solution for one day, then were rinsed with distilled water, followed by immersion in 0.1 M NaOH solution for one day then rinsed again with distilled water and remain stored in distilled water until use.

2.3 Data Analysis

NaCl conductivity was measured using conductometer (LUTRON CD-4301) and the data was processed into salt concentration value (g/L). The electrolyte pH was measured at the beginning and the end of the experiment using pH meter (EUTECH Instrument Model EcoTestr pH 2). Desalination performance was known by salinity reduction (g/L) and the percentage of salt removal was calculated using equation:

$$SR = \frac{c_o - c_i}{c_o} \times 100\% \quad (1)$$

Where Co and Ci is the initial and final concentration of saline solution (g/L) respectively.[4] Morphology of coconut shell charcoal bioelectrode observed with Scanning Electron Microscopy (SEM) Carl Zeiss EVO MA10. SEM test to observe the surface morphology specifically on coconut shell charcoal bioelectrode with 1000 times magnification.

3. Result and Disscusion

3.1 Effect of Rice Husk Charcoal and Sodium Percarbonate Concentration on Desalination Performance

MDC using the rice husk charcoal biolectrode with sodium percarbonate catholyte, produced the highest salt removal percentage by SP 0.1 M with percentage of salt removal 14,36% and salinity reduction from 31.55 g/L up to 27.02 g/L (Figure 2).

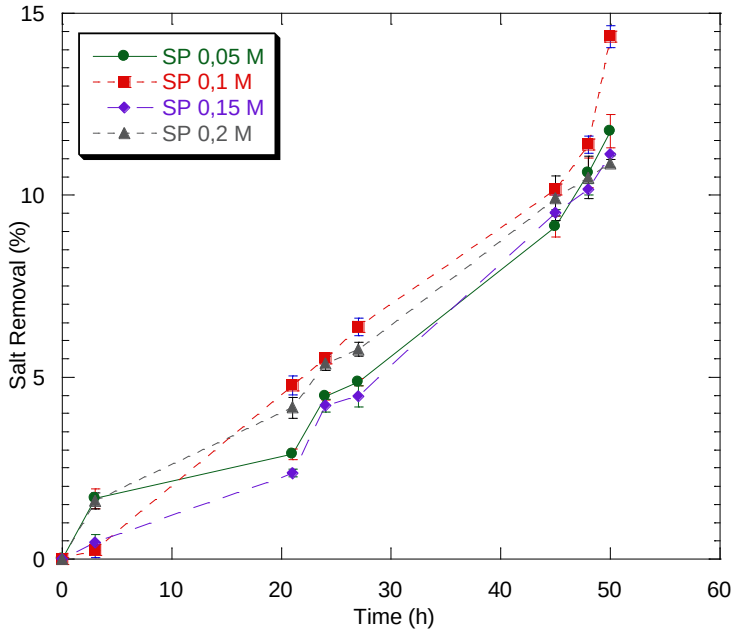

Fig 11.Salt Removal Percentage of MDC at Different Concentration Sodium Percarbonate (SP)

The high ability of desalination on MDC SP 0.1 M due to the high concentration of microbes. High density of leachate, indicates a high concentration of cells in the substrate. Thus, the more concentrated leachate, the more electrons are generated. This resulted in a large flow of electrons through the circuit and will have an impact on the magnitude of the rate of migration of ions Na^+ and Cl^- to cross the membrane, cations and anions of the chamber desalination. MDC with 0.1 M Sodium Percarbonate is having the highest rate of

osmosis due to a large concentration gradient with salt concentration indicated by a high desalination range[7].

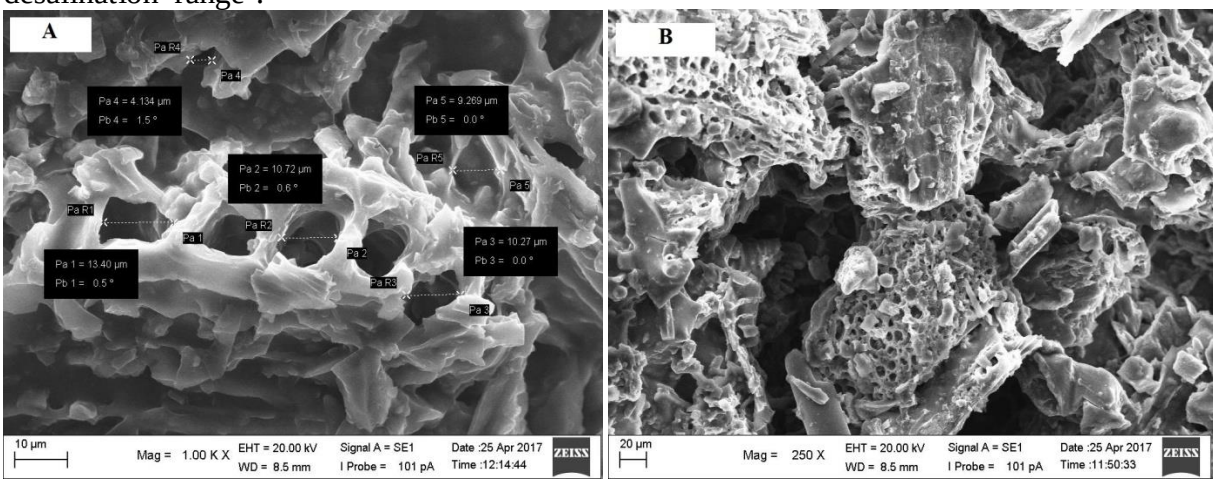

Fig 12.SEM of Rice Husk Charcoal Bioelectrode Structure [A] Before Experiment and [B] After Experiment

Figure 3 (a) shows a 1000x magnification of the rice husk charcoal surface before being used as an anode on the MDC system. The surface of this charcoal shows a considerable pore. When compared to Figure 3 (b) there is a collection of microorganisms that cover the pores of the charcoal surface so that the pores appear smaller. The structure of the pores which owned charcoal increases the surface area that can enhance the electrochemical activity on microrganism. Characteristics of biomass has a surface area of and a high adsorption capacity[2]. Some of the larger pores can be accessible for microbial adhesion, and smaller pores may contribute to the increased conductivity due to increases specific surface area for electron transfer[2]. One of the factors that affect the performance of MDC, the activity of biocatalyst[13], where the bacteria oxidize organic material and release the protons and electrons. Bacteria will form an aggregate of cells known as biofilm and will stick to the surface of the anode[9]. The establishment of biofilms as a major role in the electrochemical process and affect the production of electricity. The surface of the carbon in the rice husk charcoal can support the establishment of microbial communities and increasethe transfer of electrons on the anode space through the formation of biofilms.

3.2 Comparison of Catholyte Performance between Sodium Percarbonate and Phosphate Buffer

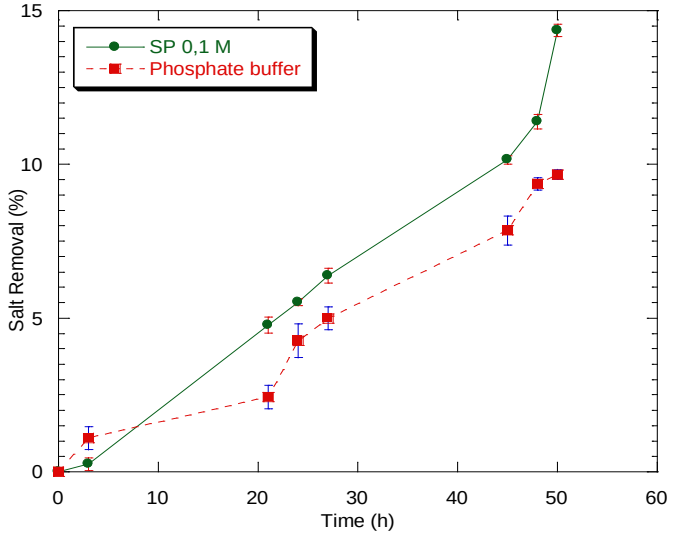

Fig 13. Comparison of MDC desalination performance experiments comparison of catholyte performance between sodium percarbonate and phosphate buffer

From the graph of salinity decrease in Figure 4 shows the MDC system with catholyte Sodium Percarbonat is superior with the increase of salt removal percentage of 14.36%. The product of the decomposition of sodium carbonate in water one of which is a carbonate species which can then react back and forth into bicarbonate (HCO_3^-) with water aid based on bicarbonate reaction ($CO_3^{2-} + H_2O \rightleftharpoons HCO_3^- + OH^-$). The carbonate ⇌ bicarbonate reaction has a pKa value of 10.3[8] so it can be said that sodium percarbonate is a strong base and contains many OH-ions. The number of carbonate specimens in an electrolyte solution can increase the transfer of hydroxide (OH^-) ions from the cathode so that the MDC system with its sodium catholyte (its use still with buffer addition) has a high enough power density when aligned with MDCs that use other commercial catholytes.

3.3 MDC Experiment on Optimum Conditions

Experiment on optimum condition of MDC done using optimum variable, i.e. sodium percarbonate catholyte with concentration of 0.1 M. The decrease in salinity produced at 456 h was 32.23 g/L up to 15.28 g/L with salt removal percentage of 52.60%. experiment on the optimum conditions in this MDC, the driving factor that influence the occurence of desalination is osmosis water from the cathode chamber to the desalination chamber.[4, 5] This can be seen by the existence of a decrease in the volume of catholyte in the cathode chamber. The measurement of the final catholyte volume in this experiment was 125 ml.

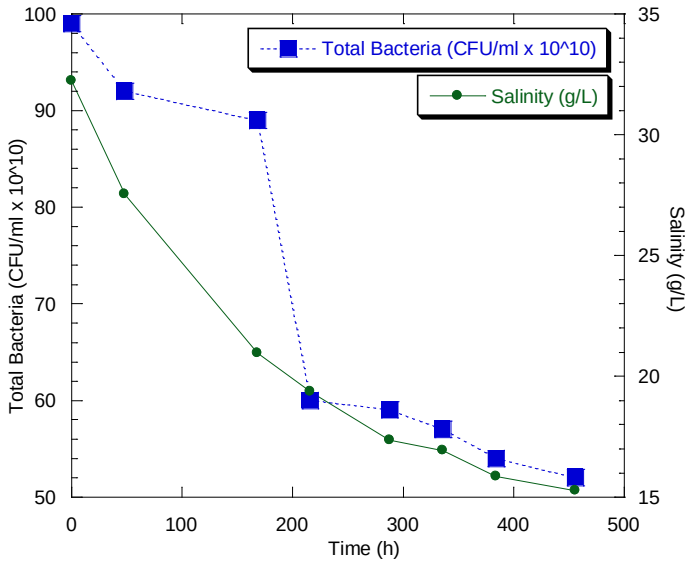

Figure 14. The Growth Curve of Bacteria and Salinity Reduction

During experiment on optimum condition of MDC underway, seen also the growth of bacteria by using the method of Total Plate Count (TPC). In Figure 5 show relevant result among the bacterial growth with salinity reduction during experiment on optimum condition of MDC. In the range of 0 to 168 hour happening decrease salinity significantly, this result indicate that metabolic activity of bacteria is still quite high. In the range of 288 to 456 hour decrease salinity has already approached the constant, similarly with the result of bacterial growth began to wane, because the smaller transfer of electrons from bacteria to the anode, the electrons produced may not be transferred to the anode, but transferred to the cells of the other consortium which could be used for benefit of the electron recipient cell metabolism[6].

3.4 pH Changes

Table 8. pH Changes in Anode and Cathode Chamber

Experiment MDC	Anode Chamber			Cathoda Chamber		
	Initial pH	Final pH	Δ pH	Initial pH	Final pH	Δ pH
AL-SP 0.05 M	8.5	8.6	+0.1	11.8	11.7	-0.1
AL-SP 0.1 M	8.5	8.8	+0.3	11.7	11.6	-0.1
AL-SP 0.15 M	8.5	8.6	+0.1	11.9	12.1	+0.2
AL-SP 0.2 M	8.7	8.8	+0.1	12.1	11.9	-0.2
AL-SP	8.5	8.8	+0.3	11.7	11.6	-0.1
AL-BF	8.7	8.9	+0.2	7	7	0
Optimum Conditions	8.5	8.75	+0.25	11.6	11.2	-0.4

Table 1 shows the range of pH differences in anode chamber ranging from 0.1 to 0.3. The increase pH also occurs in leachate anolyte with a range from 0.1-0.3, caused by the reduction of protons (H^+ ions) in leachate water consumed by bicarbonate ions for the formation of methane

$$H^+ + HCO_3^- \rightarrow CO_2 + H_2O \quad (2)$$

$$4H_2 + CO_2 \rightarrow CH_4 + 2H_2O \quad (3)$$

In the cathode chamber occurs rise in pH of 0.2. Sodium percarbonate ($2Na_2CO_3.3H_2O_2$) will release the hydrogen peroxide (H_2O_2) as electron acceptors.The OH^- ions formed from the results of the reduction of hydrogen peroxide (H_2O_2) will bind with Na^+ that comes from the decomposition of sodium carbonate (Na_2CO_3) and also from the desalination chamber migration result, thus forming NaOH in the cathode chamber. The formation of NaOH cause increased pH in the cathode chamber.

However, sodium percarbonate has the ability as a natural buffer that comes from bicarbonate ions (HCO_3^-) so as to maintain the pH value. A decrease in pH of sodium percarbonate catholyte occurs due to the events of osmosis water which causes a decreased concentration of sodium percarbonate in the cathode chamber. this make the reduced OH^- which can be consumed to CO_3^{2-} by HCO_3^-.

4. Conclusion

This research proves that rice husk charcoal can be used as bioanode in MDC system. Sodium percarbonate with a concentration of 0.1 M has the highest desalination performance seen from the salt removal percentage of 14.36%. Sodium percarbonate as catholyte in MDC system of this experimental pest has better desalination performance (SR = 14,36%) compared with phosphate buffer (SR = 9,67%) at same concentration that is 0,1 M.

5 Acknowledgements

This research was supported by Laboratory of Bioprocess Engineering, Department of Chemical Engineering, Faculty of Engineering, Universitas Indonesia.

References

1. Chen, X., Xia, X., Liang,P., Cao, X. Sun, H.T., & Huang, X. (2011) Stacked microbial desalination cells to enhance water desalination efficiency.*Environ. Sci. Technol*., 45, 2465–2470.

2. Huggins, T., Wang, H., Kearns, J., Jenkins, P., & Ren, Z. J. 2014. Biochar as a Sustainable Electrode Material for Electricity Production in Microbial Fuel Cells. *Bioresource Technology,* **157**, 114–119.
3. Hsu, W. H., and Luh, B.s. 1980. Rice hulls. In *Rice: Production and Utilization,* edited by B. S. Luh. Westport, CT: AVI, pp. 736-63
4. Jacobson, K. S., Drew, D. M., & He, Z. 2011. Use of a Liter-Scale Microbial Desalination Cell As a Platform to Study Bioelectrochemical Desalination with Salt Solution or Artificial Seawater. *Environmental Science & Technology,* **45**, 4652-4657.
5. Kamila, E. D., Utami, T. S., & Arbianti, R. 2016. Natrium Perkarbonat sebagai Katolit Berpenyangga Alami dalam Sistem Microbial Desalination Cell.*Journal UI Proceeding on Science and Technology,* **1**.
6. Logan, B. E., & Regan, J. M. 2006. Electricity-Producing Bacterial Communities in Microbial Fuel Cells. *Trends in Microbiology,* **14,** 512-518.
7. Mehanna, M., Saito, T., Yan, J., Hickner, M., Cao, X., Huang, X., & Logan, B. E. 2010. Using Microbial Desalination Cells to Reduce Water Salinity Prior to Reverse Osmosis. *Energy & Environmental Science,* **3**, 1114–1120.
8. MP Biomedicals, Sodium Bicarbonate, http://www.mpbio.com/product.php?pid= 02194553, 2016.
9. Saeed, H. M., Husseini, G. A., Yousef, S., Saif, J., Al-Asheh, S., Fara, A. A., Azzam, S., Khawaga, R., Aidan, A. 2014. Microbial desalination cell technology: A review and a case study. *Desalination,* **359**, 1-13.
10. Shehab, N.A., G.L. Amy, B.E. Logan, P.E. Saikaly. 2014. Enhanced water desalination efficiency in an air-cathode stacked microbial electrodeionization cell (SMEDIC). *Journal of Membrane Science* 469(2014): 364 - 370.
11. Suharno, (1979), Komposisi Kimia Sekam Padi, di dalam: Sigit Nugraha dan JettySetiawati, 2001, Peluang Agribisnis Arang Sekam, Badan Penelitian Pascapanen Pertanian, Jakarta
12. Tumimomor, F. R. 2014. *Pemanfaatan Karbon Aktif Berbasis Sabut Kelapa dan Bambu sebagai Elektroda Superkapasitor*. Tesis, Program Studi Biofisika, Institut Pertanian Bogor, Bogor, Indonesia.
13. Yang, S., Du, F., & Liu, H. 2012. Characterization of Mixed-Culture Biofilms Established in Characterization of Microbial Fuel Cells. *Biomass and Bioenergy,* **46**, 531-537.
14. Zhang, F., & He, Z. 2015. Scaling Up Microbial Desalination Cell System with a Post-Aerobic Process for Simultaneous Wastewater Treatment and Seawater Desalination. *Desalination,* **360**, 28-34.
15. Zhang, F., Saito, T., Cheng, S., Hickner, M. A., & Logan, B. E. 2010. Microbial Fuel Cell Cathodes With Poly(dimethylsiloxane) Diffusion Layers Constructed around Stainless Steel Mesh Current Collectors. *Journal of Environmental Science & Technology,* **44**, 1490-1495.

Utilization of Biocharcoal as Bioelectrode in Microbial Desalination Cell for Leachate Treatment

Syafira Andyah Putri[1], Rita Arbianti[1], Tania Surya Utami[1*]

[1]*Bioprocess Engineering Laboratory, Department of Chemical Engineering, Universitas Indonesia, Depok 16424, Indonesia*

** Corresponding Author's E-mail nana@che.ui.id*

Abstract
Microbial Desalination Cell (MDC) is a bioelectrochemical device that uses microorganisms to produce electricity from the metabolism in the breakdown of organic compounds. The electrode material in the bioelectrochemical system can contribute up to 20-50% of the total construction. Therefore, this study will examine the ability of biocharcoal as a bioelectrode in MDC. There are two type of bioelecrode that will be used as anode, biocharcoal from coconut shell and biocharcoal from rice husk. Use of sodium percarbonate without electrolyte solution in the cathode chamber was also carried out with variations in concentrations of 0.05 M, 0.10 M, 0.15 M and 0.20 M. This study used leachate from TPST Bantargebang as anolyte and focused on wastewater treatment aspect determined by reduction of COD and BOD5 levels. The research shows that MDC using rice husks biocharcoal as anode with a concentration of 0.05 M sodium percarbonate give the best performance by COD removal 57,21%, BOD5 removal 86,14%, and salt removal 41,15%.

1. Introduction

Microbial Desalination Cell (MDC) is a bioelectrochemical device intergration of Microbial Fuel Cell (MFC) that has the ability to desalinate seawater as well as produce electricity from the metabolism in the breakdown of organic compounds. The electrode material in the bioelectrochemical system can contribute up to 20-50% of the total construction. Most of the electrode materials in MDC systems use expensive carbon materials and will be a hindrance to large-scale applications. Therefore, the present study examines the ability of biocharcoal as a bioelectrode in the MDC. Coconut shell charcoal and rice husk charcoal are selected because aside from its cheap price, charcoal has a porous structure that allows gas transportation, water flow, and conductive[1].

This study is expected to improve seawater desalination performance and able to reduce the COD and BOD_5 level of leachate on a large scale and can be used as an alternative of leachate treatment in Indonesia.

2. Materials and Method

2.1 Reactor Configuration

Cube-shaped three chamber MDC reactor which made of acrylic was used in this experiment. The volume of each chamber is 480 mL of the anode chamber, 120 mL of saline chamber, and 240 mL of cathode with a ratio of 4: 1: 2^2. AEM membrane inserted between the anode and saline chambers, whereas the CEM membrane inserted between the saline and cathode chamber. Each membrane has length and width of 7 x 7 cm was prepared by immersing it in 5% NaCl solution at 40°C for 24 hours. There are two type of anode that will be used, charcoal from coconut shell and charcoal from rice husk. The cathode used is CFC.

In the reactor circuit, the anode and cathode electrodes are connected to a 10-ohm resistor using a copper wire.

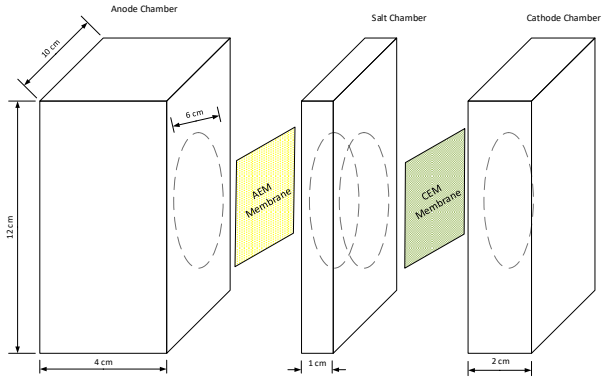

Fig. 1. MDC Reactor Scheme

Leachate from TPST Bantargebang was used as anolyte and taken periodically when new experiments are performed. At the beginning of the experiment, the type of leachate should be determined to ensure that the leachate type of all variations in this study is uniform.

2.2 Biocharcoal as an Electrode

Powdered charcoal will be coated on stainless steel. The type of stainless steel used is SS 304 mesh shape with size 12.5 cm x 9.5 cm and the size of coating charcoal is 10 cm x 9.5 cm. Before the coating process, stainless steel soaked at room temperature in H_2SO_4 for 24 hours. After that, PVA solution made with composition of 3 g of PVA, 30 mL of water and 24 mL of ethanol heated at 120°C and continuously stirred until all of the composition mixed. PVA solution then mixed with 12 g of charcoal. Stainless steel mesh then coated with charcoal paste horizontally.

2.3 Electrode Preparation

Before used, the electrode was prepared. CFC and Bioelectrode immersed in a 0.1 M HCl solution for 1 day and then rinsed with distilled water. It was soaked again into a 0.1 M NaOH solution for 1 day and then rinsed again using distilled water.

2.4 MDC Experiment

MDC was operated in a batch system at room temperature, where the electrolyte was only added to the system at the beginning of the cycle. First experiment was anode variation in which anode from coconut shell charcoal and anode from rice husks charcoal would be compared its performance as anode in MDC. The anode with best performance at reducing COD and BOD_5 would be selected to be used as anode in the next experiment which is concentration of sodium percarbonate variations. The concentration variations used were 0.05 M, 0.1 M, 0.15 M, and 0.20 M to be put into cathode chamber and compared. After that, sodium percarbonate will be compared with phosphate buffer solution 0.05 M. Operation time for anode variation, variation of sodium percarbonate concentration, and catholyte performance ratio was 50 hours. Furthermore, experiment of optimum time conditions was conducted. MDC will continue until COD values are reduce to zero or stagnant.

2.5 Data Analysis

The pH, COD, and BOD_5 values are measured before and after the experiment for all variations. COD was measured using BELL UV-M90 Spectrophotometer. Reagents used are HACH COD Cat reagents. 2125925 20-1500 mg/L. Before COD is measured, a calibration

curve was created to determine the COD value in leachate. Measurement of BOD_5 is done by winkler method using DO meter. pH meter was measured using a pH meter EUTECH Instrument Model EcoTestr pH 2.

3. Results and Discussion

3.1 Leachate Type

Leachate was taken at every experiment and to know which type of leachate used in experiment, pH and COD value would be measured. Table. 1. shows pH and COD value of leachate that was taken during experiment.

Table. 4. pH and COD value during experiment

No	Date	COD (mg/L)	pH
1	5 March 2017	5.123,07	8,7
2	14 March 2017	5.094,63	8,5
3	29 March 2017	2.373,01	8,4
4	5 April 2017	2.266,61	8,5
5	12 April 2017	2.342,97	8,5
6	26 April 2017	4.227,44	8,5

3.2 Anode Variation

Fig. 2. shows COD value in leachate as an anolyte in the anode chamber for 50 hours of MDC operation using both different anode types decreased.

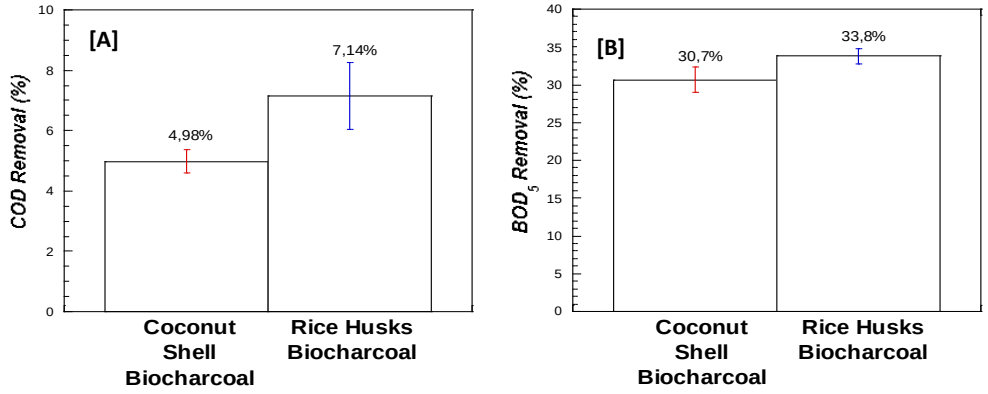

Fig. 2. COD Removal[A] and BOD Removal[B] by using two kinds of anode

The reduced of COD value by using rice husk biocharcoal is higher than using coconut shell biocharcoal. It is found that adsorption, both chemically and physically, plays an important role in wastewater treatment in MFC systems[3]. High adsorption capacity also plays an important role in bacterial colonization and biofilm formation in carbon. Factors that cause high adsorption capacity are surface area, microporosity, coarse surface, and mineral composition in the material[3].

The thing that distinguishes coconut shell biocharcoal with rice husk biocharcoal is its mineral composition. Rice husk ash contains silica (SiO_2) with a range of 93.4408%[4]. While the coconuts shell biocharcoal contains 37.97% silica in the ashes[5]. In addition to the adsorption capacity of the carbon material used as an electrode, another factor that causes reduction in the value of COD and BOD_5 is the formation of biofilms in the electrode. Biofilms grow on the anode and act as anodic catalysts and help accelerate respiration from

bacteria and produce protons and electrons. The larger the surface area of an electrode, the easier the biofilm to form.With biofilm formation, bioelectrochemical systems will occur and will degrade COD in leachate[6].

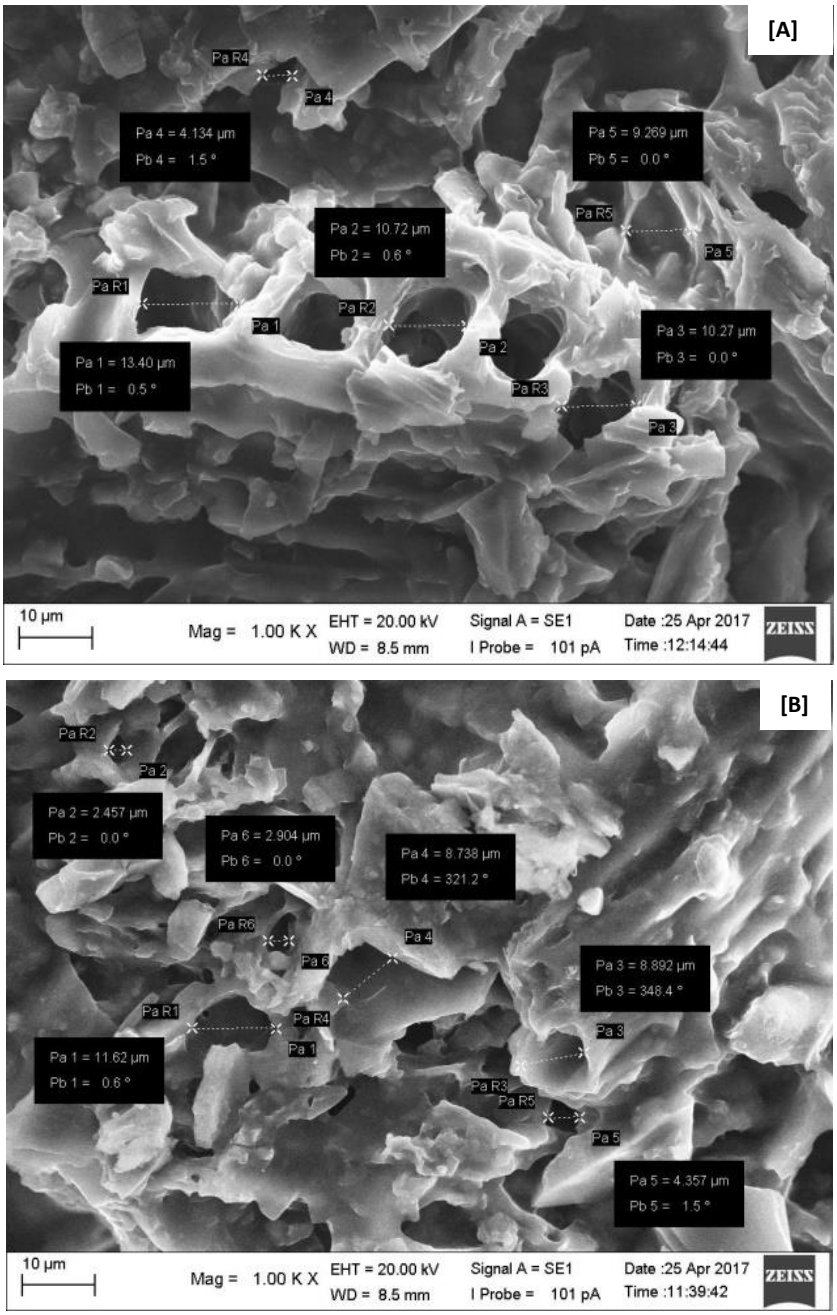

Fig. 3. Surface profile of rice husks biocharcoal with 1000x magnification: [A] Before dan [B] After

In Fig. 3. [A] it is seen that the surface of the biocharcoal contains many loopholes that could become a new spot for microbial growth. After the MDC experiment was done (Fig. 3. [B]) the size of the pores smaller. The decrease in BOD_5 content of rice husk rice is higher than that of coconut shell charcoal.

Electrode materials for bioelectrochemical systems contribute 20-50% of total cost[3]. The calculation of the price is based on the total mass of raw materials used as anode. Table. 2. is the price comparison compared to the percentage reduction in COD.

Table. 2. Cost comparison between anode and its COD removal

Variable	Cost/COD Removal
Coconut Shell Biocharcoal	Rp. 2.895,17,-
Rice Husks Biocharcoal	Rp. 2.082,79,-
Carbon Brush[a]	Rp. 23.549,49,-

[a]7

Based on the table above can be seen that the cost of raw material rice husk biocharcoal is more economical compared to coconut shell biocharcoal.

3.3 Variation of sodium percarbonate concentration

Based on the previous experiment, rice husk biocharcoal is the best biocharcoal in the comparison of anode. This study aims to determine the relationship between sodium percarbonate concentration as catholyte to reduce in COD and BOD_5 levels in MDC system.

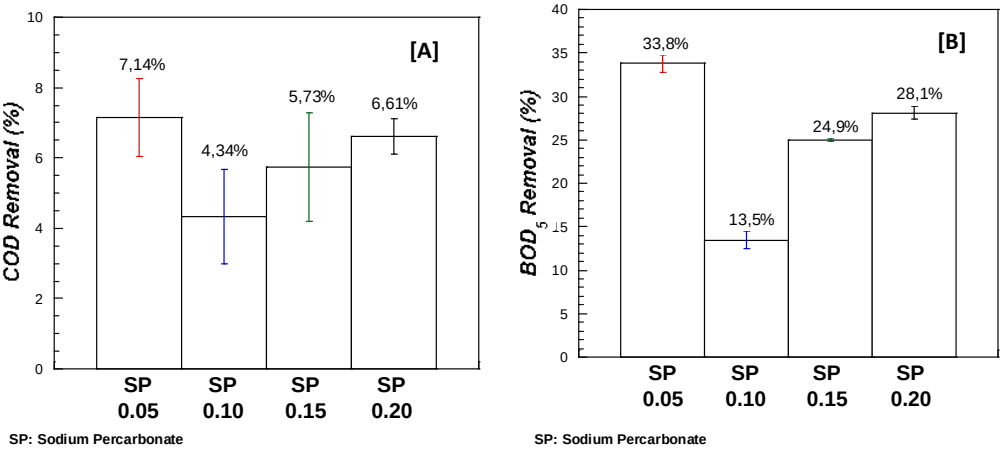

Fig. 4. Comparion of concentration variation of sodium percarbonate catholyte: [A] COD, [B] BOD_5

The highest COD removal was obtained by MDC NP 0.05 M, from 2,266.61 mg/L to 2,105.10 mg/L (COD Removal = 7.1%). The highest BOD_5 removal was also obtained by MDC NP 0.05 from 134.25 mg/L to 88.9 mg/L (BOD5 Removal = 33.78%). COD removal occurs not only because of the bioelectrochemical process in the MDC system alone, but also because of the adsorption capacity of the anodes used[3].

3.4 Comparison of catholyte performance

This experiment will see the effect of buffer-based catholyte on the decrease of COD and BOD_5 in MDC.

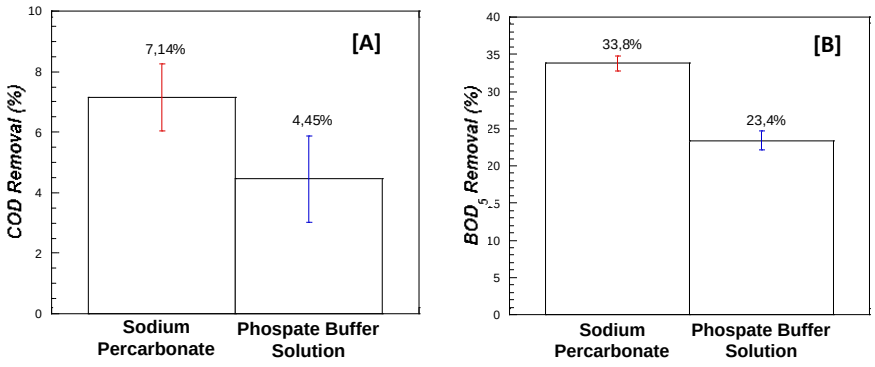

Fig. 5. Comparison using different catholyte: [A] COD removal and [B] BOD_5 removal

The use of a phosphate buffer solution has the potential to cause environmental problems by releasing phosphorus substances into water bodies as byproducts[8]. Sodium percarbonate has a rating of 2 health hazards and precautions should be taken, but the byproduct resulting from the reduction process is not environmentally harmful[9].

3.5 MDC Optimum Operation Time

MDC experiments on optimum conditions using the best variables of the previous variation. The anolyte used is leachate and the catholyte is sodium percarbonate 0.05 M. The MDC system operated until the COD and BOD_5 decrease reaches zero or is already close to stagnant.

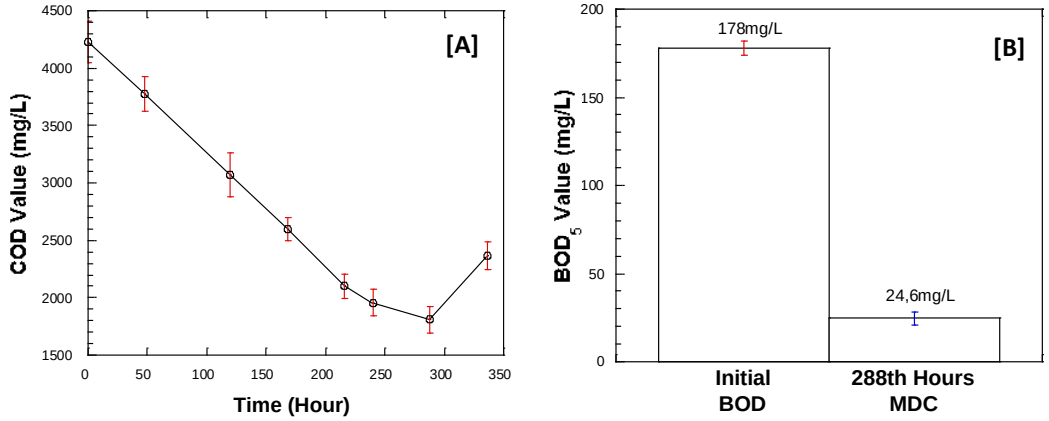

Fig. 6. MDC experiment at optimum conditon: [A] COD Removal dan [B] BOD_5 Removal

Although the experiment stopped at 336 hours, but the optimum time of MDC system in this experiment was at 288 hours (12 days). Termination at 336 hours is done because the COD value generated increased by 13.143% from the 288th hour. This is due to the increased concentration of salt in leachate due to the migration of Cl^- ions from the saline chamber. COD MDC has the potential to be an alternative process in wastewater treatment at TPA Bantargebang. High BOD_5 removal indicates MDC can replace treatment in facultative pond. Facultative ponds serve to decompose and reduce the organic content present in the waste. The use of facultative ponds can lower the BOD_5 value by 70-80% with a residence time of 5-30 days. Water-soluble sodium carbonate is safe when released to the environment[9].

3.6 Bacterial growth

Bacterial growth was observed when MDC operated at optimum condition with *Total Plate Count* (TPC) method. Data can be seen at Fig. 7.

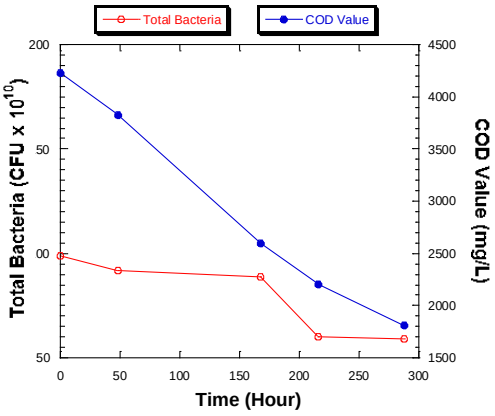

Fig. 7. Bacterial growth curve during optimum condition experiment

From Fig. 7, it can be said that COD removal is not so well suited to the bacterial growth. When bacterial growth decreases from 0 to 288 hours, the COD value in leachate decreases steadily or remains high.

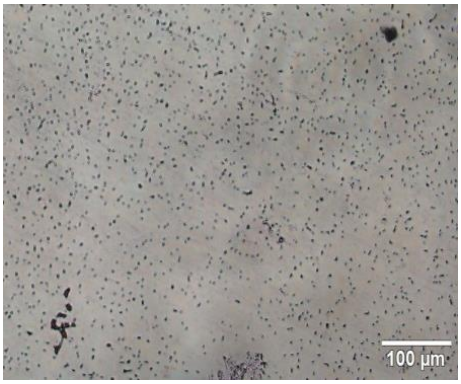

Fig. 8. Bacteria coloring test results

The 20x magnification results in Fig. 8 [A] and [B] show that blue colonies are quite dominant. The stable ability of the gram-positive bacteria that is the dominant bacteria in leachate strongly supports the MDC system as a leachate treatment. At the time of staining, gram-positive bacteria showed blue-violet color retention derived from complex crystal violet reactions with iodine in the cell membrane of the organism followed by washing with alcohol.[10]

3.6 Desalination performance

Aside from its ability degrade COD and BOD_5 in leachate, one of the main functions of MDC was reducing salinity in seawater. This study also looked at salt removal that can be done at optimum time MDC degrades COD and BOD_5. According to Figure 10, salt removal was 41.15% from the original 33.25 mg/L to 18.98 mg/L when the MDC trial was operated for 288 hours.

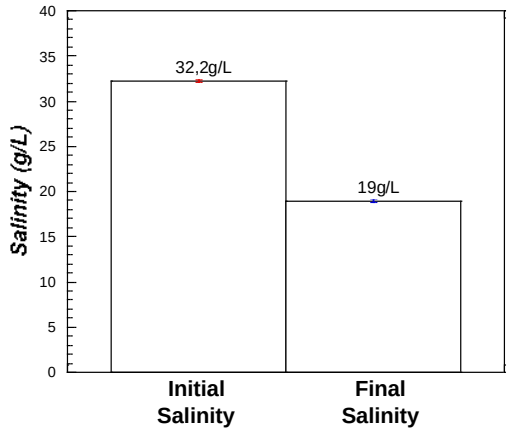

Fig. 9. Desalination performance of MDC with rice husks biocharcoal as anode at optimum condition

4. Conclusion

Biocharcoal with the best performance as anode in MDC is rice husk biocharcoal with optimum concentration of 0.05 M sodium percarbonate. COD and BOD5 removal is 7.1% and 33.78%. The best buffer-based catholyte is sodium percarbonate. The optimum time of MDC operation is 288 hours or 12 days. The percentage of COD and BOD5 removal is 57.21% and 86.14%. Salt Removal at optimum time at the MDC system for waste treatment is 41.15%

References

1. Rao, M. 2013. The Novel Implementation of Biochar Cathodes in Microbial Fuel Cell. Oregon: Jesuit High School Portland.
2. Zhang, F., & He, H. 2015. Scaling up microbial desalination cell system with a post-aerobic process for simultaneous wastewater treatment and seawater desalination. Bioresource Technology, 429 – 432.
3. Huggins, T. M., Latorre, A., Biffinger, J. C., and Ren, Z. J. 2016. Biochar Based Microbial Fuel Cell for Enhanced Wastewater Treatment and Nutrient Recovery. *Sustainability*, 1-10.
4. Abdian, R. M. and Herbudiman, B. 2010. Pengaruh Kehalusan dan Kadar Abu Sekam Padi Pada Kekuatan Beton Dengan Kuat Tekan 50 MPa. Konferensi Teknik Sipil 4 (KoNTeKS 4). Bali: Sanur
5. Utsev, J.T., Taku, J.K. 2012. Coconut Shell Ash As Partial Replacement of Ordinary Portland Cement In Concrete Production. International Journal of Scientific and Technology Research, Vol 1, Issue 8, 1-4.
6. Saeed, H. M., Husseini, G. A., Yousef, S., Saif, J., Al-Asheh, S., Fara, A. A., et al. 2015. Microbial desalination cell technology: A review and a case study. Desalination, 1-13.
7. Sevda, S., Abu-Reesh, I., Yuan, H., & He, Z. 2016. Bioelectricity generation from treatment of petroleum refinery wastewater with simultaneous seawater desalination in microbial desalination cells.
8. Yossan, S., Xiao, L., Prasertsan, P., & He, Z. 2013. Hydrogen production in microbial electrolysis cells:Choice of catholyte. International Journal of Hydrogen Energy, 9619-9624.
9. Forrestal, C., Huang, Z., & Ren, Z. J. 2013. Percarbonate as a naturally buffering catholyte for microbial fuel cells. Bioresource Technology, 429-432.
10. Yazdankhak, P, S., Sørum, H., Larsen, H. J., Gogstad, G., Yazdankhak, et al. 2001. Use of magnetic beads for Gram staining of bacteria n aqueous suspension. *Journal of Microbiological Methods*, 369-371.

POSTER PRESENTATION SESSION

Effect of Extraction Methods on Nyamplung (*Calophyllum inophyllum* L.) Seed Oil Quality

Danu Ariono [1,*], Ryan Adhimukti Prayitno [1]

[1]*Chemical Engineering, Institut Teknologi Bandung, Jalan Ganesha No. 10, Bandung 40132, Indonesia*

* *Corresponding Author's E-mail danu@che.itb.ac.id*

Abstract

The oil reserves in Indonesia are decreasing until now with increasing oil consumption. Biofuel is a fuel derived from renewable natural resources which can be processed into vegetable oil obtained from plants. Nyamplung oil that contain 40-73% on the kernel seeds as a source of biofuel. Nyamplung seed oil were obtained at 70-90°C preheating temperature for 10-30 minutes by mechanical press and extraction with n-hexane using Solvet at 20-40 mesh kernel sieving and temperature of 80°C for 6-8 hours. The characterization of the oil consisted of acid value, saponification value, iodine value, peroxide value, unsaponification matter content, and phosphorus content. The result showed that oil obtained from mechanical extraction are better than Solvet extraction. Mechanical press oil contained 21.97 mg KOH/g oil acid value, 178.63 mg KOH/g oil saponification value, 75.35 g I_2/100 g oil iodine value, 17.86 meq O_2/kg oil peroxide value, 0.19%-w/w unsaponification matter content, and 282.79 mg P/kg oil phosphorus content.

Keywords : Nyamplung, mechanical extraction, Solvet

1. Introduction

Oil consumption in Indonesia are increasing until now while oil reserves have declined. The fuel used to date is fossil fuel. Therefore, it is necessary to find alternative energy resources. One of the alternative energy resource is biofuels. Fuel comes from renewable natural resources. These natural resources can be processed into vegetable oils. The oil can be obtained from plants. This can be a solution to solve the problem about decreasing petroleum reserves. Several sources of vegetable fatty oil have been identified as potential sources of biofuels, one of them is Nyamplung (Calophyllum inophyllum L.). The diameter of the kernel seed is 1.5 cm, covered with soft and hard seed shells. In Indonesia, nyamplung is spreaded in Sumatra, Java, Kalimantan, Sulawesi, Maluku, East Nusa Tenggara, and Papua. Nyamplung contains 40-73% oil at kernel seed (Atabani et al., 2014). Nyamplung kernel seed oil contains fatty acid mostly 14.40% palmitic acid, 15.57% stearic acid, 34.41% oleic acid, and 28.34% linoleic acid Therefore, nyamplung needs to be developed more in order to become an alternative energy resource. Nyamplung seed oil can be obtained by a method called extraction. Nyamplung seed oil extraction can be conducted in two ways, mechanical extraction and Solvet extraction. Mechanical extraction is performed by crushing oil-containing materials and pressed using a hydraulic press while Solvet extraction by using n-hexane as a solvent in this study.

Nyamplung seed oil application as fuel can be used in the form of biodiesel. Most of the research on extraction leaded to the quantity of oil, so there is no information about the effect of extraction on the quality of nyamplung seed oil and need to be studied in this study. Therefore, the purpose of this study was to determine the effect of extraction on the quality of nyamplung seed oil to obtain quality nyamplung seed oil.

2. Materials and Methods

2.1 Sample and sample preparation

Nyamplung seeds were gathered from Carita Ministry of Environment and Forestry. The size of the seed is 2.5-5 cm, weight 0.5-2 grams, and dried under the sun for 7 days. 40 grams of kernel seeds were removed from the shell, then dried in an oven at 110^{o}C for 1 hour.

2.2 Mechanical extraction

Kernel seeds were heated at 70-90°C for 5 minutes. The kernels were inserted into hydraulic press. Extraction of nyamplung seed oil was performed for 10-30 minutes.

2.3 Solvet extraction

Kernel seeds were crushed until smooth. Flour were sieved with variation of size 20-40 mesh. Flour were put into the extraction tube and corked. The boiling stones are put into a round flask. The n-hexane solvent is poured from the condenser to the round flask until the extraction tube is half filled, then the round flask is placed on the water bath. Extraction of nyamplung seed oil was performed at 80^{o}C for 6-8 hours. The mixture of nyamplung oil and n-hexane is separated by distillation at 80°C.

2.4 Extraction yield

Determination of oil yield from each variation of extraction operation condition is obtained by dividing the mass of oil obtained by the mass of the extracted kernel seed.

2.5 Acid value determination

2 grams of oil were dissolved in 50 ml of 95% ethanol, then added 3 drops of phenolphthalein and titrated with 0.1 N KOH until pink and not disappeared for 15 seconds. This procedure is also conducted in the same way on the blank.

2.6 Saponification value determination

2 grams of oil were dissolved in 25 ml of KOH in 95% ethanol, then boiled for 1 hour. The solution was then cooled, then 0.5 ml of phenolphthalein was added and titrated with 0.5 N HCl until the pink color disappeared. This procedure is also conducted in the same way on the blank.

2.7 Iodine value determination

0.13 grams of oil were dissolved in 15 ml of chloroform, then added 25 ml of Wijs solution and stored in dark place for 30 minutes. Next, 20 ml of 10% KI and 150 ml of distilled water were added, then titrated with 0.1 N $Na_2S_2O_3$ until yellow. After that, 2 ml of the starch solution were added and the titration were continued until the blue color disappeared. This procedure is also conducted in the same way on the blank.

2.8 Peroxide value determination

1 gram of oil were dissolved in 30 ml of glacial acetic acid and chloroform mixture with a volume ratio of 3:2, then 0.5 ml of saturated KI were added and stirred for 2 min. Next, 30 ml of distilled water and 1 ml of starch solution were added and then titrated with 0.01 N $Na_2S_2O_3$ until the blue color disappeared. This procedure is also conducted in the same way on the blank.

2.9 Unsaponification matter content determination

5 grams of oil were dissolved in 30 ml of 95% ethanol and 5 ml of 50% KOH 50%, then boiled for 1 hour. Next, extracted with 25 ml of n-hexane 3 times. The n-hexane layer was

washed with 25 ml of 10% ethanol and the ethanol layer was removed. The n-hexane layer was evaporated at 80°C. After that, it was cooled in a desiccator and weighed. After weighing, the pulp was dissolved in 50 ml 95% ethanol which had been added with 3 drops of phenolphthalein at 50°C and titrated with KOH 0.02 N pink color appeared.

2.10 Phosphorus content determination

3 grams of oil and 0.5 g of ZnO is heated in a crucible by using an electric heater until thickened, then the temperature is raised slowly until ashes were formed at 540°C. After that, it is stored at room temperature. 5 ml of distilled water and 5 ml of 37% HCl were added to the ashes, then the crucible was covered with a watch glass and heated until boiled slowly for 5 minutes. Next, the solution is filtered to a 100 ml measuring flask. After that, the solution was cooled to room temperature and 50% KOH was added dropwise until neutral, then added dropwise 37% HCl until ZnO dissolved and added 2 drops of 37% HCl, the solution was diluted until the limit marker reached. 10 ml of solution was taken to 50 ml measuring flask, then added 38 ml of $N_2H_4SO_4$ and 2 ml Na_2MoO_4. The measuring flask is loosened and heated in a boiling water bath for 10 minutes, then cooled to 25°C and diluted with distilled water until the limit marker reached. Next, the absorbance of the solution was measured using a UV-Vis spectrophotometer at 650 nm of maximum wave length. This procedure is also conducted in the same way on the blank.

3. Results and Discussion

3.1 Mechanical extraction

The effect of preheating temperature on the quality and quantity of nyamplung seed oil is shown in Table 1 and Fig. 1. The higher the temperature, the higher the yield of oil. However, the increment in percent yields decreases in temperature from 80°C to 90°C. The increase in yield percent of oil is caused by damaged cell wall, while a decrease in the percent increase in oil yields is caused by faster water evaporation and faster dry oil (Tambunan et al., 2012). An increment in preheat temperature also caused acid value, saponification value, iodine value, and phosphorus content rise. The increment in these parameters was similar to the percent increment in oil yield. The increment in the initial temperature increased the oil hydrolysis rate, so it was predicted that there was still water content in the kernel seed and drying in the oven at 110^{o}C for 1 hour was not enough, so it needed to extend the drying time. The large acid value difference of preheat temperature resulted a large difference of saponification value as well. Increased phosphorus content due to the dissolution of phospholipids in the oil along with the initial warming temperature and unsaponification matter content stabilize at 0.19% - w/w (Subroto et al., 2014). The rise in iodine value to the rise in preheat temperature caused by more unsaturated fatty acid extracted and active oxygens were reduced oil so that active oxygen reaction with double bonds are avoided. This incidence is characterized by a decrement in the peroxide value against preheating temperature. When the initial heating temperature is raised from 80^{o}C to 90^{o}C, the peroxide rate remains at 15.87 meq O_2/kg oil. Optimum preheating temperature at 70^{o}C.

Table.1. Nyamplung seed oil quality and quantity at various preheating temperatures of mechanical extraction for 10 minutes

Parameter	**Preheating Temperature (°C)**		
	70	80	90
Oil Yield (%-w/w)	33.15	33.75	33.80
Acid Value (mg KOH/g oil)	21.97	30.81	33.02
Saponification Value (mg KOH/g oil)	178.63	187.49	189.71
Iodine Value (gr I_2/100 g oil)	75.35	92.85	96.74
Peroxide Value (meq O_2/kg oil)	17.86	15.87	15.87
Unsaponification Matter (%-w/w)	0.19	0.19	0.19
Phosphor (mg P/kg oil)	282.79	353.48	388.83

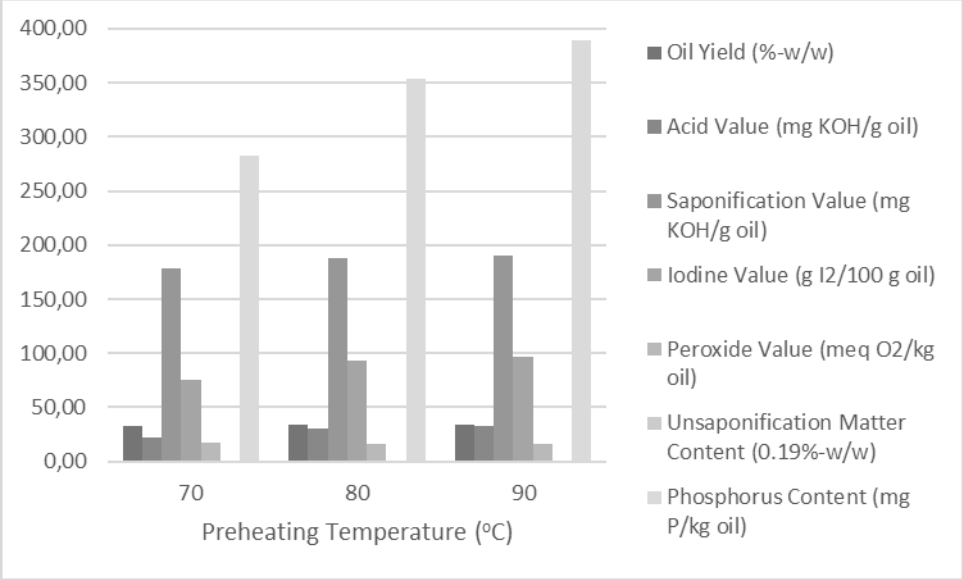

Fig.1. Nyamplung seed oil quality and quantity at various preheating temperatures of mechanical extraction for 10 minutes

The effect of mechanical extraction time on the quality and quantity of nyamplung seed oil is shown in Table 2 and Fig. 2. The longer the extraction time, the percentage of oil yield increases. The increment in percent of oil yield against extraction time is greater than that of the preheating temperature. However, the percent increment in oil yield from 20 minutes to 30 minutes decreased compared with from 10 minutes to 20 minutes. This was due to the longer extraction time, the nyamplung kernel seed formed like a cake mixture mixed with oil, making it difficult to separate (Mpagalile and Clarke, 2005). Increased extraction time also caused iodine value and phosphorus content rised. Acid value 21.97 mg KOH/g oil, saponification value 178.63 mg KOH/g oil, peroxide value 17.86 meq O_2/kg oil, and unsaponification matter content 0.19%-w/w were stabilized. These parameters were not changed because the extraction process is too short. The rise in phosphorus content is due to the dissolved phospholipids in the oil described earlier, so that the extraction time also affects the dissolution of phospholipids in the oil. So, the iodine number caused by the extraction of more unsaturated fatty acid. The optimum extraction time at 10 minutes, so that the optimum conditions of mechanical extraction at the initial heating temperature 70°C.

Table.2. Nyamplung seed oil quality and quantity at various extraction time of mechanical extraction at preheating temperature 70°C

Parameter	Extraction Time (min)		
	10	20	30
Oil Yield (%-w/w)	33.15	37.45	39.05
Acid Value (mg KOH/g oil)	21.97	21.97	21.97
Saponification Value (mg KOH/g oil)	178.63	178.63	178.63
Iodine Value (gr I_2/100 g oil)	75.35	96.74	116.19
Peroxide Value (meq O_2/kg oil)	17.86	17.86	17.86
Unsaponification Matter (%-w/w)	0.19	0.19	0.19
Phosphor (mg P/kg oil)	282.79	388.83	424.18

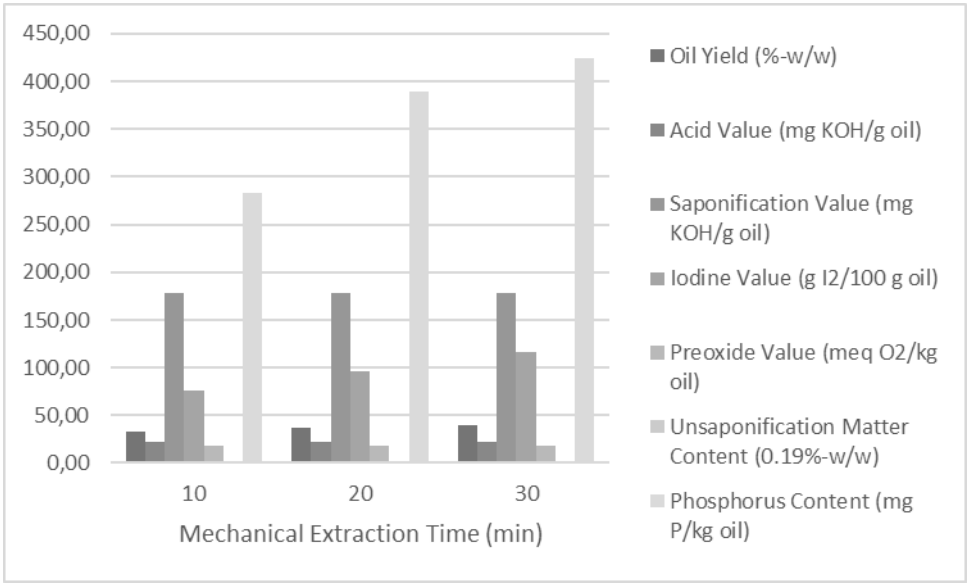

Fig.2. Nyamplung seed oil quality and quantity at various extraction time of mechanical extraction at preheating temperature 70°C

3.2 Solvent extraction

The effect of nyamplung kernel seed sieving on oil quality and quantity is shown in Figure 3 and Table 3. The smaller the size of the kernel seed, the higher the yield of oil. This is because the smaller size of the kernel seed, the larger the surface area, so that n-hexane solvent absorbs oil more easily from kernel seed. On the other hand, minimizing the size of kernel seed caused acid value, saponification value, peroxide value, and phosphorus content rose. The increased peroxide value caused by active oxygen reacted easily with oil when the surface area was large, especially unsaturated fatty acids, so that the acid value and saponification value also became bigger. The increase of phosphorus content caused by phospholipid was easily absorbed by n-hexane along with the small size of kernel seed, but at kernel seed size of 40 mesh n-hexane cannot longer absorbed phospholipid so that phosphorus content was 989,75 mg P/kg of oil from kernel seed size 35 mesh. The fixed iodine number was 82.16 g I_2 / 100 g oil and the unsaponification matter content remained 0.2%-w/w. The size of nyamplung kernel seed was optimum at 20 mesh.

Table.3. Nyamplung seed oil quality and quantity at various kernel seed size of Solvet extraction for 6 hours

Parameter	Nyamplung Kernel Seed Size (mesh)		
	20	35	40
Oil Yield (%-w/w)	58.38	62.35	63.30
Acid Value (mg KOH/g oil)	33.02	38.55	39.80
Saponification Value (mg KOH/g oil)	188.97	194.87	197.83
Iodine Value (g I_2/100 gr oil)	82.16	82.16	82.16
Peroxide Value (meq O_2/kg oil)	16.37	19.35	20.34
Unsaponification Matter (%-w/w)	0.20	0.20	0.20
Phosfor (mg P/kg oil)	777.66	989.75	989.75

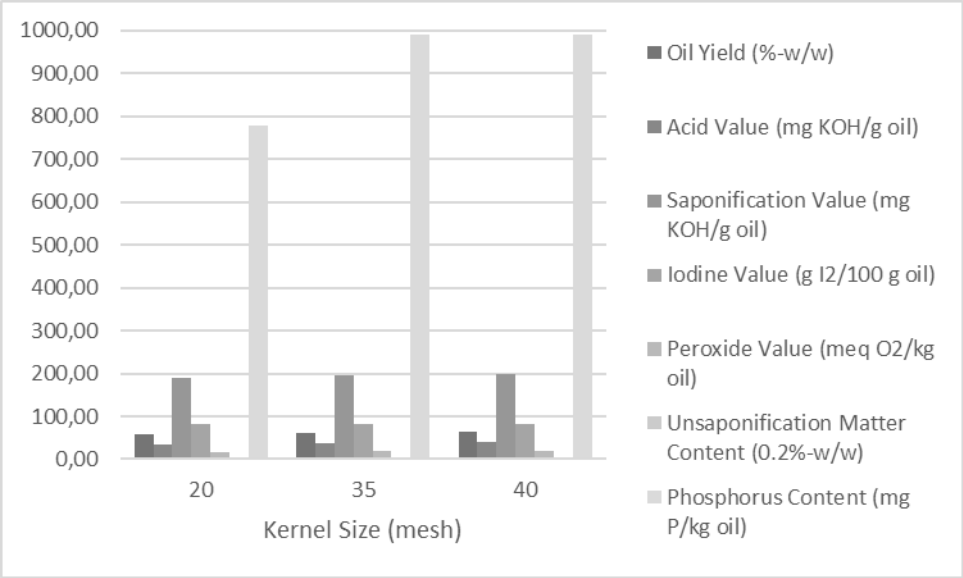

Fig.3. Nyamplung seed oil quality and quantity at various kernel seed size of mechanical extraction at preheating temperature 70ºC

The influence of Solvet extraction time on the quality and quantity of nyamplung seed oil is shown in Fig. 4 and Table 4. Increased percent yield of oil was exactly the same as mechanical extraction time. However, the time required for oil extraction was longer and the increment was smaller. Extraction temperatures can be reached at least 1 hour, while about 30 minutes later the oil were gathered in a round flask. Therefore, the required extraction time was at least 2 hours. 2 hours later no oil extracted anymore. It can be said that the extraction time of 6 hours up to 8 hours was too long, so it needed to reduce extraction time. Adding extraction time caused acid value, saponification value, iodine value, and phosphorus content rose. When the extraction time increased from 7 hours to 8 hours, the saponification value remained at 193.40 mg KOH / g oil. Peroxide value decreased dramatically from 16.37 meq O_2 / kg oil at 6 hours until 2.48 meq O_2 / kg oil at 8 hours. The longer the extraction time, the active oxygen in the oil decreased and the volatile compounds also decreased (Budiadnyani et al., 2015). The increment of phosphorus content was exactly the same as the effect of nyamplung kernel seed size, while the iodine value increased along with the length of extraction time which was accompanied by the heating, which was supposed to increase peroxide value. The content of unabsorbed matter remains 0.2%-w/w. The optimum time of Solvet extraction was 6 hours, so the optimum condition of Solvet extraction was 20 mesh particle size for 6 hours.

Table.4. Nyamplung seed oil quality and quantity at various extraction time of Solvet extraction kernel seed size 20 mesh

Parameter	Solvet Extraction Time (hr)

	6	7	8
Oil Yield (%-w/w)	58.38	59.50	61.50
Acid Value (mg KOH/g oil)	33.02	36.89	37.17
Saponification Value (mg KOH/g oil)	188.97	193.40	193.40
Iodine Value (g I_2/100 gr oil)	82.16	91.39	101.60
Peroxide Value (meq O_2/kg oil)	16.37	4.46	2.48
Unsaponification Matter (%-w/w)	0.20	0.20	0.20
Phosfor (mg P/kg oil)	777.66	989.75	989.75

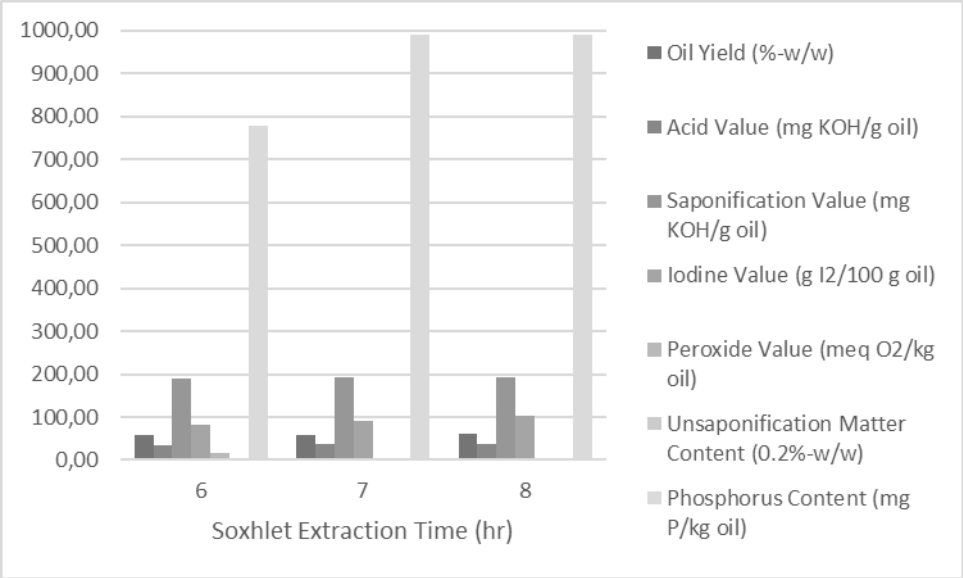

Fig.4. Nyamplung seed oil quality and quantity at various extraction time of Solvet extraction kernel seed size 20 mesh

2.3 Extraction Methods Comparision

Fig. 5 and Table 5 show the comparison of optimum oil mechanical extraction with the optimum oil Solvet extraction from nyamplung seed.

Table.5. Nyamplung seed oil extraction methods comparision

Parameter	**Extraction Method**	
	Mechanical	Solvet
Oil Yield (%-w/w)	33.15	58.38
Acid Value (mg KOH/g oil)	21.97	33.02
Saponification Value (mg KOH/g oil)	178.63	188.97
Iodine Value (g I_2/100 g oil)	75.35	82.16
Peroxide Value (meq O_2/kg oil)	17.86	16.37
Unsaponification Matter (%-w/w)	0.19	0.20
Phosphor (mg P/kg oil)	282.79	777.66

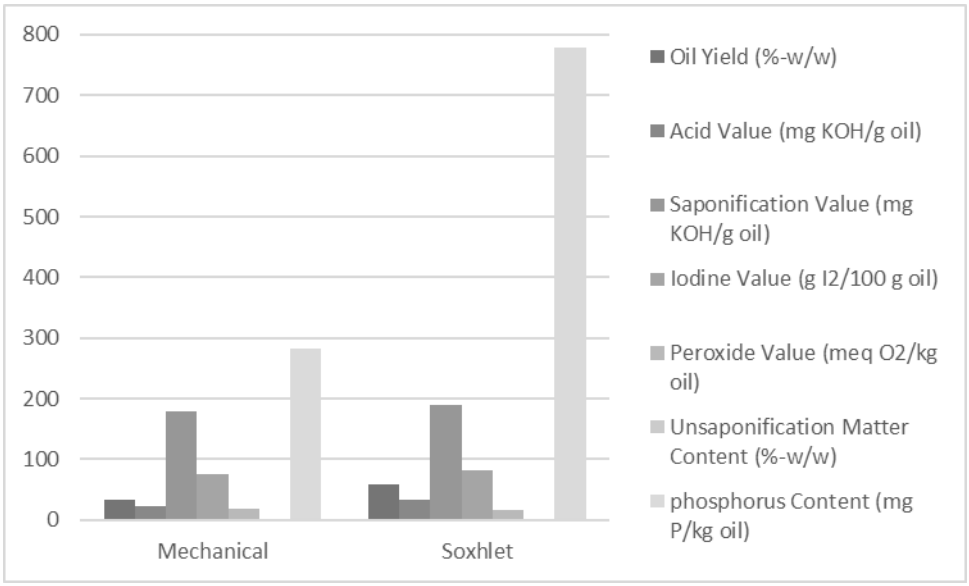

Fig.5. Nyamplung seed oil extraction methods comparision

Overall, mechanical extraction was better than Solvet extraction although the yield percentage of nyamplung seed oil was lower. This is in contrast to research done by Delfan-Hossseini et al. (2016) on purslane kernels which states that there aws no significant effect of extraction methods on oil quality. The most influential method of extraction was the n-hexane solvent. The solvent absorbed oil components such as free fatty acids, sterols, and more phospholipids. Mechanical extraction did not use solvents at all, so the method is cheaper operational costs, faster processing, energy saving, and less environmentally damaging than Solvet extraction.

4. Conclusions

In mechanical extraction, raising the preheating temperature raised acid value, saponification value, iodine value, and phosphorus content, and decreases the peroxide value; while the addition of extraction time only increased iodine value and phosphorus content. In Solvet extraction, the size of the nyamplung kernel seed increased acid value, saponification value, peroxide value, and phosphorus content; while the addition of extraction time increased acid value, saponification value, iodine value, and phosphorus content, and decreased peroxide value.

References

1. Aparamarta, H.W., Saputra, T., Claratika, A., Ju, Y., and Gunawan, S. Separation and purification of triacylglycerols from nyamplung (Calophyllum inophyllum) oil by batchwise solvent extraction. *Industrial & Engineering Chemistry Research*; 55: 3113-3119(2016).
2. Atabani, A. E., and César, A. D. S. Calophyllum inophyllum L. – A prospective non-edible biodiesel feedstock. Study of biodiesel production, properties, fatty acid composition, blending and engine performance. *Renewable and Sustainable Energy Reviews*; 37, 644–655(2014).
3. Budiadnyani, I.G.A., Estiasih, T., and Yunianta. Characteristics and fatty acid profile of refined fish oil from byproduct of yellowfish tuna (Thunnus albacores) meal processing. *Journal of Life Science and Biomedicine*; 5, 132-136(2015).
4. Chavan, S. B., Kumbhar, R.R., and Deshmukh, R.B. Callophyllum inophyllum Linn ("honne") oil, a source for biodiesel production. *Journal of Chemical Science*; 11; 24-31(2013).
5. Delfan-Hosseini, S., Nayebzadeh, K., Mirmoghtadaie, L., Kavosi, M., and Hosseini, S.M. Effect of extraction process on composition, oxidative stability and rheological properties of purslane seed oil. *Food Chemistry*; 222, 61-66(2016).

6. Mahanta, P. and Shrivastava, A. *Technology Development of Bio-Diesel as an Energy Alternative*. Guwahati: Department of Mechanical Engineering Indian Institute of Technology Guwahati.
7. Mpagalile, J.J., and Clarke, B. Effect of processing parameters on coconut oil expression efficiencies. *International Journal of Food Sciences and Nutrition*; 56, 125-132(2005).
8. Orwa, C., Mutua, A., Kindt, R., dan Simons, A.J. *Agroforestree Database: a tree reference and selection guide version 4.0*. Kenya: World Agroforestry Centre (2009).
9. Prabowo, S.E, Dwinugroho, M.P., Baruna, E.S., Ajiwihanto, N., Idarwati, F., Ambarsari, L., Yusuf, M., Suzanty, V.M., Pratama, D.P., Thaib, Z., Yuanningrat, H., and Anutomo, I.G. *Handbook of Energy & Economic Statistics of Indonesia*. Jakarta: Mining of Energy and Mineral Resources Republic of Indonesia (2016).
10. Ruiz-Mendez, M. and Dobarganes, M.C. Oil Refining. *AOCS Lipid Library* (2011).
11. Subroto, E., Manurung, R., Heeres, H.J., and Broekhuis, A.A. Mechanical extraction of oil from Jatropha curcas L. kernel: Effect of processing parameters. *Industrial Crops and Products*; 63, 303-310(2015).
12. Tambunan, A.H., Situmorang, J.P., Silip, J.J., Joelianingsih, A., and Araki, T. Yield and physicochemical properties of mechanically extracted crude Jatropha curcas L. oil. *Biomass Bioenergy*; 43, 12-17(2012).

Preliminary Study of Recovery of Vitamin E from Magnesium Salt of Palm Fatty Acid Distillate (PFAD)

Reni Yuniarti[1], Listianingrum[1], R.H.M.T. Al-Aziz[1], Defry Rizaldy[2], Muhamad Insanu[2], Ardiyan Harimawan[1], and Dianika Lestari[1,*]

[1]*Department of Chemical Engineering, Institut Teknologi Bandung, Jl. Ganesha 10, Bandung 40132, Indonesia*
[2]*School of Pharmacy, Institut Teknologi Bandung, Bandung 40132 Indonesia*
**E-mail: dianika@che.itb.ac.id*

Abstract
Vitamin E is one of the products that can be obtained from the processing of waste refinery, namely PFAD. Palm fatty acid distillate (PFAD) contains 82%-wt of free fatty acids which can be utilized as a raw material for magnesium salts of fatty acids (Mg-PFAD) and 0,5%-wt vitamin E or five times higher than crude palm oil (CPO). The objective of this research is to investigate the optimum condition of the recovery process of Vitamin E through extraction Mg-PFAD using food grade organic solvents. Optimization of the extraction process using ethanol is determined by performing variations on the experiment duration and weight ratio of Mg-PFAD salts with ethanol (as solvent). In addition, this research compares the recovery process of vitamin E by the method of direct extraction and soxhlet extraction. Physical and chemical properties of ethanol extraction phase were determined by the analysis of acid value and levels of vitamin E by spektrofotodensitometry. Data show that the duration of extraction process significantly affects the extraction process. For any variation of the solvent comparison note optimum at 30-60 minutes. After 60 minutes the first time, the duration of extraction is no significantly affect the process. Optimum levels of vitamin E is 35,37% by soxhlet extraction method.

1. Introduction

PFAD is known as a by-product of the CPO refining process of the deodorization unit, with a high fatty acid content of 82% and is estimated to be about 4-5%-wt from the CPO produced[1]. On the process of purification in the deodorization unit, most vitamin E is carried away from the CPO to PFAD so that the levels of vitamin E in the PFAD increased up to 5 times higher than the CPO which is about 4000-5000 ppm or about 0.5%-wt[2]. Vitamin E in the PFAD contains 70% of tocotrienol, where the content higher than other sources. Therefore, PFAD potentially as raw material for getting vitamin E. The method of separation of vitamin E from PFAD can be through the saponification process of fatty acids with alkaline or metal oxide magnesium, followed by extraction process of vitamin E using food grade organic solvents.

Vitamin E and its derivatives is a compound that is very beneficial to humans. In essence, vitamin E and its derivatives can cause apoptosis (death) against cancer cells. According to Packer (1991), vitamin E, especially α-tocopherol, can set the reaction rate of peroxidase and the production of free radical. According to FAO (2005), everyone needs vitamin E about 3-10 mg per day. According to BPS, the population in Indonesia at the year 2015 about 254,9 million. Based on that data, the minimum requirement of vitamin E in Indonesia is about 764,7 kg/day. For the sake of satisfying the needs of vitamin E, Indonesia relies on imports from China (53% of imports) and United States (17% of imports) with a fairly high import costs.

2. Experimental

In this research, first, we did the saponification process of fatty acids with alkaline or metal oxide magnesium. The main raw materials used namely PFAD with specifications as indicated in Table 1 and MgO. Briefly, 2 kg of PFAD and 271 g of MgO was mixed at 80°C. Afterward, this saponification reaction occurred at 98°C. The reaction was completed when the temperature reaches around 105°C[3]. Fig. 1 displays the experimental scheme for the saponification process.

Table 1. Physical and chemical properties of PFAD

	Range
Titre (°C)	50
Iodine value (mg I_2/g sample)	60
Acid value (mg KOH/g sample)	197,19
Free Fatty Acid	88.28%
Myristic acid	1,69%
Palmitic acid	30,48%
Stearic acid	9,7%
Oleic acid	32,39%
Linoleic acid	14,02%

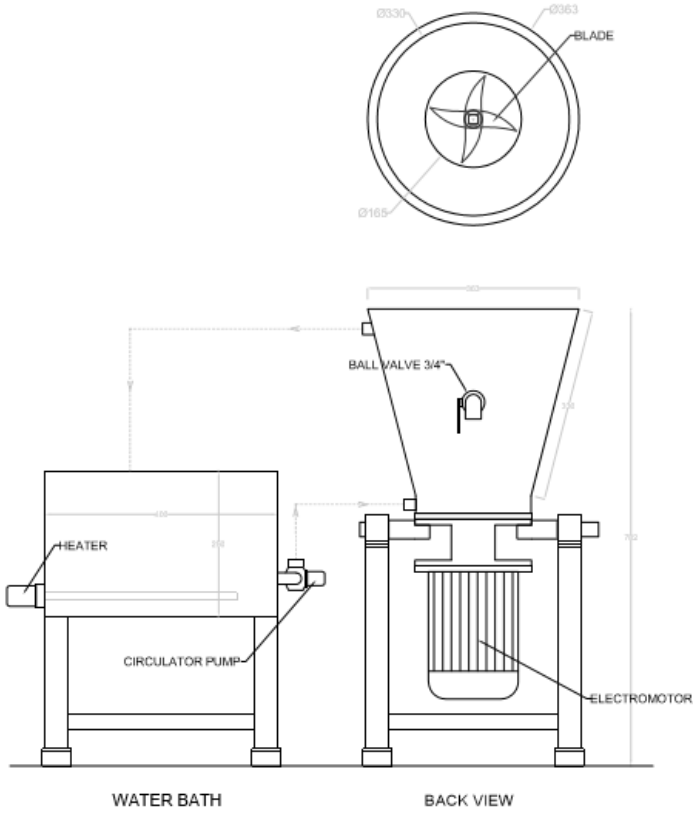

Fig.1. Schematic of saponification reactor

After getting Mg-PFAD salts continued with the extraction process of Mg-PFAD salts with ethanol (as solvent). Optimization of the extraction process using ethanol is determined by performing variations on the experiment duration and weight ratio of Mg-PFAD salts with ethanol. In addition, this research compares the recovery process of vitamin E by the method of direct extraction and soxhlet extraction. Experimental variations are presented by Table 2 and Table 3.

Table 2. Variations of duration extraction

No	The duration of extraction (minutes)
1	10
2	30
3	60
4	90

Table 3. Variations of weight ratio Mg-PFAD salts with ethanol

No	The weight Mg-PFAD salts with ethanol
1	1:3
2	1:5
3	1:10

The flow diagram of experiments is shown in Fig. 2. Physical and chemical properties of ethanol extraction phase were determined by the analysis of acid number and levels of vitamin E by spektrofotodensitometry.

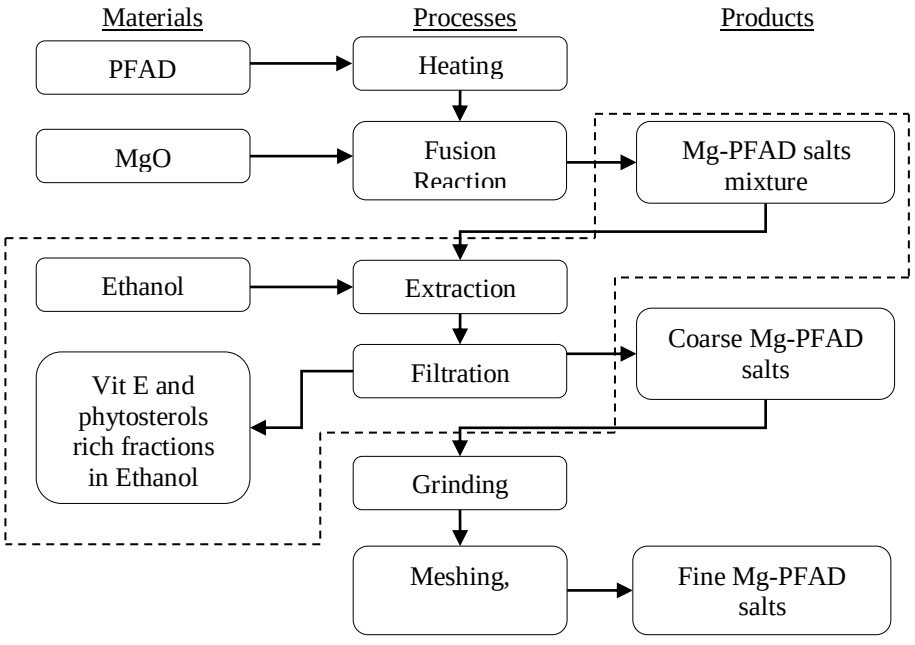

Fig.2. Research flow diagram

3. Results and discussion

3.1. The Effects of the duration extraction and weight ratio of Mg-PFAD salts with ethanol on % FFA of ethanol phase and Mg-PFAD salts phase

Vitamin E in the PFAD didn't react to form Mg-PFAD salts and be carried away in the ethanol fraction at extraction process along with a number of squalene, sterols and fatty acids that didn't react. An evaluation of this process is %free fatty acids of Mg-PFAD salts phase and ethanol phase after extraction process. %fatty acids obtained from convert of the acid value that measurable. The profile effect variation of the duration of extraction process and the ratio of the weight of the Mg-PFAD salts with ethanol against %FFA indicated on Fig. 3 and Fig. 4.

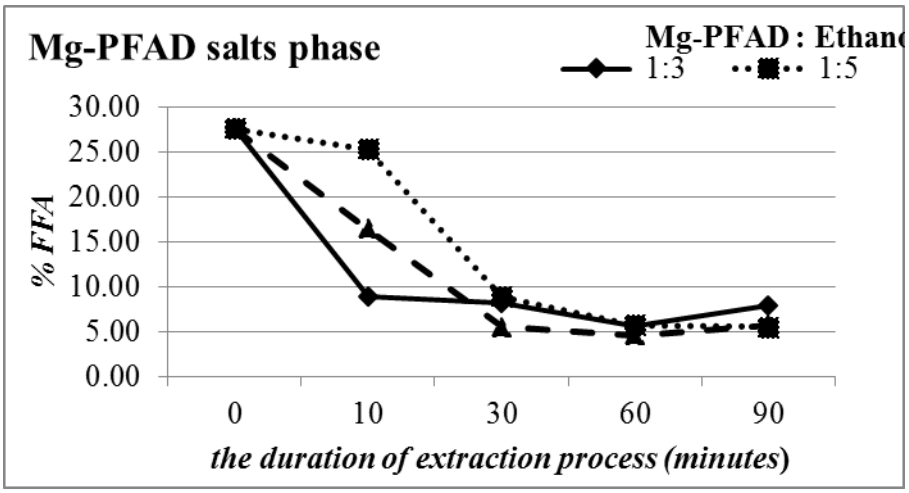

Fig. 3. The effects of the duration extraction and weight ratio of Mg-PFAD salts with ethanol on % FFA of ethanol phase

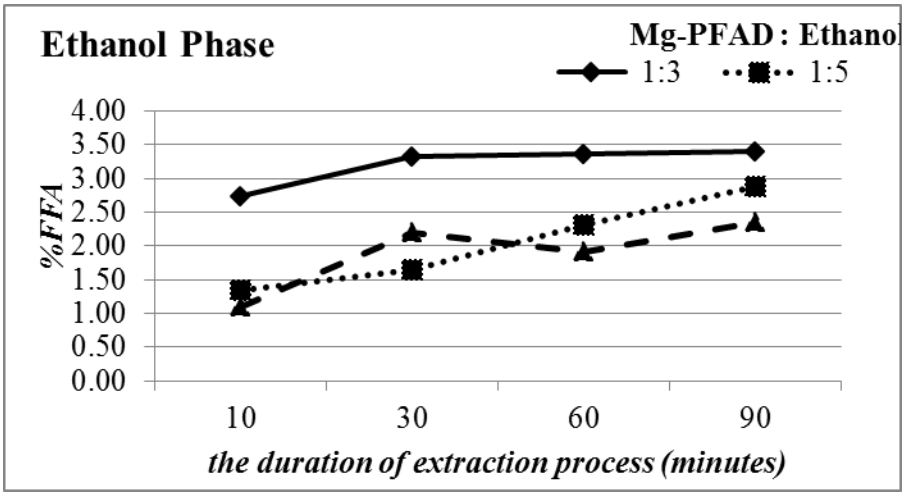

Fig. 4. The effects of the duration extraction and weight ratio of Mg-PFAD salts with ethanol on % FFA of ethanol phase

Data show that the duration of extraction process significantly affects the extraction process. For any variation of the solvent comparison note optimum at 30-60 minutes. %FFA of Mg-PFAD salts after extraction process for 30-60 minutes about 5-10% of FFA. After 60 minutes the first time, the duration of extraction is no significantly affect the process. Optimum conditions the ratio of weight Mg-PFAD salt with ethanol is 1:3. At this ratio, the %FFA of

ethanol phase during extraction process for 30-90 minutes (3,33-3,39% of FFA) is greater than the other variations ratio.

3.2. The Effects method of extraction process on levels of vitamin E

Determination of the levels of vitamin E by the spektrofotodensitometry method with motion phase: hexane – ethyl acetate (9:1), 500 µg/ml of sample, and 3µl of points volume. The recovery process of vitamin E by the method of soxhlet extraction (35,37% of vitamin E) is better than the direct extraction method (23,56% of Vitamin E).

Table 4. The levels of vitamin E on each extraction process method

Extract of Vitamin E	C of comparison (µg/ml)	AUC of comparison	AUC of sample	Vitamin E of sample (µg)	%Vitamin E
direct extraction	100	577,5	680,2	0,35	**23,56**
soxhlet extraction	250	1.455,9	1.029,9	0,53	**35,37**

4. Conclusions

The duration of extraction process significantly affects the extraction process. For any variation of the solvent comparison note optimum at 30-60 minutes. After 60 minutes the first time, the duration of extraction is no longer significantly affect the process. Optimum conditions the ratio of weight Mg-PFAD salt with ethanol is 1:3. The recovery process of vitamin E by the method of soxhlet extraction is better than the direct extraction method.

Acknowledgements

This research was funded by Grant Research Sawit (GRS, K-16) Programme from BPDPKS, Indonesian Ministry of Finance, 2016.

References

11. Ab Gapor Md Top. Production and utilization of palm fatty acid distillate (PFAD). Lipid Technology 22 (2010), 11-13.F. De Lillo, F. Cecconi, G. Lacorata, A. Vulpiani, EPL, 84 (2008).
12. Maarasyid C, Muhamad II, Supriyantob E. Potential source and extraction of vitamin E from palm-based oils: a review. *J Teknologi*. 2014;69(4):43–50.
13. Rogers, Russell and Blew, William. Manufacture of Metal Soaps. *US Patent 2,890,232*.

Scale up Production of Magnesium Salt of Palm Fatty Acid Distillate (Mg-PFAD) for Food, Nutraceuticals, and Pharmaceuticals Industries

R. Habib R.M.T. Al-Aziz[1], Listianingrum[1], Reni Yuniarti[1], Defry Rizaldy[2], Muhamad Insanu[2], Ardiyan Harimawan[1], and Dianika Lestari[1*]

[1] *Department of Chemical Engineering, Institut Teknologi Bandung, Jalan Ganesha 10, 40132 Indonesia*
[2] *School of Pharmacy, Institut Teknologi Bandung, Jalan Ganesha 10, 40132, Indonesia*
[*] *E-mail: dianika@che.itb.ac.id*

Abstract

The aim of this research is to explore the effect of scale up production of Mg-PFAD to the reaction yield using technical grade of MgO. The scale up was conducted using a water jacketed reactor with propeller. A waterbath was installed to the main reactor to adjust the temperature while no pressure modification. The variation of experiments were the volume of reaction up to 2 kg. Furthermore, the assessment of scaling up production was based on Acid value (AV). For up to 2 kg scale up production, this study recommends to use 1,5 molar ratio of MgO to PFAD with 2 hours pre-heating for PFAD and to conduct the reaction at temperature of 80 ^{o}C and 20 Hz of propeller speed.

1. Introduction

Palm Fatty Acid Distillate or PFAD is a by-product of palm oil refinery process. PFAD contain approximately 82%-w of free fatty acid and can be used as a raw material for Mg-PFAD production[1]. One of further process of Mg-PFAD product is magnesium stearate. A magnesium stearate is known as a food additive or most widely used lubricant during tablet compaction or capsule filling at pharmaceutical industries. The average national need in 2010-2015 is about 5627 tonne/year, and it still imported.

Magnesium stearate is a mixture of magnesium salts of fatty acid which consist mainly of magnesium stearate and palmitate in varying proportion. Magnesium stearate can be produce by following process: (a) direct process wherein fatty acids are directly reacted with a magnesium source, (b) indirect process where a sodium soap is produced by the reaction of fatty acids with sodium hydroxide in water[2,3].

A magnesium salt or magnesium stearate production by fatty acid has been founded at several patent or journal and produced commercially. Despite its potential, it has not been tested with PFAD from Indonesian palm oil industries.

A preliminary research result an operational condition of Mg-PFAD production. A previous research use a direct fusion reaction by reacting melted PFAD with magnesium oxide at several conditions. As a part of the research of development magnesium stearate and vitamin E production by PFAD, an experiment scale will be improved to maximum 3 kg PFAD per hour. The aim of this research is to explore the effect of scale up production of Mg-PFAD to the reaction yield using technical grade of MgO.

2. Material and Methods

2.1 Material

A PFAD were supplied from SMART Tbk, Jakarta, Indonesia contain about 92% of free fatty acid. MgO powder using technical grade ny chlorogreen, Bandung, Indonesia. Analytical material such as ethanol, chloroform, KOH and phenophthalein were using by Merck with p.a grade.

2.2. Reactor Setup

Scale up of Mg-PFAD production to maximum reactor 3 kg PFAD per hour consisting of main reactor, waterbath and electrical pannel. A main reactor has a double jacketed and propeller and its made by stainless steel SUS-304 material. Diameter of inner tank at bottom part is 165 mm and at the upper part is 330 mm with the height of tank is 320 mm. Maximum

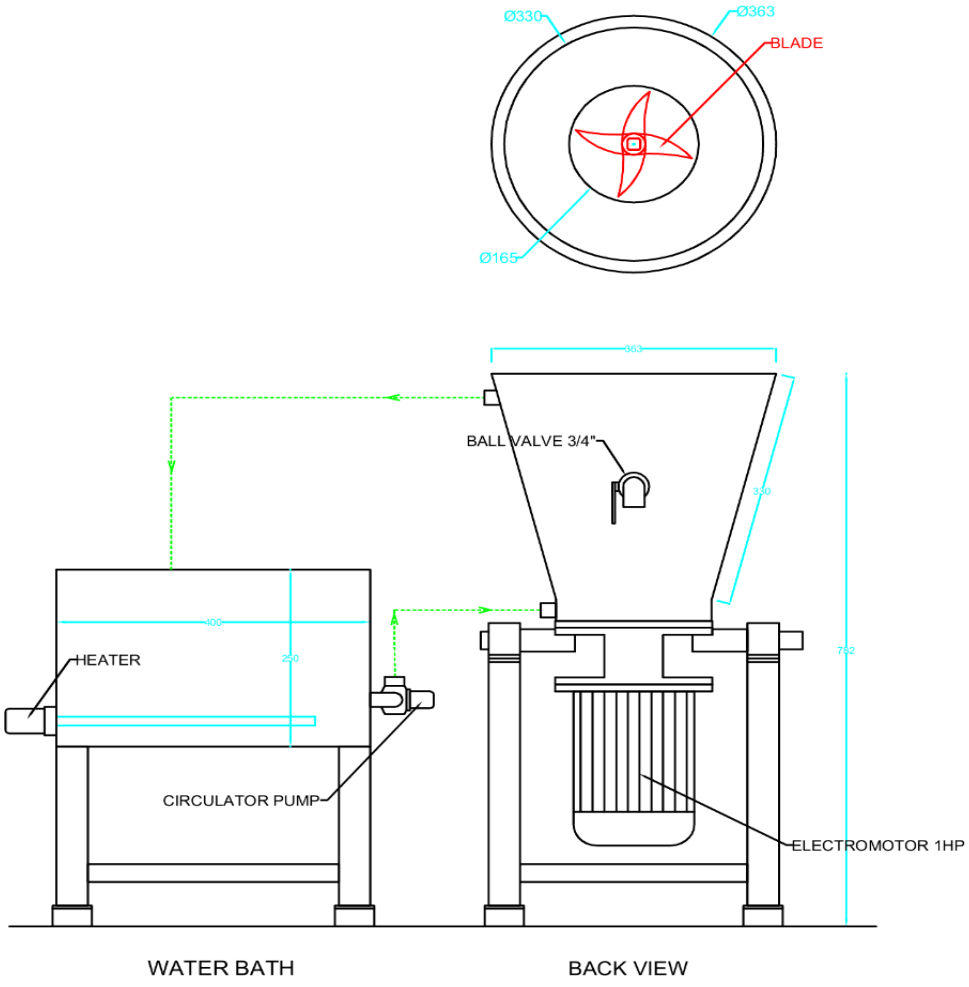

Fig. 1. Scheme of Mg-PFAD Reactor

volume of reactor is 15 L. Figure 1 shown a scheme of reactor and figure 2 is shown a real image of the reactor.

A main reactor is equipped by motor with inverter to spin the blade at the inner reactor. A blade is made by stainless steel SUS-316 and it can removed from reactor easily. A maximum volume of waterbath is 20 L with material of tank is made by stainless steel SUS-304. Waterbath equipped with heater, thermocontroller and circulation pump. At the next of waterbath, electrical panel is installed. Electrical panel is consist of temperature panel to control a temperature of heater, circulation panel is to discharged hot water to a main reactor and propeller panel is to control propeller cycle.

Fig. 2. Mg-PFAD Reactor

2.3. Reaction Methodology

In the laboratory scale, several Mg-PFAD reaction methode were carried out. As a final result, we use Rogers patent methode (1959), US Pat. 2,890,232 with some modification and its adapted to this scale up Mg-PFAD production research. The flow diagram of experiment is shown in figure 3.

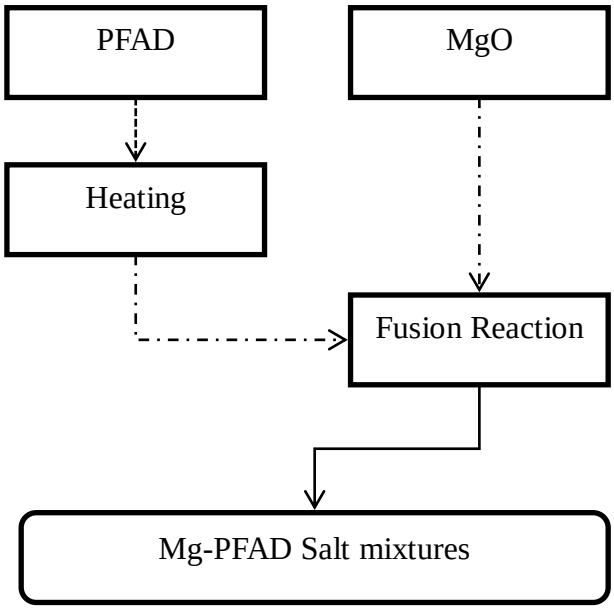

Fig. 3. Flow Diagram of Experiment

Firstly we added PFAD with certain variation to main reactor and heated at 80°C. After 2 hours of preheated, turn on propeller panel and set the spin of propeller at 20 Hz. Then added MgO to melted PFAD with molar ratio 1:1,5 of PFAD:MgO. Reaction was completed when reaction is expand and maximum temperature are reached.

2.4. Experimental Variation and operational condition of reaction

Operational condition of reaction is adapted by previous research at laboratory scale with some modification. The reaction was conducted at 80°C without pressure modification. The agitation speed is about 20 Hz and it start to turned on after 2 hours. A molar ratio of PFAD to MgO were 1:1,5. An experimental variation is shown in table 1.

Table 1. Experimental Variation of the Research

Mass of PFAD (g)	Mass of MgO (g)	Molar Ratio of PFAD : MgO
1000	184.7	1 : 1.5
1500	277.1	
2000	369.5	

2.5. Analytical Methode

Acid value analytical methode was selected because it was efficient methode and it doesnt need specialized equipment. The aim of acid value analysis is to determine the fatty acid conversion.

First, phenophthalein indicator was added to 100 ml ethanol-chloroform at elenmeyer flask and titrate with KOH-ethanol solution until the color is change to pink color. Then added five gram of sample and titrate again with KOH-ethanol solution until the color change again to pink. Acid value (A.V.) was determined according to the equation given below.

$$A.V. = \frac{56.1 * N * V}{M} mg\ KOH gram\ fatty\ acid \quad (1)$$

Where:
N: Normally of KOH solution
V: the volume of solution employed for titration, ml
M: weight of fatty acids sample, g

3. Result and Discussions

Magnesium stearate is the major product of this research. Operating condition of Mg-PFAD production is adapted by previous research. To get an optimum condition of operation we have to perform some preliminary study of scale up reactor with several condition. When its

Fig. 4. Step Process of preheated of PFAD

applied to scale up production, some problem occured because there are different condition between laboratory scale and scale up reactor. So we should modified some condition to get a better result such as preheated PFAD until 2 hours and change a molar ratio PFAD to MgO from 1:1,25 to 1:1,5. A purpose preheated is to maximize the heat of reaction.

Reaction time was completed within 5-7 minutes when the reaction is expand. After that, the propeller cannot stirred because the product become hardened. At laboratory scale, a reaction will expand after added some water as a catalyst. But at scale up reactor, even some water

Fig. 5. Step Process when reaction is expand after added some MgO.

didn't add to the reactor, the reaction is still expand. It assumed the agitation in this reactor increased surface area of melted PFAD to react more faster with MgO.

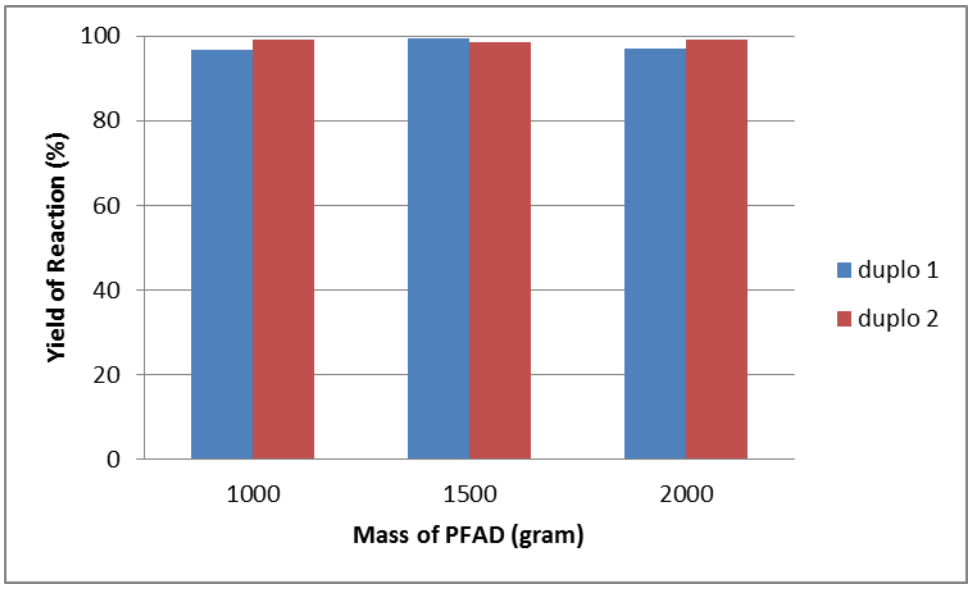

Fig. 6.The Effect of Scale up Mg-PFAD Production to the Reaction Yield

Reaction yield at experimental variation is shown at figure 6. A Maximum conversion of this research is 99.32% at 1500 gram of initial PFAD. Amount of initial PFAD its not affected the yield of reaction. Its still need further analysis to know this phenomenon.

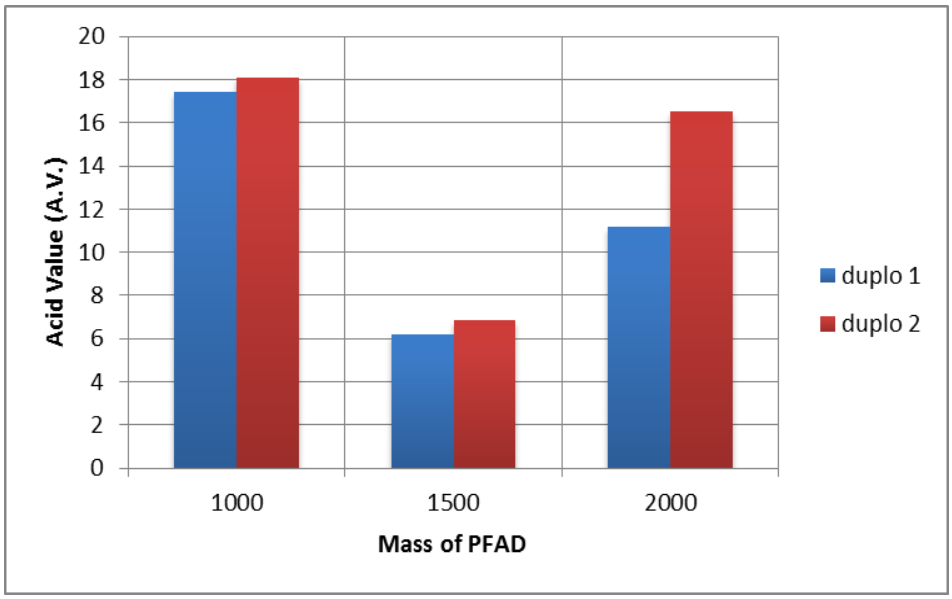

Fig. 7. Acid Value Number of Scale Up Production

Acid value analysis resulting a fatty acid conversion. Figure 7 shown an acid value graphic at experimental variation. It show that 1500 gram of initial PFAD show a smallest acid value number. It assumed that a scale up production cannotinfluence a yield conversion.

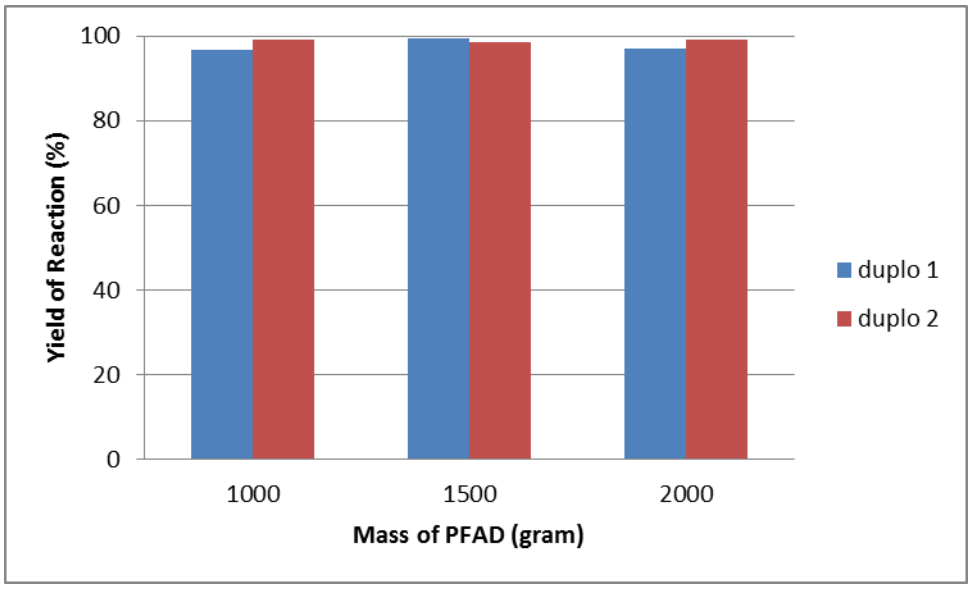

Fig. 6.The Effect of Scale up Mg-PFAD Production to the Reaction Yield

4. Conclusions

A1500 gram of PFAD resulting highest coversion and smallest acid value number, A scale up production didn't effect to the yield of reaction.

5. Acknowledgment

This research was funded by Grant Research Sawit (GRS, K-16) Programme from BPDPKS, Indonesian Ministry of Finance, 2016

References

1. Ab Gapor Md Top, Production and utilization of palm fatty acid distillate (PFAD), *Lipid Technology* 22 (2010).
2. FAO,Magnesium stearate – 80th Joint FAO/WHO Expert Commitee on Food Additives (JEFCA) Meeting, *Chemical and Technical Assesment*, (2015)
3. Roger, R.H., et al., Manufacture of metal soaps., *US Patent Office*, 2890232, (1959)

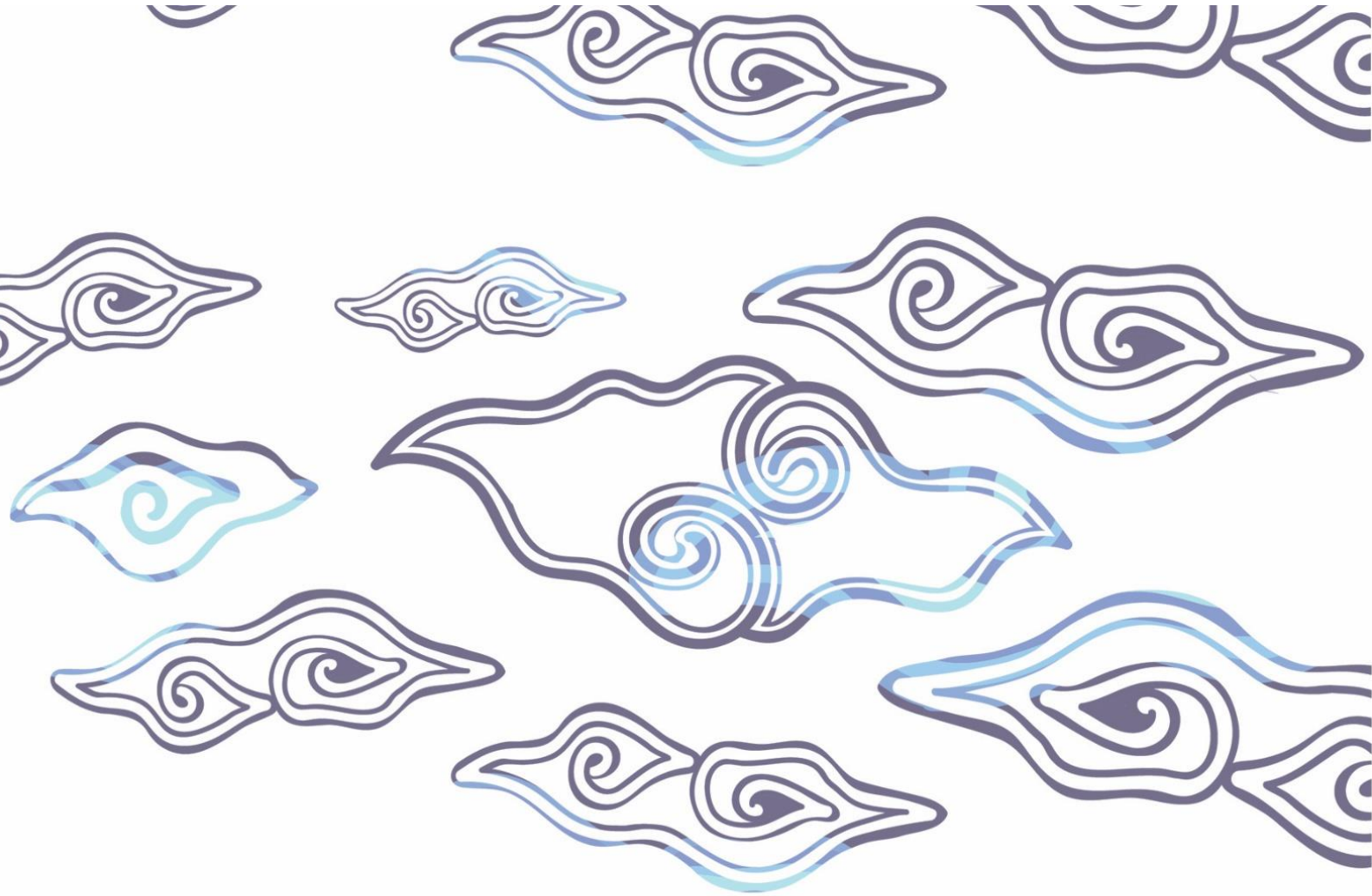

Department of Chemical Engineering
Faculty of Industrial Technology
Institut Teknologi Bandung

ISSN: 2354-5917